ERDC/CHL TR-11-6

Coastal and Hydraulics Laboratory

US Army Corps
of Engineers®
Engineer Research and
Development Center

Morganza to the Gulf of Mexico Floodgate Study

Tate O. McAlpin, Ian E. Floyd, Christopher J. Callegan,
Thad C. Pratt, and Danielle M. Washington

October 2011

ERDC/CHL TR-11-6
October 2011

Morganza to the Gulf of Mexico Floodgate Study

Tate O. McAlpin, Ian E. Floyd, Christopher J. Callegan, and Thad C. Pratt

Coastal and Hydraulics Laboratory
U.S. Army Engineer Research and Development Center
3909 Halls Ferry Road
Vicksburg, MS 39180

Danielle M. Washington

U.S. Army Engineer District, New Orleans
7400 Leake Ave.
New Orleans, LA 70118-3651

Final report

Prepared for U.S. Army Engineer District, New Orleans
7400 Leake Ave.
New Orleans, LA 70118-3651

Under Military Interdepartmental Purchase Request (MIPR) W42HEM92266908,
"ERDC ADH Gate Modeling/Morganza to the Gulf of Mexico"

Abstract: The Adaptive Hydraulics model, AdH, was used to investigate the circulation tendencies in and around numerous proposed structure locations for the Morganza to the Gulf of Mexico project utilizing its two-dimensional shallow-water module. This study characterizes existing water levels and currents in the vicinity of six proposed structures and predicts any potential impacts that may result. Comparing model-generated currents and water-surface elevations between pre- and post-construction conditions provides insight into whether a particular alternative will adversely impact velocity conditions. AdH was used to develop time varying current fields for the base and plan conditions.

Contents

Figures and Tables

Figures

Tables

Preface

This study was conducted for the U.S. Army Engineer District, New Orleans under Military Interdepartmental Purchase Request (MIPR) W42HEM92266908, "ERDC ADH Gate Modeling/Morganza to the Gulf of Mexico" dated 2009. Project coordination at the New Orleans District was provided by Danielle Washington of the New Orleans District.

The work described herein and the preparation of this report was performed from August 2009 through August 2010 by the U.S. Army Engineer Research and Development Center Coastal and Hydraulics Laboratory (ERDC-CHL), Vicksburg, MS. The work was performed under the general supervision of Dr. William D. Martin, Director, ERDC-CHL, and, Jose E. Sanchez, Deputy Directory, ERDC-CHL. Direct supervision was provided by Bruce Ebersole, Chief, Flood and Storm Protection Division; and Dr. Robert McAdory, Chief of the Estuarine Engineering Branch, Tate O. McAlpin, Ian E. Floyd, Christopher J. Callegan, Thad C. Pratt, all of the Estuarine Engineering Branch, and. Danielle M. Washington, New Orleans District, conducted this study and prepared the report.

At the time of publication of this report, COL Kevin J. Wilson, was Commander and Executive Director of ERDC, and Dr. Jeffery P. Holland was the Director.

Unit Conversion Factors

Multiply	By	To Obtain
cubic feet	0.02831685	cubic meters
cubic inches	1.6387064 E-05	cubic meters
cubic yards	0.7645549	cubic meters
degrees (angle)	0.01745329	radians
feet	0.3048	meters
foot-pounds force	1.355818	joules
Inches	0.0254	meters
inch-pounds (force)	0.1129848	newton meters
knots	0.5144444	meters per second
miles (nautical)	1,852	meters
miles (U.S. statute)	1,609.347	meters
miles per hour	0.44704	meters per second
slugs	14.59390	kilograms
square feet	0.09290304	square meters
square inches	6.4516 E-04	square meters
square miles	2.59 E+06	square meters
square yards	0.8361274	square meters
yards	0.9144	meters

1 Introduction

Background

The U.S. Army Engineer District, New Orleans is in the process of determining the correct sizing for sail-through structures to be constructed along the new proposed Morganza to the Gulf levee system in southern Louisiana. In the aftermath of Hurricane Katrina, numerous new levees are being constructed to reduce the risk of storm- induced flooding. In addition to the economic and loss of life impact of such flooding, there is also a significant negative impact on the local ecosystem (Fredrickson et al. 2007; Suedal et al. 2008).

To provide the best protection, waterways north of the new levee system will be shut off from the Gulf of Mexico during storm events. In order to accomplish this protection with minimum impact on the natural environment and waterborne transportation, numerous sail-through structures — each capable of being closed as necessary — are being constructed to allow for continued waterborne transportation between the Gulf of Mexico and areas north of the new levee system. These structures will also allow for the continued movement of water to and from the Gulf of Mexico, thereby minimizing the impact of the new levee system on natural habitat. Also included along the levee system are numerous environmental structures to increase the connection between the Gulf of Mexico and areas north of the proposed levee system during normal tidal exchange.

At the request of the New Orleans District, the U.S. Army Engineer Research and Development Center (ERDC) performed a number of engineering studies in support of efforts to determine the proper sizes of six proposed structures (Bush Canal, Bayou Terrebonne, Lapeyrouse Canal, Placid Canal, Bayou Petit Caillou, and Humble Canal). These structure sizes will be determined through numerical modeling using the Adaptive Hydraulics Code (AdH). The study area along with the proposed levee alignment and structure locations are shown in Figure 1.

Once all navigational and environmental structure sizes are determined using AdH then the final configuration will be modeled using a previously validated TABS-MDS model. This model will determine the effects of the levee system on the salinity conditions throughout the system. The

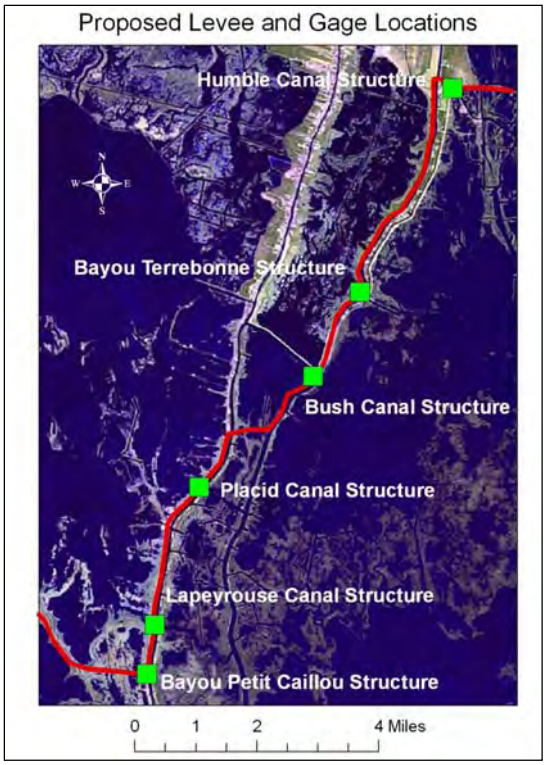

Figure 1. The proposed levee alignment (red line) with the proposed structure locations (green squares).

validated TABS-MDS model will also be used to investigate different operational methods and their impacts on the salinity fields. This two pronged modeling approach was accepted as the best means of utilizing the more computationally efficient AdH model (to obtain the proper structure velocities) and the already available validated TABS-MDS salinity model (to obtain the base versus plan salinity fields). Only the AdH hydrodynamic results are discussed in this report.

Objective

The primary objective of this study was to determine the smallest structures that resulted in reasonable velocity fields for the six proposed locations.

Approach

Data sources and acquisition, and model development methods using AdH, are described in detail in Chapters 2–4, with the model validation included in Chapter 5. Several design alternatives were simulated using the validated numerical model and are detailed in Chapter 6 with base

versus plan model comparisons provided in Chapter 7. The resulting conclusions for this project are presented in Chapter 8.

Description of site

The project is located south of Houma, LA, on the southern coast of Louisiana. The study site is centered between the Plaquemines-Modern Delta Complex (bird's foot delta) and the Atchafalaya River at the distal end of the Lower Mississippi River Valley (Frazier 1967; Brown et al. 2000). The primary waterways of interest are Bayou Petit Caillou, Bayou Terrebonne, and Bush Canal. Bayou Petit Caillou and Bayou Terrebonne lie almost parallel to each other, with approximate north-south orientations. The primary means of waterborne transportation connecting Bayou Petit Caillou and Bayou Terrebonne is Bush Canal. Bayou Petit Caillou extends south to Cocodrie, where it joins the Houma Navigational Canal. It also has connections to the west to Lake Boudreaux and Lake Quitman. Bayou Terrebonne extends south to Lake Barre and has connections to the east to Madison Bay. Bayou Petit Caillou and Bayou Terrebonne join north of the study area and extend northward to join the Gulf Intracoastal Waterway (GIWW) in Houma, LA. The study area is shown in Figure 2.

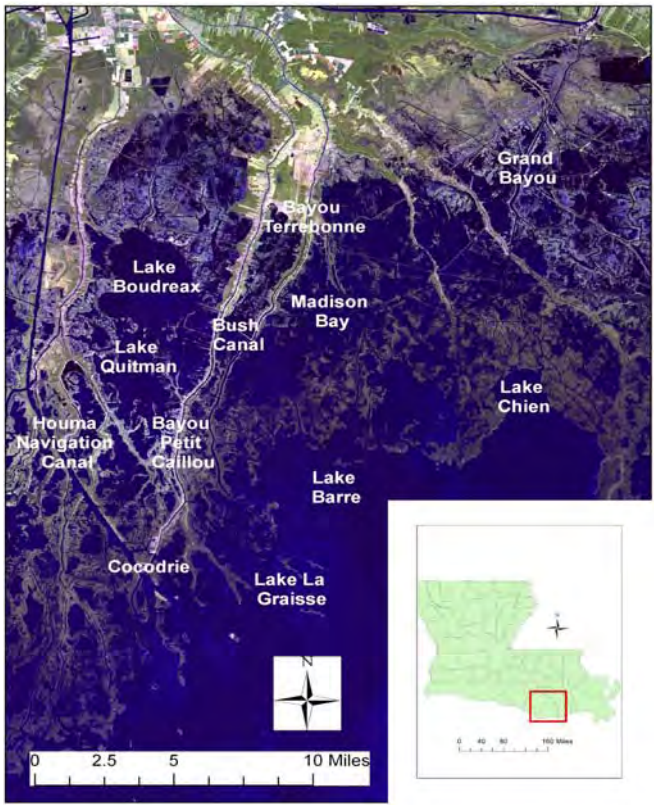

Figure 2. Study area location map.

2 Field data

U.S. Geological Survey data

The U.S. Geological Survey (USGS) maintains numerous water related gages (hydrodynamic and water quality) throughout the United States. Some of these USGS gages are in the current AdH model domain and as such were utilized in the numerical model validation. The water surface and discharge gage locations are shown in Figure 3 with Table 1 showing the longitude and latitude along with the available gage data for each. A more detailed explanation of the data collection methods used by the USGS is provided in Wahl et al. 1995.

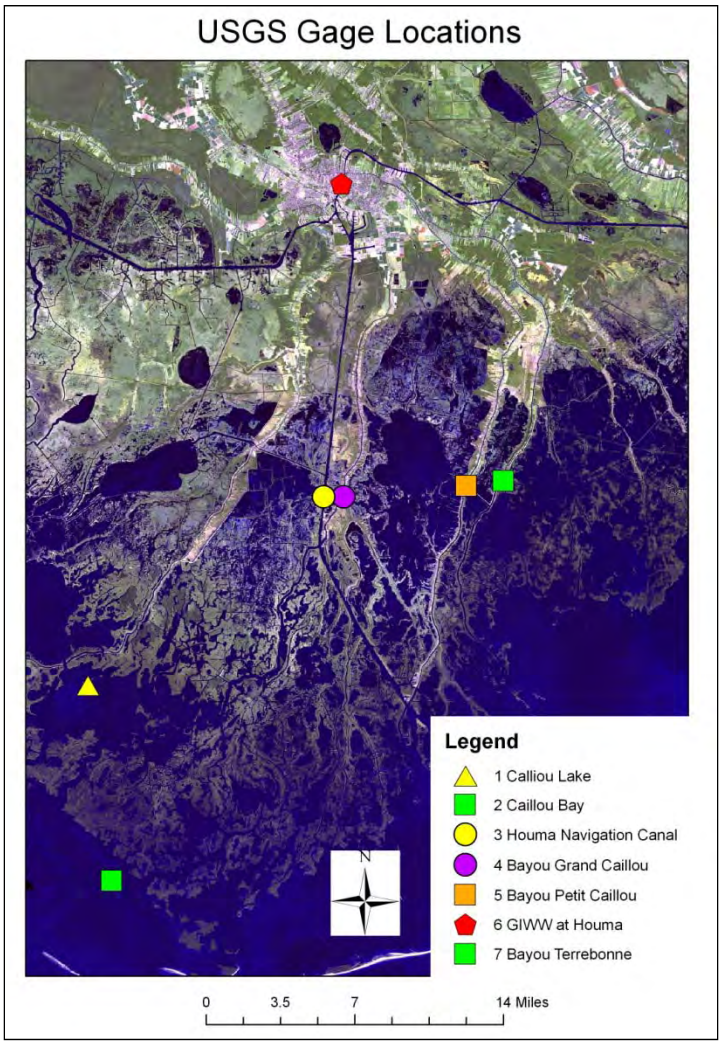

Figure 3. USGS gage locations.

Table 1. Latitudes and longitudes of USGS gages.

Gage Name	Discharge Data	Water Level Data	Wind Data	Latitude	Longitude
Caillou Lake		X	X	29.24917	-90.92111
Caillou Bay		X	X	29.07806	-90.87139
Houma Navigation Canal	X	X	X	29.385	-90.72972
Bayou Grand Caillou	X	X		29.38278	-90.71528
Bayou Petit Caillou		X	X	29.38697	-90.61803
GIWW at Houma	X	X		29.58806	-90.71
Bayou Terrebonne		X		29.38988	-90.5882

Coastal and Hydraulics Laboratory data

The ERDC Coastal and Hydraulics Laboratory (CHL) field crew deployed numerous gages for the current modeling effort (locations shown in Figure 5 and listed in Table 2). The deployed gages recorded water surface elevation and velocity measurements from 26 October 2009 to 22 January 2010. The data were measured using Argonaut side-looking Doppler current meters (Model SL500) and Teledyne RD Instruments ChannelMaster Horizontal Acoustic Doppler current profiler (ADCP) meters. The SL500 uses a vertical acoustic beam to determine water levels to an accuracy of ±0.02 ft or ±0.1% (whichever is greater) while measuring velocity ranges of ±20 ft/s to an accuracy of ±0.015 ft/s or ±1% (whichever is greater) (Sontek). The Teledyne RD Instruments Channel H-ADCP Meters

Table 2. CHL gage and latitudes and longitudes.

Gage Number	CHL Gages	Latitudes	Longitudes
1	GIWW near Houma	29.56195	-90.74453
2	Falgout Canal	29.4156	-90.791
3	Bayou Dularge	29.40772	-90.78696
4	Bayou Grand Caillou	29.33733	-90.73289
5	Bayou Petit Grand Caillou	29.29684	-90.64823
6	Lapeyrouse Canal	29.30858	-90.64552
7	Placid Canal	29.34174	-90.63247
8	Bayou Terrebonne	29.38988	-90.58821
9	Humble Canal	29.43606	-90.56275
10	Grand Bayou	29.53599	-90.40213
11	GIWW at Bayou Lafourche	29.58891	-90.37252

(600 kHz) use an acoustic sensor to determine water levels to an accuracy of ±0.0003 ft or ±0.25% (whichever is greater) while measuring velocity ranges of ±16 ft/s to an accuracy of ±0.006 ft/s or ±0.5% (whichever is greater) (Teledyne RD Instruments 2006). For the remainder of this report these two meter types will be combined and referred to simply as side-looking ADCP meters.

The side-looking ADCP meters were used to record velocity measurements every 15 min at a given horizontal level (Figure 4).

Figure 4. Side-looking ADCP meter operation (Sonteck).

Since these meters only record velocity measurements across the channel at a given water level, a correlation was determined between their measured average velocity and the actual cross-sectional averaged velocity. The cross-sectional averaged velocities were measured using a boat mounted Rio Grande ADCP (1,200 kHz). The Rio Grande ADCP can measure velocity ranges of ±16 ft/s with an accuracy of ±0.25% of the velocity (boat + water) or ±0.008 ft/s (whichever is greatest) (Teledyne RD Instruments 2009). These two velocity measurements (side-looker and boat-mounted ADCP measurements) will be related assuming the channels possess uniform flow (logarithmic flow profile) with no significant stratification. For this area, this should be an accurate assumption.

After deployment of the side-looking ADCP meters, the boat-mounted ADCP was used to measure the actual cross-sectional averaged velocity of the channel. A number of boat-mounted ADCP transect measurements were taken at each channel location. The boat mounted cross-sectionally averaged velocity measurements were correlated to the corresponding side- looking ADCP meter average velocity at that location to obtain a time series set of cross-sectional averaged velocities for each gage location (the correlation plots and equations are shown in Figures 6 to 16 with the correlation values listed in Table 3).

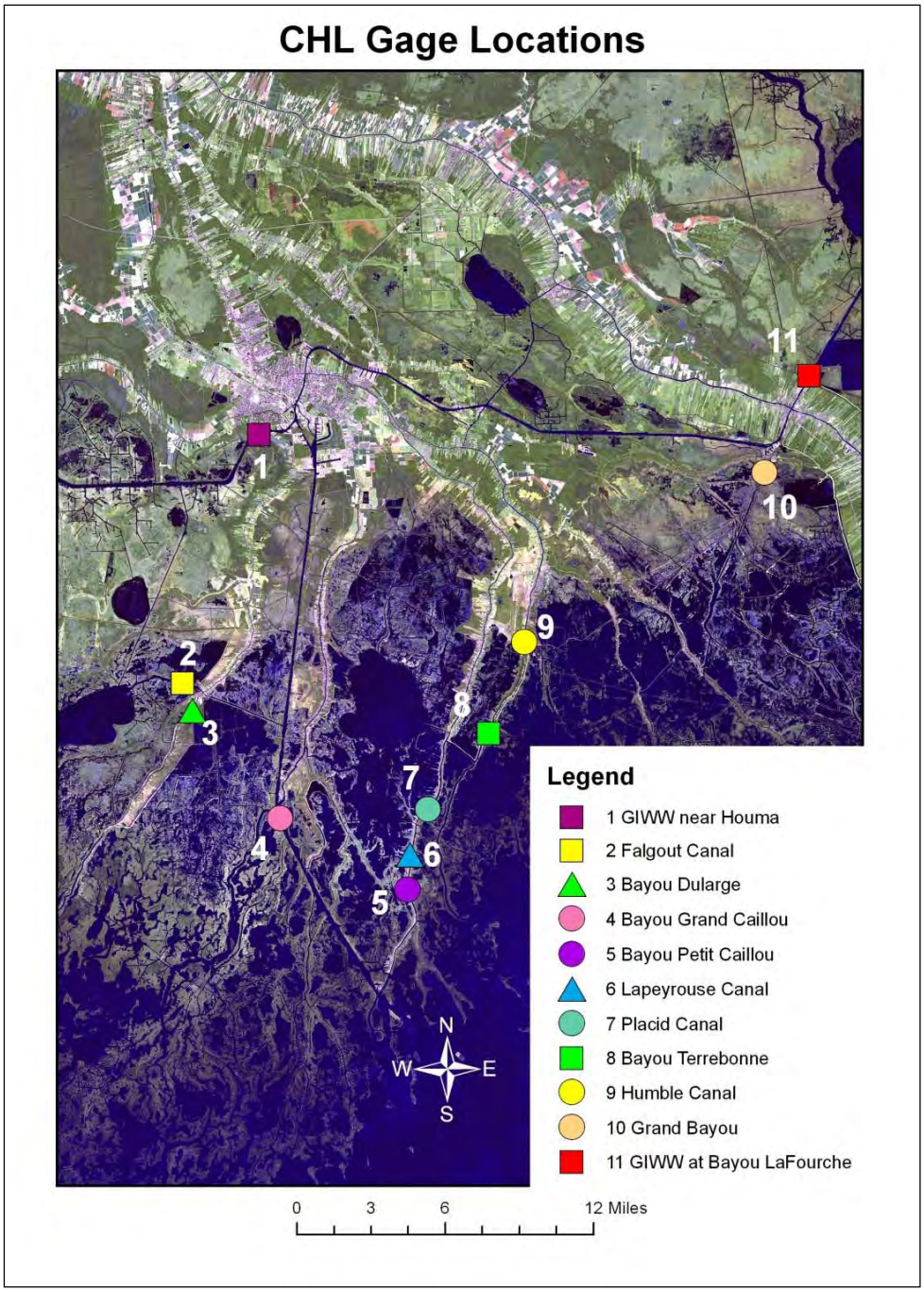

Figure 5. CHL gage locations.

Using Q=VA (Q is discharge, V is the average velocity for the cross section, and A is the cross-sectional area), the correlated velocity values were converted to discharge measurements by multiplying by the channel area (determine from boat-mounted ADCP measurements) to obtain time series discharge measurements to be used in the numerical model validation.

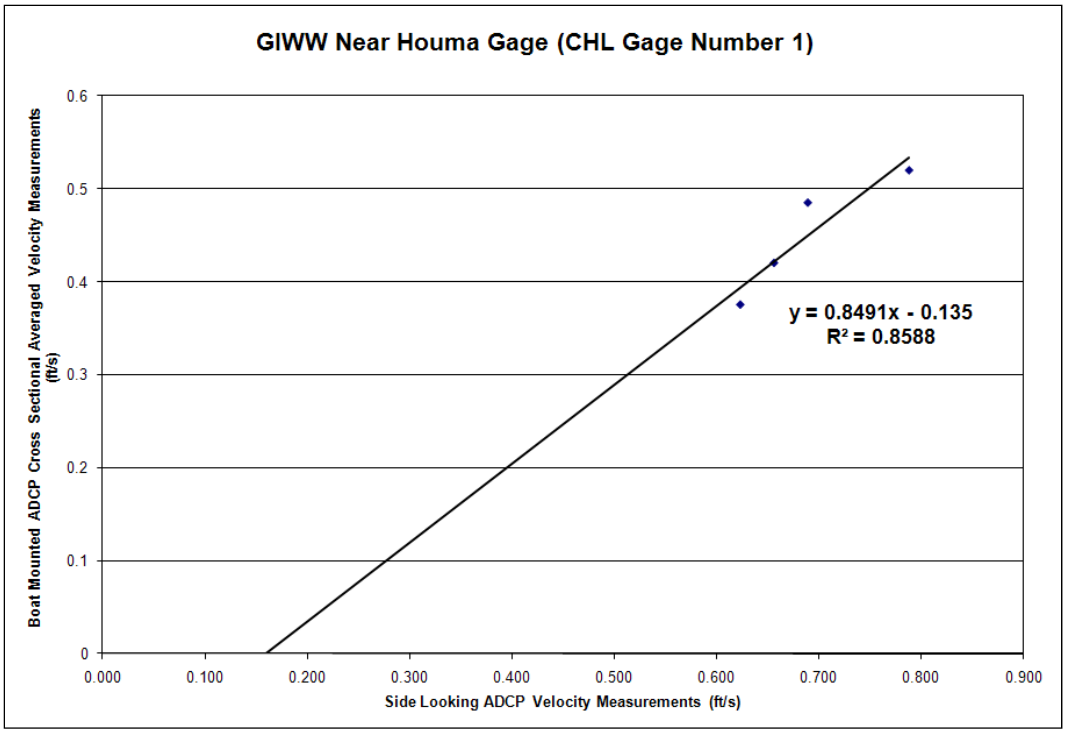

Figure 6. Velocity correlation of ADCP data at GIWW near Houma.

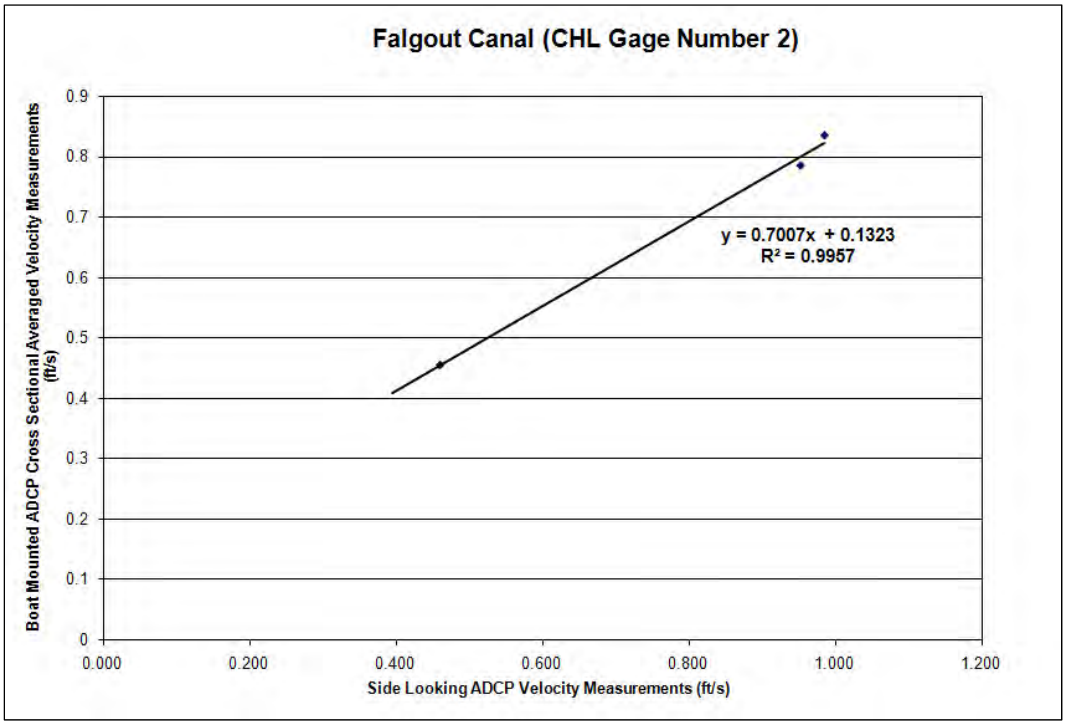

Figure 7. Velocity correlation of ADCP data at Falgout Canal.

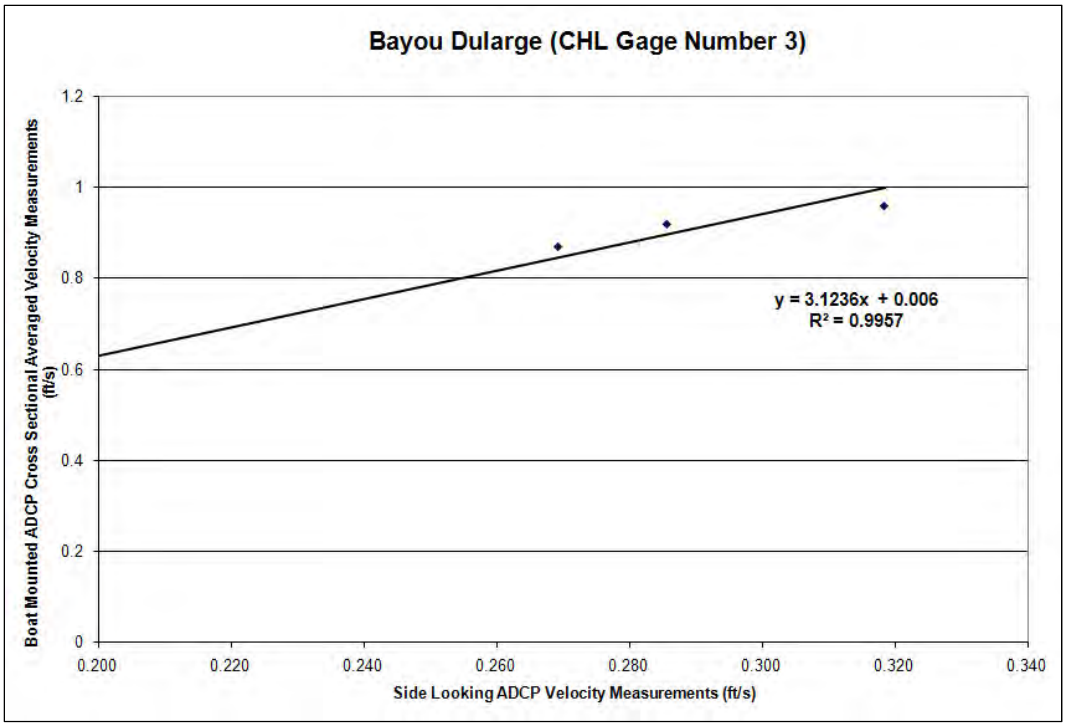

Figure 8. Velocity correlation of ADCP data at Bayou Dularge.

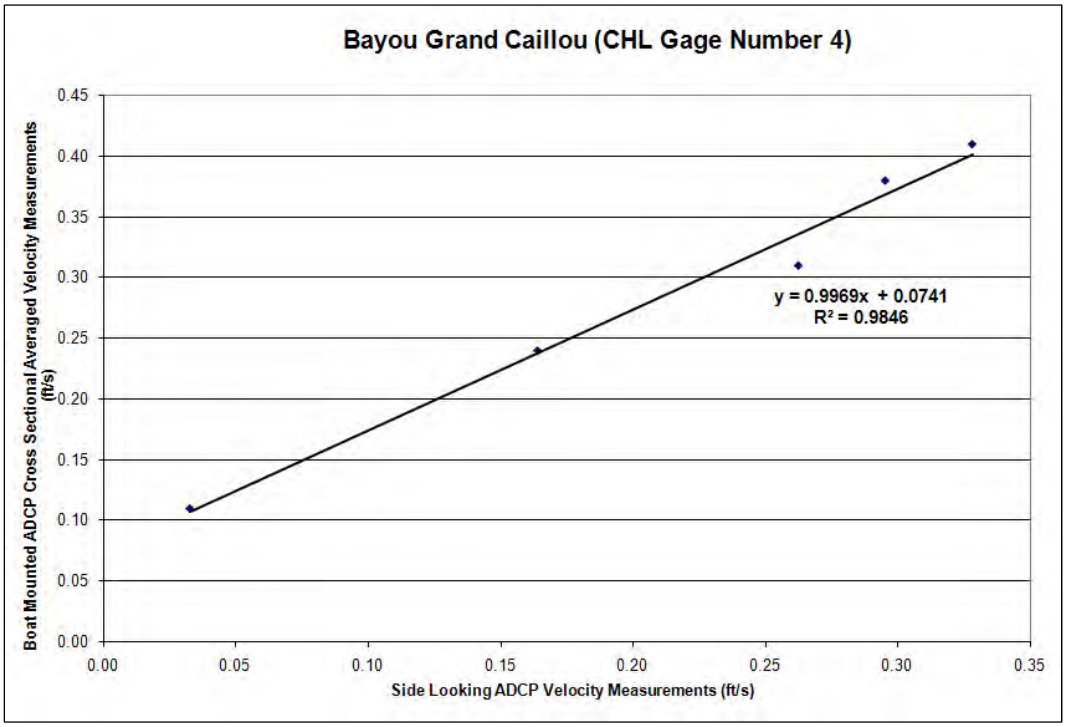

Figure 9. Velocity correlation of ADCP data at Bayou Grand Caillou.

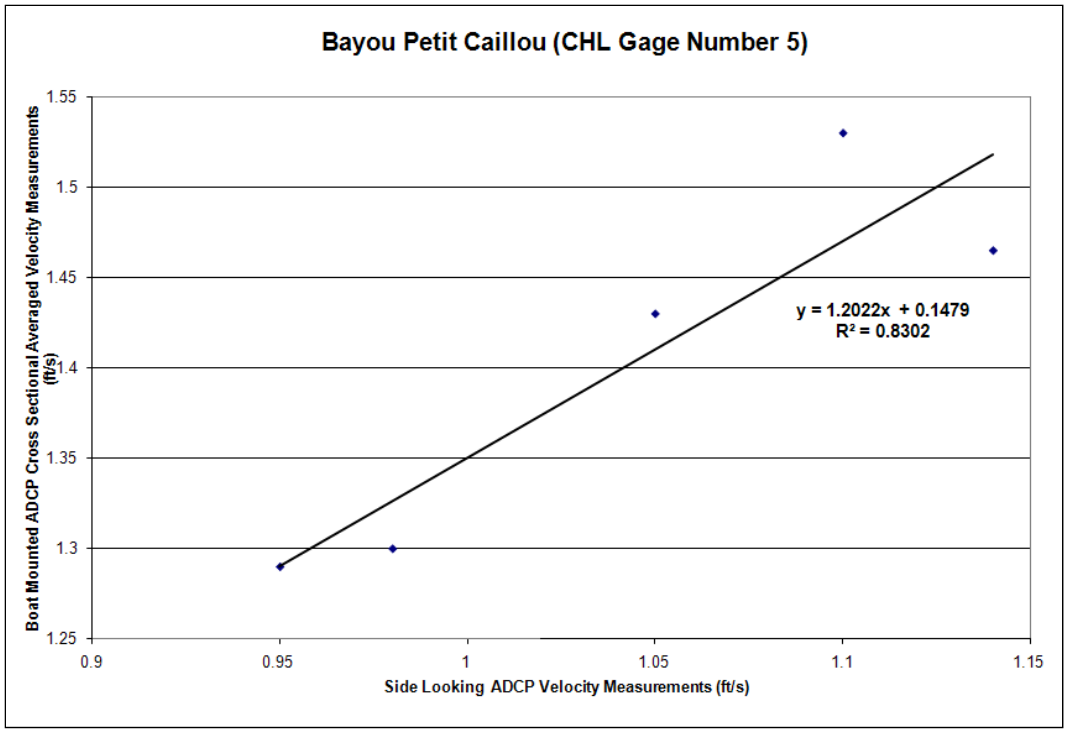

Figure 10. Velocity correlation of ADCP data at Bayou Petit Grand Caillou.

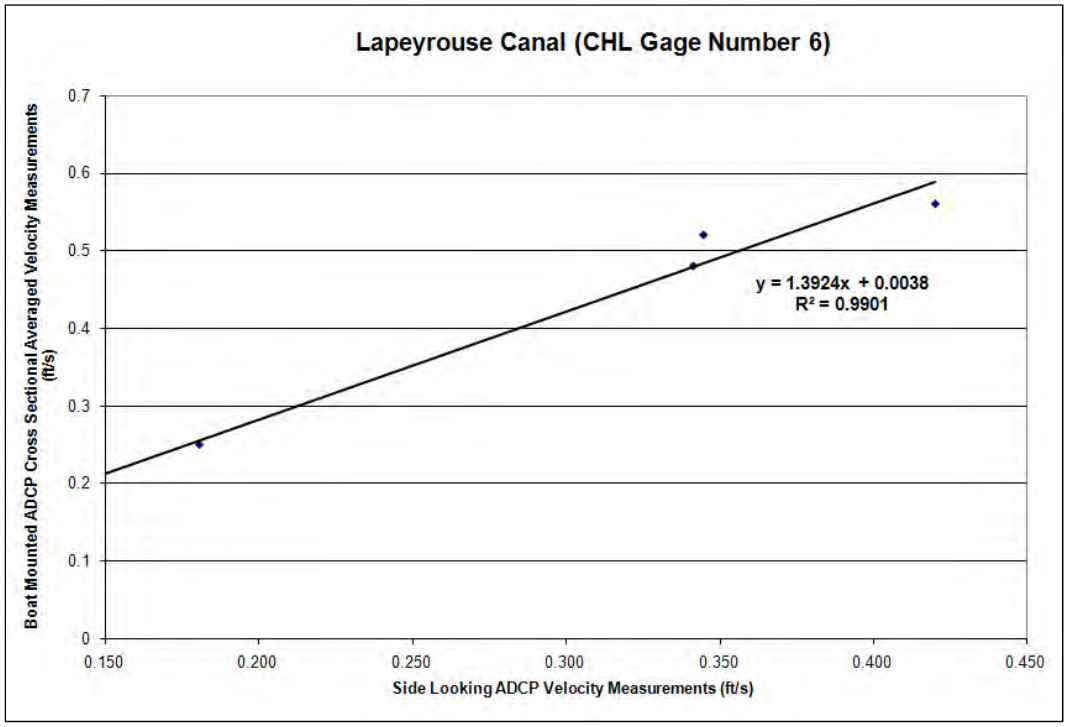

Figure 11. Velocity correlation of ADCP data at Lapeyrouse Canal.

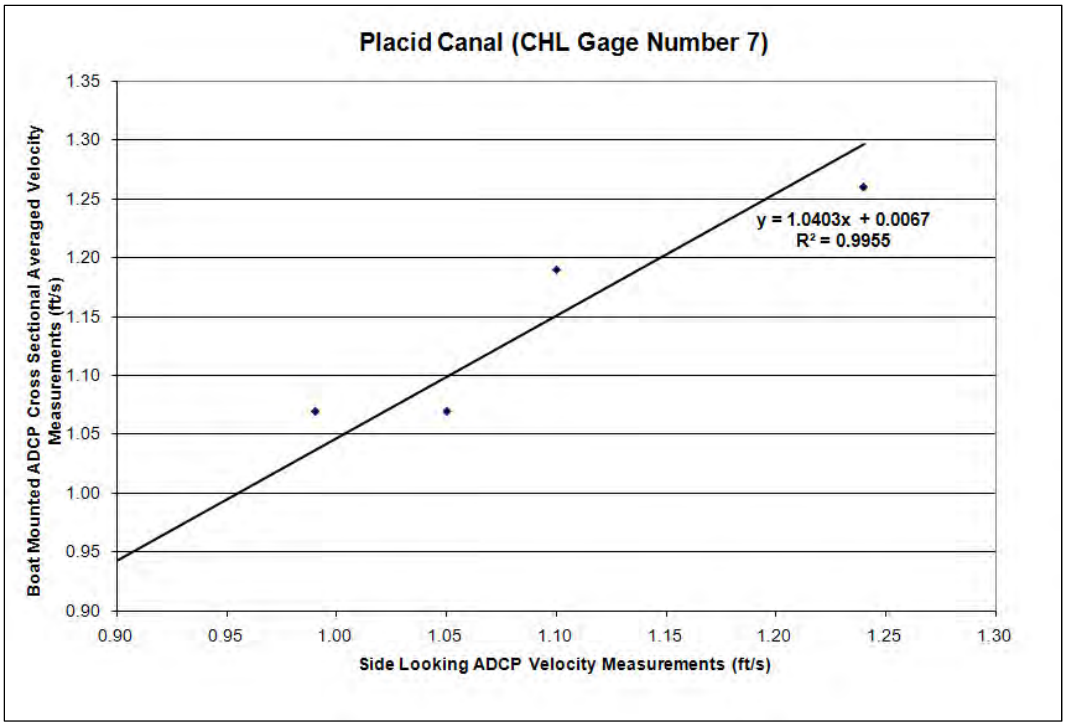

Figure 12. Velocity correlation of ADCP data at Placid Canal.

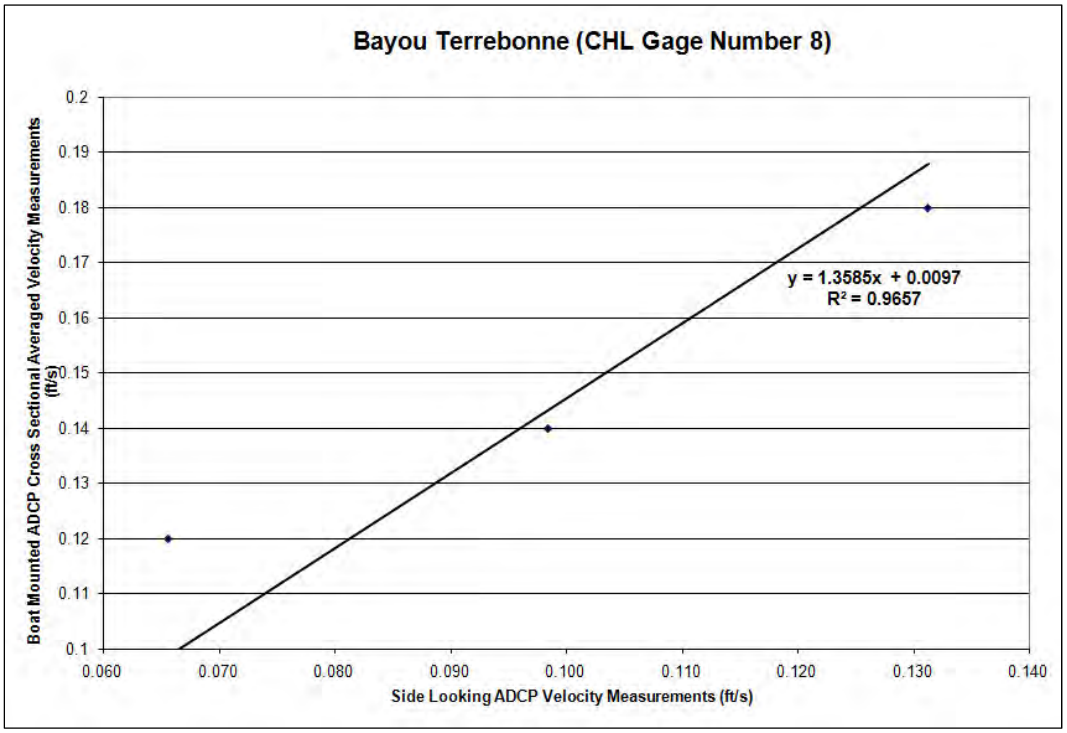

Figure 13. Velocity correlation of ADCP data at Bayou Terrebonne.

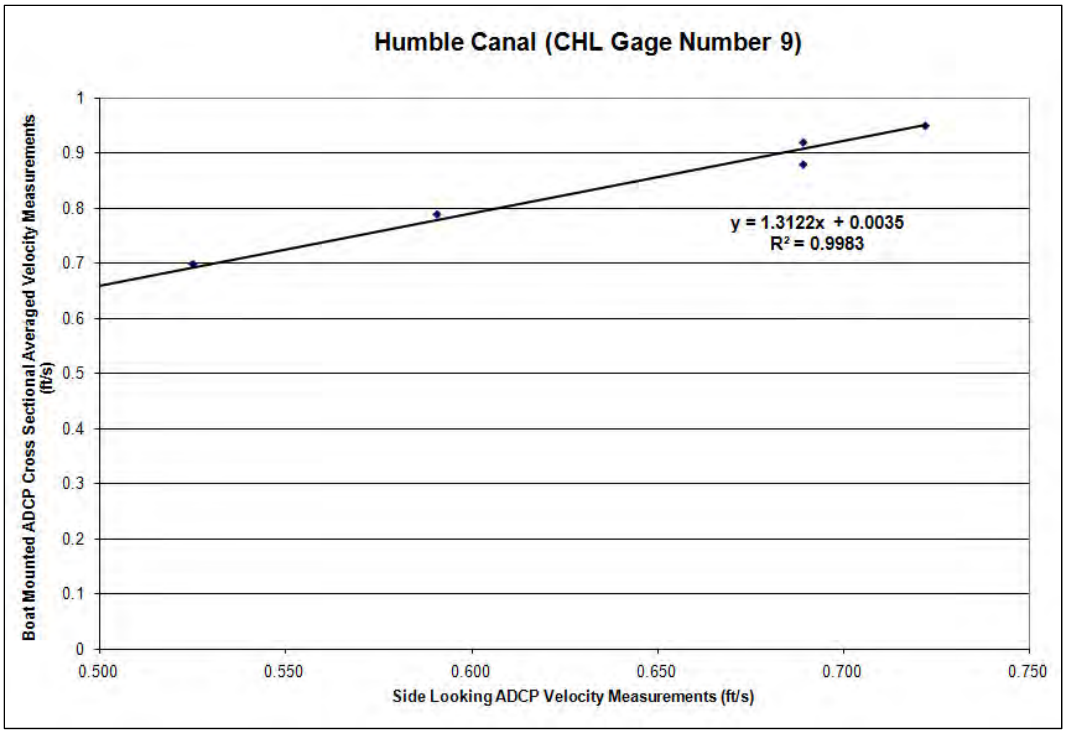

Figure 14. Velocity correlation of ADCP data at Humble Canal.

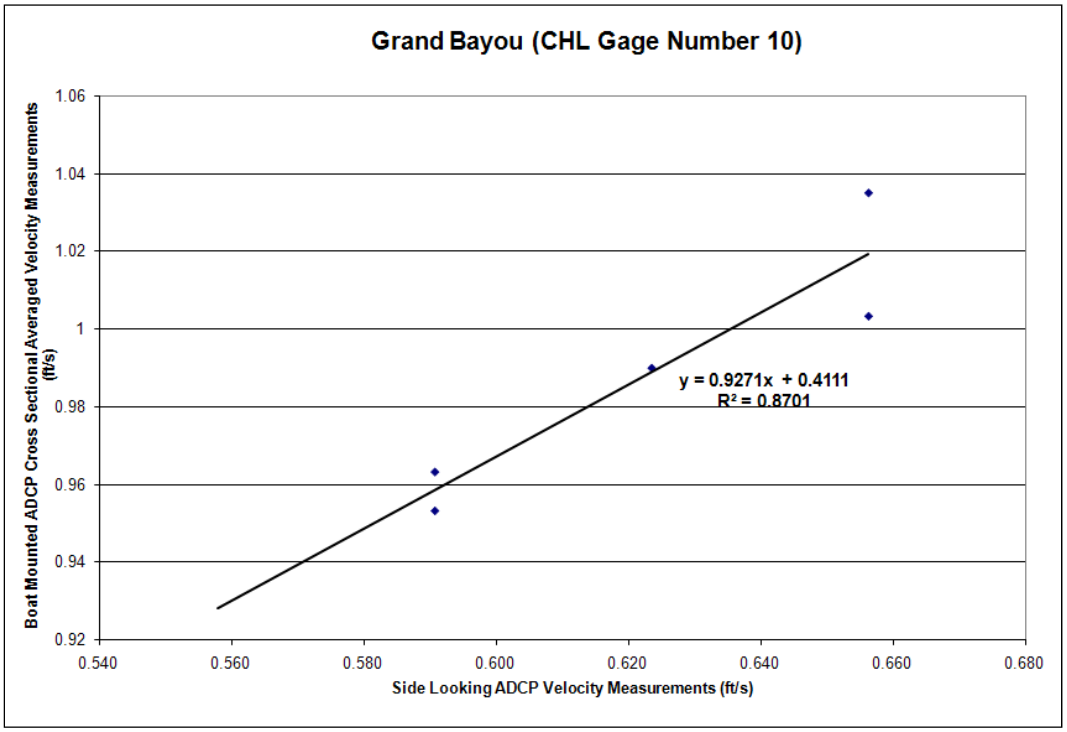

Figure 15. Velocity correlation of ADCP data at Grand Bayou.

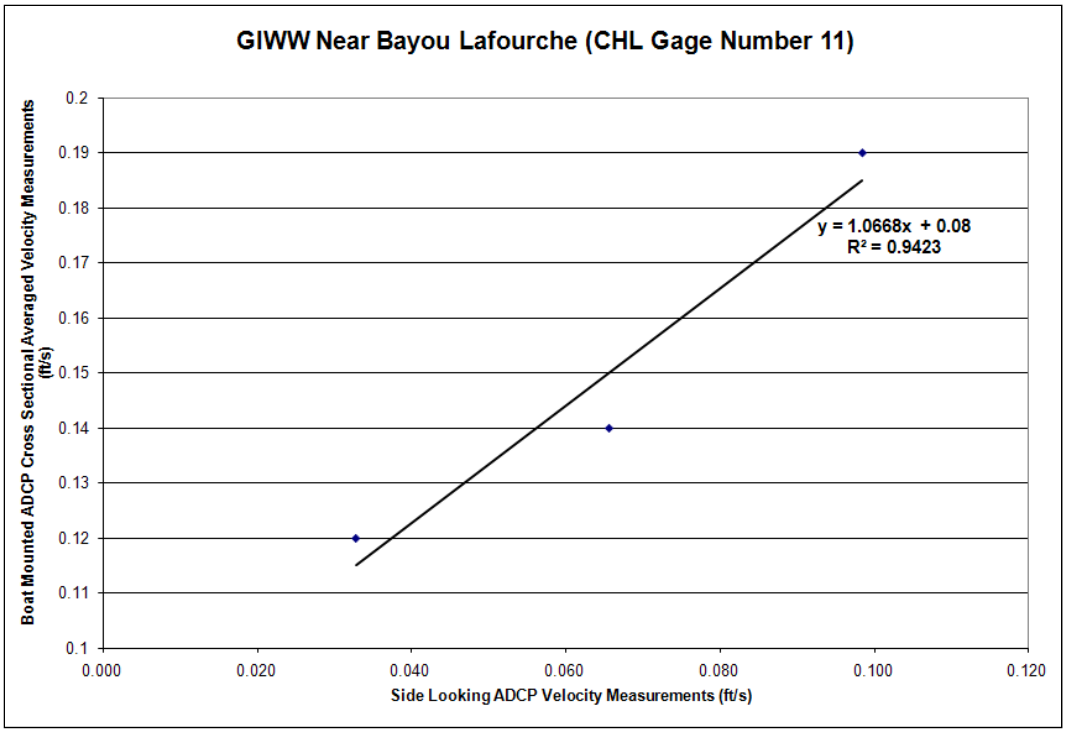

Figure 16. Velocity correlation of ADCP data at GIWW near Bayou Lafourche.

Table 3. Parameters used for the ADCP velocity correlations.

Gage Location	Slope	Y-Intercept	R^2
GIWW near Houma*	0.8491	-0.135	0.8588
Falgout Canal	0.7007	0.1323	0.996
Bayou Dularge	3.1236	0.0060	0.996
Bayou Grand Caillou	0.9969	0.0741	0.985
Bayou Petit Caillou	1.2022	0.1479	0.8302
Lapeyrouse	1.3924	0.0038	0.990
Placid Canal	1.0403	0.0067	0.996
Bayou Terrebonne	1.3585	0.0097	0.966
Humble Canal	1.3122	0.0035	0.998
Grand Bayou	0.9271	0.4111	0.8701
GIWW near Bayou Lafourche**	1.0668	0.08	0.9423

* The GIWW near Houma discharge values were increased by 38 % due to the previously discussed comparisons with data reported by Swarzenski, 2003.

**The GIWW near Bayou Lafourche discharge values were increased by 800 cfs due to comparisons with a nearby USGS gage.

It should be noted that discrepancies were observed between measured discharge values for the two CHL GIWW gages and nearby USGS gages and data reported from a USGS report (Swarzenski 2003). Since these two locations were utilized as model boundary conditions (the remaining gages were used for validation comparisons), it was vitally important they be applied accurately. The following two paragraphs detail the adjustments made to the data for these two locations.

For the eastern GIWW gage (GIWW at Bayou Lafourche), the correlated CHL gage measurements were approximately 800 cfs below the USGS gage measurements at a different location along the GIWW (no significant side channels between the gages so the flows should have been equal). Since the CHL gage correlation was obtained for extremely low flows (when higher flows are the norm), it is expected that the USGS measurements are much more representative of the actual flows since their correlation utilized a wider range of flow values. Therefore the CHL measurements were offset by 800 cfs to better reflect the more general USGS measurements.

For the western GIWW gage (GIWW near Houma), it was observed that the flows were less than the expected flows reported by Swarzenski (2003). Analysis of the USGS flow measurements at the Houma Navigational Canal and the GIWW at Houma also supported increasing the flows for this location. Since the GIWW and the Houma Navigation Canal are the primary pathways for flow, the sum of the discharges for the GIWW at Houma USGS gage (out) and the Houma Navigation Canal USGS gage (out) should approximately equal the GIWW near Houma (CHL) discharges (in), but that is not the case. Increasing the GIWW near Houma (CHL) discharge measurements by 38 % produced results approximately equal to the sum of the GIWW at Houma (USGS) and the Houma Navigation Canal (USGS) discharges while also agreeing with the values reported by Swarzenski (2003). Therefore the GIWW near Houma (CHL) discharges were increased by 38 %. Additional data were going to be taken upon gage retrieval to verify these assumptions but both gages had been struck by navigation vessels making an improved correlation impossible.

3 Mesh Development

An existing RMA2 mesh of the south central Louisiana coast was provided by the New Orleans District. This initial mesh was created by Dr. Joseph V. Letter, Jr., for an Atchafalaya Bay study using RMA2 (Donnell et al., 1991). It was later modified by Mr. David Elmore and again by Ms. Amena Henville (both of MVN) for the Morganza to the Gulf of Mexico project, also using RMA2. This initial mesh, shown in Figure 17, extends from the Atchafalaya Bay on the west to Port Fourchon on the east. It contains a large area to the west of the study area that was not necessary for the current numerical model study.

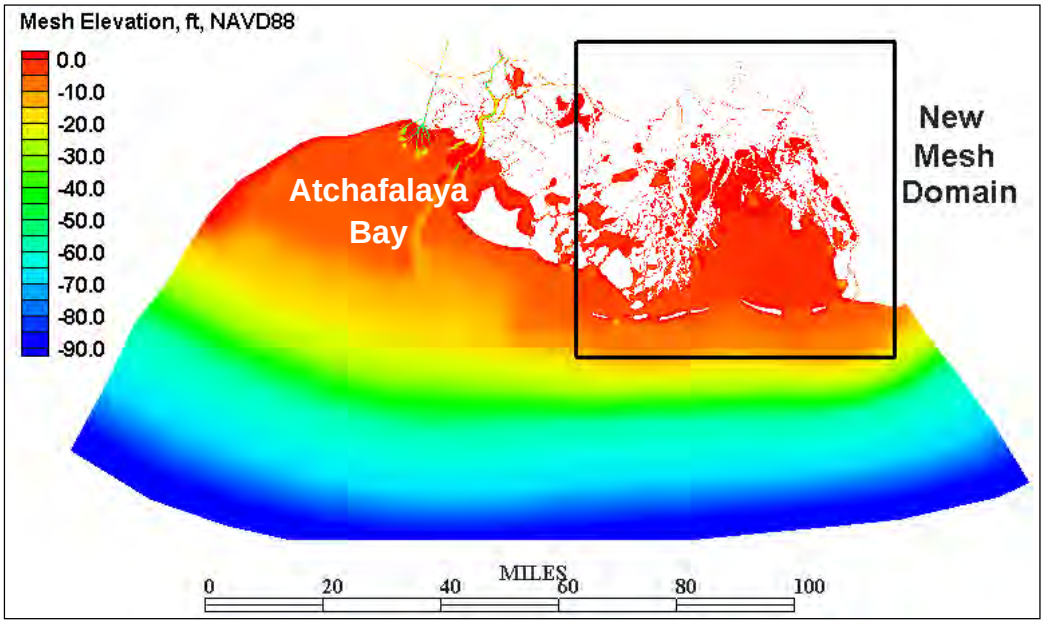

Figure 17. Initial RMA2 mesh developed for previous study, with current study area indicated.

The western area outside the greater study location was removed and the remaining mesh converted to an AdH compatible format for the Bush Canal study (McAlpin et al. 2009). For the current Morganza to the Gulf of Mexico gate sizing study, the resolution in the study area near proposed gate locations was significantly increased. Bathymetry data were also taken near the proposed structure locations by the CHL field crew and incorporated into the model.

These mesh modifications were performed in the Surface Water Modeling System (SMS), a graphical user interface developed for use in setting up

and running numerical models (Aquaveo 2009). The final model domain and bathymetry used in this study are shown in Figure 18, with Figure 19 showing the increased resolution in different parts of the study area. The horizontal and vertical coordinate systems were State Plan 83, Louisiana South, feet and NAVD88(2004.65), ft respectively.

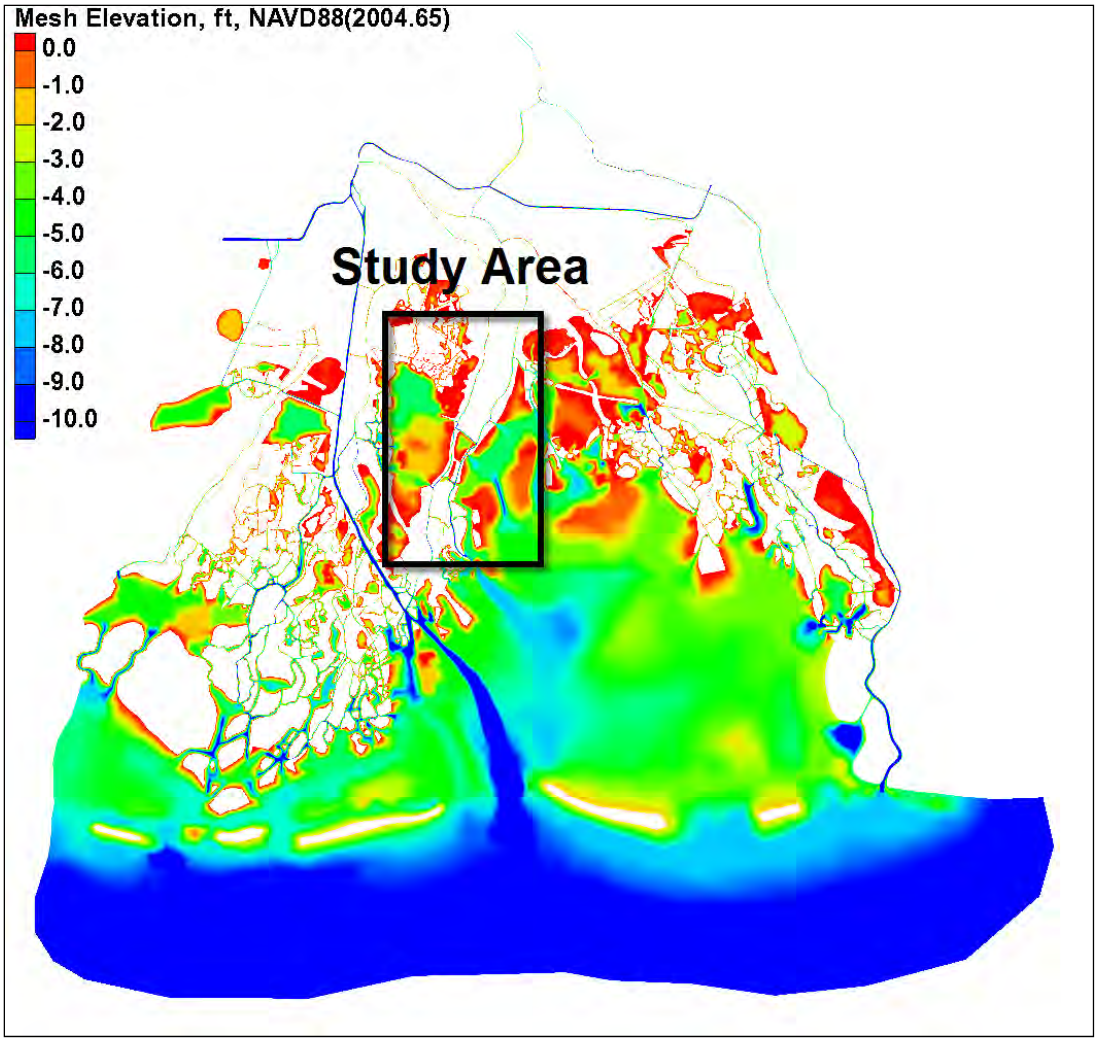

Figure 18. Model domain for current study.

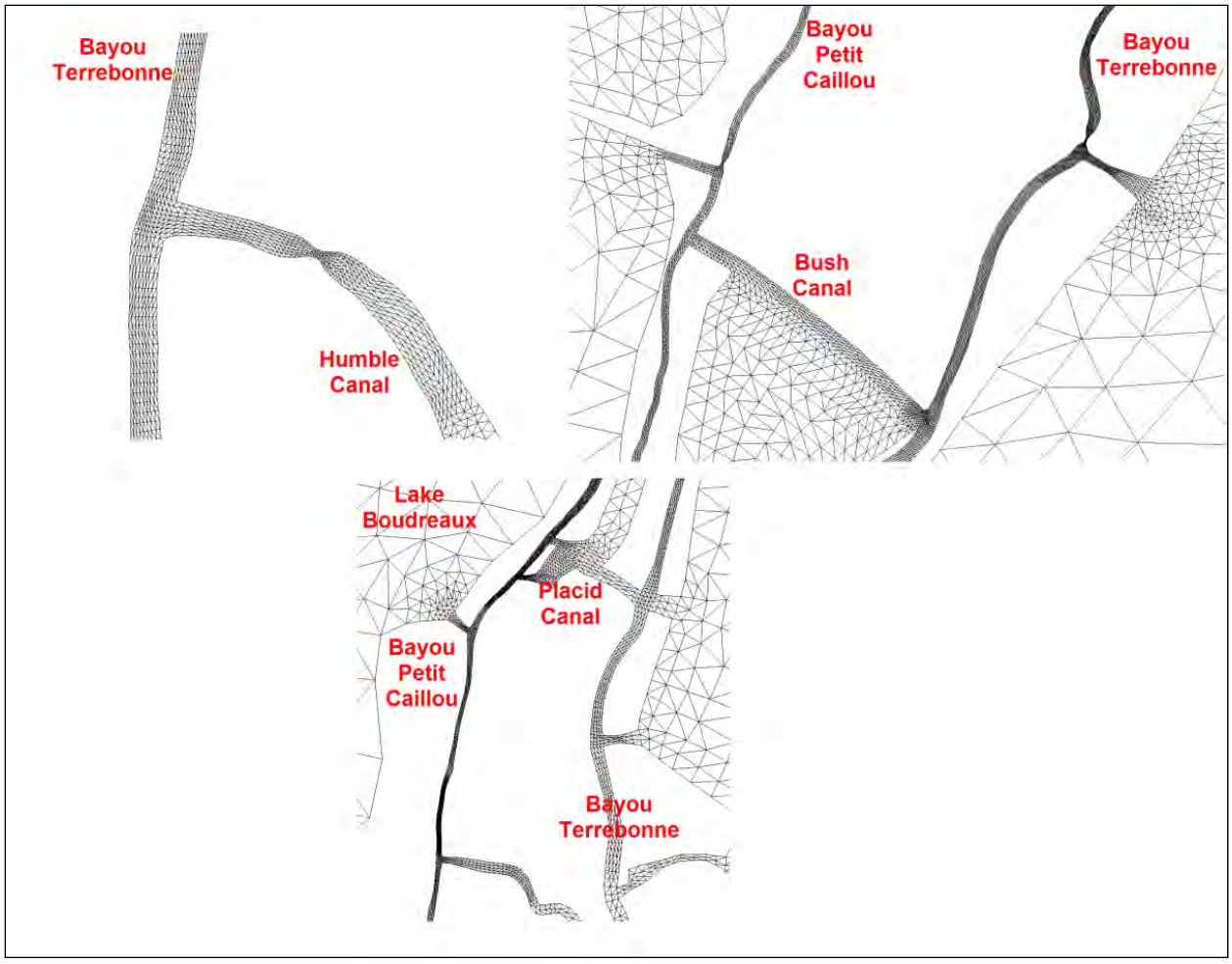

Figure 19. Illustration of increased resolution in the study area.

4 Boundary Conditions Development

Tidal boundary conditions

The model tidal boundary (shown in Figure 20) was specified using the National Oceanic and Atmospheric Administration (NOAA) Port Fourchon measured tidal signal. The observed tidal signal at Port Fourchon was filtered to remove extraneous noise and to improve model stability. A simple box car filter was used to remove any portions of the signal that possessed a period of less than 4 hr. This removed the extraneous noise associated with measurement errors and resulted in a smoother representation of the tidal signal.

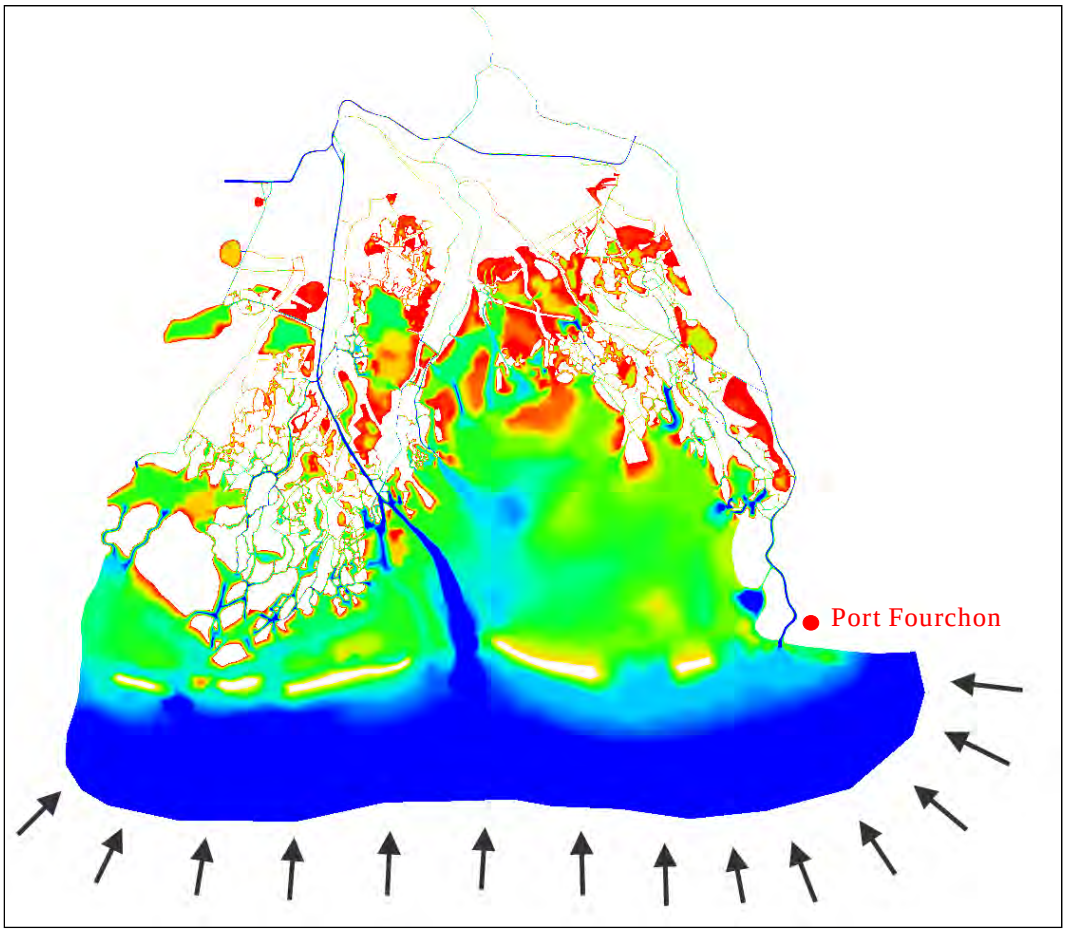

Figure 20. Model tidal boundary.

When comparing the Port Fourchon model and field tidal values, it was determined that there was a slight phase lag (~1 hr) and amplitude

reduction for the model from applying the Port Fourchon tidal signal farther out in the Gulf of Mexico. Therefore the applied tidal boundary consisted of the Port Fourchon measured signal with a time offset (1 hr) and a slight increase in the tidal range (7 %). A comparison of the raw and applied Port Fourchon signals, shown in Figure 21, shows the 1-hr temporal shift in the data along with the smoothing of the signal. This adjustment resulted in an accurate model replication of the measured Port Fourchon signal at the Port Fourchon measurement location (see Figure 22).

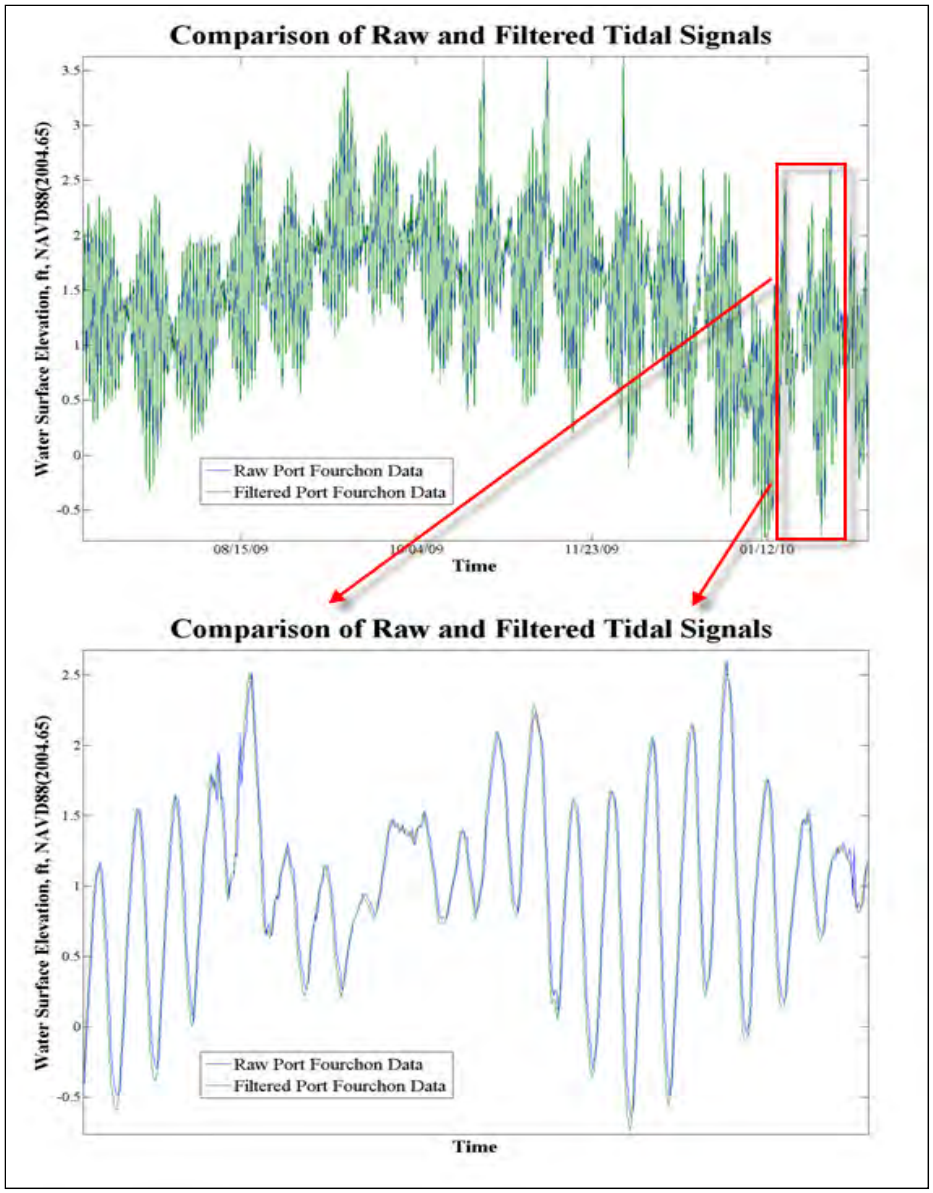

Figure 21. Comparison of the raw and filtered tidal signals.

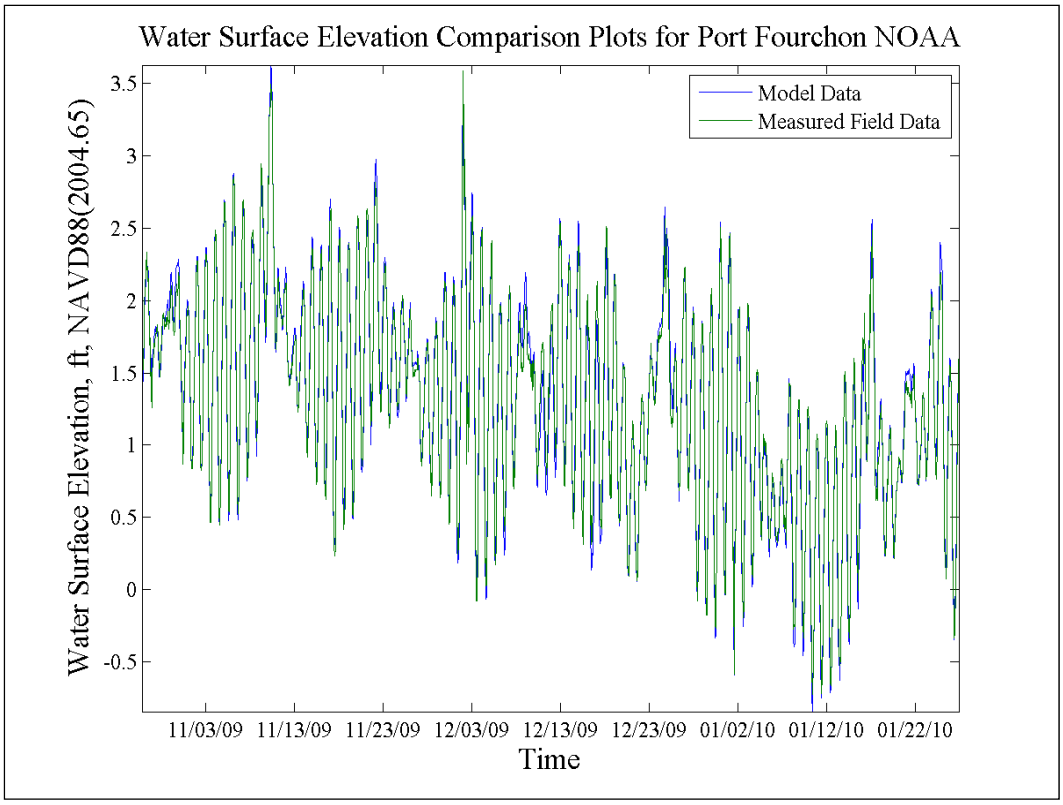

Figure 22. Comparison of observed and model water surface elevations.

Inflow boundary conditions

There were three inflows/outflows (shown in Figure 23) to the system deemed significant enough to include in the model boundary conditions. These were the eastern and western boundaries of the GIWW and the Bayou Lafourche inflow. The inflow measurements for these locations were filtered to reduce the numerical shocks and to remove any extraneous noise. The filter applied to the discharges was a simple running average filter to insure that the cumulative flow in and out of the model was not altered. Comparisons of the raw and filtered data are shown in Figures 24-26. The primarily negative flows for the eastern GIWW boundary indicate a net flow out of the model for this boundary. It should also be noted that gaps in the discharge measurements (primarily for Bayou Lafourche) were filled by means of a linear interpolation. The displayed GIWW discharges in Figures 24 and 25 are the adjusted values from the USGS comparison analysis.

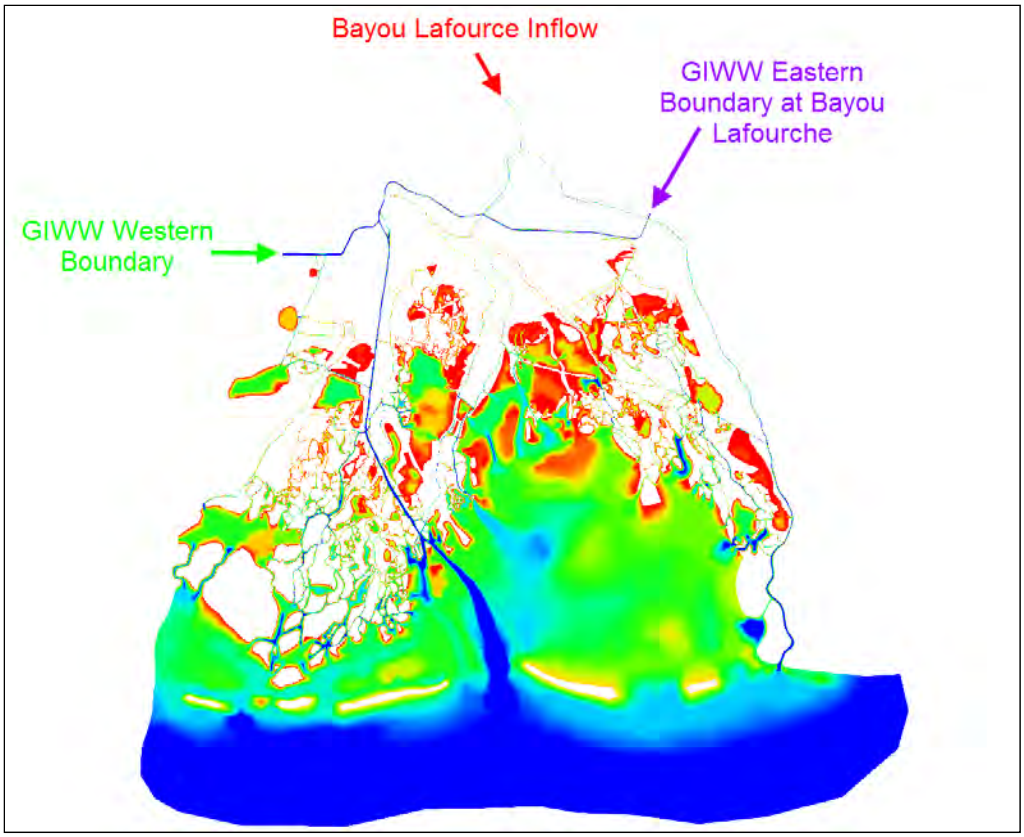

Figure 23. Inflow locations.

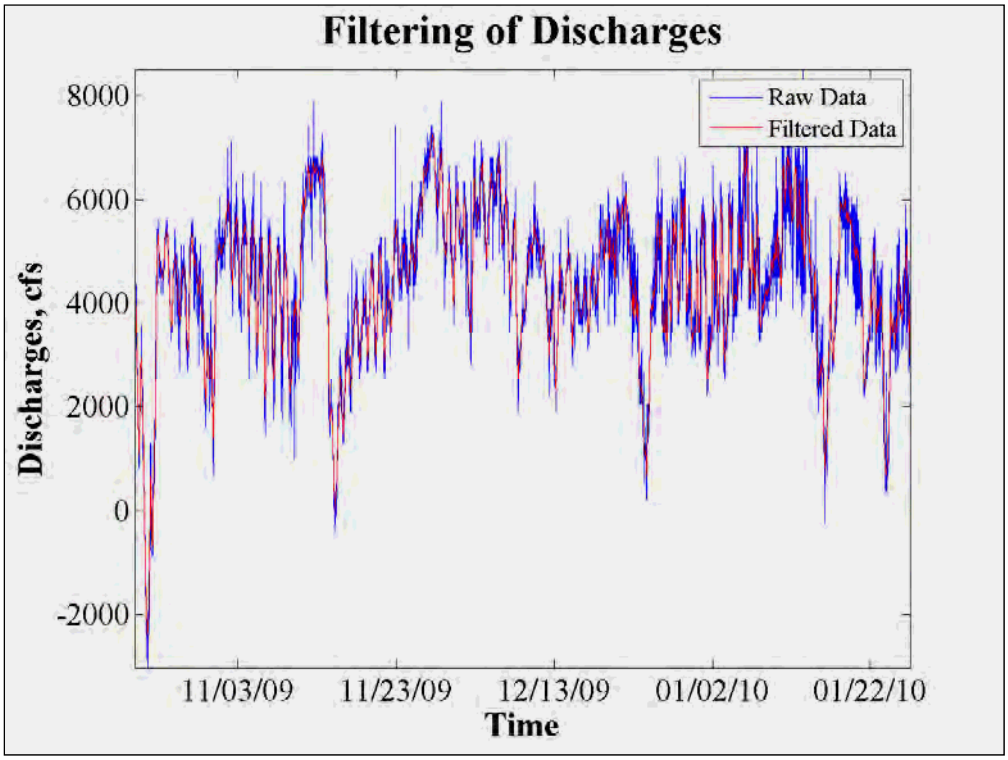

Figure 24. GIWW West of Houma inflow.

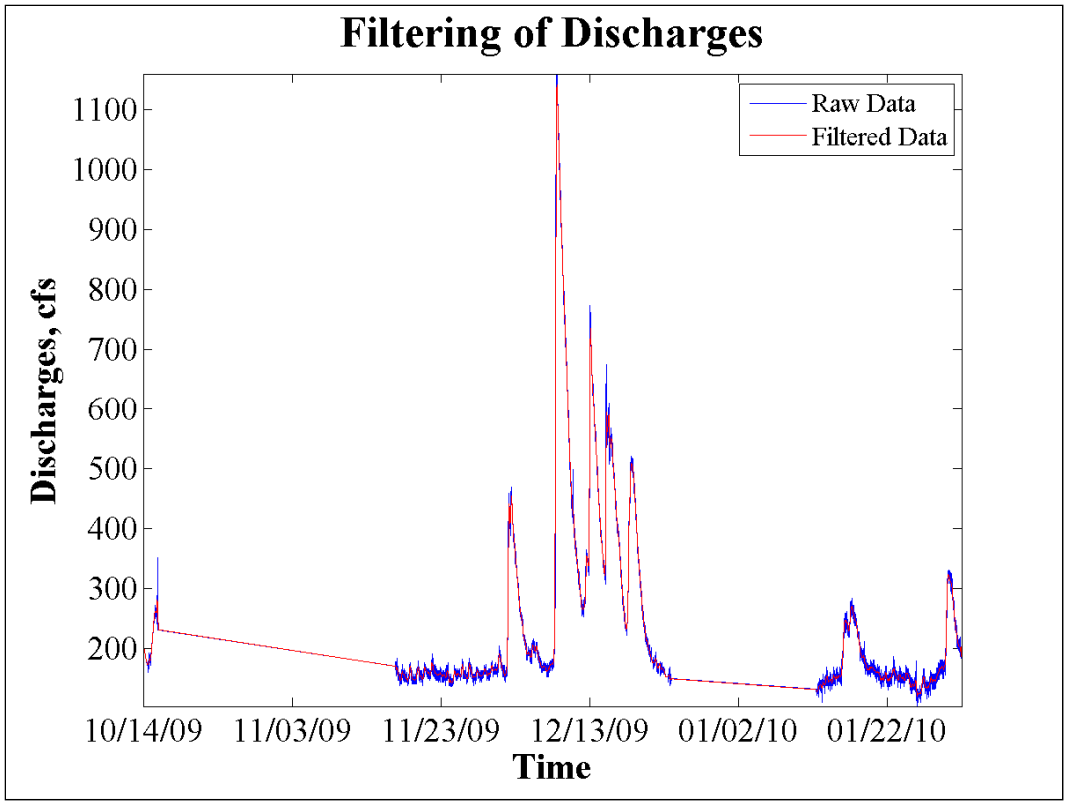

Figure 25. Eastern GIWW Boundary east of Bayou Lafourche.

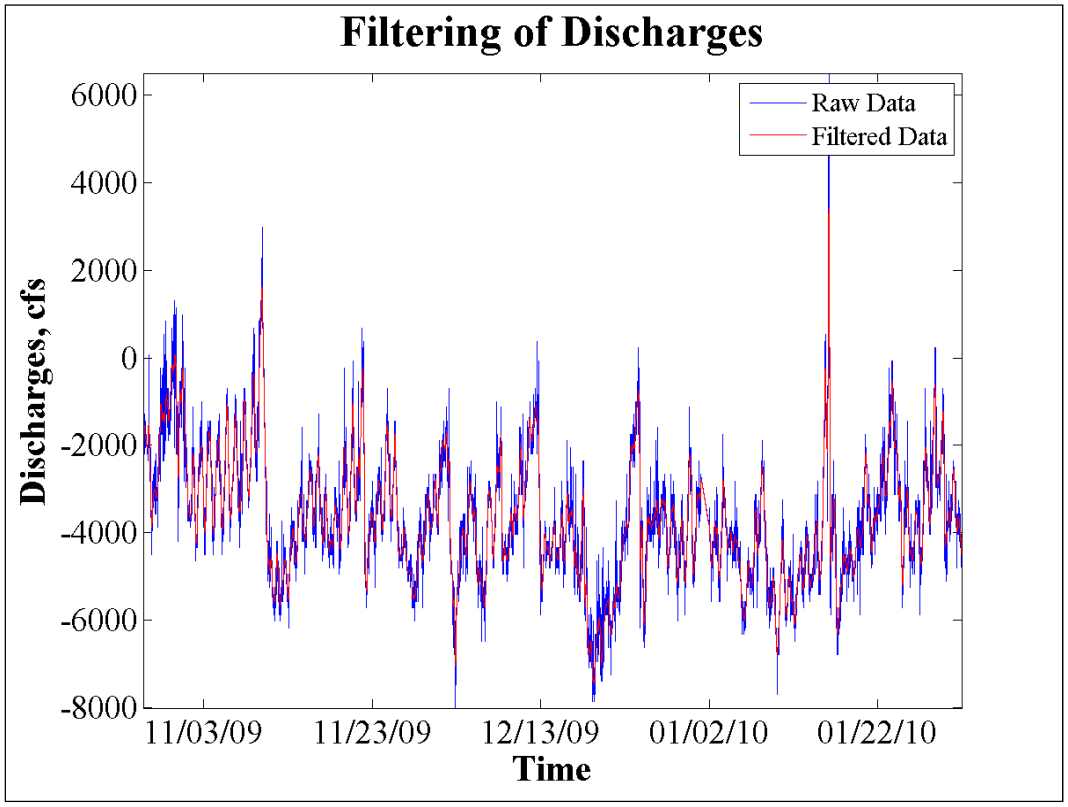

Figure 26. Bayou Lafourche inflow data.

Wind boundary conditions

Due to its shallow nature, there can be significant wind driven circulation patterns in the Morganza area, requiring the inclusion of wind forcing in the current model simulations. Four USGS gages (Caillou Bay, Caillou Lake, Houma Navigational Canal, and Bayou Petit Caillou in Figure 27) had wind speed and direction measurements.

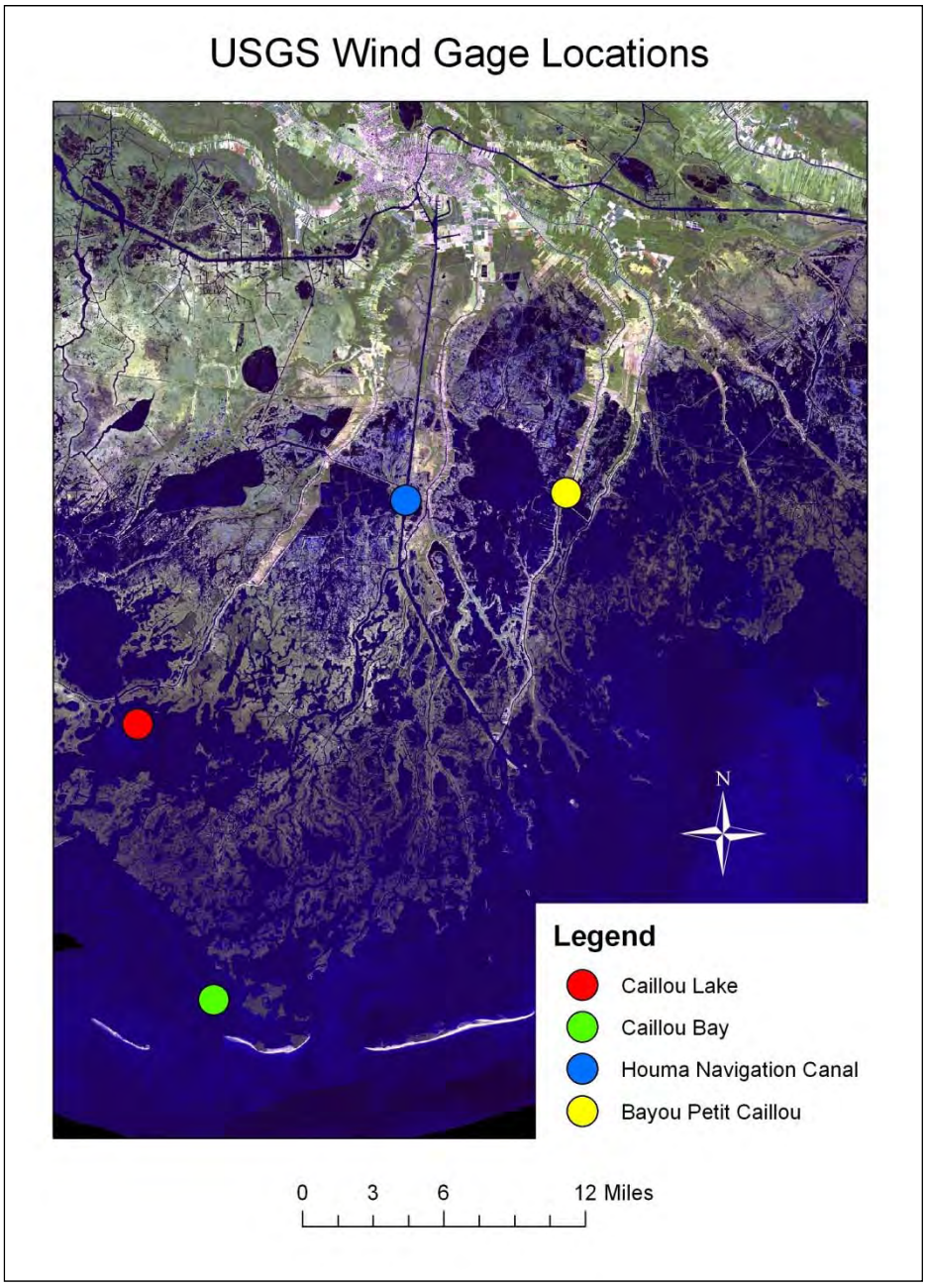

Figure 27. USGS wind measurement locations.

The Caillou Bay gage was missing a large amount of data from December 5, 2009 to January 6, 2010. Data from Caillou Lake, the closest gage to Caillou Bay, was substituted for this missing data with any remaining small gaps in the data sets being interpolated using the spline command within Matlab (Matlab 2010).

To remove extraneous noise from the wind data, a filter was applied to the x and y components of the wind measurements individually for each data set. This filter removed any components of the signal that possessed a period of less than 4 hr thereby smoothing the signals without significantly reducing the peaks. Comparisons of the raw and filtered wind signals are shown in Figures 28 to 31 (negative is a western blowing wind for the *x* component and a southern blowing wind for the *y* component).

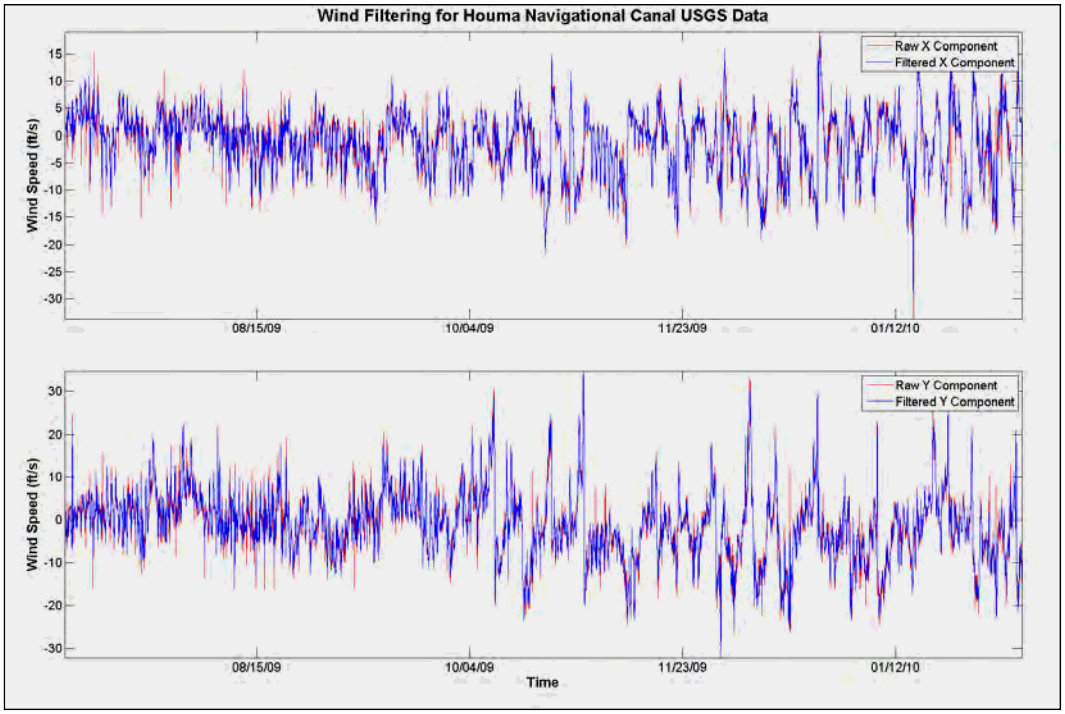

Figure 28. Houma Navigational Canal USGS wind data.

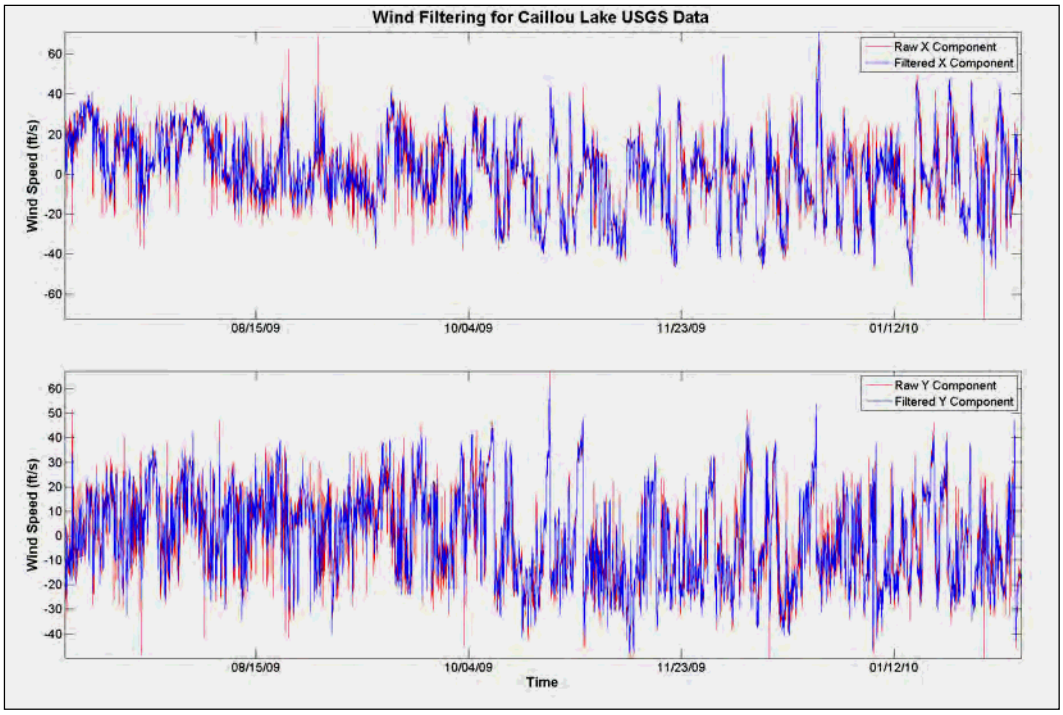

Figure 29. Caillou Lake USGS wind data.

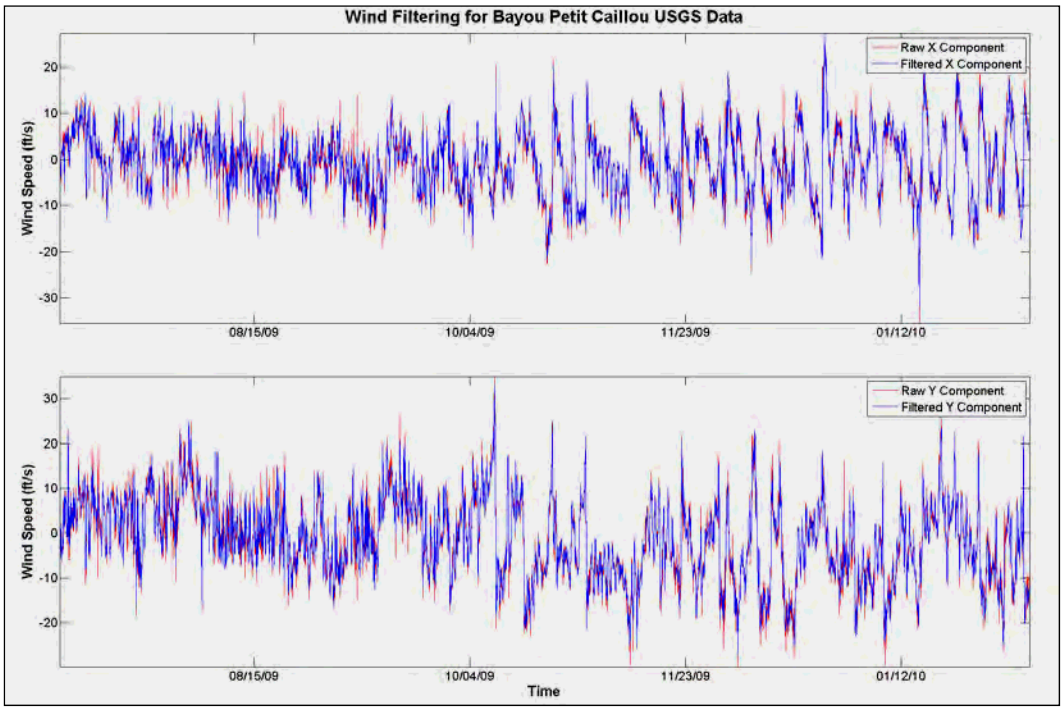

Figure 30. Bayou Petit Caillou USGS wind data.

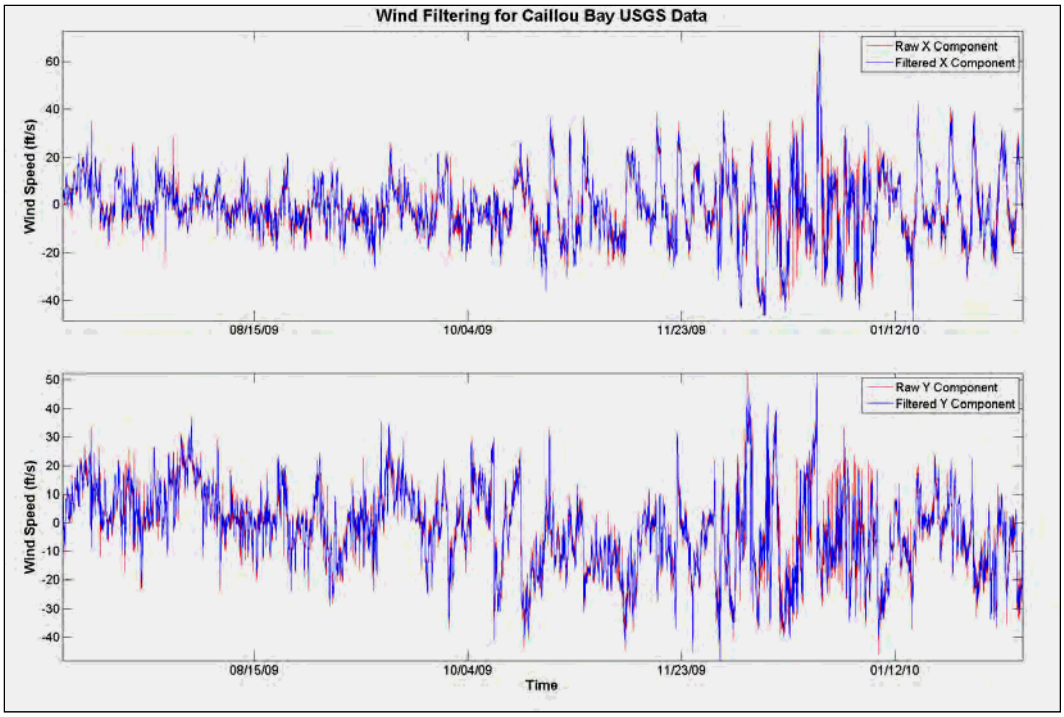

Figure 31. Caillou Bay USGS wind data.

5 Model Validation

The purpose of model validation is to ensure that the developed model represents the system adequately for useful comparisons of existing conditions and proposed alternatives. This chapter compares the model results with the field data and concludes that the model replicates the modeled system well.

Numerical model

This modeling study is an additional application of AdH to the numerous ones already completed. AdH has been utilized to study varied phenomena such as dam break (Savant et al. 2010), estuarine circulation (McAlpin et al. 2009; Tate et al. 2010; Martin et al. 2010), riverine flow (Stockstill and Vaughan 2009; Stockstill et al. 2010), and others. A brief discussion of the AdH (Version 3.01) model is provided in Appendix A but additional information can be accessed via the Internet at https://adh.usace.army.mil/

Water-surface elevation validation

The model water-surface elevations were validated through comparison to observed water-surface elevations for 26 October, 2009 to 26 January, 2010. To insure proper spin up of the hydrodynamic conditions and to remove any biasing due to the initial conditions, the model was run for 1 week prior to 26 October 2009.

USGS and CHL had numerous water-surface elevation gages in and around the study area, as previously shown in Figures 3 and 5. These gages were of vital importance in the validation process. Comparison plots, shown in Figures 32 to 48, consist of time series comparisons along with model versus field box plots.

For the box plots, points lying on the 45 deg black line represent an exact replication of the field by the model. Points below the line represent calculated model results below the observed field values with values above the line representing calculated model results above the observed field values. Additional error metrics were also calculated to obtain a “goodness” factor for the validation.

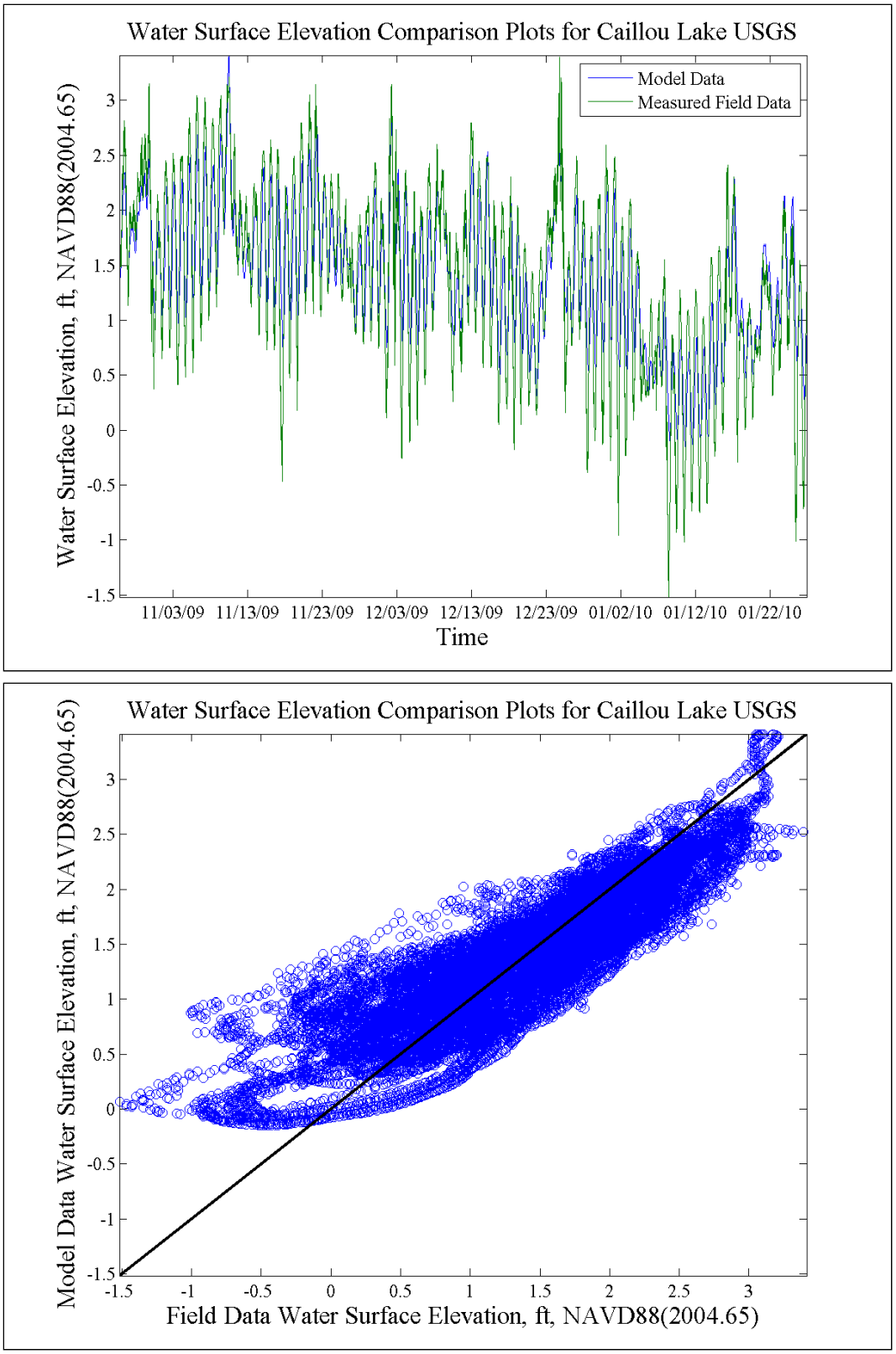

Figure 32. Caillou Lake model versus field comparisons.

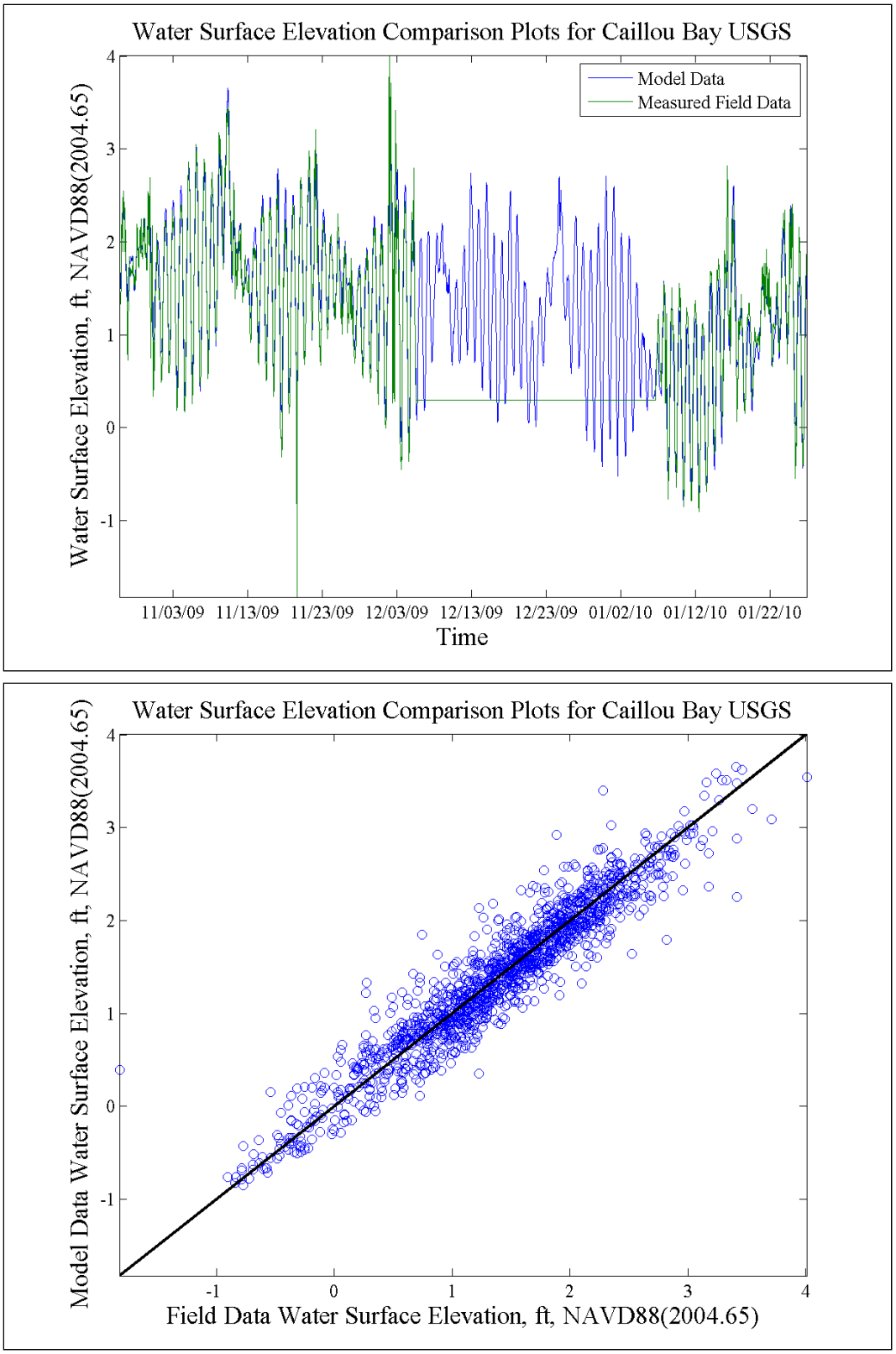

Figure 33. Caillou Bay model versus field comparisons.

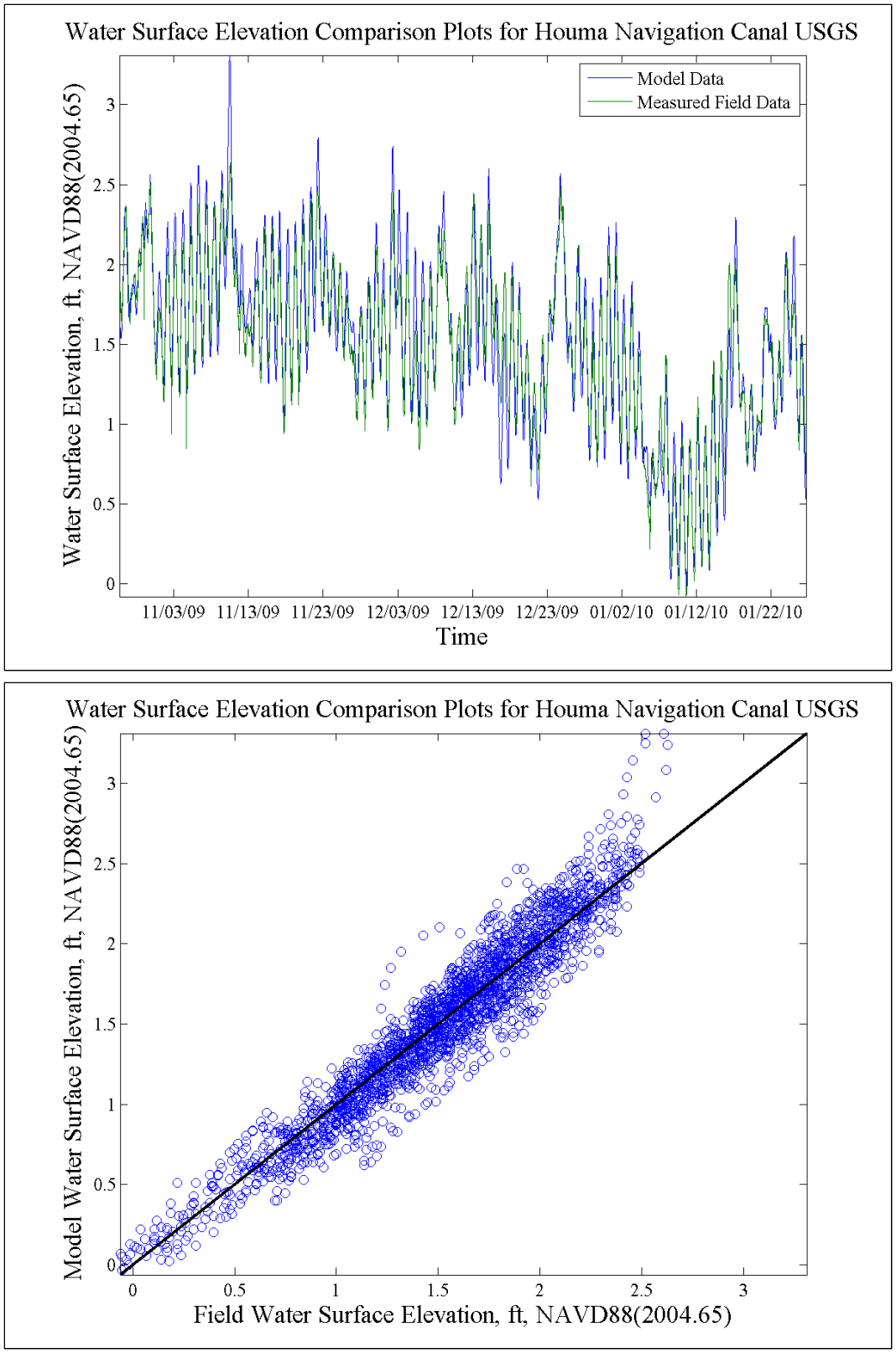

Figure 34. Houma Navigational Canal model versus field comparisons.

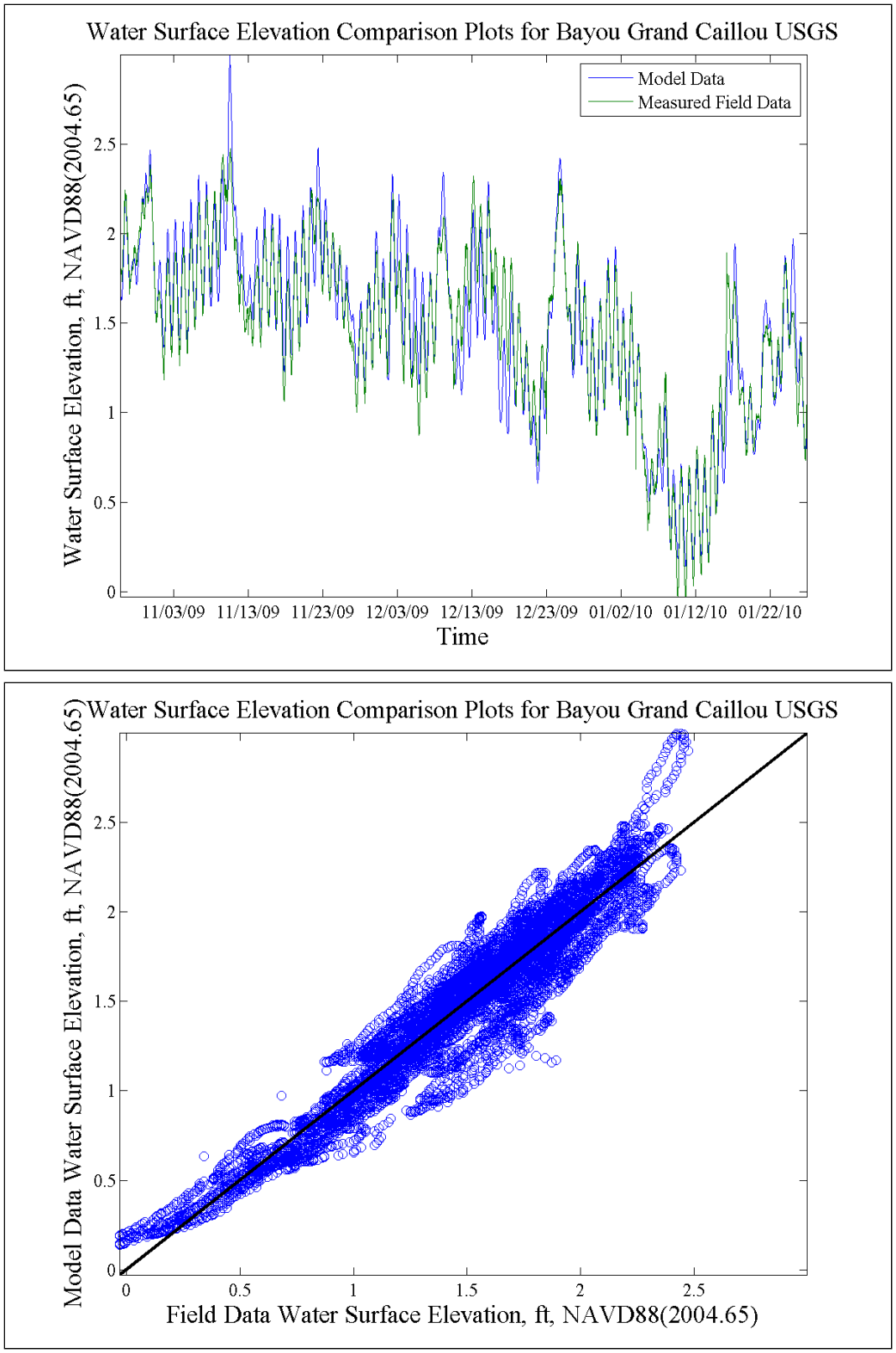

Figure 35. Bayou Grand Caillou model versus field comparisons.

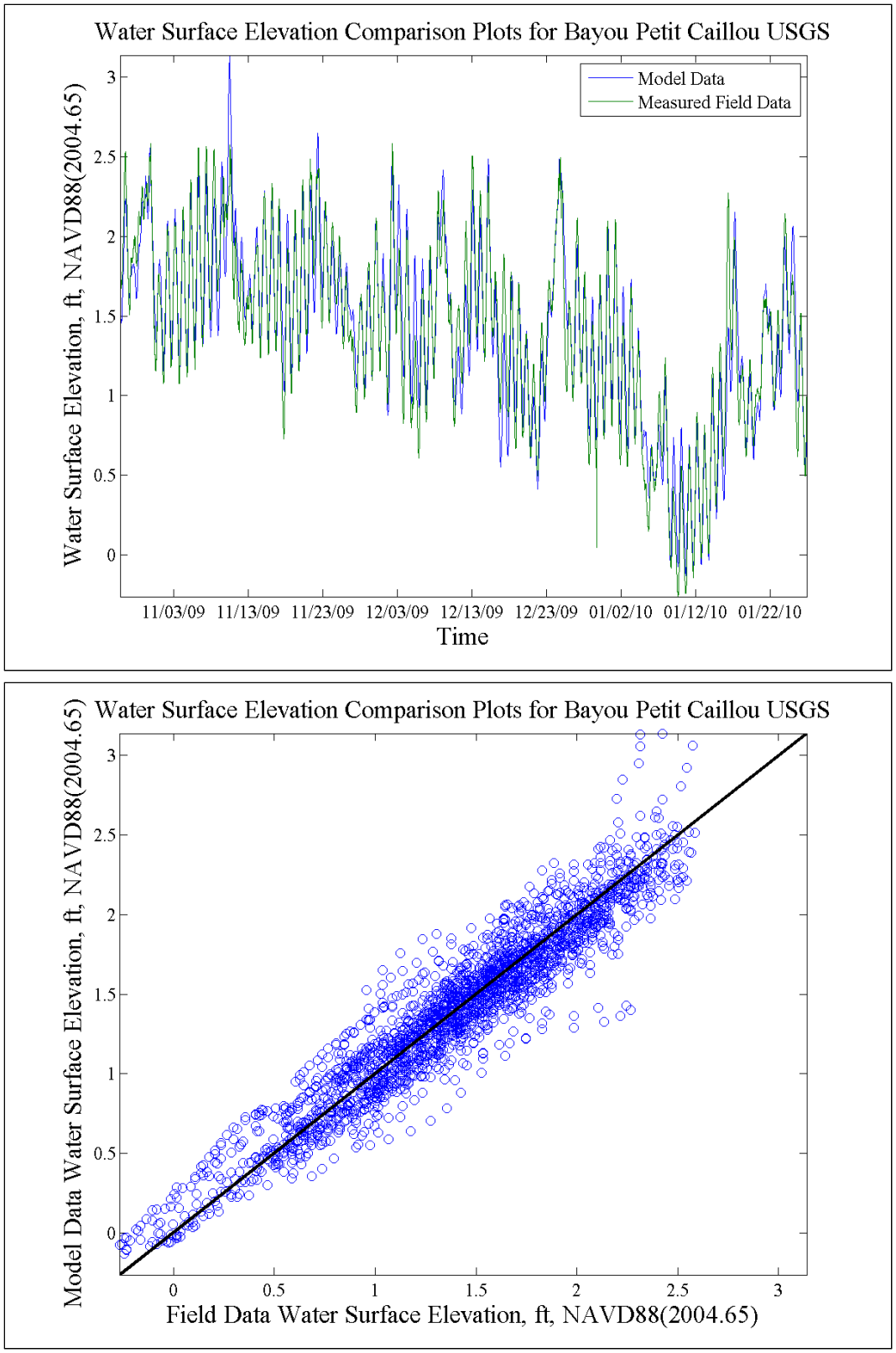

Figure 36. Bayou Petit Caillou model versus field comparisons.

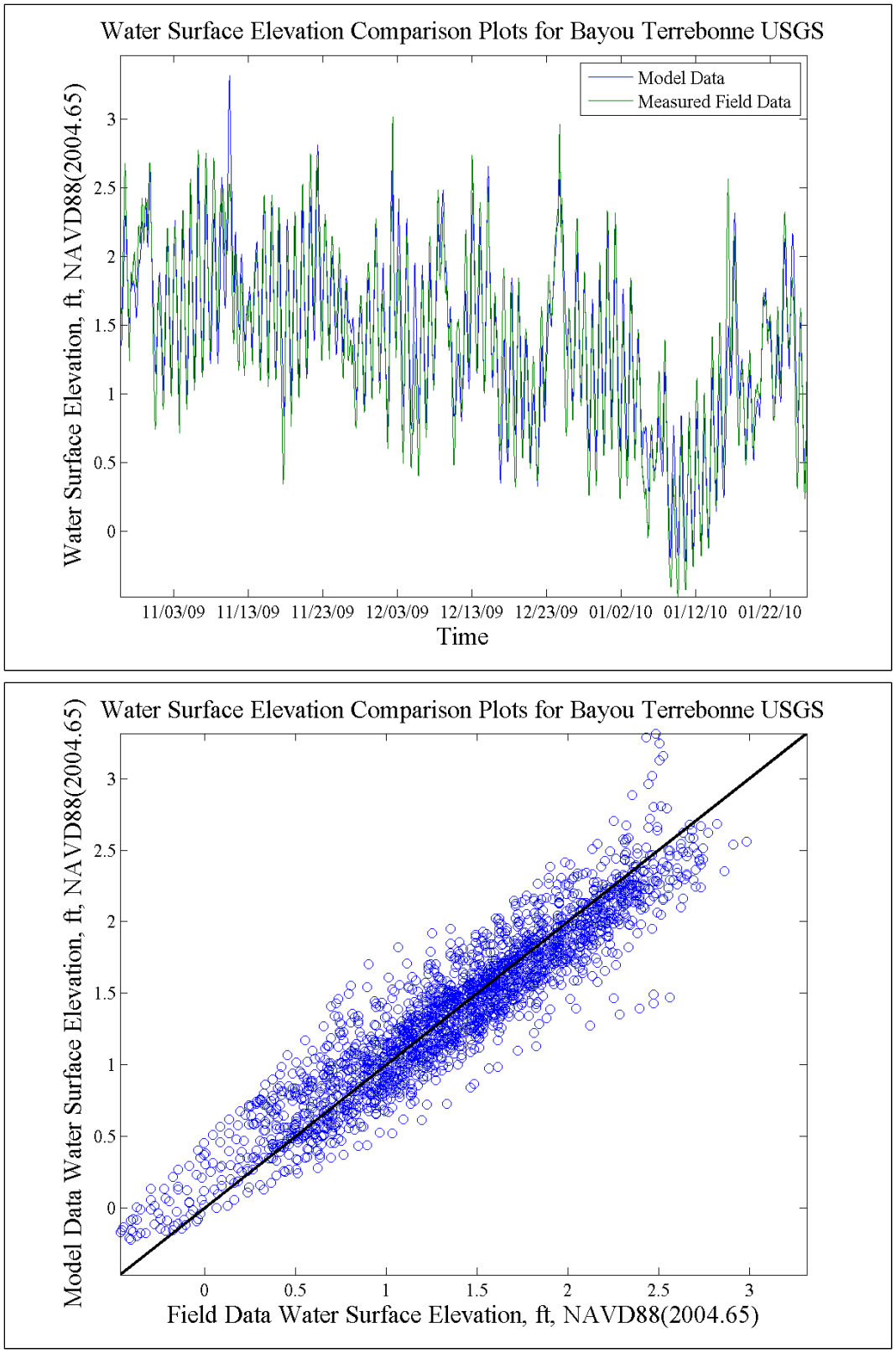

Figure 37. Bayou Terrebonne model versus field comparisons.

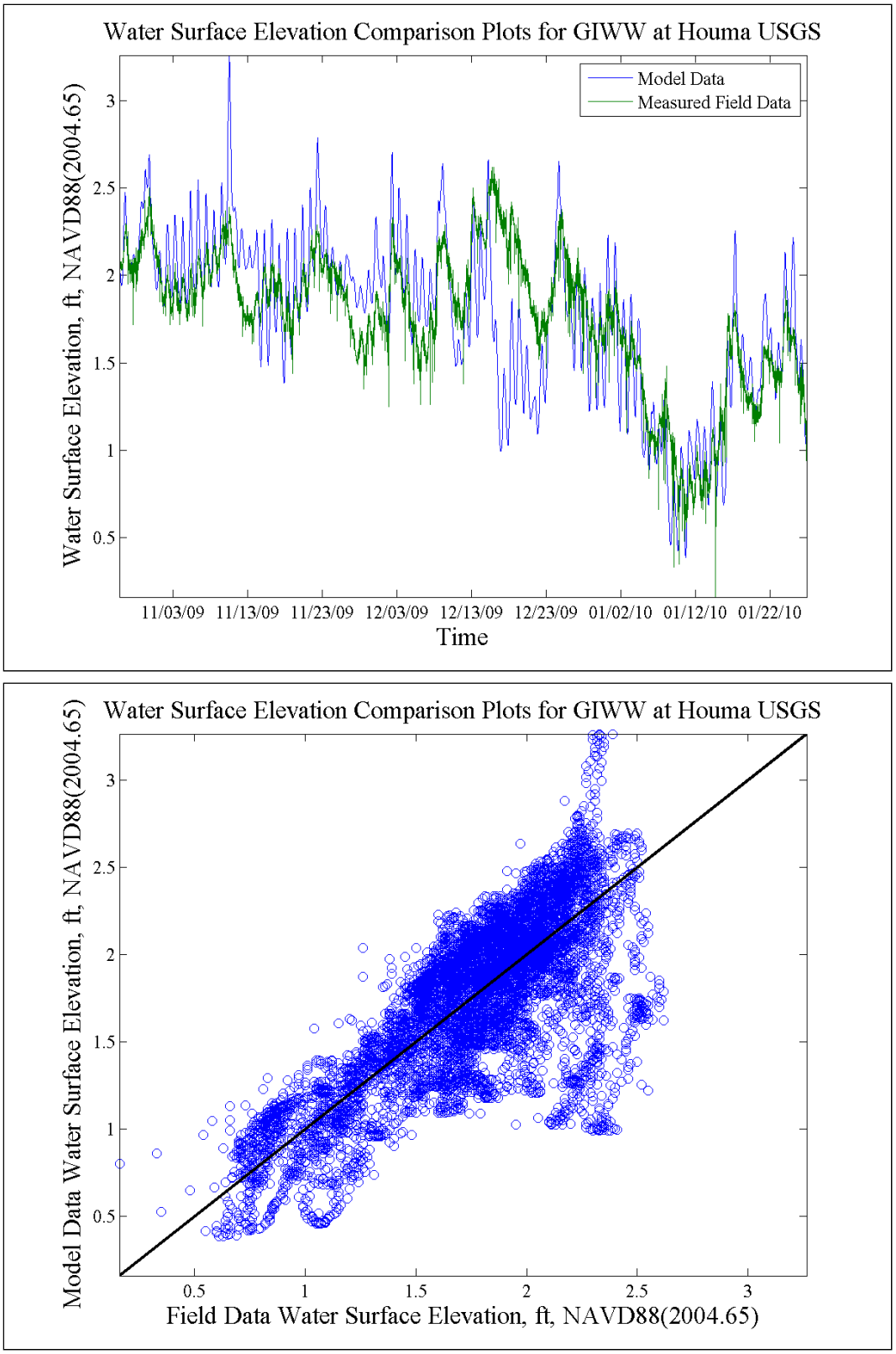

Figure 38. GIWW at Houma model versus field comparisons.

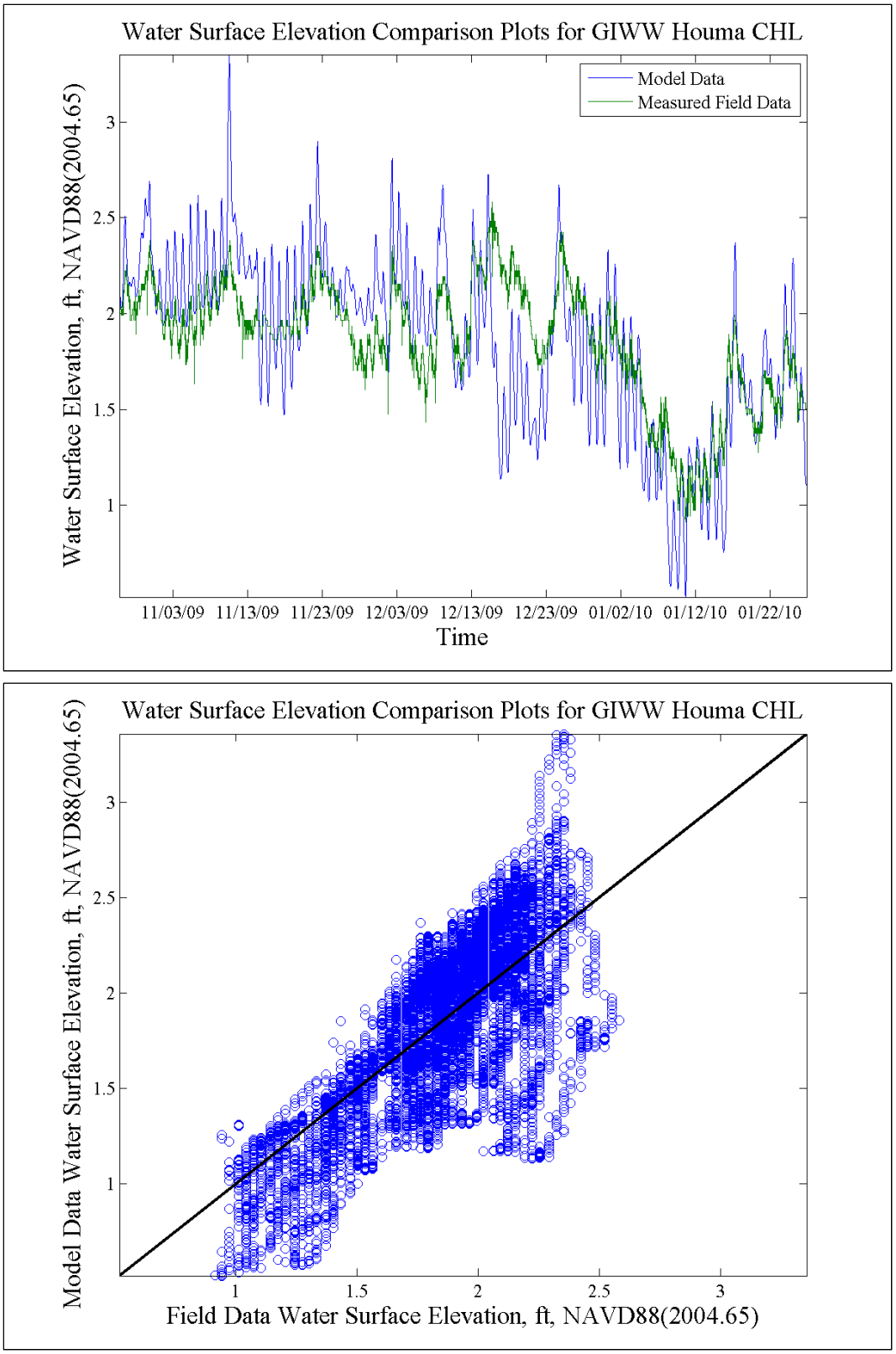

Figure 39. GIWW west of Houma model versus field comparisons.

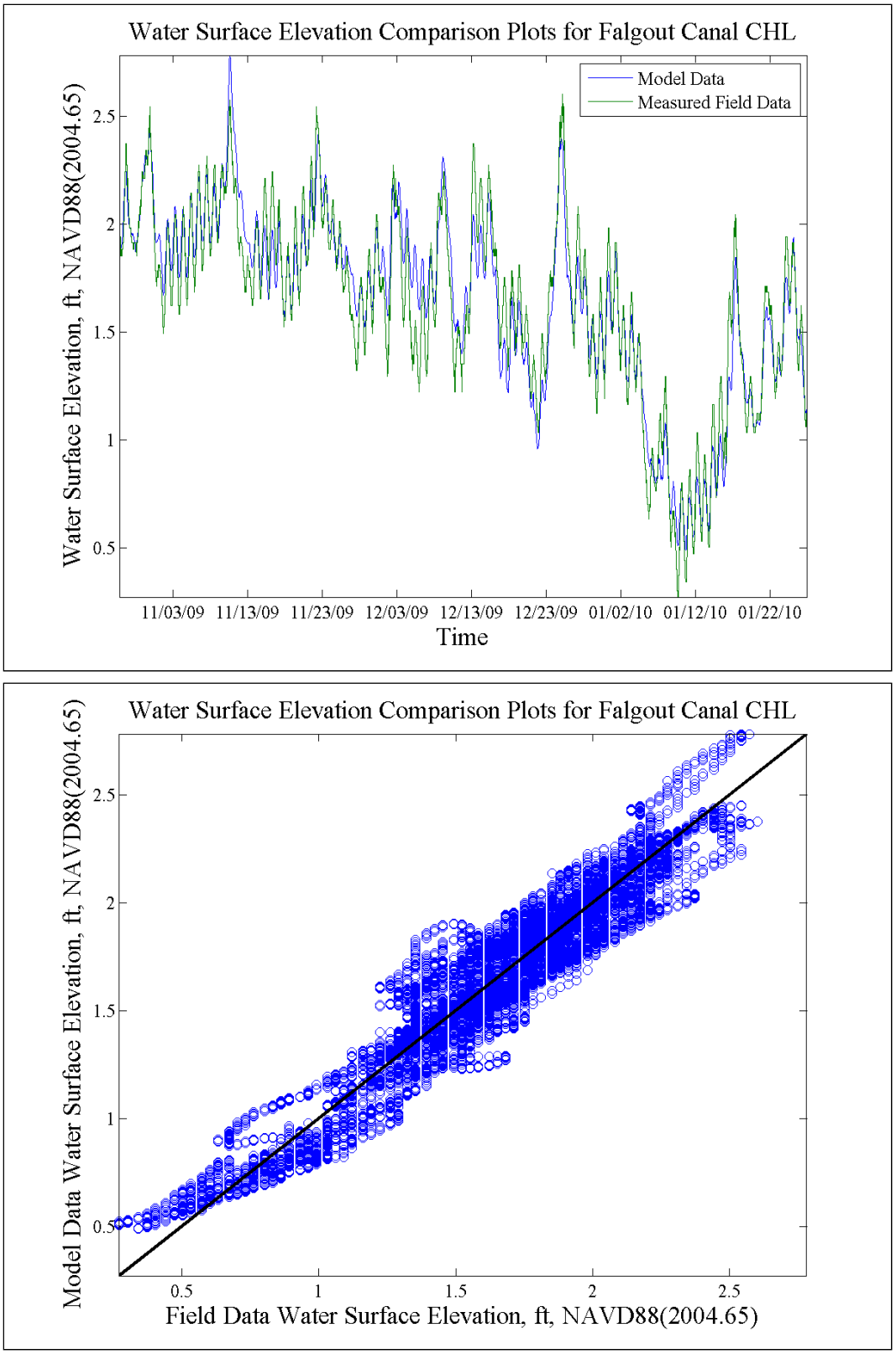

Figure 40. Falgout Canal model versus field comparisons.

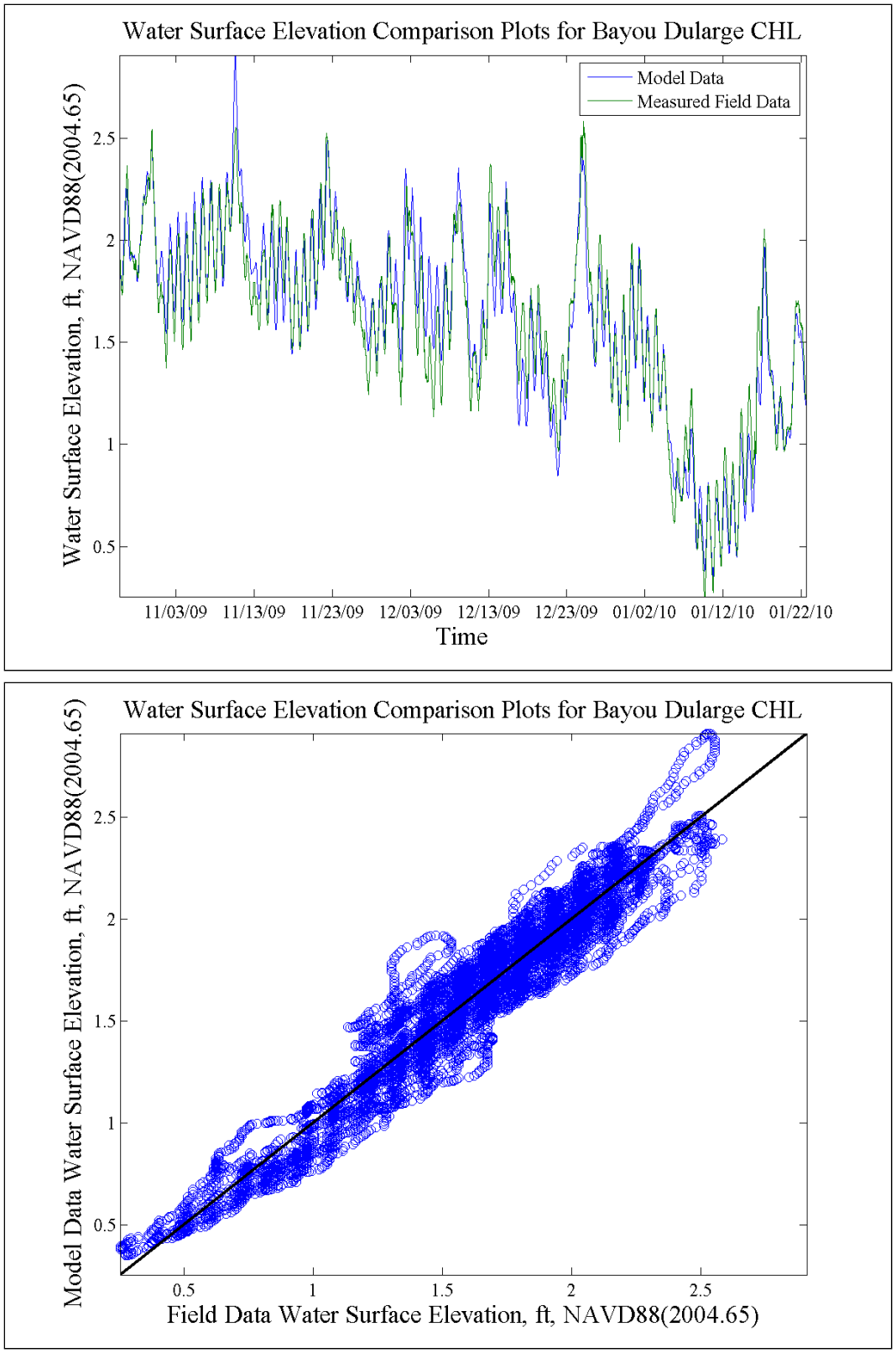

Figure 41. Bayou Dularge model versus field comparisons.

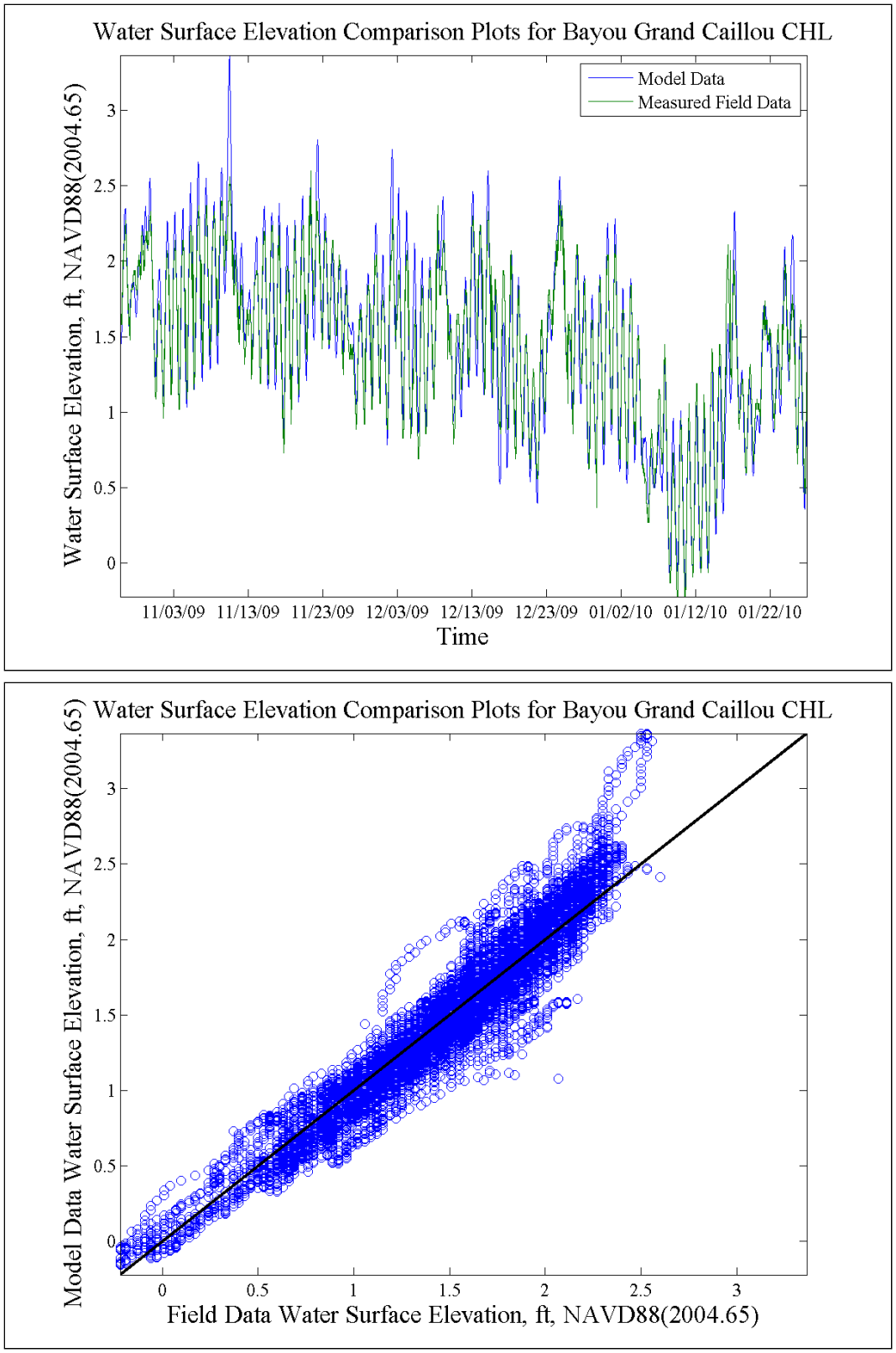

Figure 42. Bayou Grand Caillou model versus field comparisons.

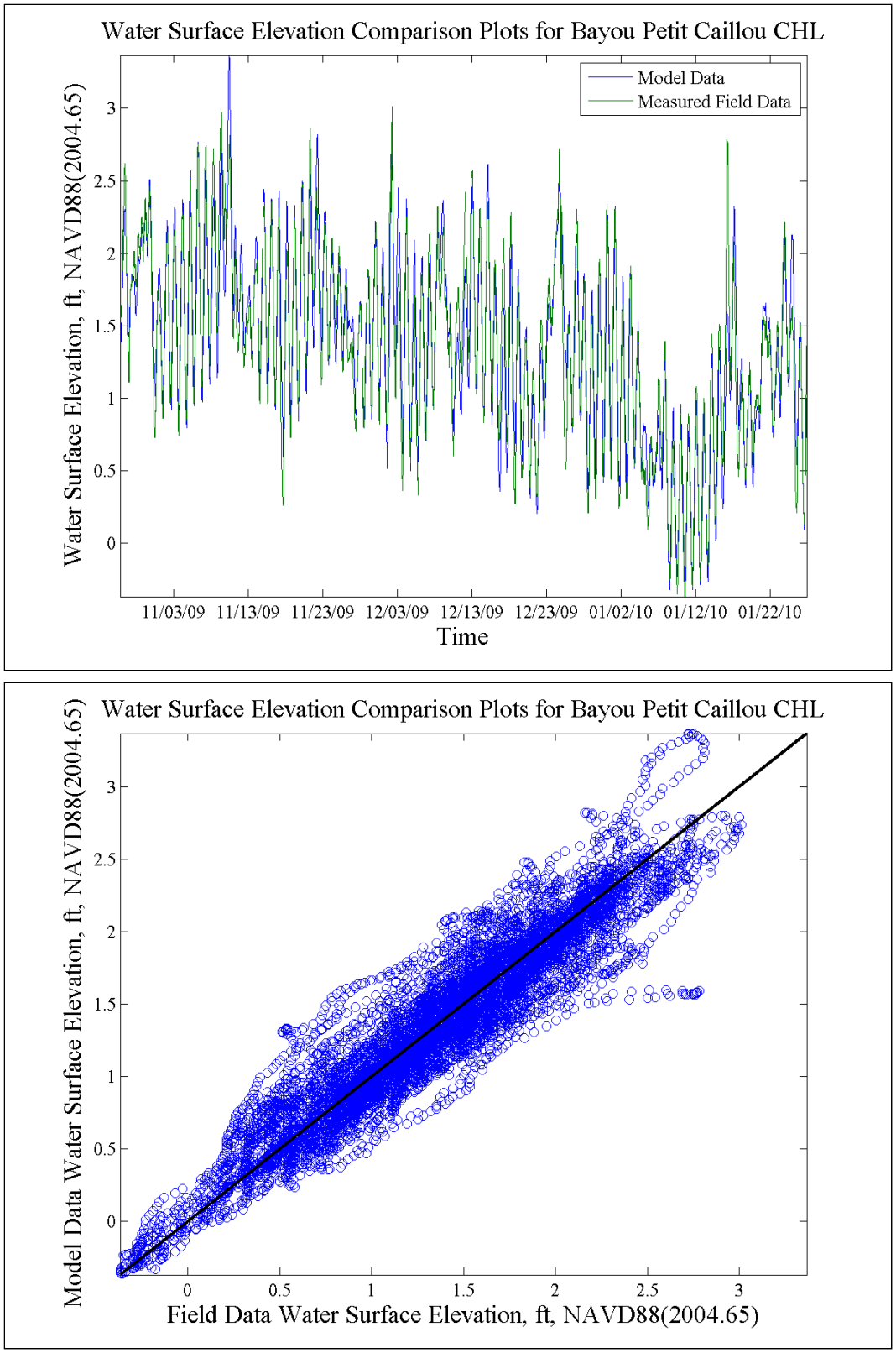

Figure 43. Bayou Petit Caillou model versus field comparisons.

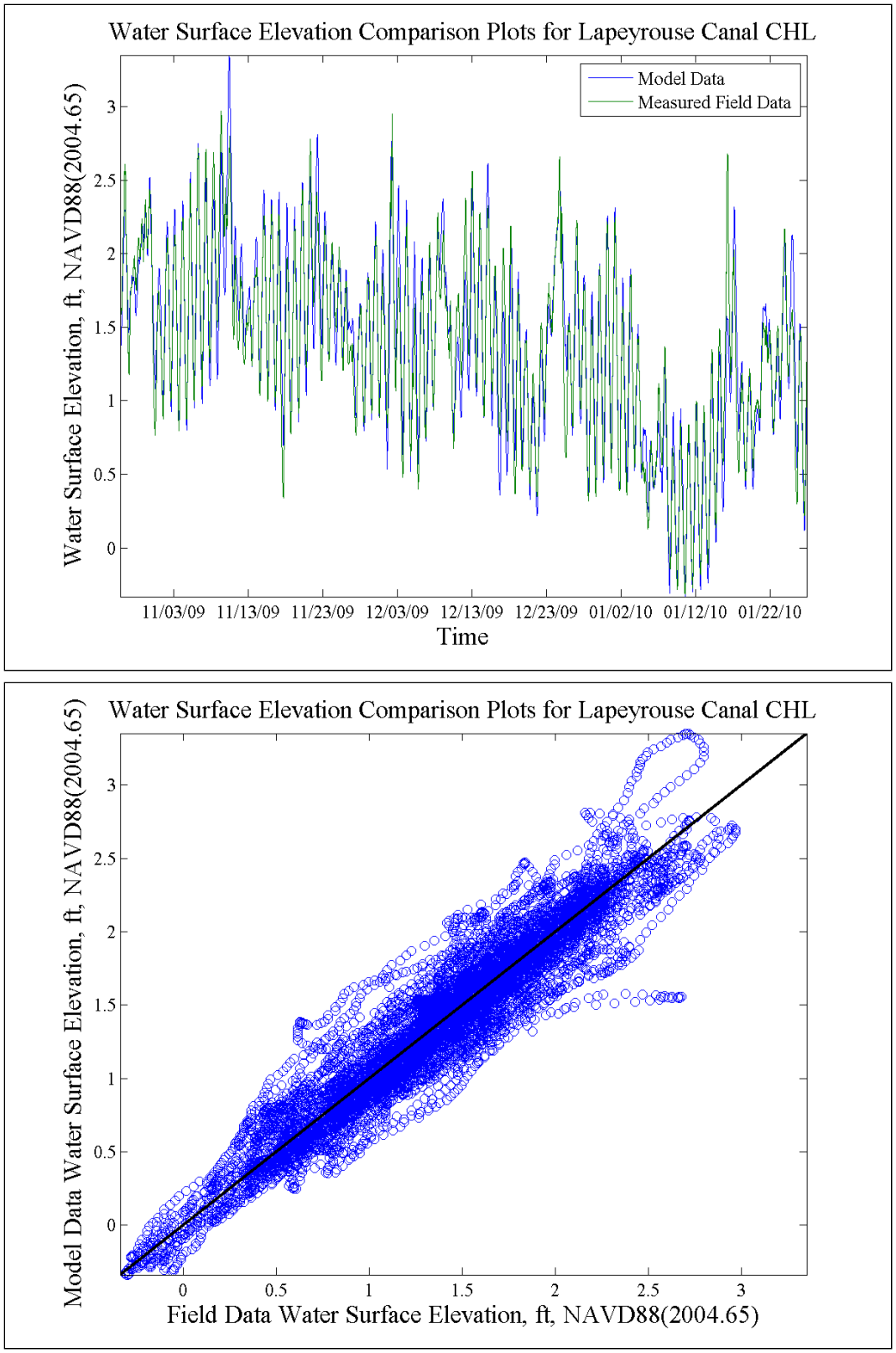

Figure 44. Lapeyrouse Canal model versus field comparisons.

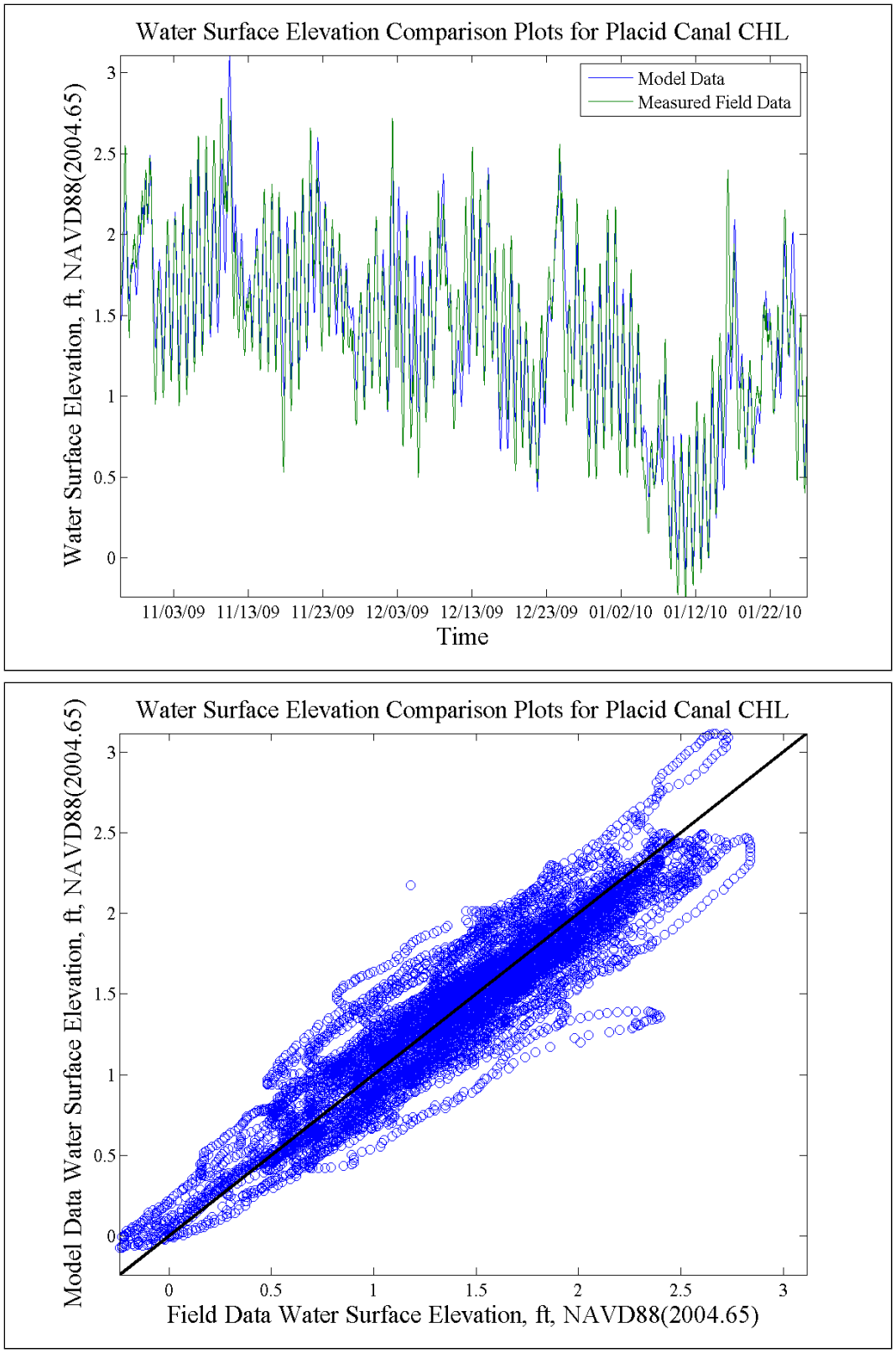

Figure 45. Placid Canal model versus field comparisons.

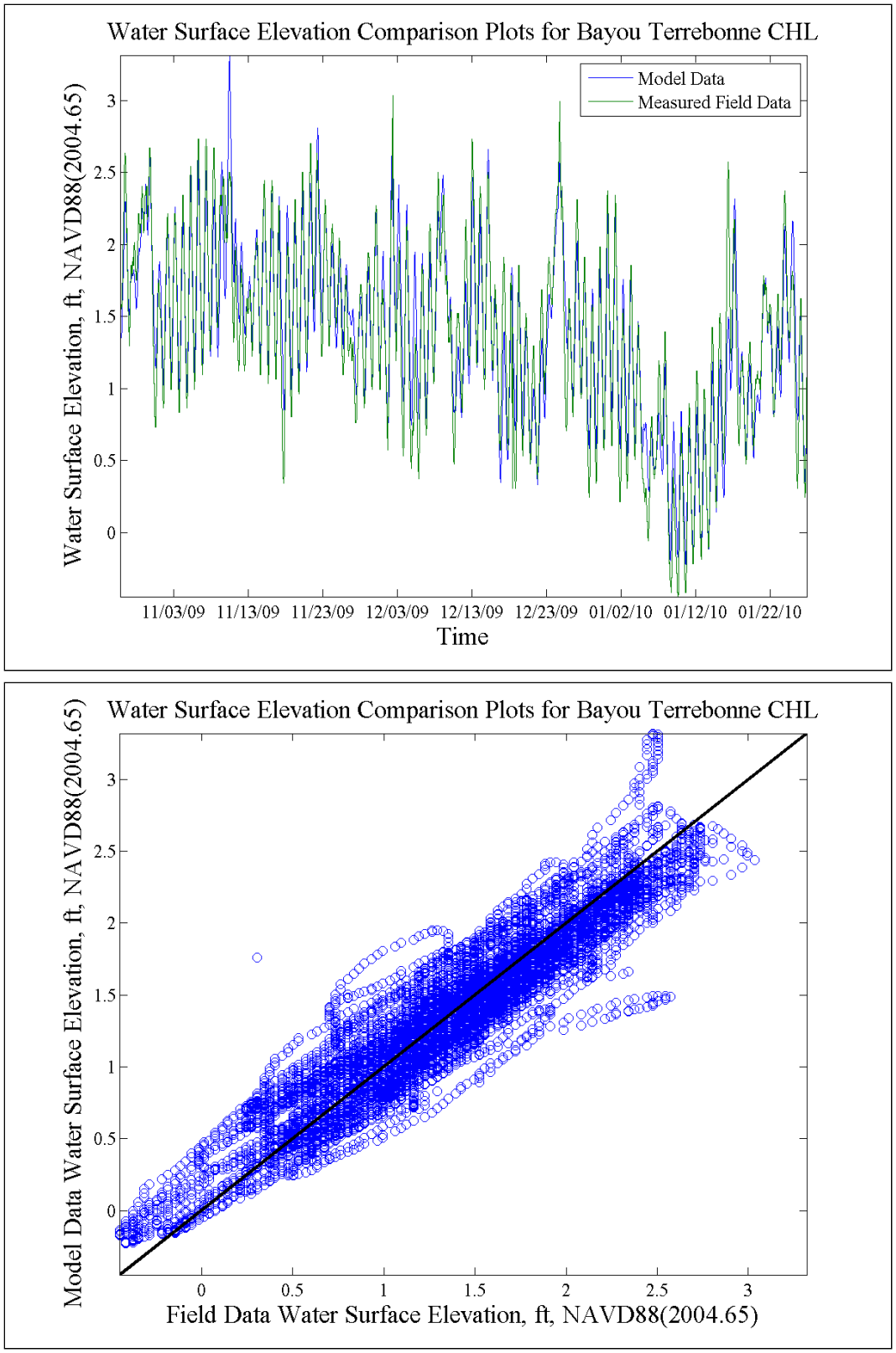

Figure 46. Bayou Terrebonne model versus field comparisons.

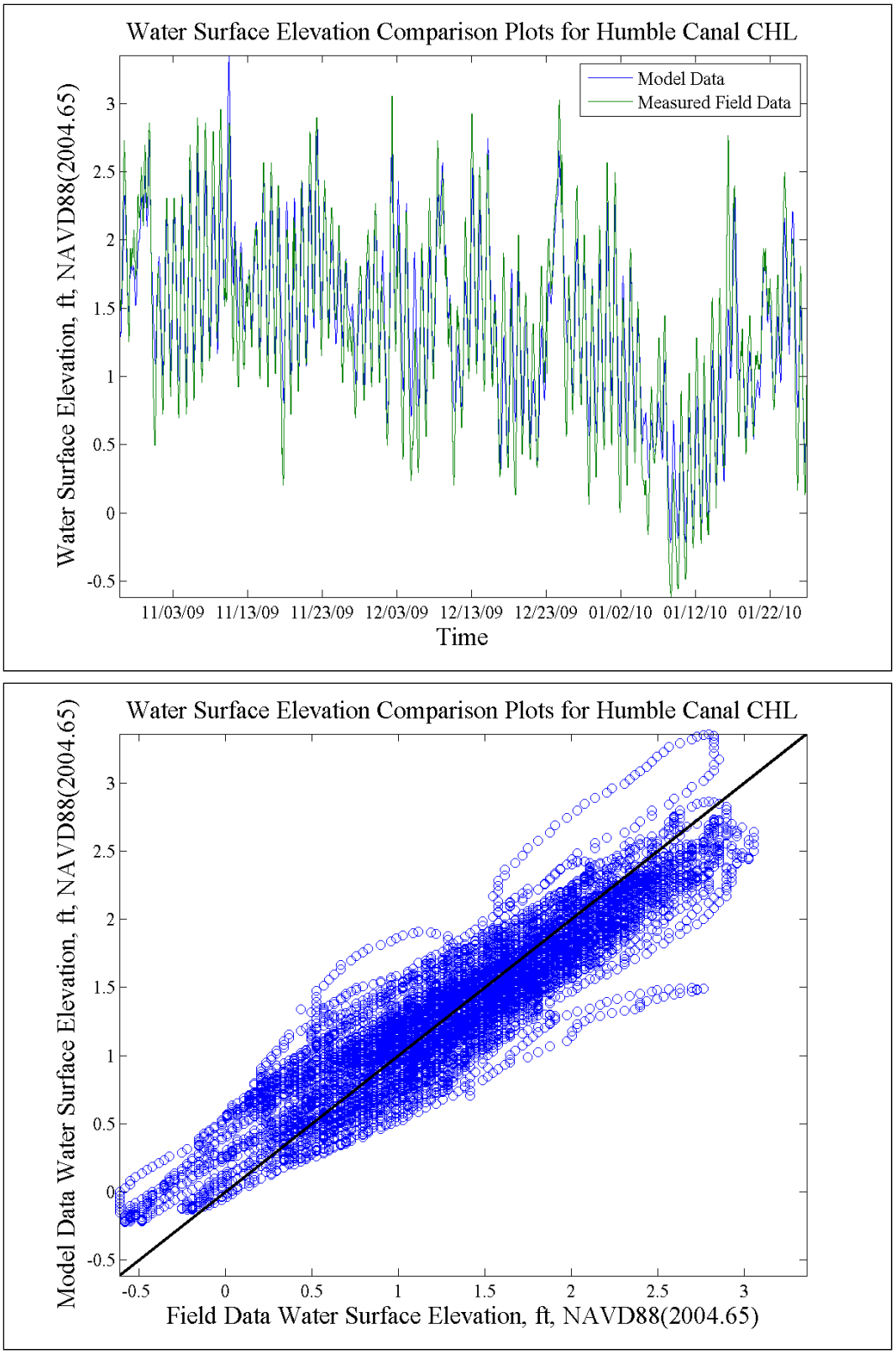

Figure 47. Humble Canal model versus field comparisons.

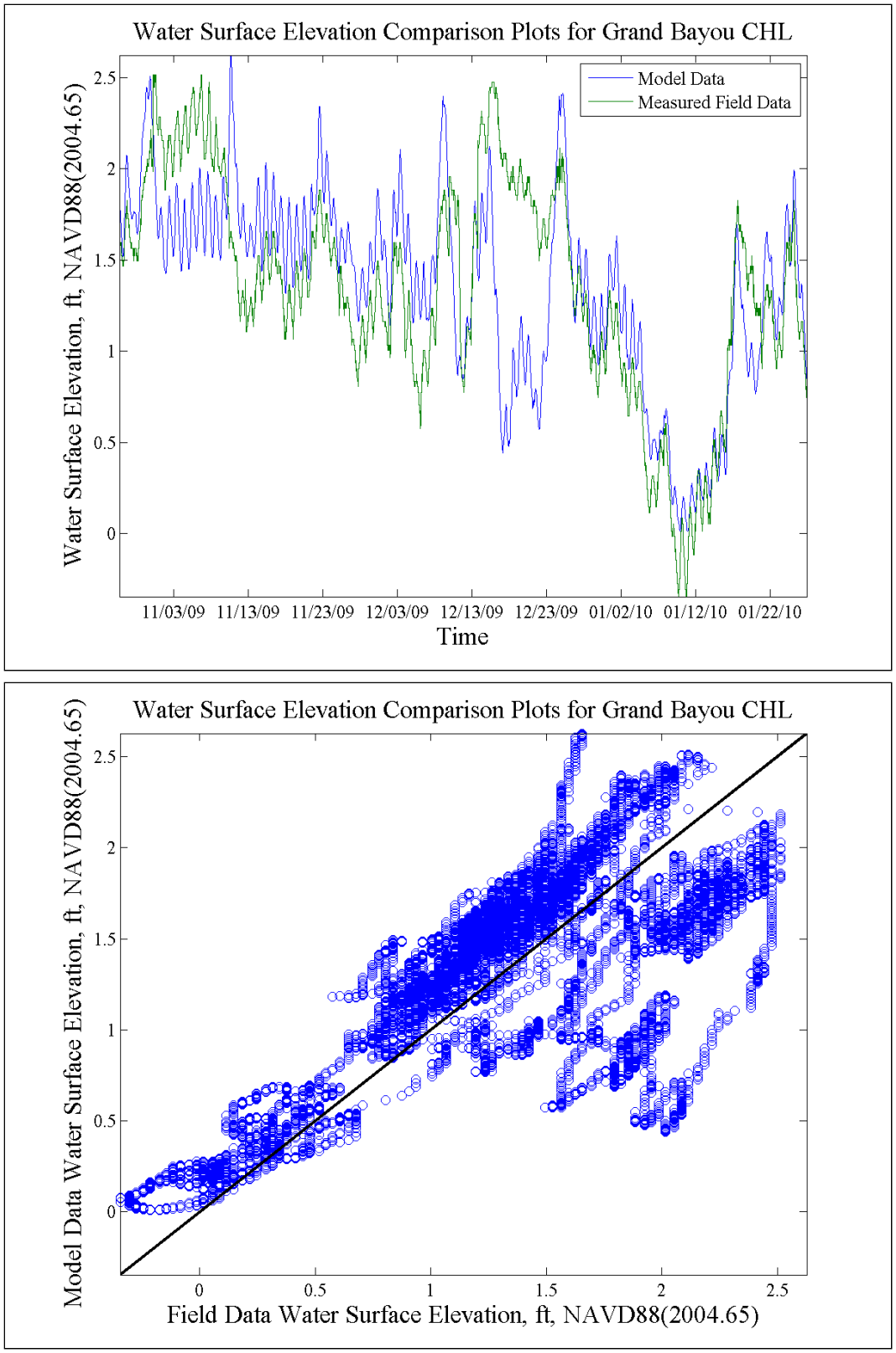

Figure 48. Grand Bayou model versus field comparisons.

One of these metrics consisted of the Normalized Root Mean Square Error (NRMSE). The equation for the NRMSE is provided in Equation 1.

$$NRMSE = \frac{\sqrt{\frac{\sum_{n=1}^{N}\left(observed_n - model_n\right)^2}{N}}}{Standard\ Deviation} \quad (1)$$

where N is the number of field measurements during the model simulated time period and n represents each field/model data point (i.e., field measurement and model value for a particular time). Lower values for NRMSE represent a lower percentage error in the model replication of the field data whereas high values represent poor skill by the model in replicating the field data (McLaughlin et al. 2003). Therefore values close to 0 indicate an excellent replication of the field data by the model whereas a value of 1 would suggest a model error of the same order of magnitude as the observed variation.

The correlation coefficients were also calculated using Equation 2.

$$Coef = \frac{N\sum_{n=1}^{N} x_n y_n - \left(\sum_{n=1}^{N} x_n\right)\left(\sum_{n=1}^{N} y_n\right)}{\sqrt{N\left(\sum_{n=1}^{N} x_n^2\right) - \left(\sum_{n=1}^{N} x_n\right)^2}\sqrt{N\left(\sum_{n=1}^{N} y_n^2\right) - \left(\sum_{n=1}^{N} y_n\right)^2}} \quad (2)$$

where x and y are the observed and model values. The correlation coefficient provides a single number that gives an indication as to how closely one variable is related to another variable (Higgins 2006). Values for the correlation coefficients range from +1 to -1 with a value of +1 representing a direct correlation between the two data sets.

The Nash-Sutcliffe Coefficients were calculated using Equation 3 with possible values ranging from -∞ to +1 (perfect model replication of the field) (McCuen et al. 2006). This Nash-Sutcliffe equation is:

$$Coef = 1 - \frac{\sum_{n=1}^{N}\left(observed_n - model_n\right)^2}{\sum_{n=1}^{N}\left(observed_n - \overline{observed}\right)^2} \quad (3)$$

where the overbar represents the mean of the observed data. The numerator of Equation 3 is the sum of the squares of the differences between the observed values and the corresponding model values. This

value represents the variation in the data that has not been replicated by the model. The denominator in Equation 3 is the sum of the squares of the observed values about their mean which represents the total variation of the observed values. Therefore the Nash-Sutcliffe coefficient is a ratio of the variation in the data not explained by the model to the variation in the observed data.

The Willmott coefficient (Equation 4) is another calculated variable to indicate a model's capabilities (Willmott 1982; Willmott et al. 1985). A value of 1 indicates a perfect agreement between the model and the observed values.

$$Coef = 1 - \frac{\sum_{n=1}^{N} \left(model_n - observed_n \right)^2}{\sum_{n=1}^{N} \left(\left(\left| observed_n - \overline{observed} \right| \right) + \left(\left| model_n - \overline{observed} \right| \right) \right)^2} \quad (4)$$

Like the Nash-Sutcliffe coefficient, the numerator for the Willmott coefficient is a representation of the variation in the data not explained by the model. The denominator is similar to the Nash-Sutcliffe coefficient denominator with the inclusion of the variation in the model about the observed value term. From comparison of Equations 3 and 4, it can be observed that the Willmott coefficient will always be closer to 1 than the Nash-Sutcliffe coefficient due to the added term of the model variation about the observed mean included in the denominator.

The coefficients for the NRMSE, correlation, Nash-Sutcliffe, and Willmott coefficients are presented in Table 4.

The water-surface elevation comparisons show an adequate model replication of the observed tidal signal. This is exemplified as well for the NRMSE error values (average value of 0.43 with a median value of 0.34), the Nash-Sutcliffe values (average value of 0.78 with a median value of 0.88), correlation coefficients (average value of 0.91 with a median value of 0.94), and the Willmott coefficients (average value of 0.95 with a median value of 0.97).

A small subset of the gages possess less than ideal comparisons (GIWW west of Houma, GIWW at Houma, and Grand Bayou). GIWW west of Houma is near an inflow boundary, located far from the model study area, making this less accurate comparison of little concern for the purpose of

Table 4. Water-surface elevation error values.

Gage Name	Origin of Data	Normalized Root Mean Square Error (0 = Perfect Replication)	Nash-Sutcliffe Coefficient (1 = Perfect Replication)	Correlation Coefficient (1 = Direct Correlation)	Willmott Coefficient (1 = Perfect Replication)
Caillou Lake	USGS	0.49	0.76	0.88	0.92
Caillou Bay	USGS	0.32	0.90	0.95	0.97
Houma Navigation Canal	USGS	0.32	0.90	0.96	0.98
Bayou Grand Caillou	USGS	0.30	0.91	0.96	0.98
Bayou Petit Caillou	USGS	0.32	0.90	0.95	0.97
Bayou Terrebonne	USGS	0.36	0.87	0.93	0.96
GIWW at Houma	USGS	0.78	0.40	0.76	0.86
GIWW West of Houma	CHL	0.95	0.10	0.76	0.84
Falgout Canal	CHL	0.30	0.91	0.95	0.98
Bayou Dularge	CHL	0.28	0.92	0.96	0.98
Bayou Grand Caillou	CHL	0.32	0.89	0.96	0.98
Bayou Petit Caillou	CHL	0.34	0.88	0.94	0.97
Lapeyrouse Canal	CHL	0.33	0.89	0.95	0.97
Placid Canal	CHL	0.36	0.87	0.93	0.97
Bayou Terrebonne	CHL	0.35	0.87	0.94	0.97
Humble Canal	CHL	0.39	0.85	0.92	0.95
Grand Bayou	CHL	0.75	0.44	0.70	0.83
AVERAGE		0.43	0.78	0.91	0.95
MEDIAN		0.34	0.88	0.94	0.97

this study. The other two gages (GIWW at Houma and Grand Bayou) with less than ideal comparisons are also sufficiently far from the study area making their larger errors of little concern for the purpose of this study. The error metrics associated with these two locations are also skewed due to a single event around 20 December 2009 which is not accurately replicated in the model.

The overall comparisons indicate that the model adequately replicates the water-surface elevations in the system.

Discharge validation

Validation of the model discharges consisted of comparisons with the measured discharge data taken from 26 October 2009 to 22 January 2010.

The discharge measurement locations were previously shown and discussed in Chapter 2. The comparison plots are provided in Figures 49 to 60. Similar to the water-surface elevations, the discharge comparison plots consist of time series comparisons and box plot comparisons. Table 5 provides a list of the error values also previously calculated for the water surface elevations with Table 6 providing a comparison of the mean, minimum, and maximum model and field discharge values.

It should be noted that there exists a large uncertainty in the discharge measurements (on the order of 10 to 20 %), making extremely accurate replications of the field data unlikely. Therefore the observed versus field discharge comparisons are expected to have uncertainties significantly higher than the previously reported water-surface elevations.

While the comparisons for the discharges are not as favorable as the water- surface elevation comparisons, the model replicates the behavior of the field accurately enough for the intended purposes of this project. While the average error values indicate acceptable skill replicating the system, this is greatly improved when the GIWW at Houma (Figure 3) and Grand Bayou (Figure 5) values are removed from consideration. There is a single event (around 20 December 2009) that is not replicated in the model. This event skews the error metrics in a non-favorable way. These two locations are also far from the current study area making their results of less importance for the objectives of this study. With the values from these two gages removed from the analysis, the average values of 0.81 (NRMSE), 0.28 (Nash-Sutcliffe), 0.75 (Correlation Coefficient), and 0.84 (Willmott Coefficient) and median values of 0.78 (NRMSE), 0.39 (Nash-Sutcliffe), 0.78 (Correlation Coefficient), and 0.87 (Willmott Coefficient) illustrate significant skill by the model in replicating the observed discharges.

The model does an adequate job simulating the discharges in the area of study in and around Humble Canal, Bayou Petit Caillou, Bayou Terrebonne, Placid Canal, and Lapeyrouse Canal. The Humble Canal discharge comparisons are less than ideal, but due to the low discharges/velocities measured for this location a greater error is expected. Therefore the Humble Canal comparisons were deemed sufficient as the greater measurement error could be the reason for the greater error in the model versus field comparisons.

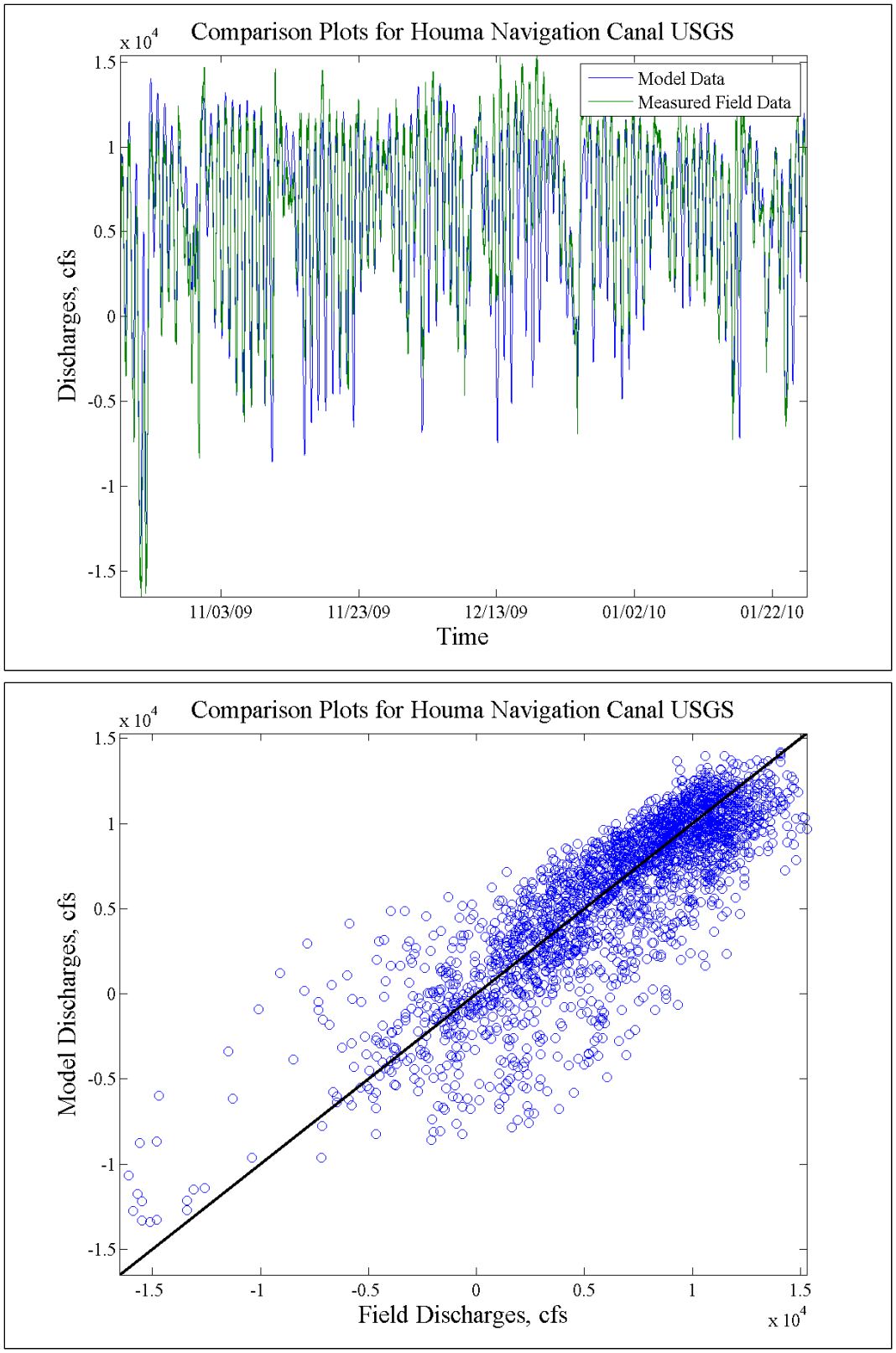

Figure 49. Houma Navigational Canal discharge comparisons.

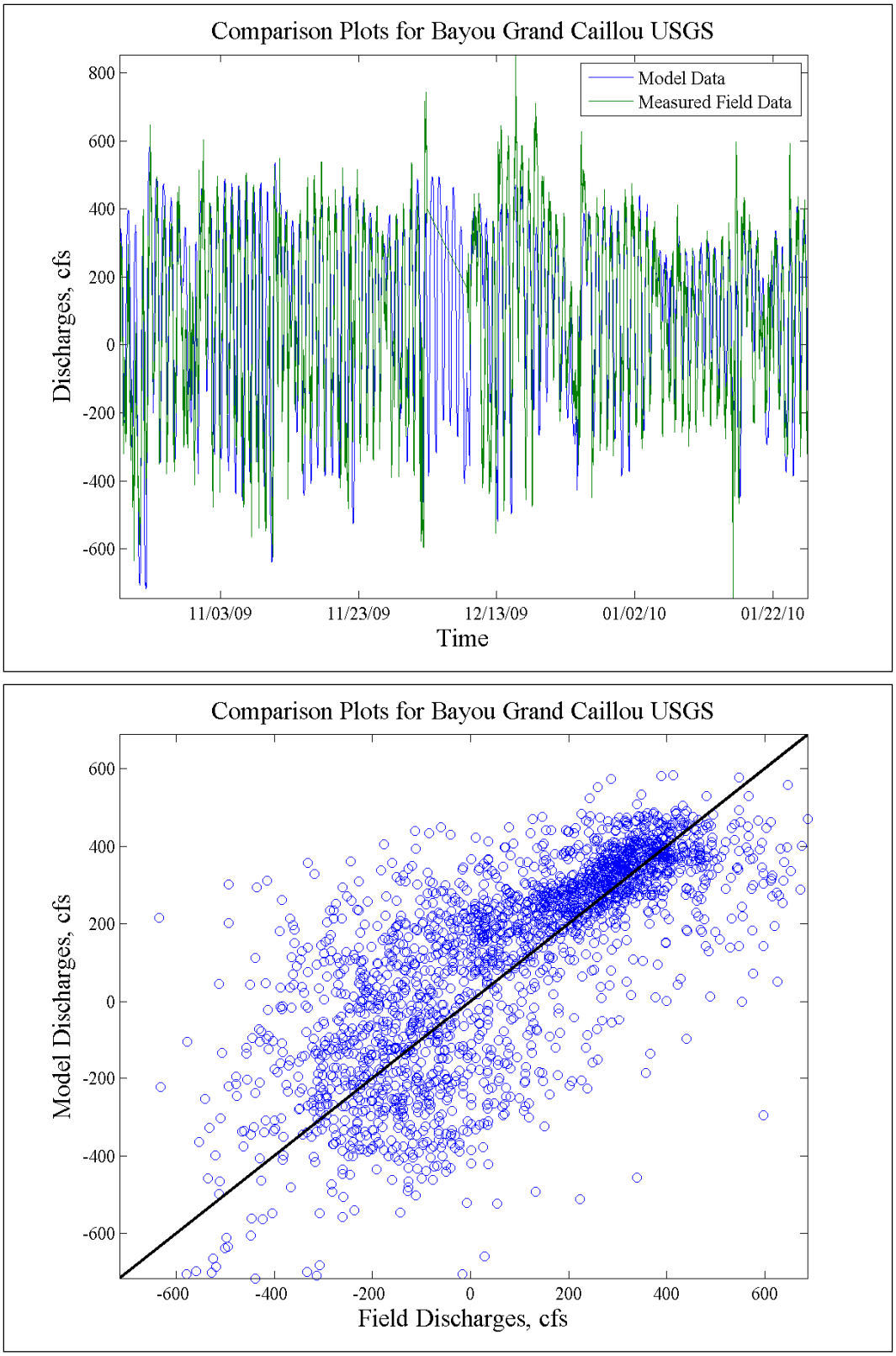

Figure 50. Bayou Grand Caillou discharge comparisons.

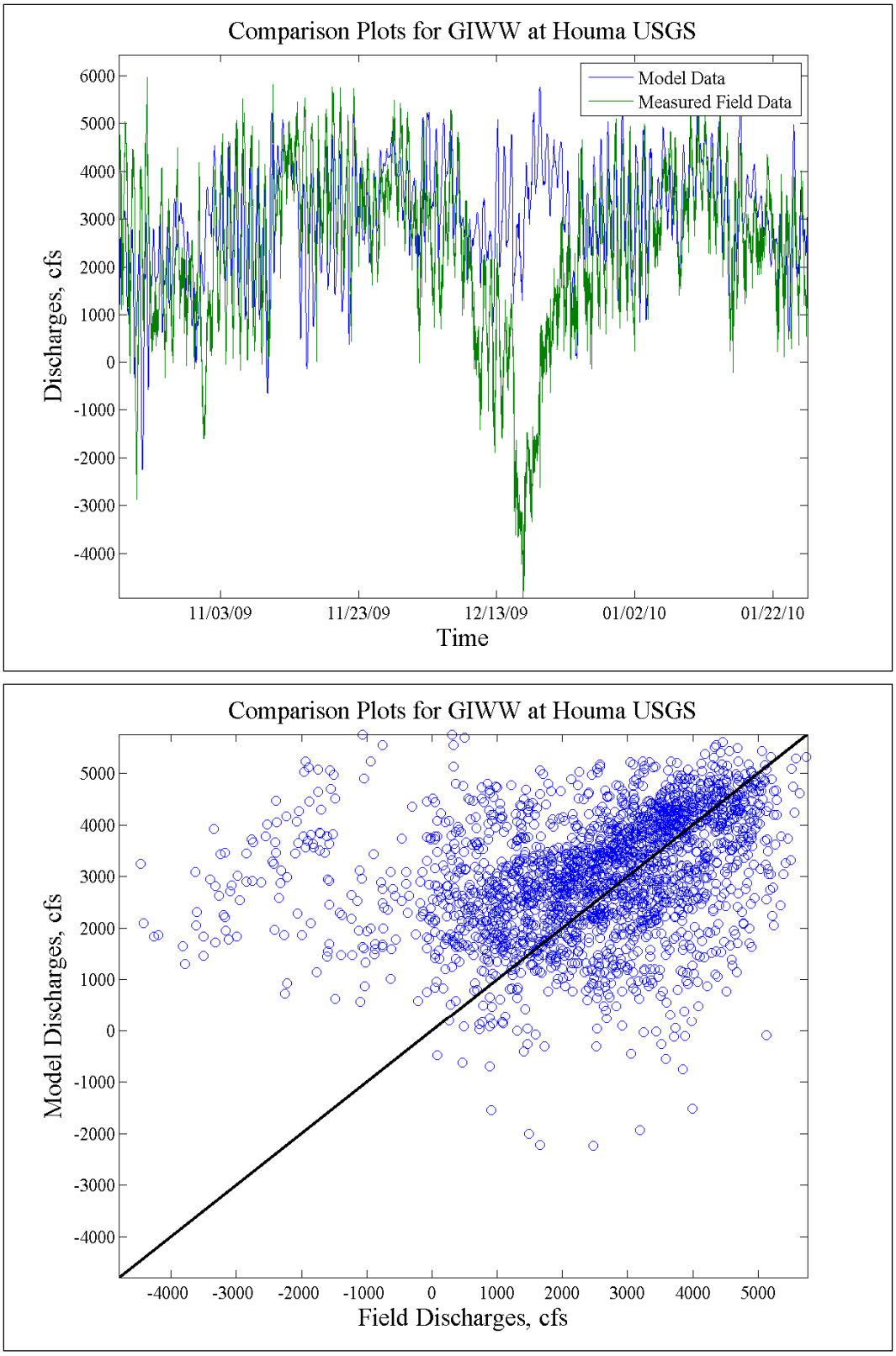

Figure 51. GIWW at Houma discharge comparisons.

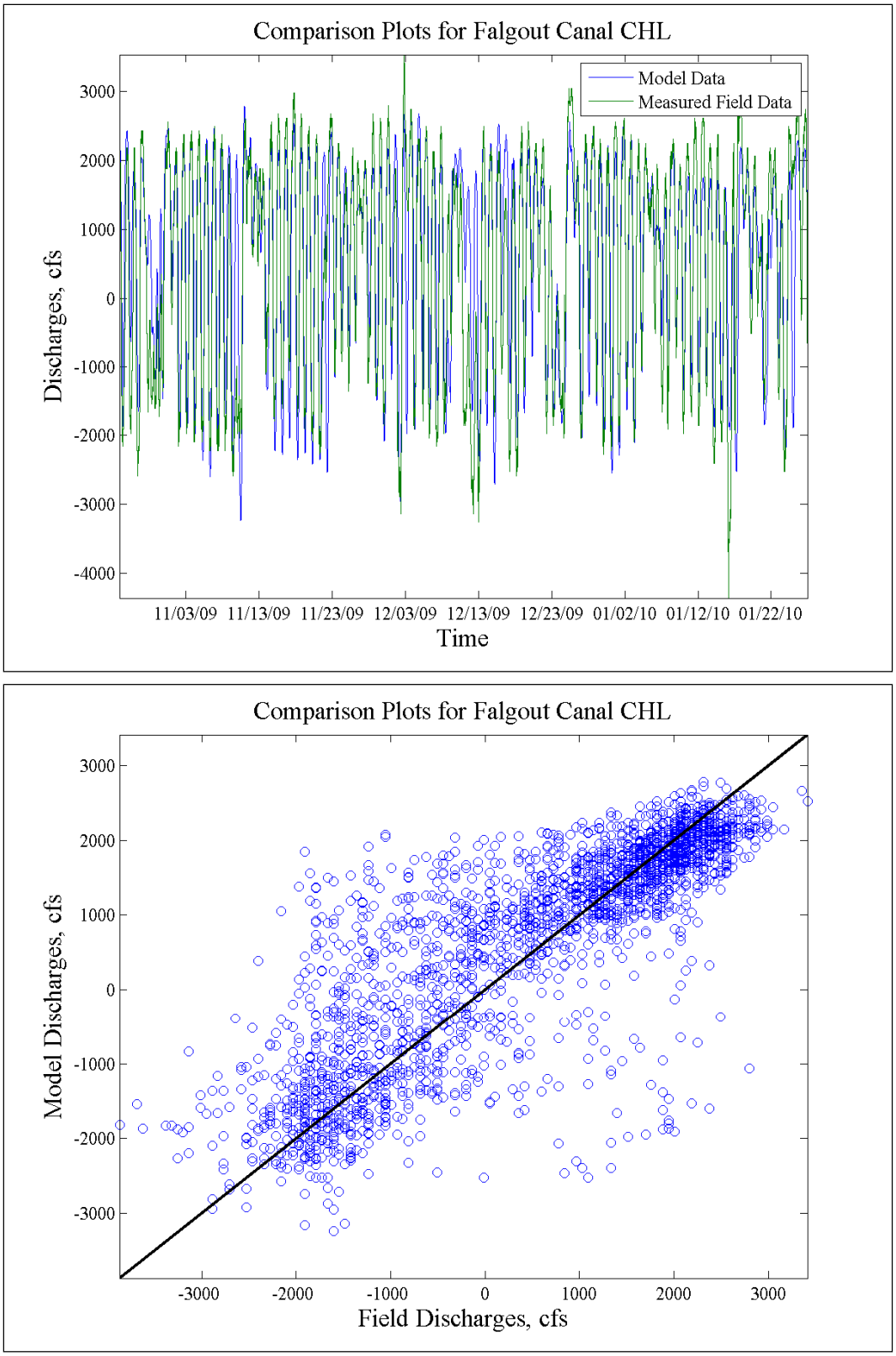

Figure 52. Falgout Canal discharge comparisons.

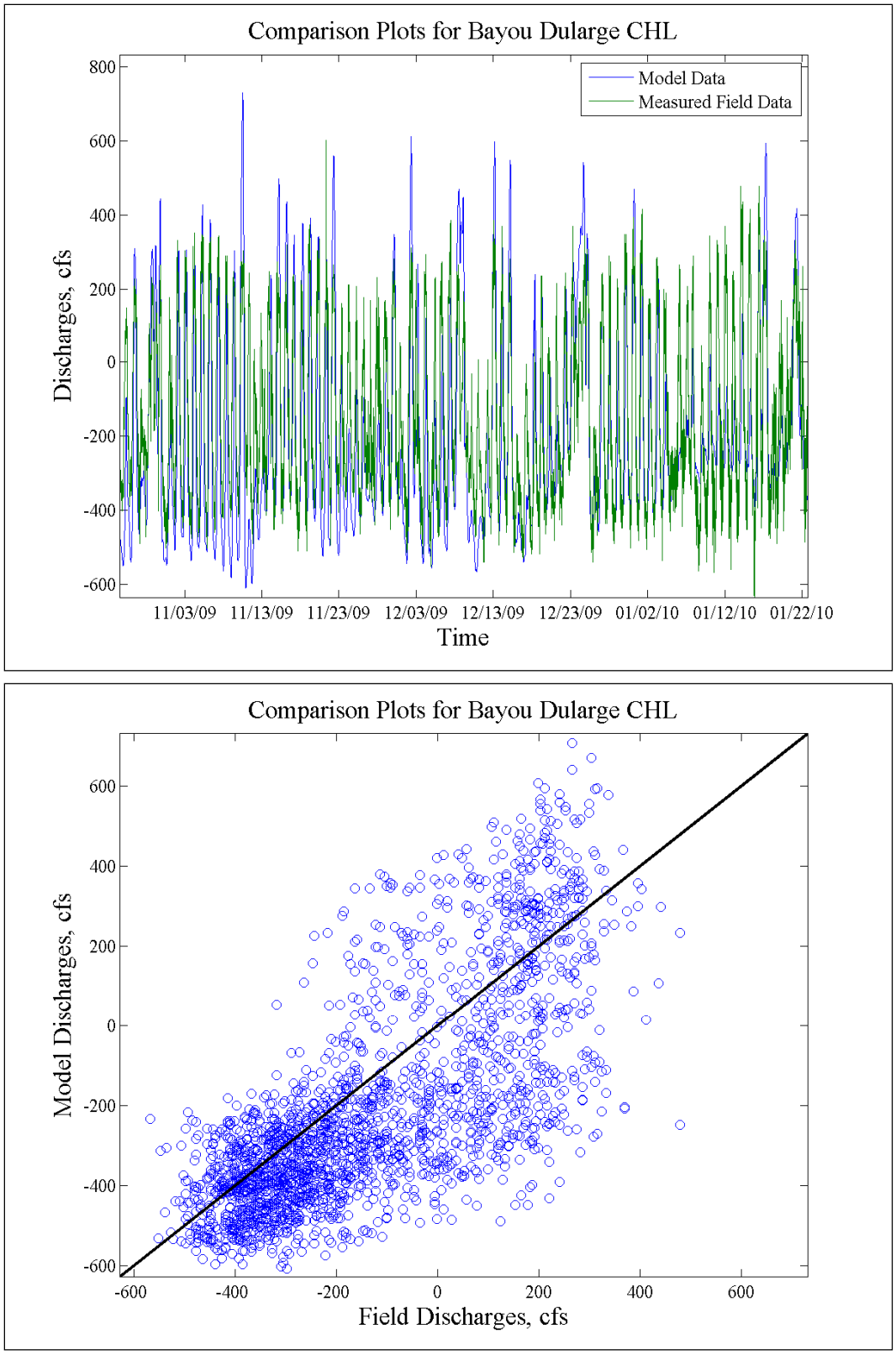

Figure 53. Bayou Dularge discharge comparisons.

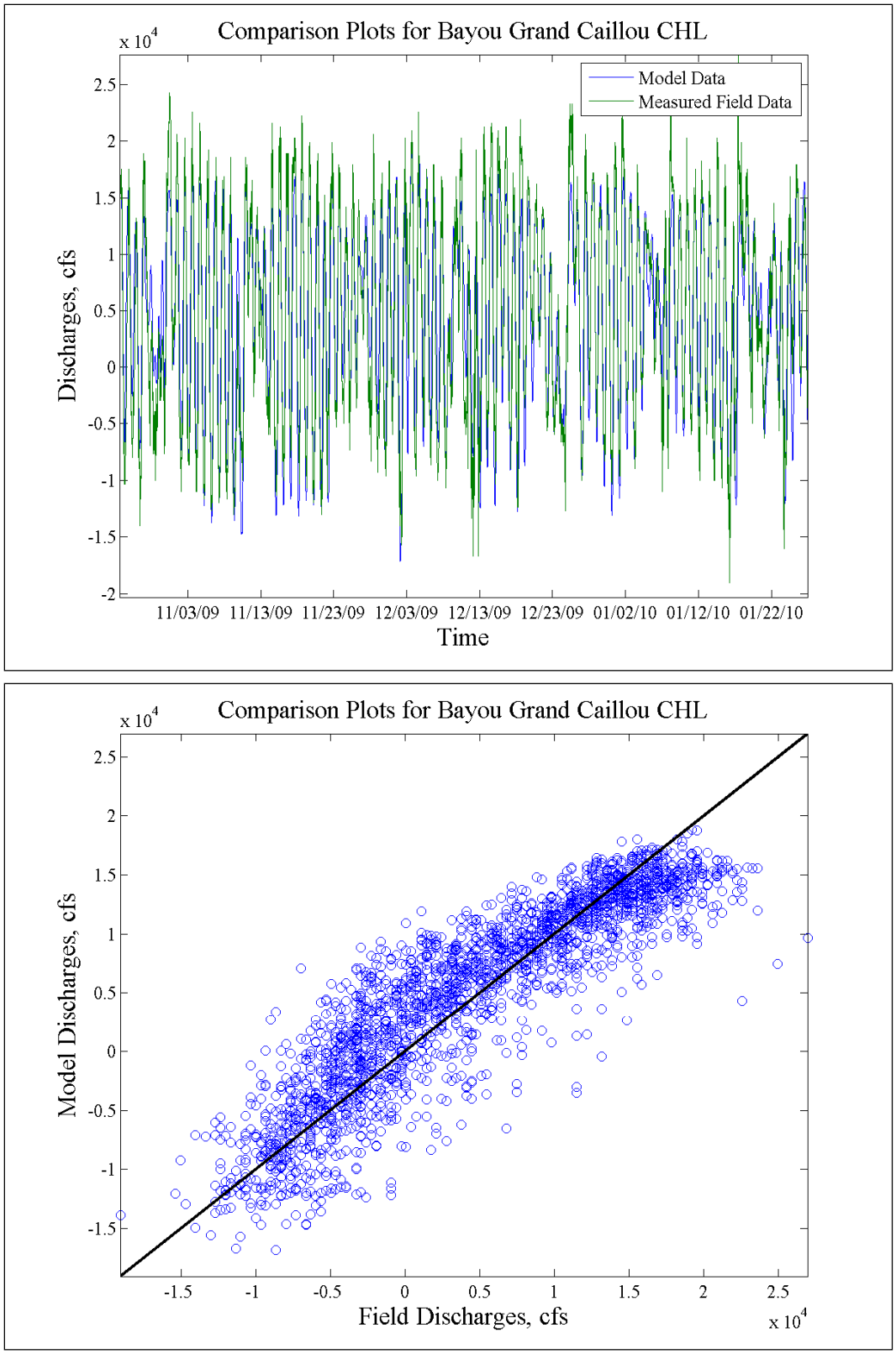

Figure 54. Bayou Grand Caillou discharge comparisons.

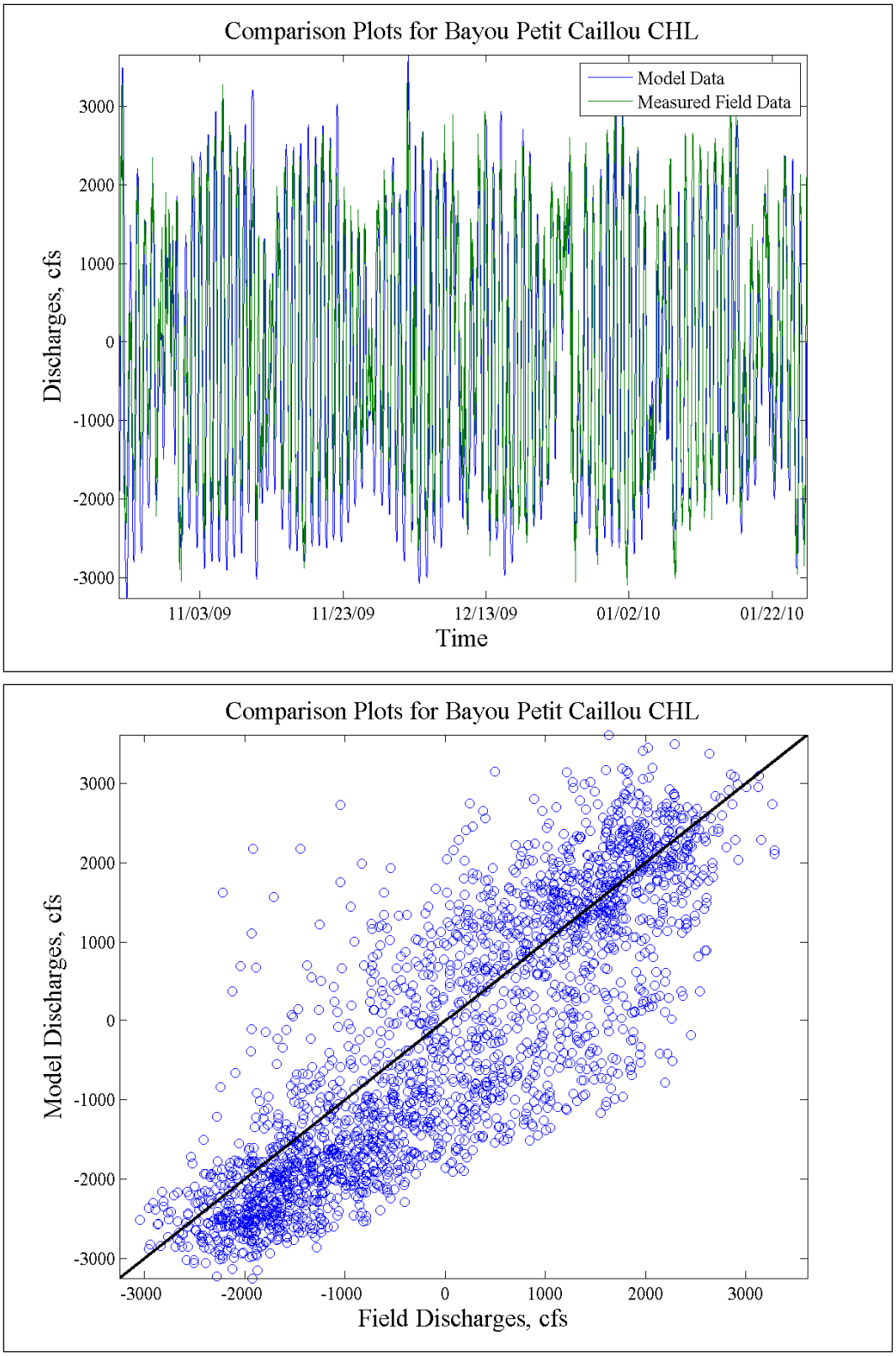

Figure 55. Bayou Petit Caillou discharge comparisons.

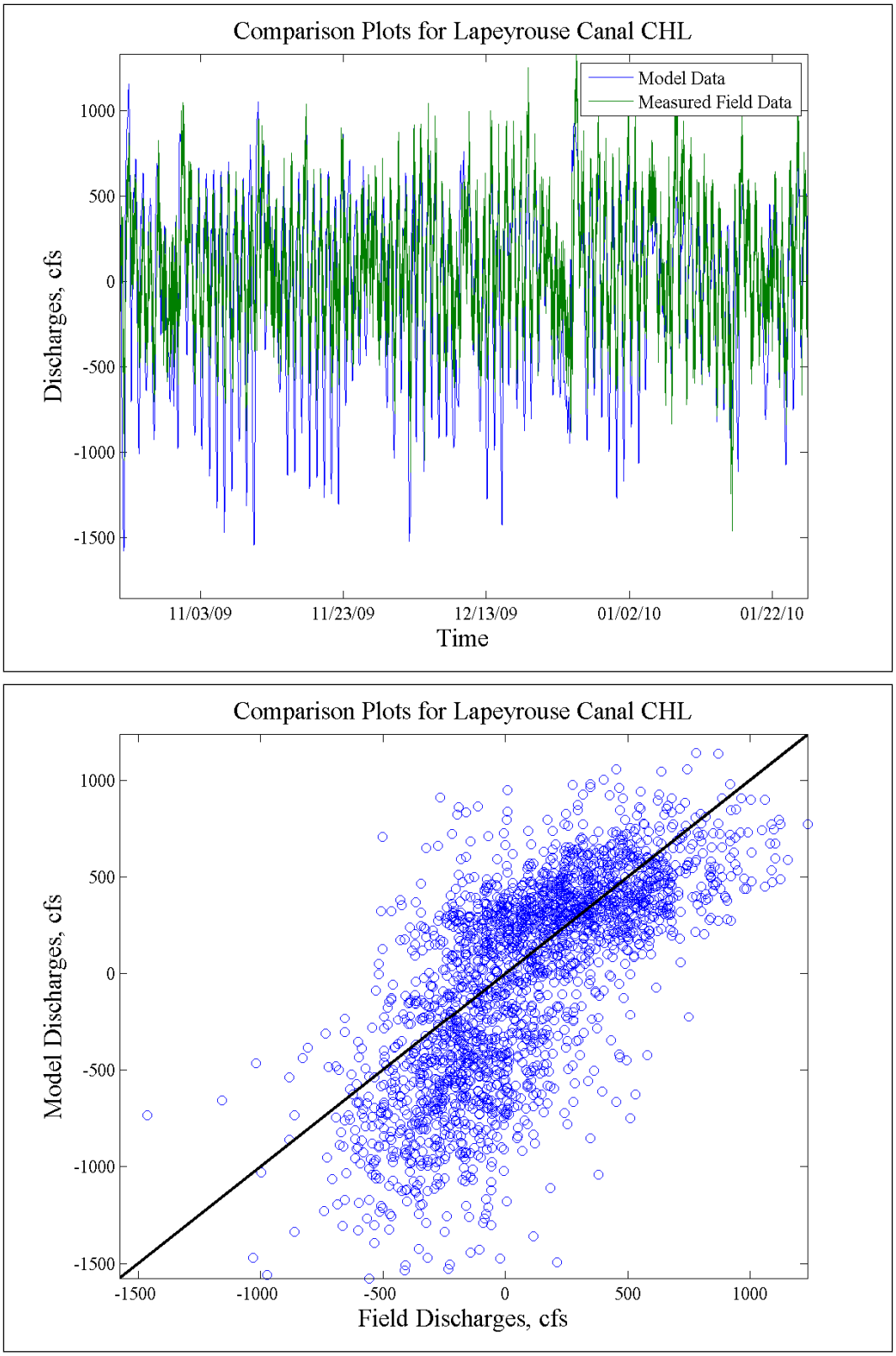

Figure 56. Lapeyrouse Canal discharge comparisons.

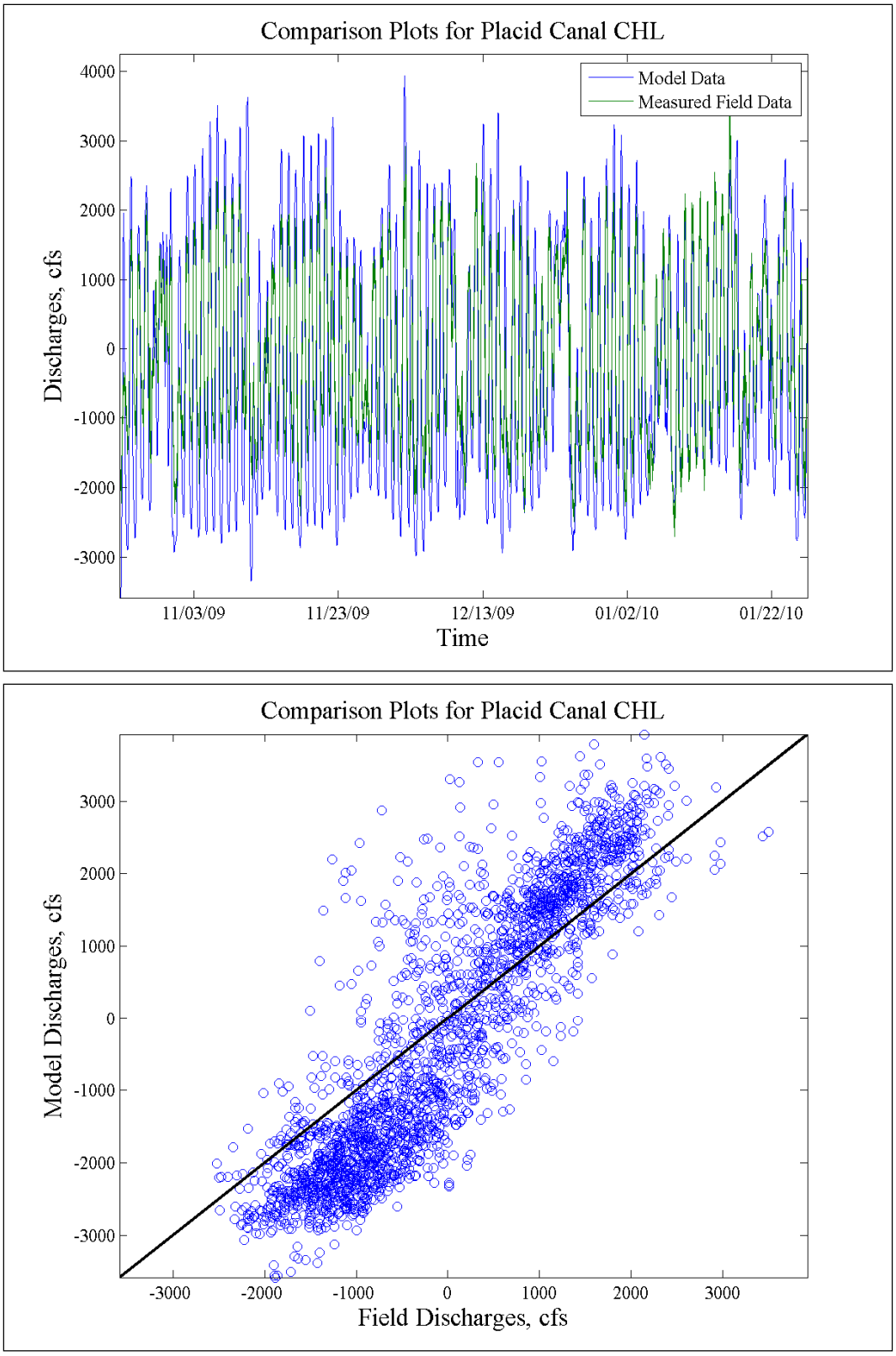

Figure 57. Placid Canal discharge comparisons.

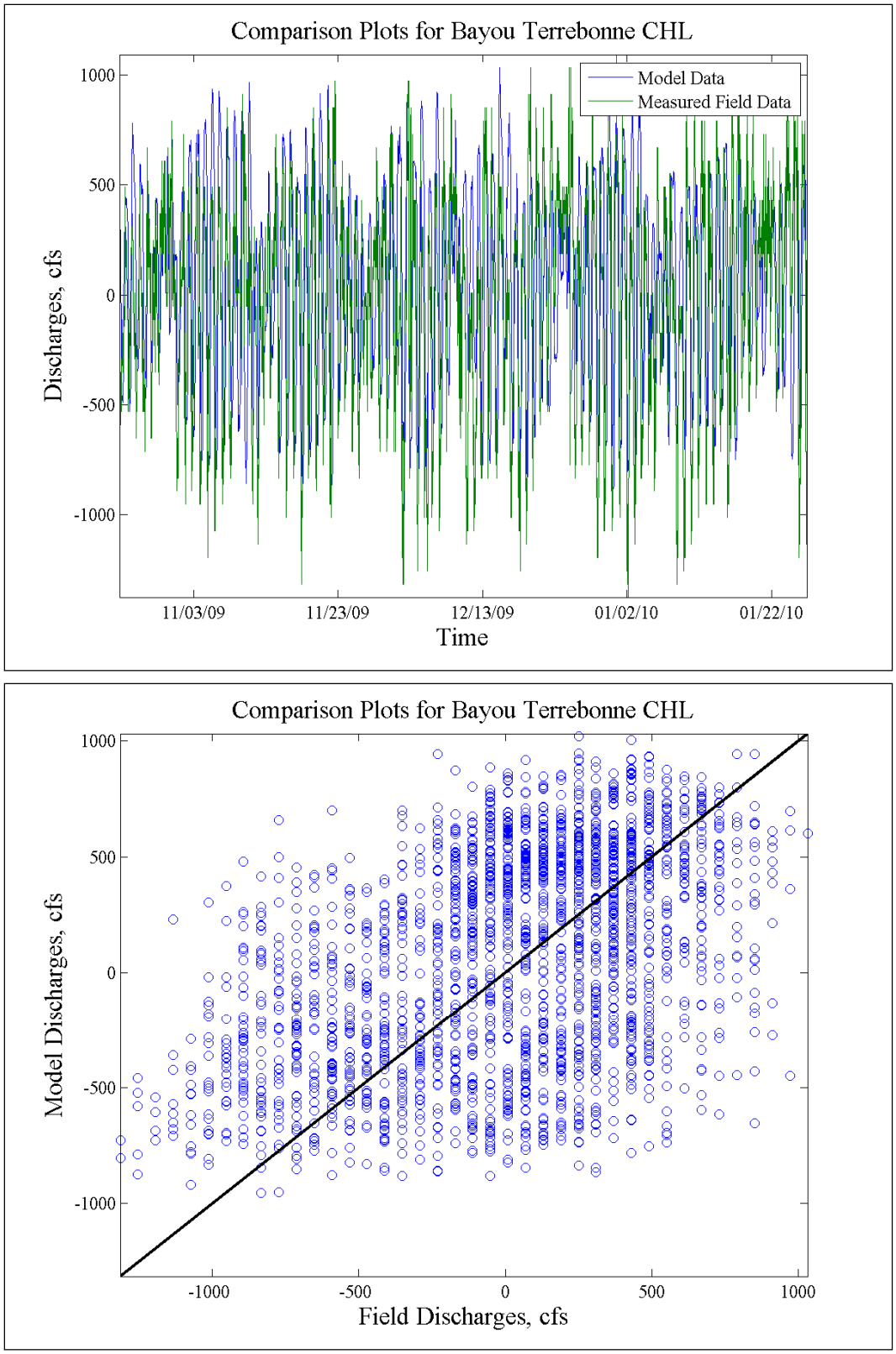

Figure 58. Bayou Terrebonne discharge comparisons.

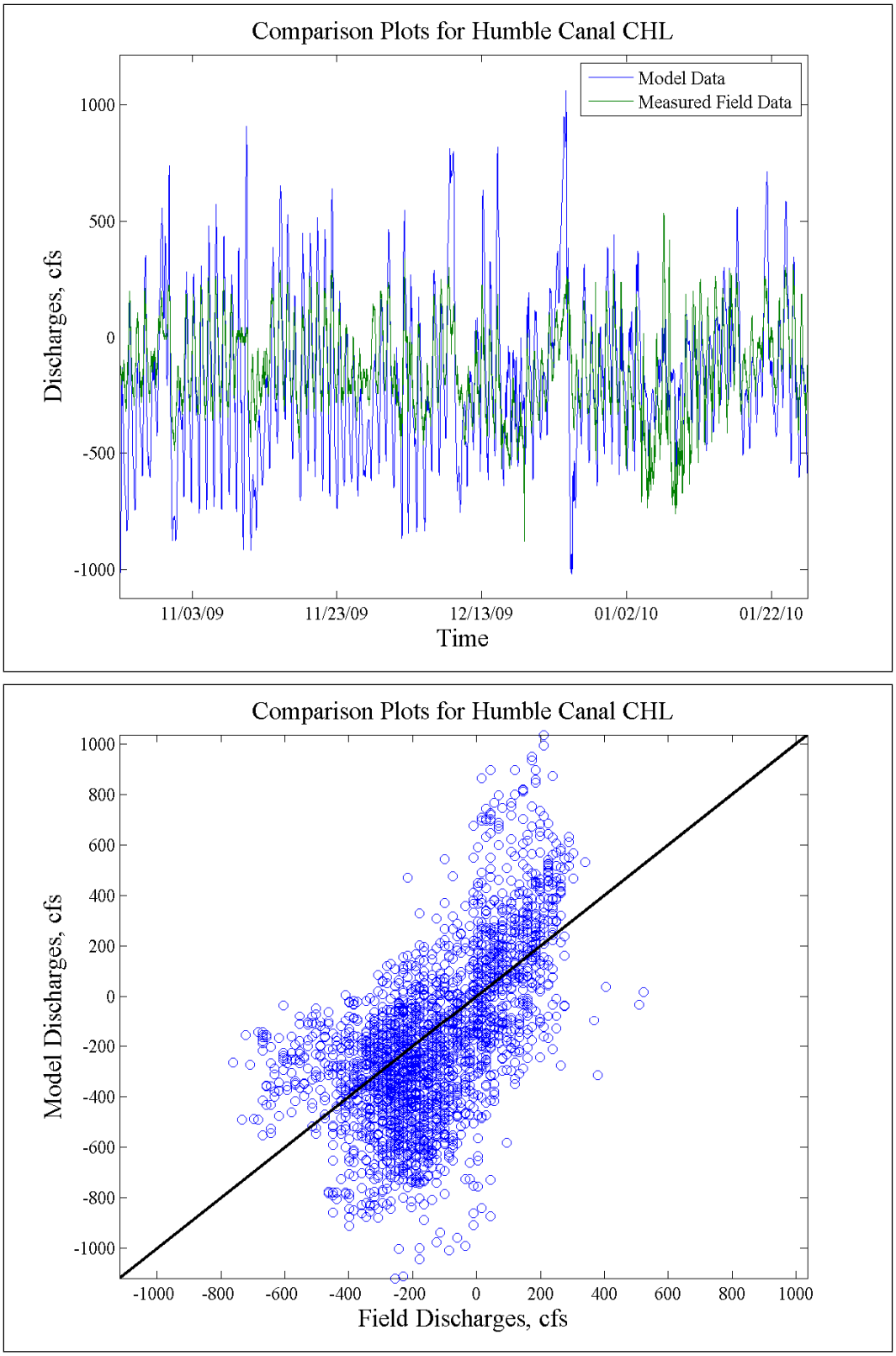

Figure 59. Humble Canal discharge comparisons.

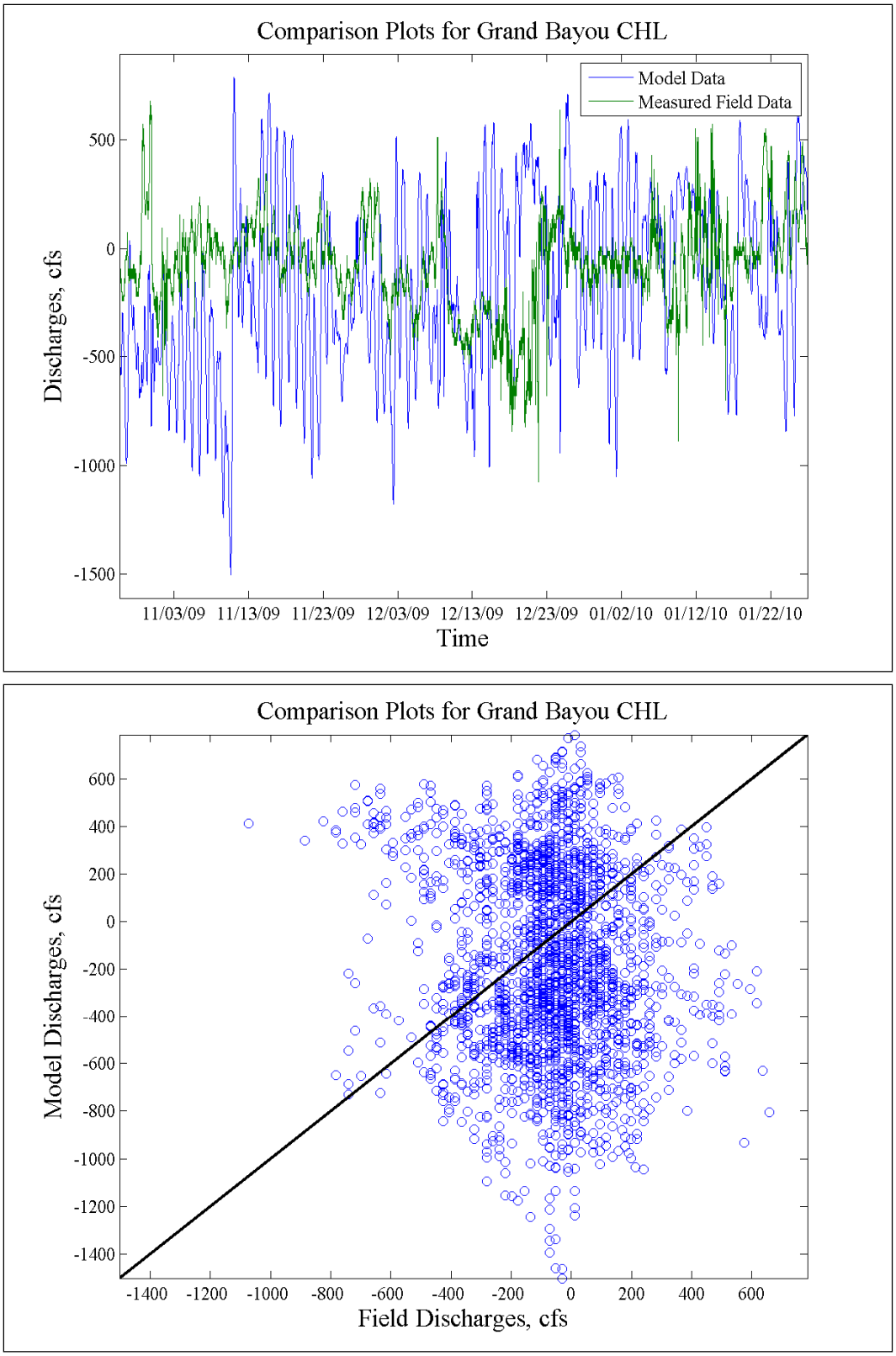

Figure 60. Grand Bayou discharge comparisons.

Table 5. Discharge error values.

Gage Name	Origin of Data	Normalized Root Mean Square Error (0 = Perfect Replication)	Nash-Sutcliffe Coefficient (1 = Perfect Replication)	Correlation Coefficient (1 = Direct Correlation)	Willmott Coefficient (1 = Perfect Replication)
Houma Navigation Canal	USGS	0.57	0.68	0.84	0.91
Bayou Grand Caillou	USGS	0.75	0.43	0.73	0.85
GIWW at Houma	USGS	1.08	-0.17	0.31	0.56
Falgout Canal	CHL	0.58	0.67	0.83	0.90
Bayou Dularge	CHL	0.87	0.24	0.73	0.83
Bayou Grand Caillou	CHL	0.45	0.80	0.89	0.94
Bayou Petit Caillou	CHL	0.64	0.59	0.85	0.91
Lapeyrouse Canal	CHL	1.06	-0.12	0.70	0.79
Placid Canal	CHL	0.81	0.34	0.89	0.89
Bayou Terrebonne	CHL	1.06	-0.12	0.45	0.68
Humble Canal	CHL	1.35	-0.83	0.59	0.70
Grand Bayou	CHL	2.27	-4.13	-0.10	0.29
AVERAGE		0.96	-0.14	0.64	0.77
MEDIAN		0.84	0.29	0.73	0.84
AVERAGE without GIWW at Houma and Grand Bayou		0.81	0.28	0.75	0.84
MEDIAN without GIWW at Houma and Grand Bayou		0.78	0.39	0.78	0.87

Bayou Petit Caillou has good model versus field comparisons exhibiting significant skill in modeling the discharges for this area. Bayou Terrebonne does an adequate job replicating the range of discharge values but due to a slight phase shift the box plots and error terms appear as unfavorable model comparisons. As this study is focused on gate sizing it is believed that this phase shift in the data is of little consequence in terms of base versus plan model comparisons.

Placid Canal and Lapeyrouse Canal possess adequate discharge comparisons. Some of the differences between the model and the field could be attributed to additional connections between Bayou Terrebonne and Bayou Petit Caillou not included in the mesh. Additional flow that should be transported through those additional smaller channels could be flowing

Table 6. Maximum, minimum, and mean discharge comparisons.

Gage Name	Origin of Data	Model (Field) Mean, cfs	Model (Field) Max, cfs	Model (Field) Min, cfs
Houma Navigation Canal	USGS	5954 (6433)	15400 (14231)	-13441 (-16500)
Bayou Grand Caillou	USGS	145 (80)	852 (584)	-719 (-744)
GIWW at Houma	USGS	3020 (2427)	5970 (5773)	-2287 (-4930)
GIWW at Bayou Lafourche	USGS	3376 (3280)	6410 (6680)	-4203 (-5500)
Falgout Canal	CHL	617 (476)	3534 (2793)	-3244 (-4360)
Bayou Dularge	CHL	-209 (-137)	603 (729)	-610 (-636)
Bayou Grand Caillou	CHL	4912 (4504)	27636 (19017)	-17114 (-19059)
Bayou Petit Caillou	CHL	-277 (11)	3614 (3285)	-3251 (-3051)
Lapeyrouse Canal	CHL	-16 (87)	1329 (1151)	-1556 (-1463)
Placid Canal	CHL	-305 (-70)	3810 (3889)	-3580 (-2707)
Bayou Terrebonne	CHL	71 (-4)	1091 (1025)	-971 (-1374)
Humble Canal	CHL	-178 (-138)	535 (1057)	-1119 (-878)
Grand Bayou	CHL	-178 (-73)	785 (658)	-1502 (-1074)
GIWW West of Houma	CHL	9137 (4534)	8633 (14603)	-5153 (-2890)

through these two connections. Therefore the model results for Lapeyrouse Canal and Placid Canal are assumed to be a better replication of the total flow connecting the two bayous which will be important for the plan configurations as these additional smaller channels will be closed to flow.

The remaining comparison locations are sufficiently far from the current study area that any less than favorable comparisons are deemed less important with little effect on the Bayou Petit Caillou, Bush Canal, and Bayou Terrebonne areas. It is noted that the Grand Bayou comparisons are not satisfactory, but the extreme distance from the Grand Bayou location to the study area made accurate modeling of the Grand Bayou area of little consequence.

Computational environment

The hydrodynamic modeling was executed on the ERDC High Performance Computing (HPC) CRAY XT4 (Jade) parallel processing supercomputer. The model mesh contained 63,754 nodes and 95,629 elements with elemental areas ranging from 177,000,000 ft^2 near the Gulf boundary to as little as 100 ft^2 in the model study area. The model was executed on 128 parallel processors and required approximately 20 hr of computational time (54.6 CPU hr) to run for three model months. The model used a time-step of 360 sec, with the ability to adapt to smaller time-steps as needed.

6 Design Alternatives

The aim of the design alternatives was to determine appropriate structure sizes that would also result in reasonable velocity fields. The initial design included navigational structures and environmental structures. This began with an initial, proposed configuration (Figure 61) that was altered due to preliminary model results. The final configurations, Plan 6 and Plan 7 (environmental structures closed), are discussed extensively in this chapter. The evolution of the plan configuration consisted solely of modifications to the Placid Canal and Bayou Petit Caillou structures (all remaining navigational and environmental structures were left unchanged from the initial plan configuration). The modifications of these structures from the initial plan to Plan 6 are provided in Table 7 at the end of this chapter along with a bar plot comparison of the maximum velocities for those two structures for all modeled configurations (Figure 77). It should be noted that the structure configurations are conceptual in nature as finalized designs have not been created.

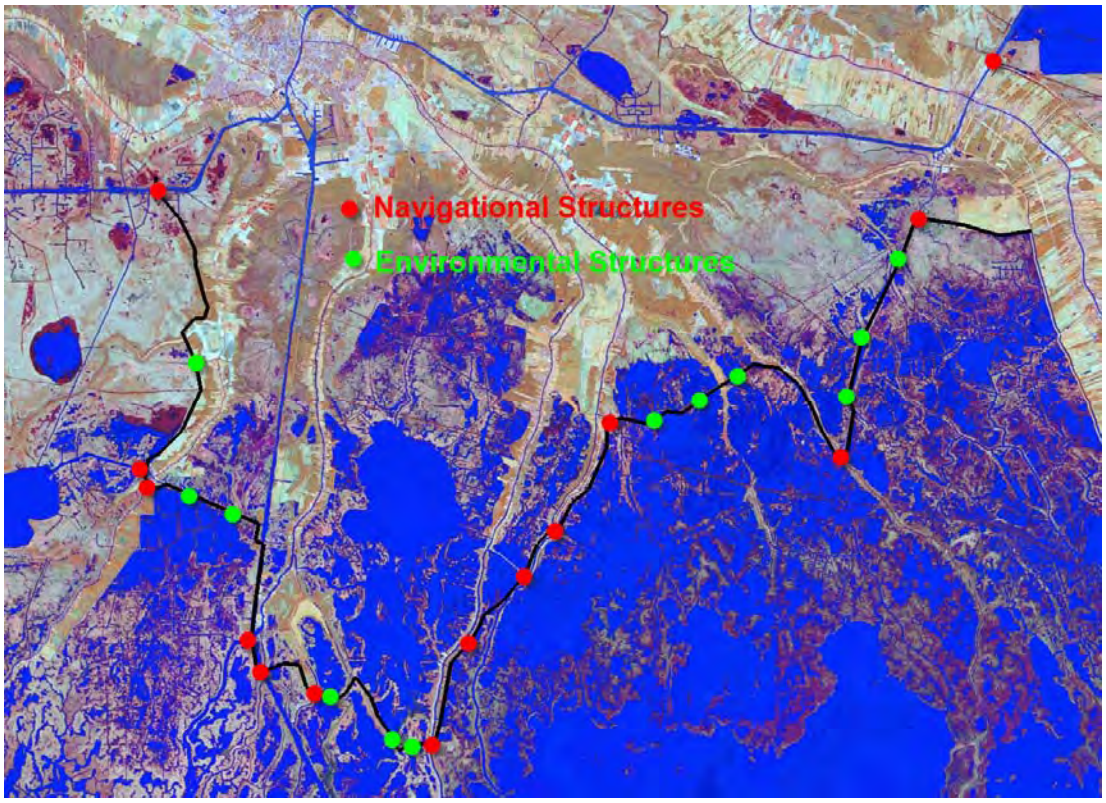

Figure 61. Structure locations.

Table 7. Evolution of the plan configuration for Placid Canal and Bayou Petit Caillou.

Alternative Number	Placid Canal Sector Gate Width (ft)	Sluice Gates for Placid Canal	Bayou Petit Caillou Sector Gate Width (ft)	Sluice Gates for Bayou Petit Caillou
Plan 1	56	0	56	0
Plan 2	30 (Barge Gate)	0	56	0
Plan 3*	56	0	56	0
Plan 4	80	0	80	0
Plan 5	100	0	100	0
Plan 6**	56	2 – 46 ft Sluice Gates	56	2 – 46 ft Sluice Gates
Plan 7**	56	2 – 46 ft Sluice Gates	56	2 – 46 ft Sluice Gates

*Plan 3 has an added structure on Lapeyrouse Canal (56-ft-wide sector gate with a bottom elevation of -10 ft, NAVD88(204.65). The Lapeyrouse Canal structure was eliminated for all other plan configurations.

**Plan 7 is the Plan 6 configuration with all Environmental Structures closed.

The GIWW west of Houma structure, shown in Figure 62, consisted of two 125-ft-wide structures with bottom widths of -20 ft, NAVD88(2004.65).

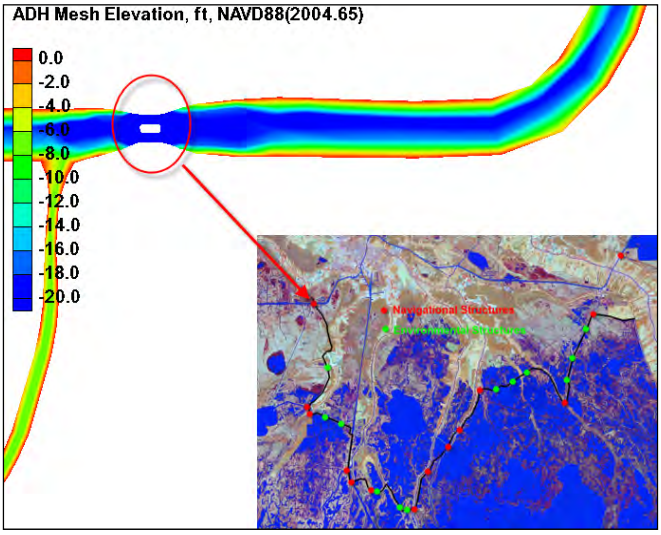

Figure 62. GIWW west of Houma structure.

The formerly free-flowing Marmande Canal is joined by a set of six culverts (6' x 6'). For this modeling effort the widths for these culverts were combined into one culvert with a width of 36 ft and a bottom invert of -4.5 ft NAVD88(2004.65)). The model representation of this configuration is shown in Figure 63.

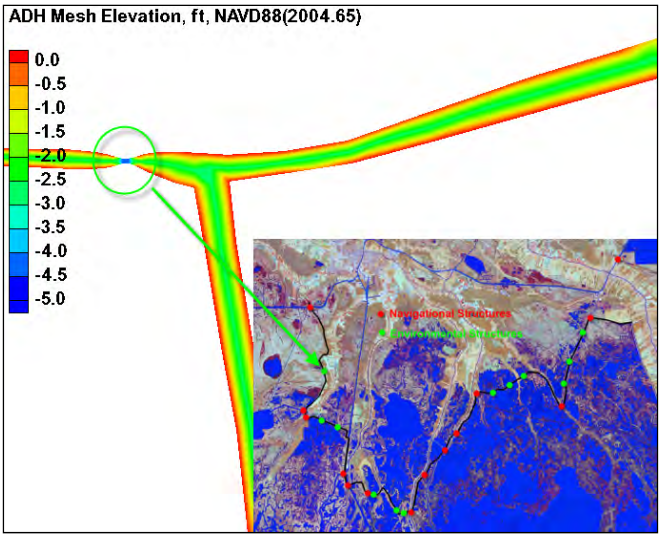

Figure 63. Model representation of the Marmande Canal culverts.

The Falgout Canal (upper left circle) and the Bayou Dularge (lower circle) structures are shown in Figure 64. The Falgout Canal structure consists of one 56-ft sector gate and three 46-ft sluice gates with -9 ft NAVD88(2004.65) bottom elevations. The Bayou Dularge structure consists of one 56-ft sector gate with a bottom elevation of -7 ft NAVD88(2004.65).

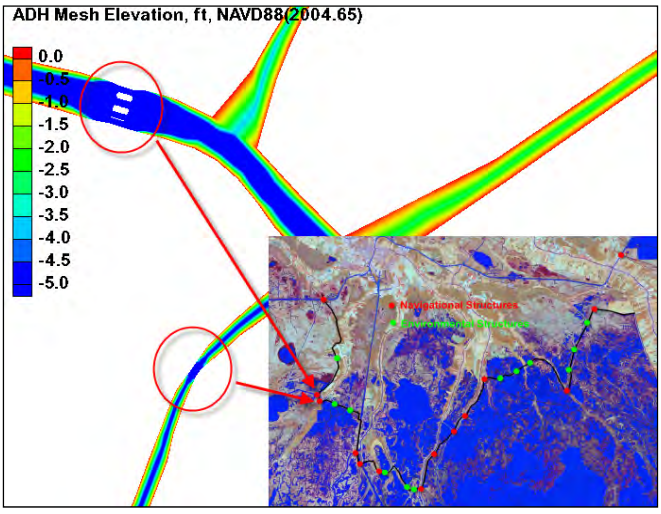

Figure 64. Model representation of the Falgout Canal and Bayou Dularge structures.

Two sets of nine culverts (6' x 6') are located along Falgout Canal. In the model, the two sets of culverts are represented as single culverts with widths of 54 ft and bottom elevations of -4.5 ft NAVD88(2004.65). This configuration is shown in Figure 65.

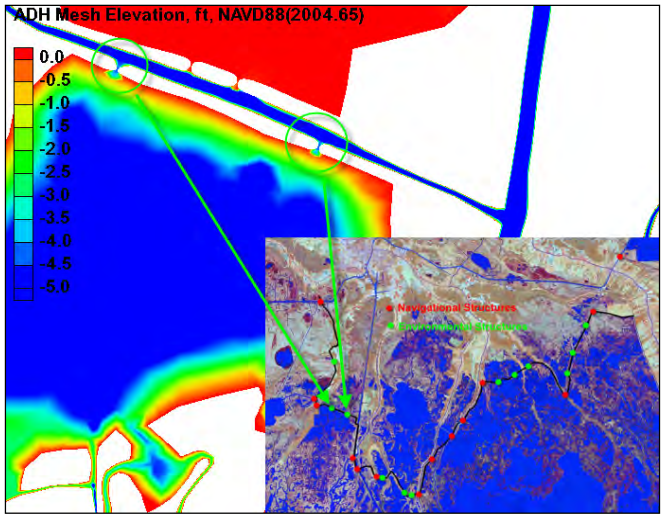

Figure 65. Model representation of the two sets of culverts located along Falgout Canal.

The Bayou Grand Caillou structure, shown in Figure 66 in the top circle, consists of three 46' sluice gates and one 56' sector gate possessing bottom elevations of -12 ft, NAVD88(2004.65). The Houma Navigation Canal structure consists of a 250-ft-wide structure and a 110-ft-wide lock, both with bottom elevations of -23 ft, NAVD88(2004.65). The -23 ft bottom elevation for this structure is based on the 50% Plans and Specifications (P&S) for the Houma Navigational Canal. The Houma Navigational Canal structure will also consist of ten 10-ft-wide sluice gates, each with a 5-ft vertical opening (from -2 ft to -7 ft NAVD88(2004.65). Four of these sluice gates will be located on the eastern side of the structure and four on the western side of the structure. Two will be located between the lock and the sector gate structures. This configuration can be observed in Figure 66.

The structure located on Bayou Fourpoints (red circle on left in Figure 67) had a 30-ft sector gate with a -8 ft NAVD88(2004.65) bottom elevation. It should also be noted that two existing earthen plugs were removed and another plug was installed farther to the north as described in Permit MVN-2008-518-CT (U.S. Army Corp of Engineers 2008). A set of six culverts (6' x 6') are located just east of Bayou Fourpoints (green circle in Figure 67). This structure was represented as a single culvert with a 36-ft width and a bottom elevation of -4.5 ft, NAVD88(2004.65).

The left circle in Figure 68 is a single culvert with a width of 6-ft and a bottom elevation of -4.5 ft, NAVD88(2004.65). Another set of six 6-ft-wide culverts are shown in Figure 68 (right circle). This culvert set also has a bottom elevation of -4.5 ft, NAVD88(2004.65).

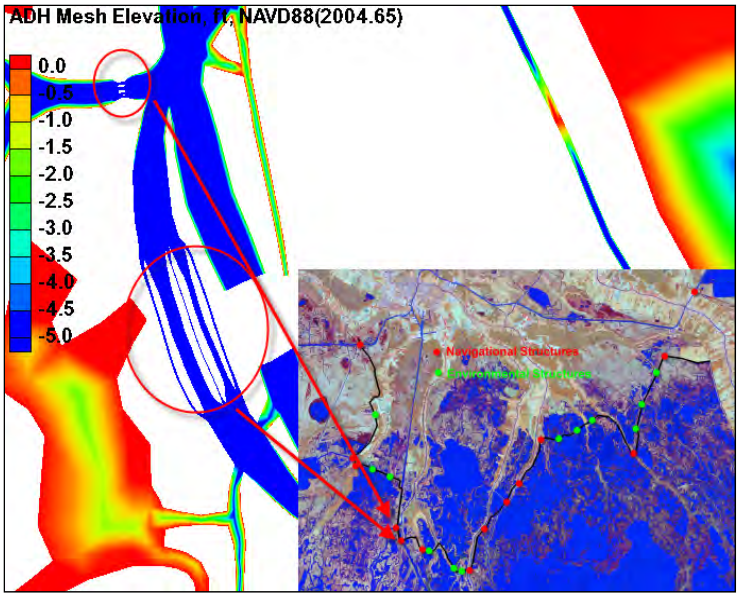

Figure 66. Model representation of the Bayou Grand Caillou structure and the Houma Navigational Canal structure and lock.

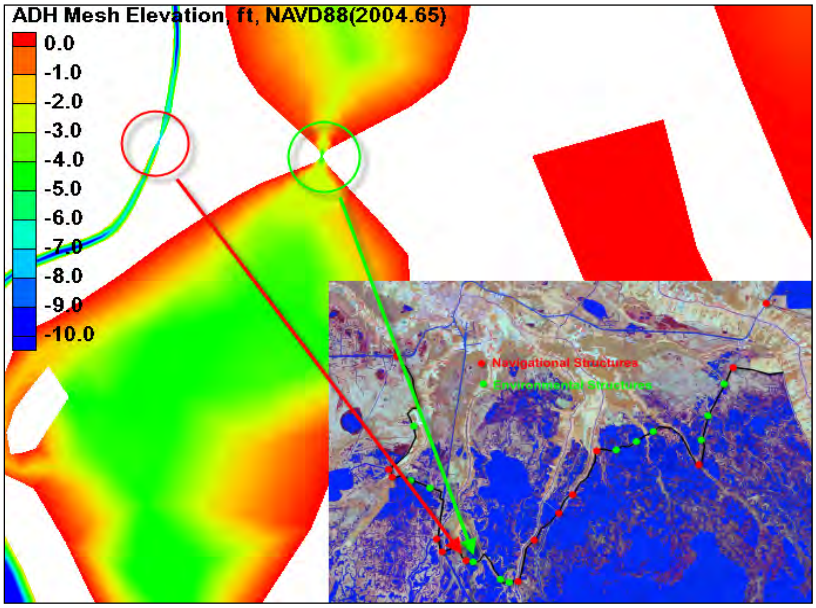

Figure 67. Model representation of the Bayou Fourpoints structure and one culvert set.

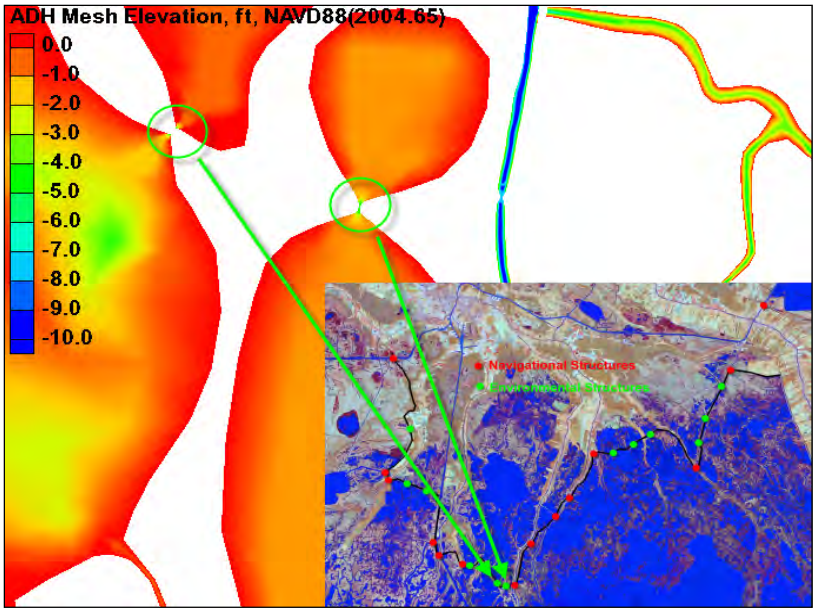

Figure 68. Two culvert sets west of Bayou Petit Caillou.

The Bayou Petit Caillou structure shown in Figure 69, is a 56-ft-wide sector gate with two 46-ft-wide sluice gates with bottom elevations of -8 ft, NAVD88(2004.65).

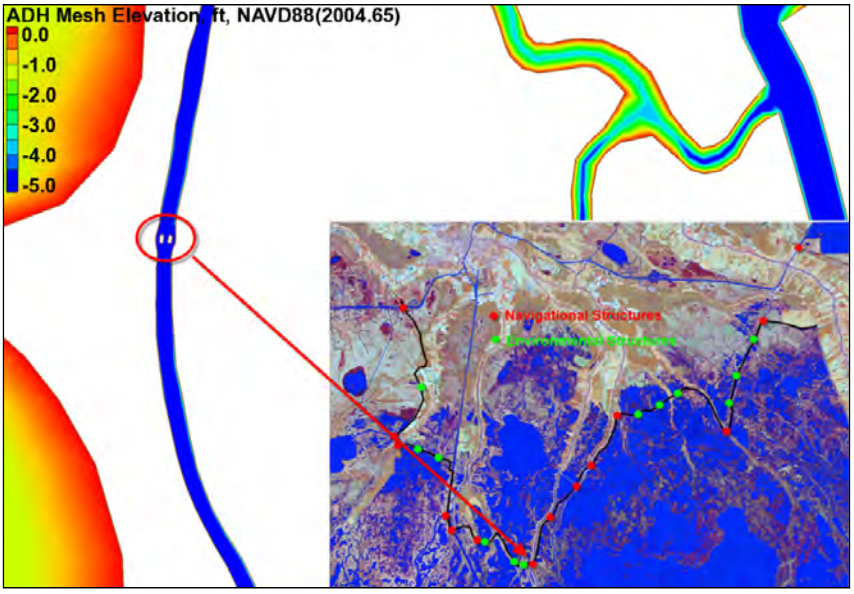

Figure 69. Model representation of the Bayou Petit Caillou structure and the Lapeyrouse Canal closure.

The Placid Canal structure, shown in Figure 70, consists of one 56-ft sector gate and two 46-ft wide sluice gates with a bottom elevation of -8 ft, NAVD88(2004.65).

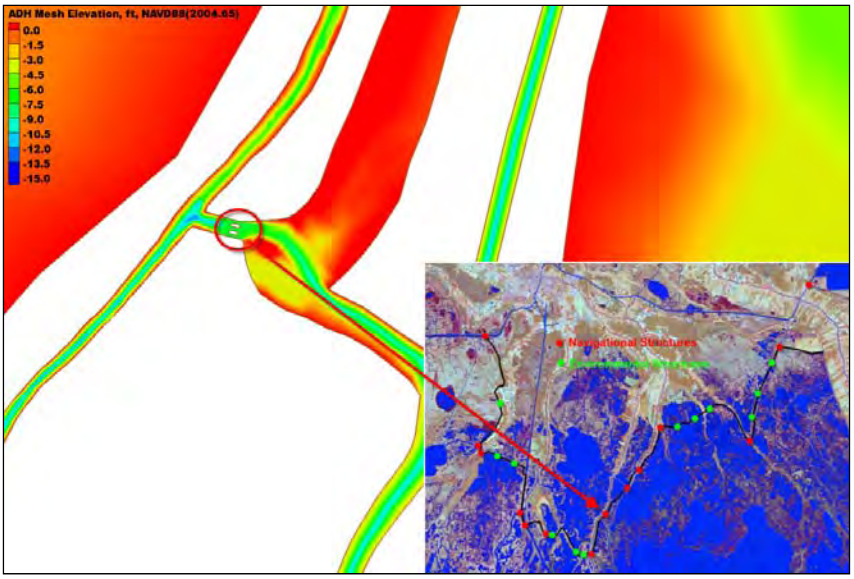

Figure 70. Model representation of the Placid Canal structure.

The Bush Canal structure, the lower circle shown in Figure 71, consists of three 46-ft sluice gates and one 56-ft sector gate. This structure had a bottom elevation of -12 ft, NAVD88(2004.65). The Bayou Terrebonne structure (upper circle) is a 56-ft sector gate with a bottom elevation of -9 ft, NAVD88(2004.65).

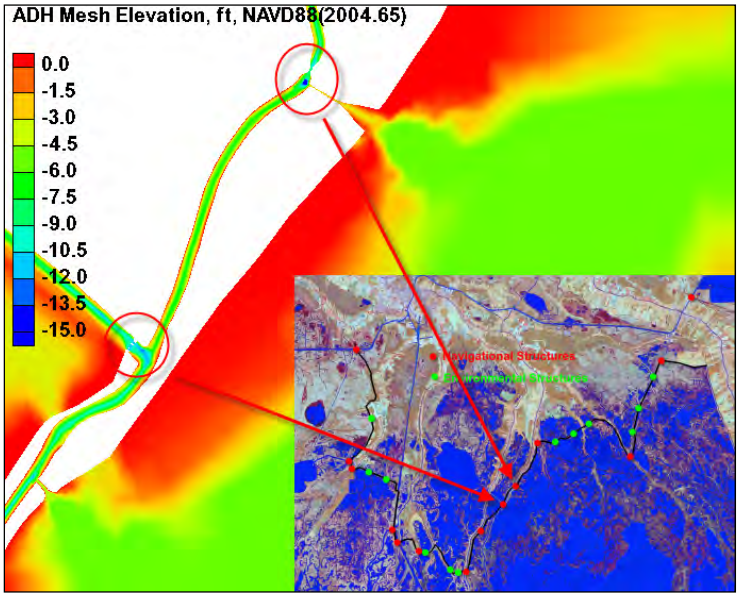

Figure 71. Model representation of the Bush Canal and Bayou Terrebonne structures.

The Humble Canal structure, shown in Figure 72, is a 56-ft sector gate with a bottom elevation of -9 ft, NAVD88(2004.65).

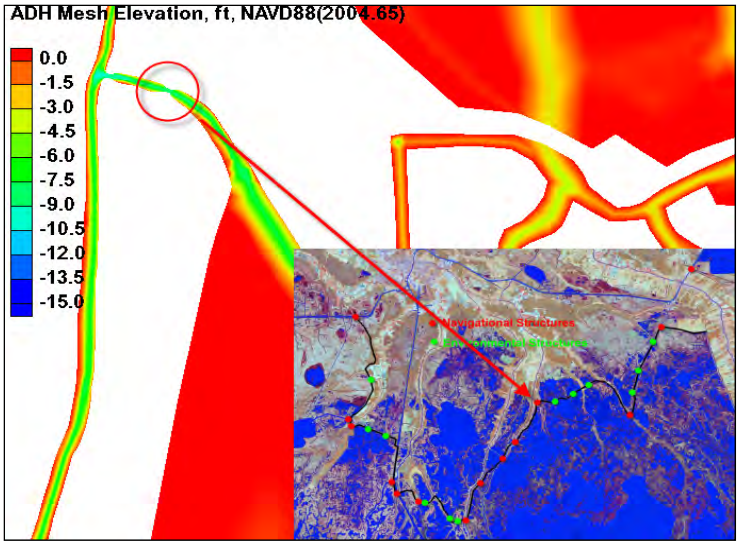

Figure 72. Model representation of the Humble Canal structure.

Shown in Figure 73 are three sets of culverts located in the Wonder Lake area (also known as the Montegut Wildlife Management Area). The left set of culverts consists of five 5' x 10' culverts which were represented in the model as having a width of 50-ft with a bottom elevation of -4.5 ft, NAVD88(2004.65). The center set of culverts consists of four 5' x 10' culverts which are represented in the model as having a width of 40 ft and a bottom elevation of -4.5 ft, NAVD88(2004.65). The right most set of culverts is a set of five 5' x 10' culverts located on the eastern part of Wonder Lake. This set had a width of 50 ft and a bottom elevation of -4.5 ft, NAVD88(2004.65).

The Pointe Aux Chenes structure, lower circle shown in Figure 74, has a 56-ft width with a bottom elevation of -6 ft, NAVD88(2004.65). Two 6' x 6' culverts, upper circle shown in Figure 74, located along Grand Bayou Canal were represented as a single culvert with a width of 12 ft and a bottom elevation of -4.5 ft, NAVD88(2004.65).

Two sets of two 6' x 6' culverts are shown in Figure 75. These two culvert sets were represented in the model as single culverts with widths of 12 ft with bottom elevations of -4.5 ft, NAVD88(2004.65).

Figure 76 is the structure located on Grand Bayou. This structure has a 56- ft-wide sector gate with two 46-ft-wide sluice gates with a bottom elevation of -9 ft, NAVD88(2004.65). The initial plan called for three sluice gates for this location but due to the width of the channel and the small measured discharges for this area only two were used for this plan configuration.

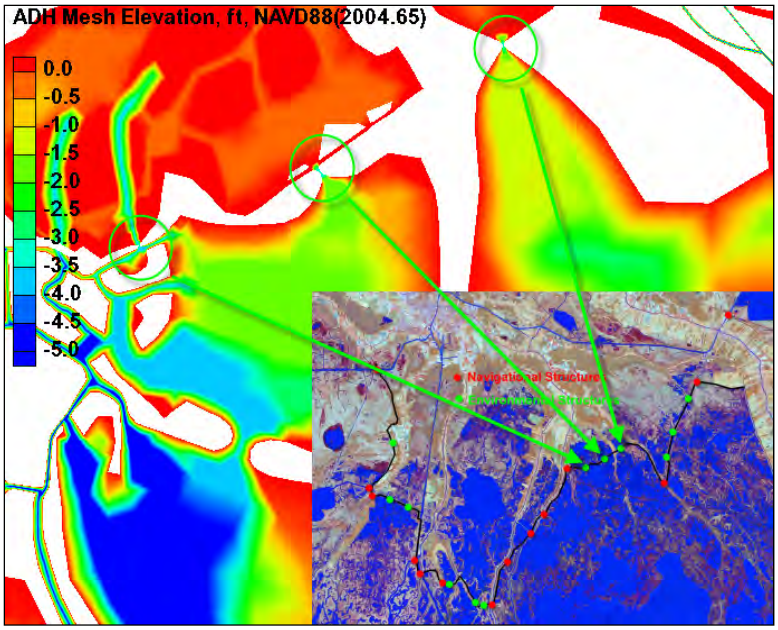

Figure 73. Model representation of the Wonder Lake (Montegut Wildlife Management Area) culvert configuration.

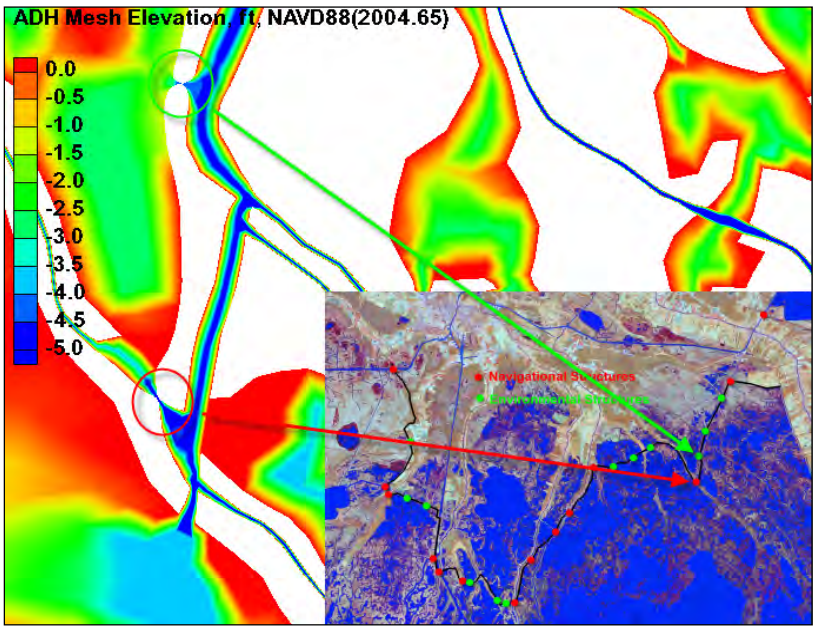

Figure 74. Model representation of the Pointe Aux Chenes structure and a culvert set.

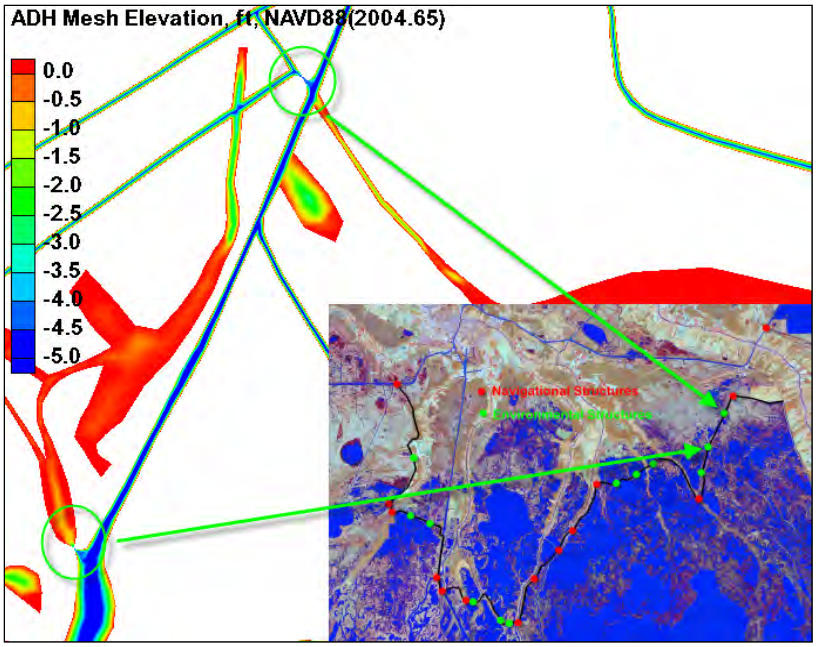

Figure 75. Model representation of the culvert sets connected to Grand Bayou.

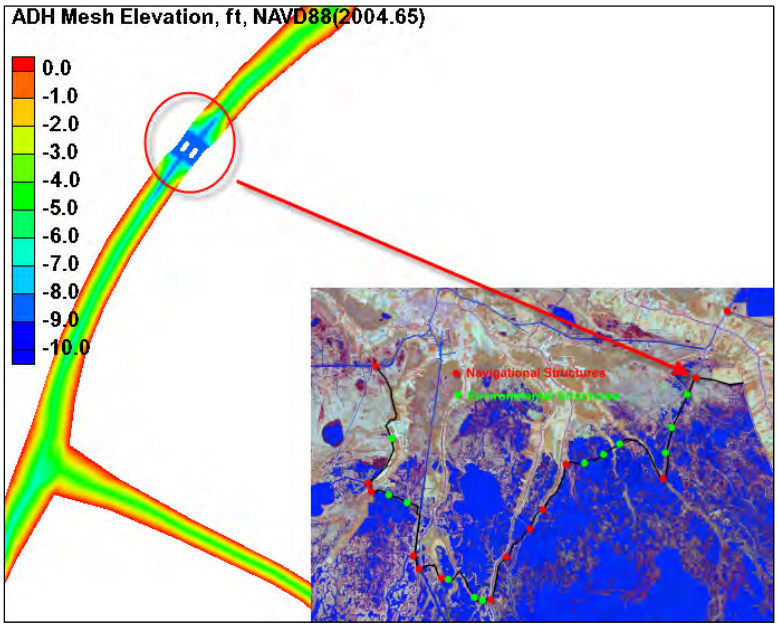

Figure 76. Model representation of the Grand Bayou structure.

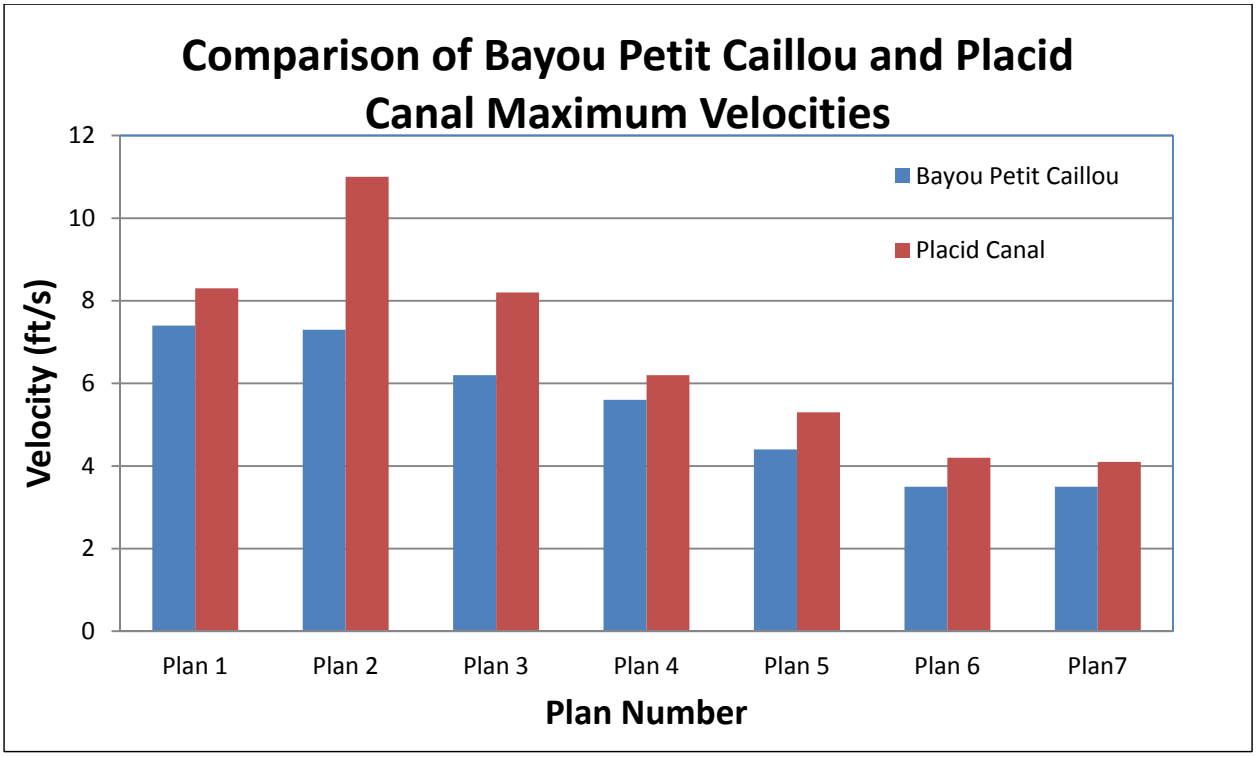

Figure 77. Comparison of Petit Caillou and Placid Canal maximum velocities.

7 Model Study Results

The plan simulations were performed using the same tidal, wind, and inflow forcing as the base validation time period. This should be a reasonably accurate representation of a normal fall time period with the occurrence of several frontal passage events. These frontal passages (approximately 2 per month from data observations) can produce significant increases and decreases in water level over a short period of time thereby creating higher velocities throughout the system. From observations of measured data, these types of metrological events are much less likely to occur during the summer months and therefore make the fall conditions more appropriate for these types of plan evaluations.

The inflow conditions for the western GIWW location are slightly higher than normal as this flow is directly related to the Atchafalaya River flow. The Atchafalaya River flow for this time period was approximately 450 kcfs (Wax Lake Outlet flow plus the Atchafalaya River at Morgan City flow) which is slightly less than the 10-year flow of 570 kcfs (FEMA 2010). From personal communication with Steve Ayres of the New Orleans District, it was determined that the flow for this time period was approximately a 2-year flow event. Therefore this flow event was a slightly higher than normal flow but not significantly so making it a good time period for this type of analysis.

A percentile analysis was performed on the base, Plan 6, and Plan 7 model simulations. Plots of the velocity exceedance values are presented in Figures 78 to 90 (line) and Figures 91 to 93 (bar) with water-surface elevation exceedance values (and differences) presented in Figures 94 to 111. This type of analysis prevents a biasing of the results by a single large event that investigation of the maximums alone would create. It should be noted that the model outputted velocities in these figures are for the sector gates only. The velocities through the sluice gates can be higher or lower than the ones shown in this section of the report.

Figure 78. Percentile analysis for the GIWW West of Houma structure.

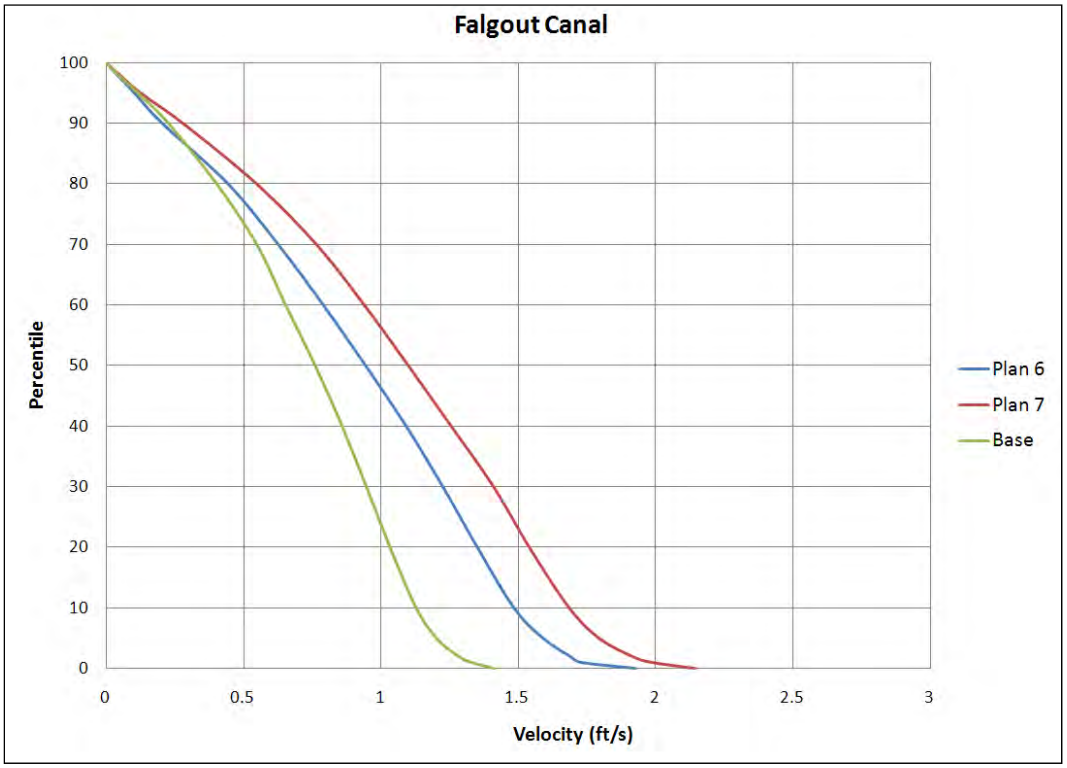

Figure 79. Percentile analysis for the Falgout Canal structure.

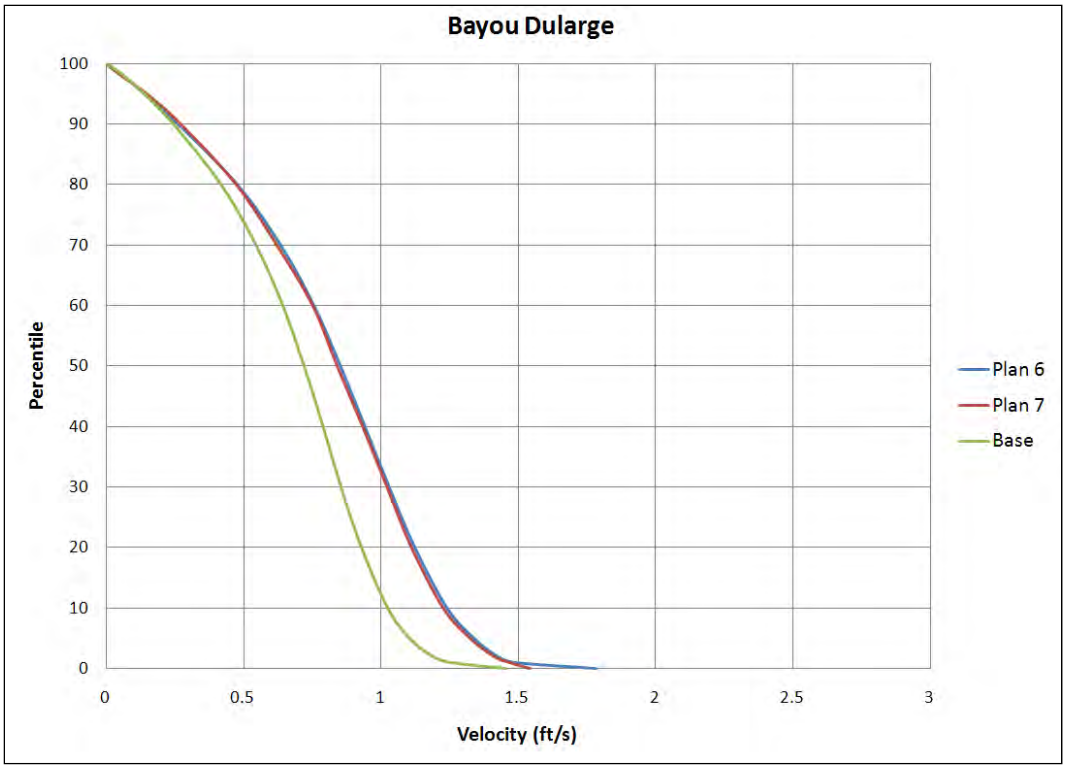

Figure 80. Percentile analysis for the Bayou Dularge structure.

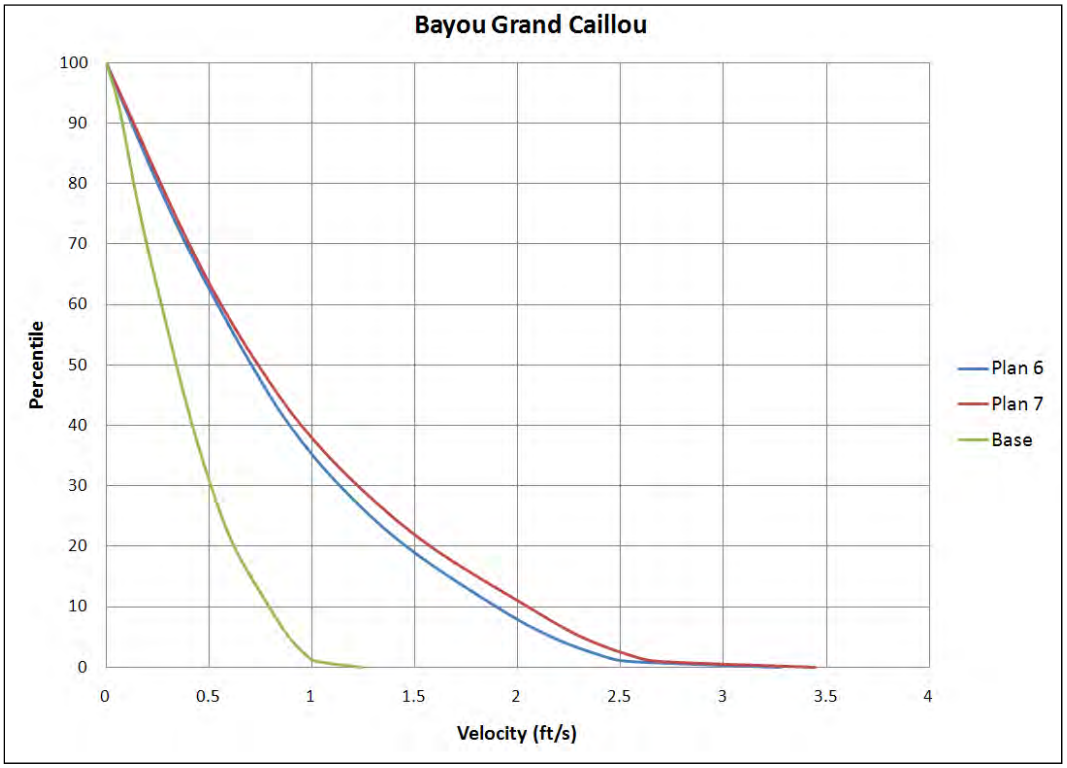

Figure 81. Percentile analysis for the Bayou Grand Caillou structure.

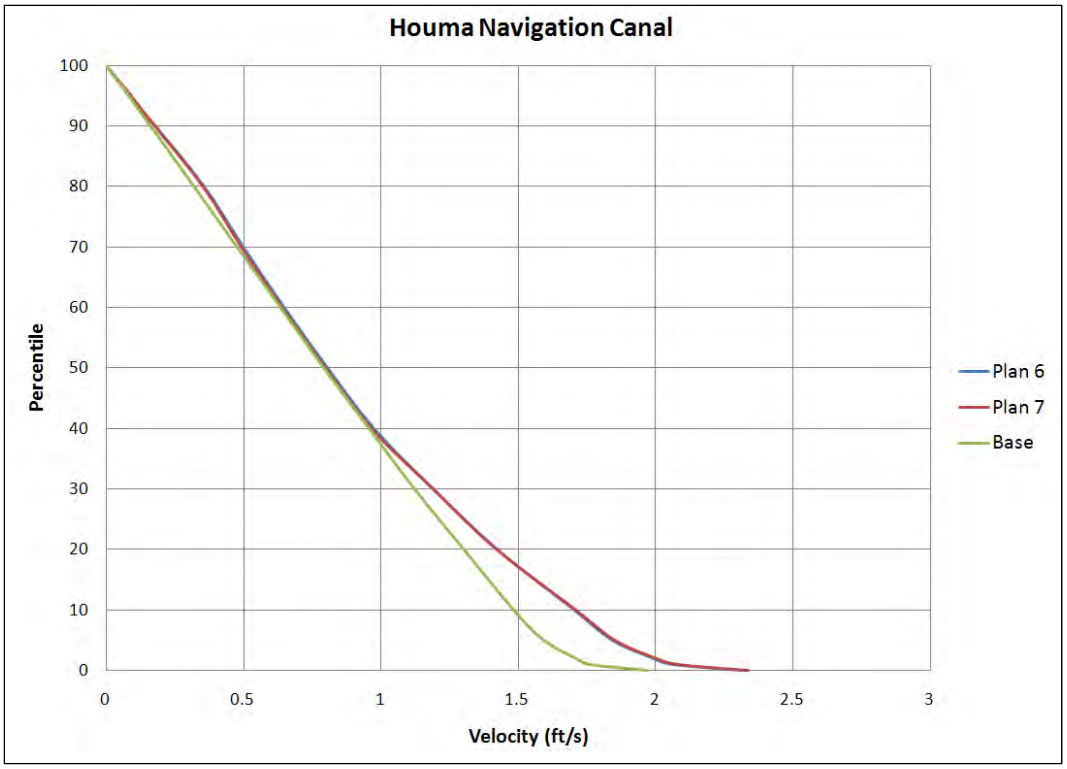

Figure 82. Percentile analysis for the Houma Navigation Canal structure.

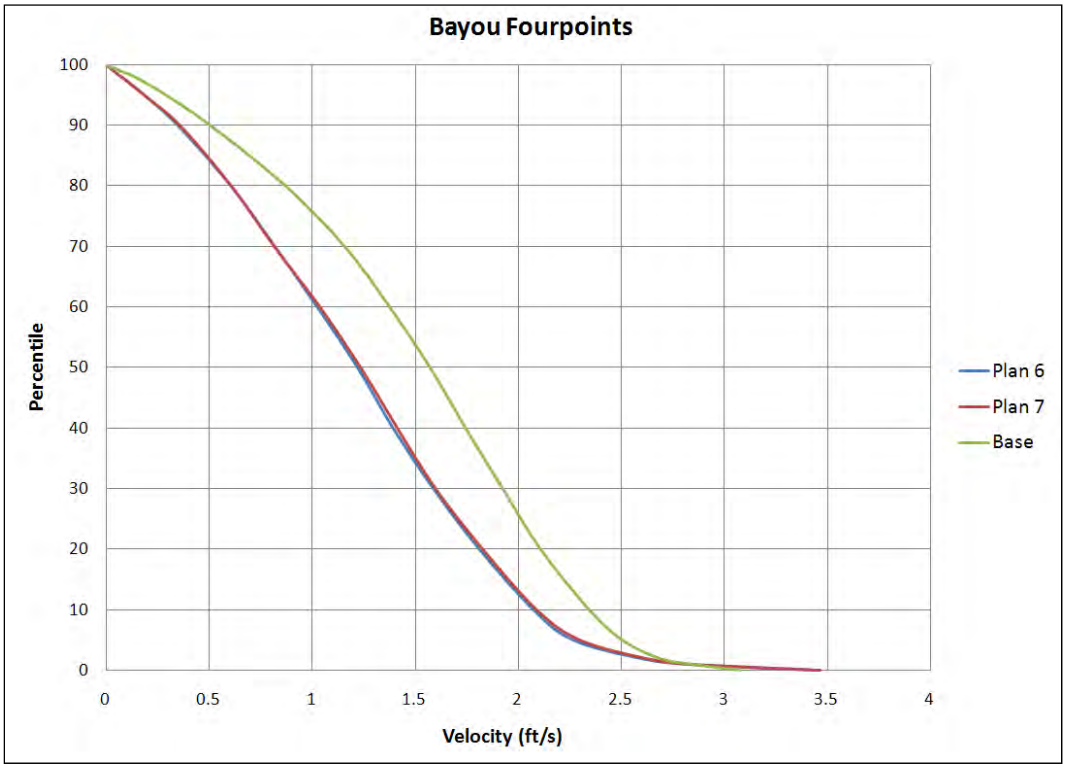

Figure 83. Percentile analysis for the Bayou Fourpoints structure.

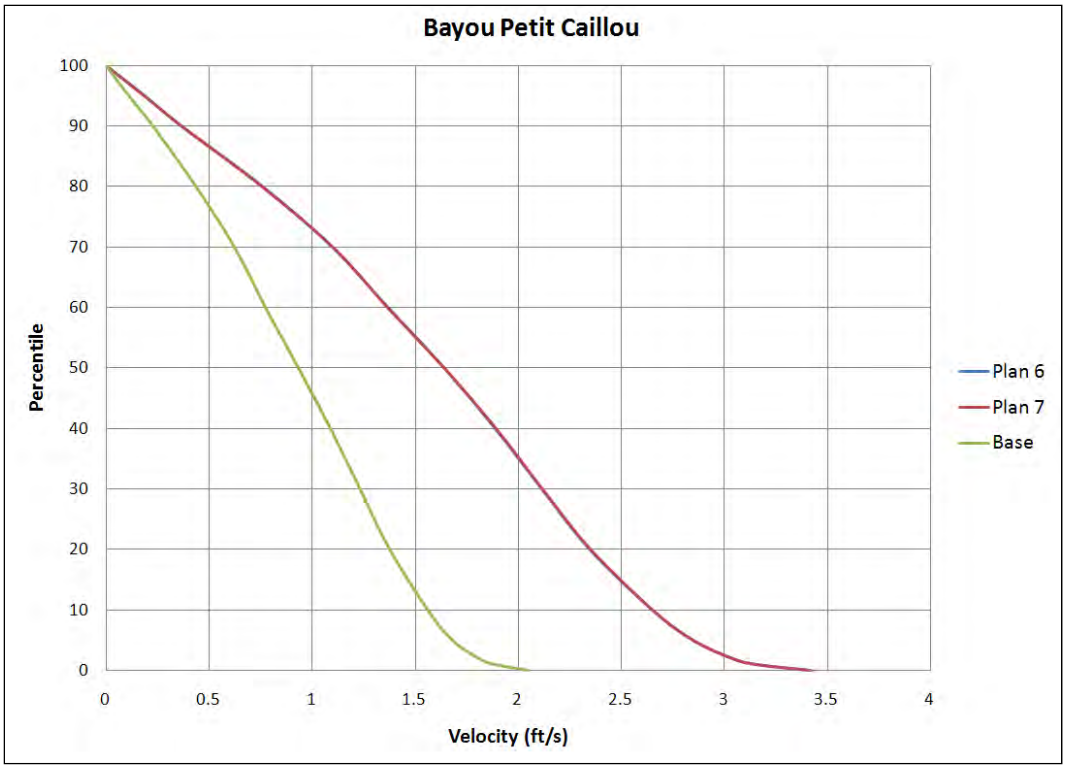

Figure 84. Percentile analysis for the Bayou Petit Caillou structure.

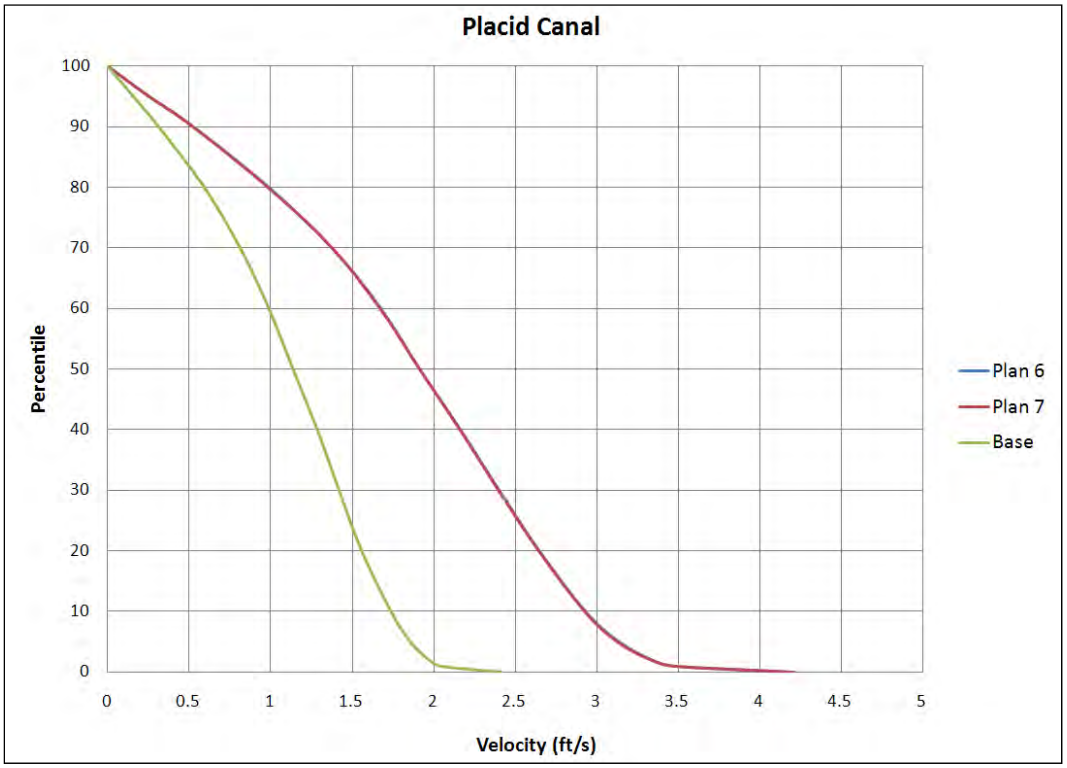

Figure 85. Percentile analysis for the Placid Canal structure.

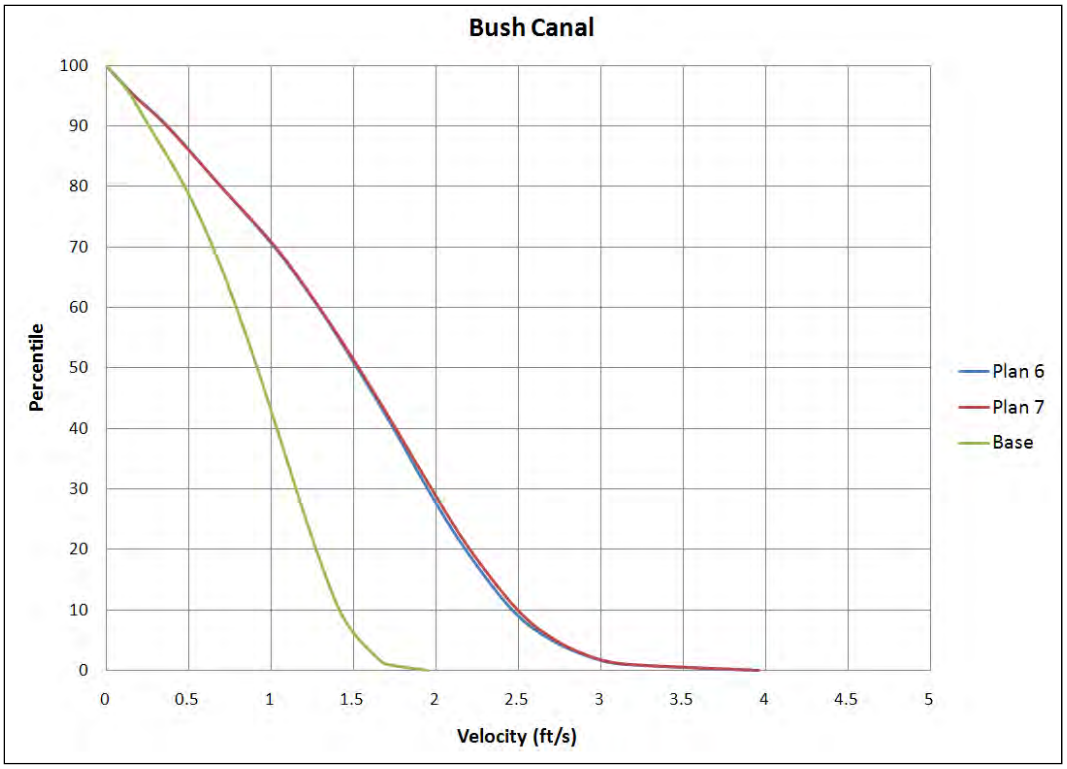

Figure 86. Percentile analysis for the Bush Canal structure.

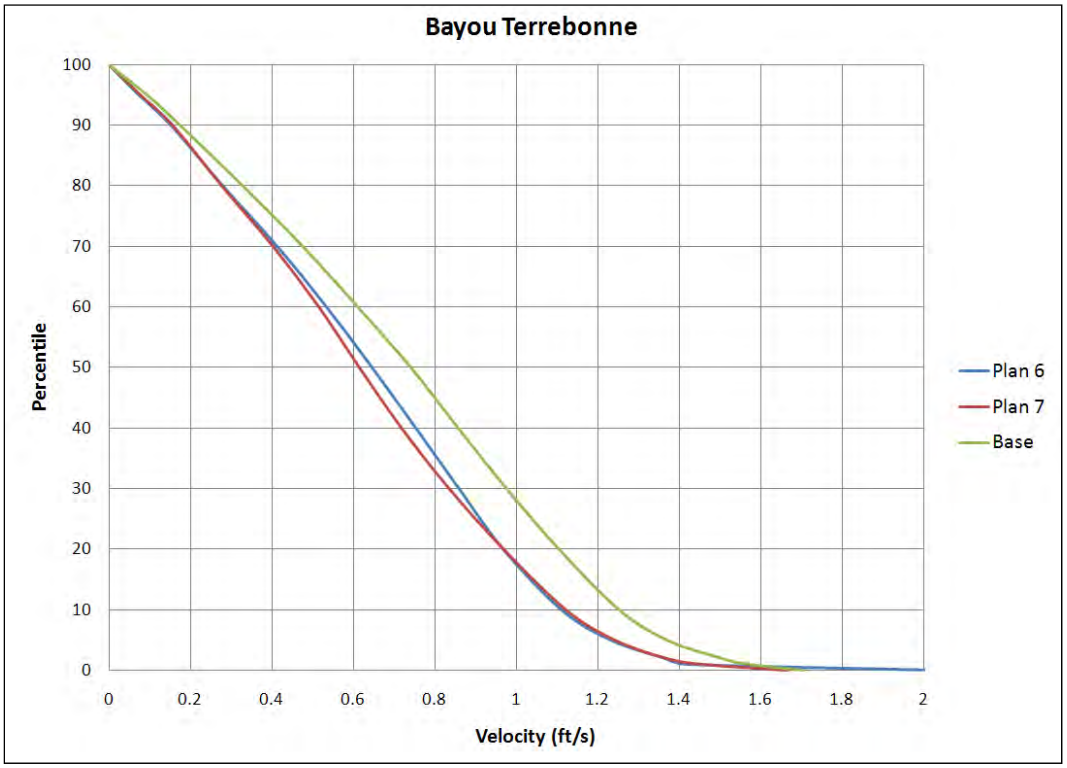

Figure 87. Percentile analysis for the Bayou Terrebonne structure.

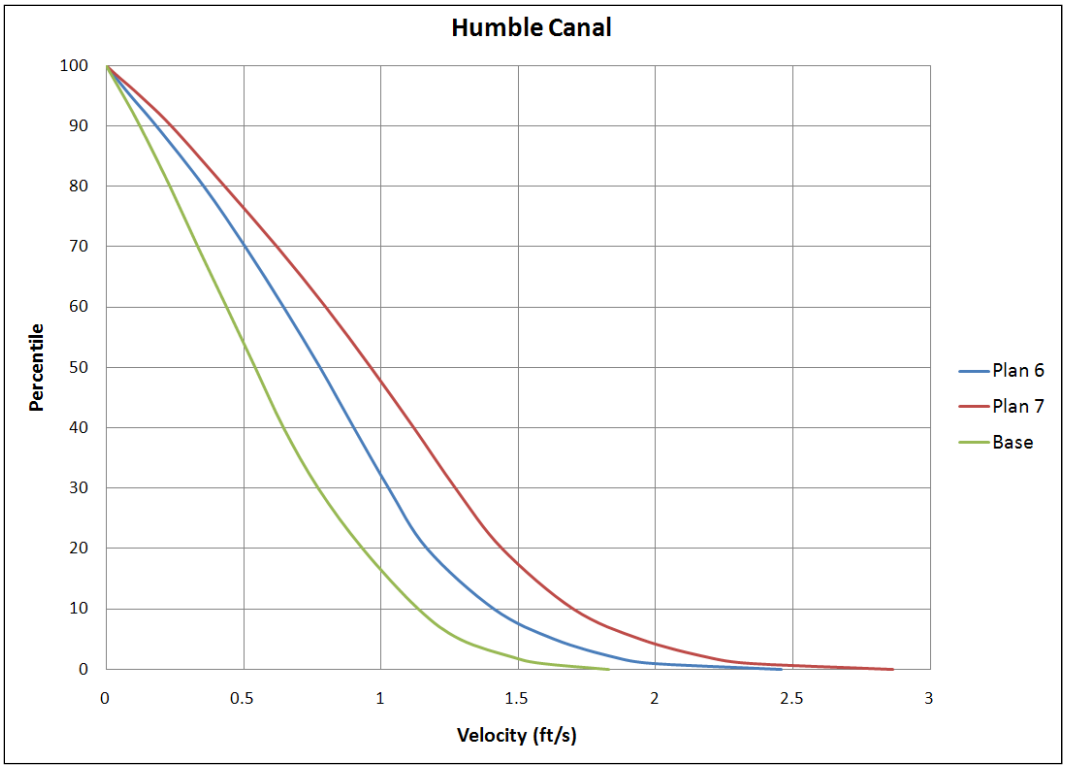

Figure 88. Percentile analysis for the Humble Canal structure.

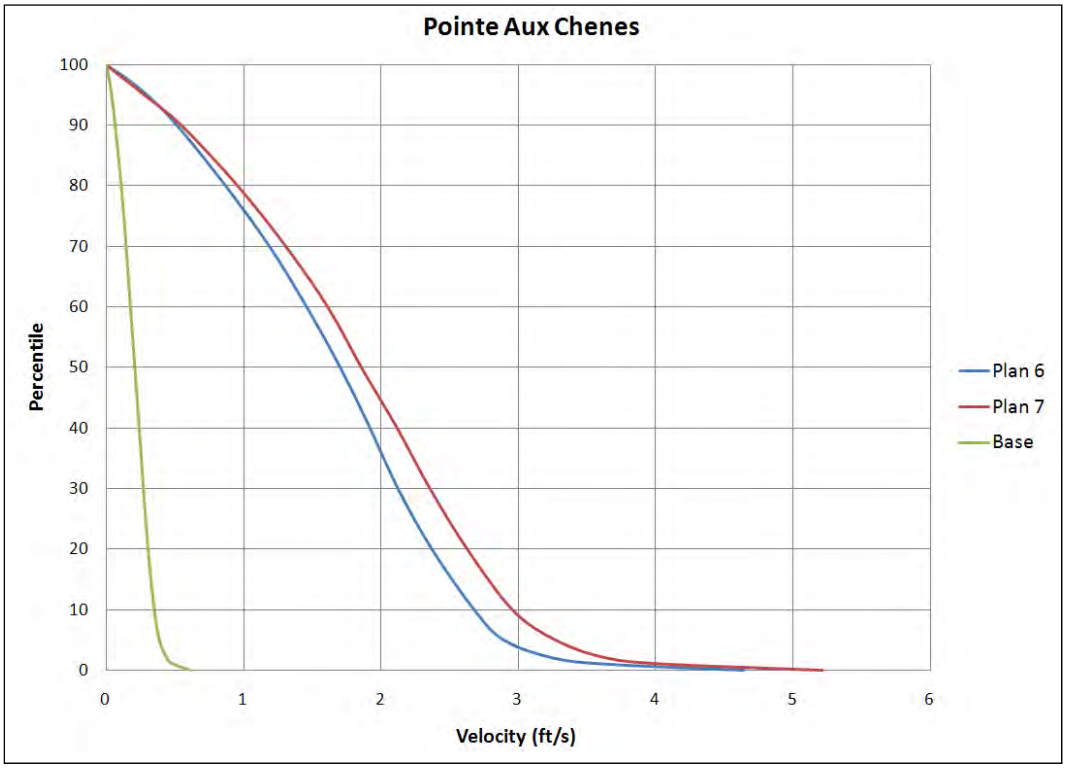

Figure 89. Percentile analysis for the Pointe Aux Chenes structure.

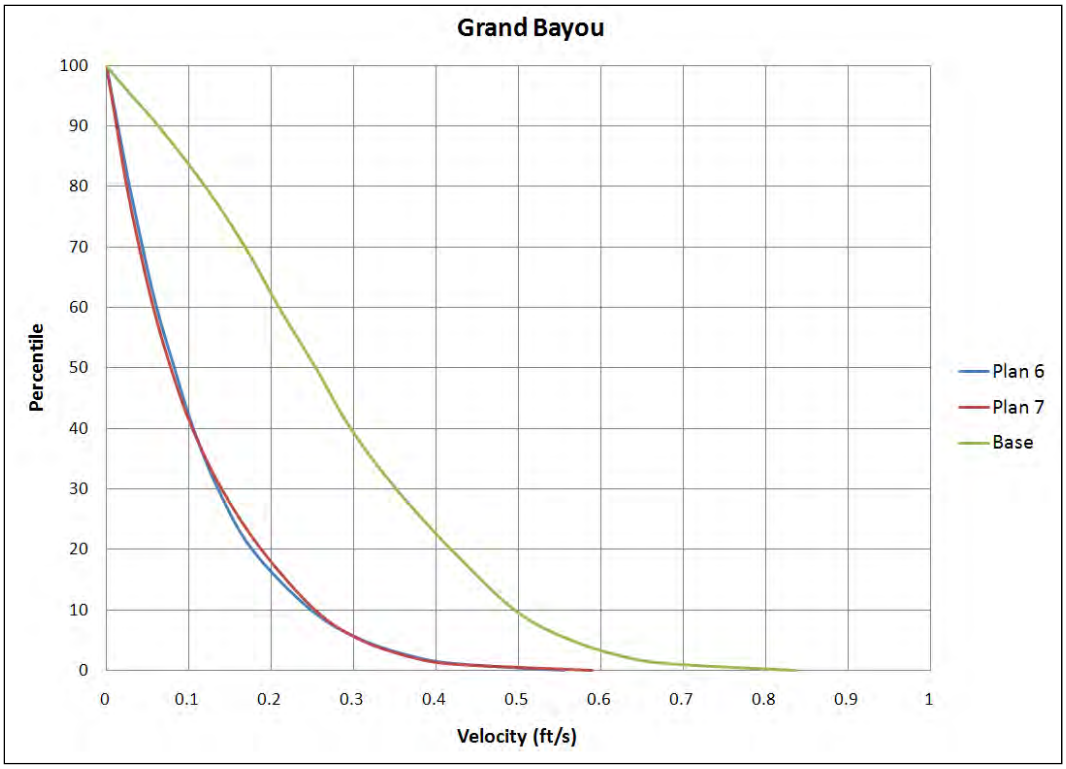

Figure 90. Percentile analysis for the Grand Bayou structure.

The exceedance plots are important in determining whether a structure's velocities are consistently increased or if the increase is primarily due to a few isolated events. The exceedance plot for the Houma Navigation Canal (Figure 82) indicates changes primarily due to isolated events since the velocity values are the same up to the 30 % and below values whereas the GIWW west of Houma exceedance plot, Figure 78, indicates a consistently higher velocity field. Knowledge about whether the velocity fields are altered consistently or just occasionally can be utilized to make inferences about possible impacts to navigation and/or fish behavior. If the changes to the velocity field are occasional then the impact to navigation and fish behavior would also only occur occasionally, but if the velocity field is consistently different then the impacts could extend for long periods of time.

Contour plots for each structure (for the base and Plan 6) are provided in Appendix B for the maximum, 10th percent exceedance (the velocity exceeds this value 10 % of the time) and the 50th percent exceedance (the velocity exceeds these values 50 % of the time) velocity magnitudes. Appendix C possesses comparison plots of the maximum flood and ebb velocity vectors for each structure for the Base and Plan 6 (environmental structures open).

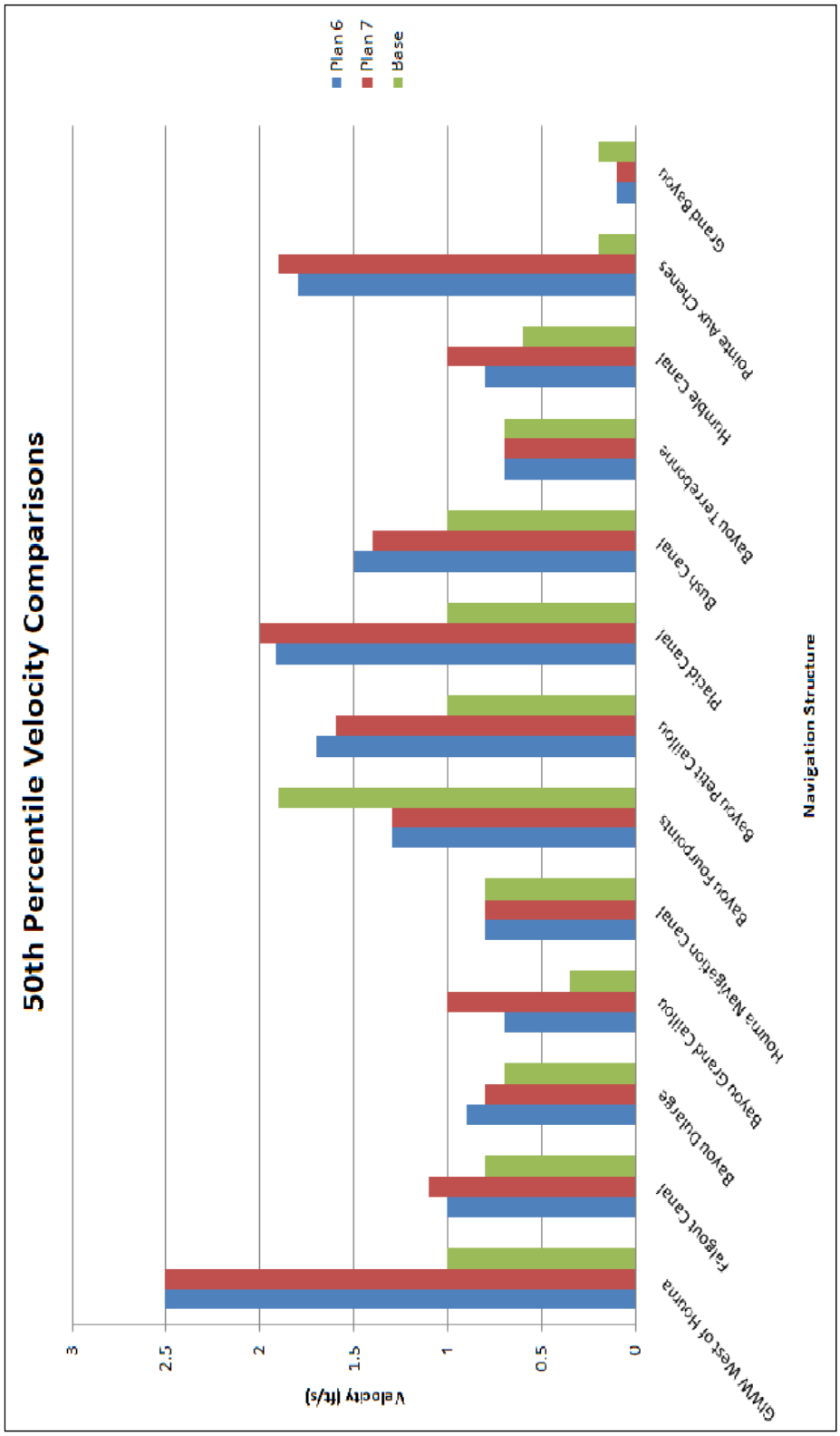

Figure 91. 50th Percent exceedance velocities for Plan 6, Plan 7 and base model simulations.

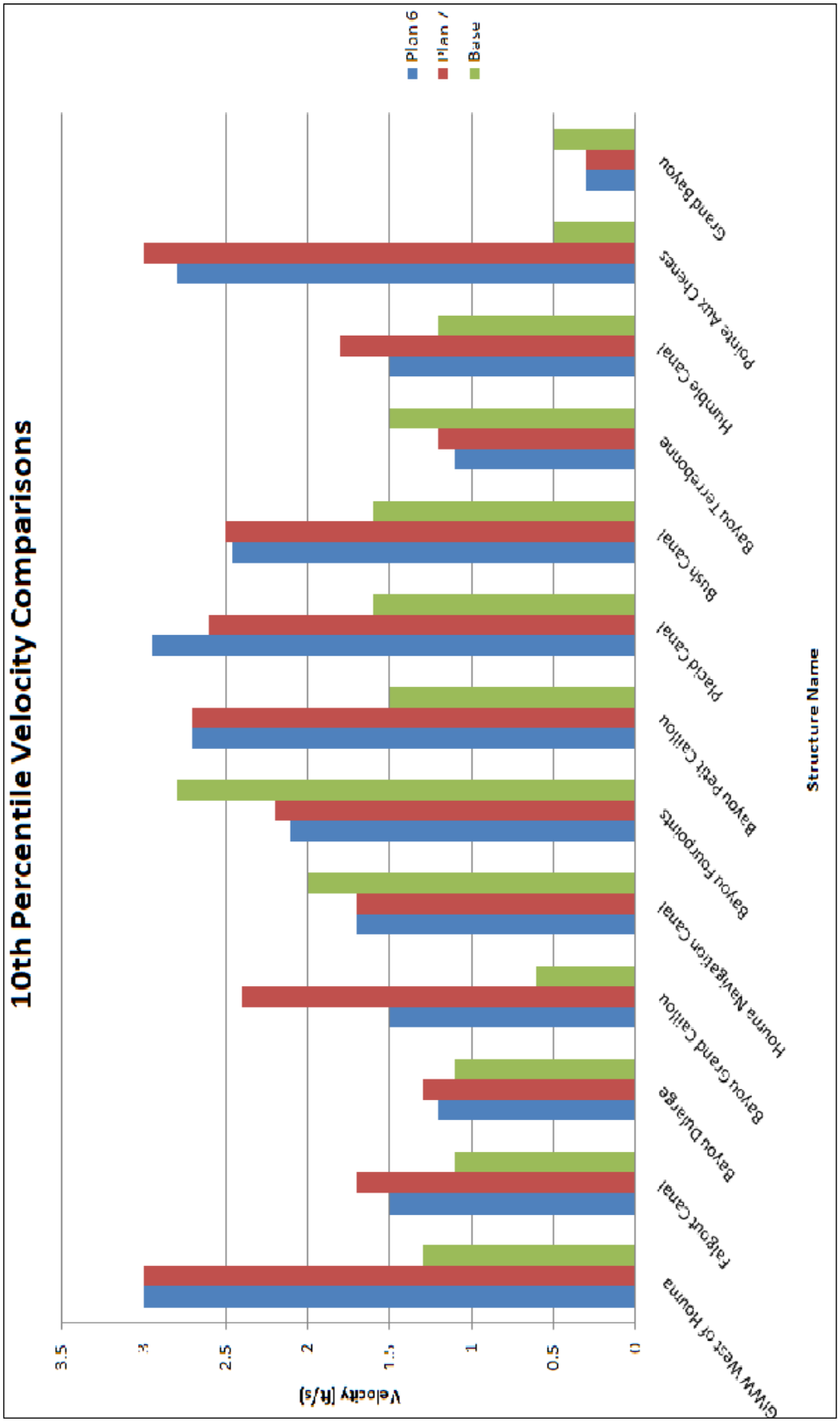

Figure 92. 10th Percent exceedance velocities for Plan 6, Plan 7 and base model simulations.

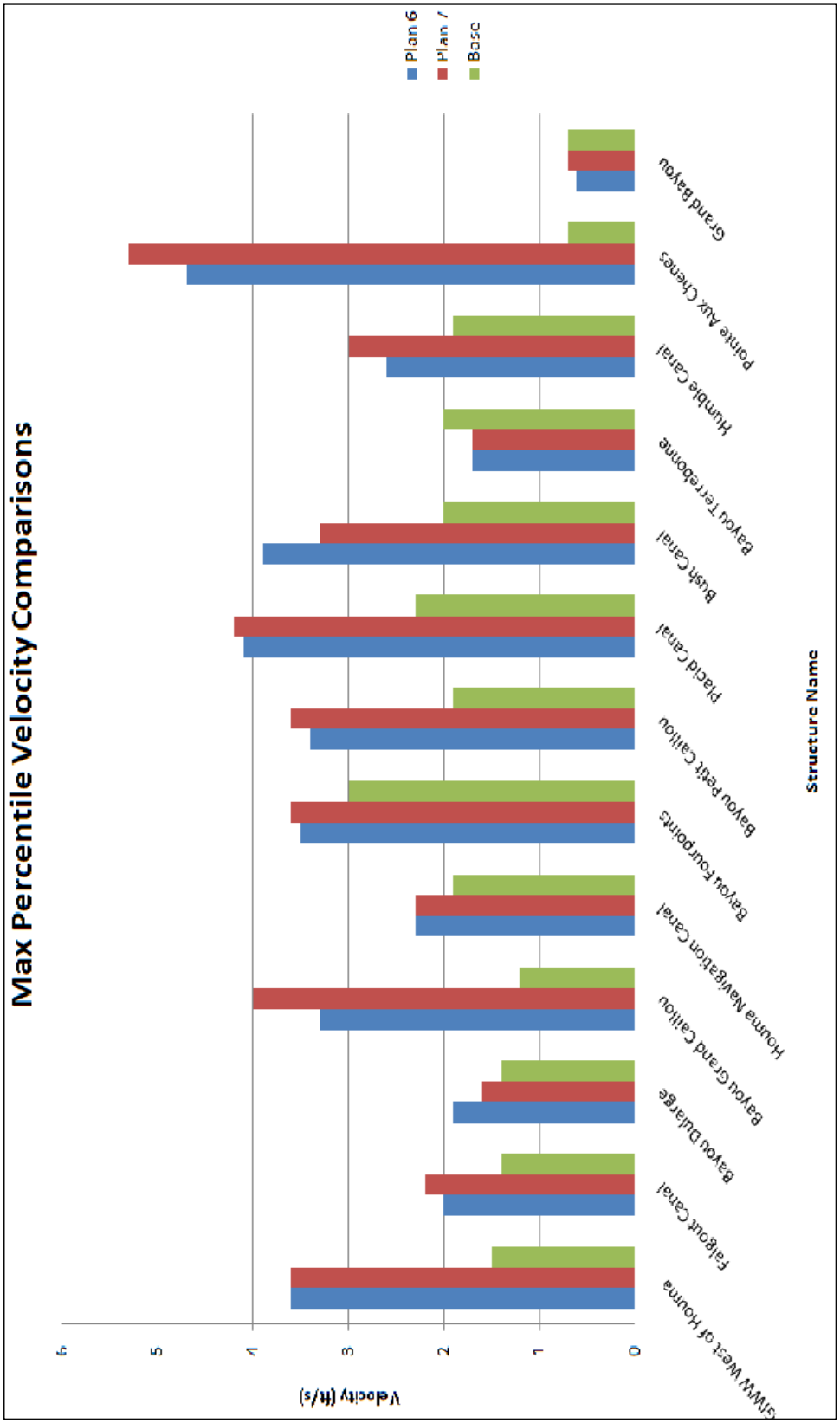

Figure 93. Maximum velocities for Plan 6, Plan 7 and base model simulations.

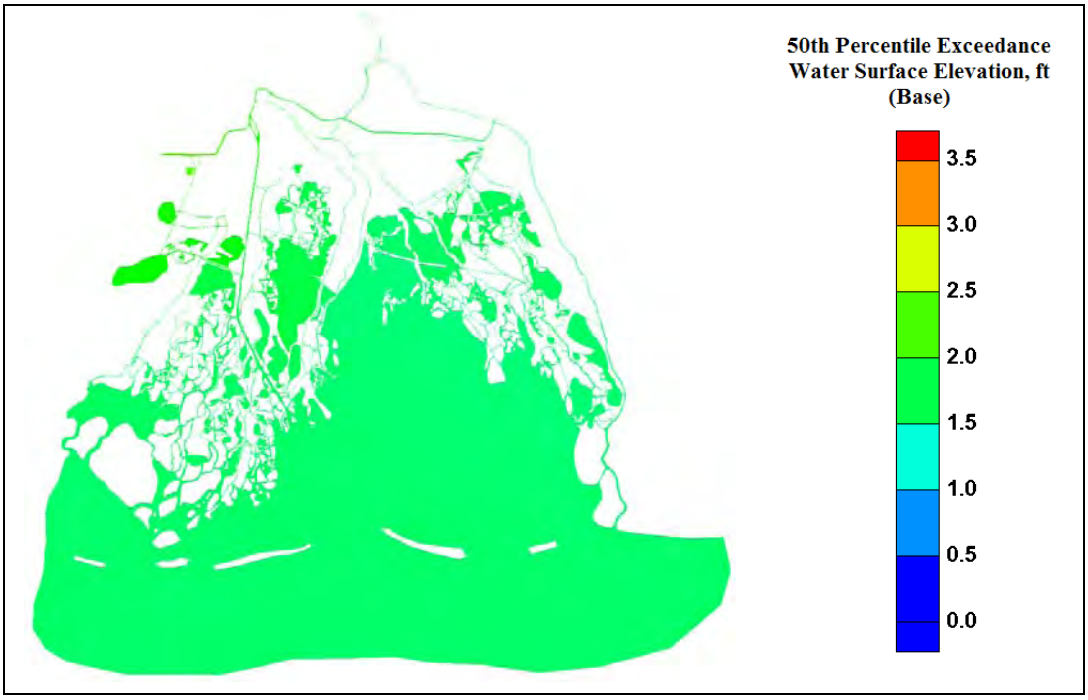

Figure 94. 50th Percentile exceedance water-surface elevation for the base conditions.

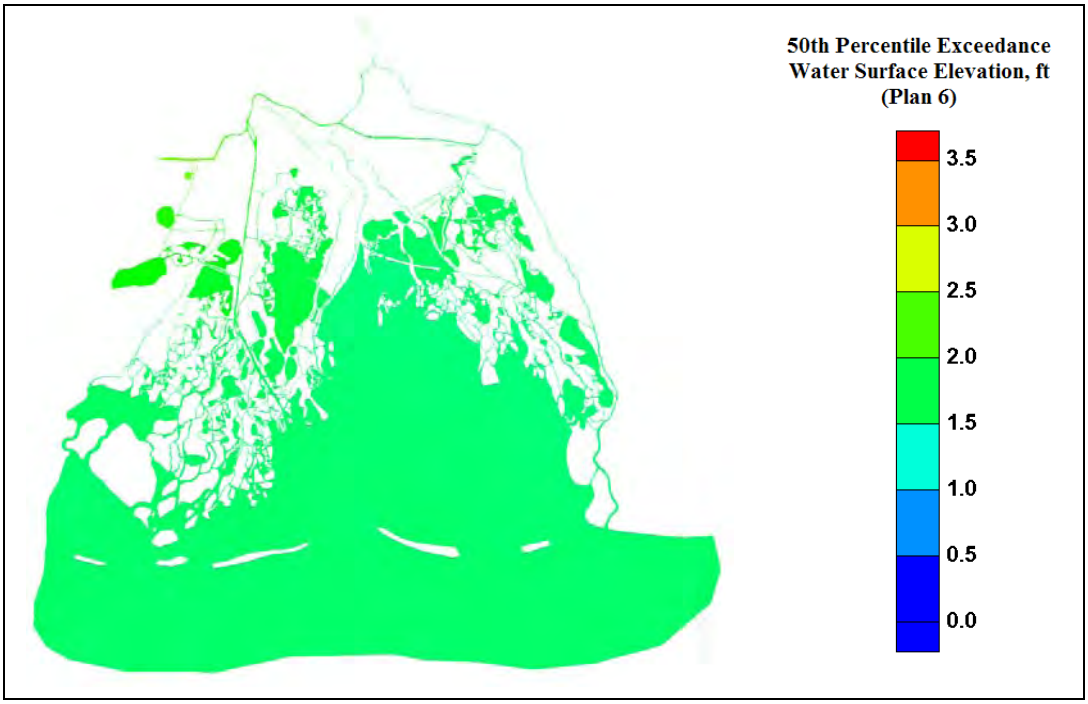

Figure 95. 50th Percentile exceedance water-surface elevation for the Plan 6 conditions.

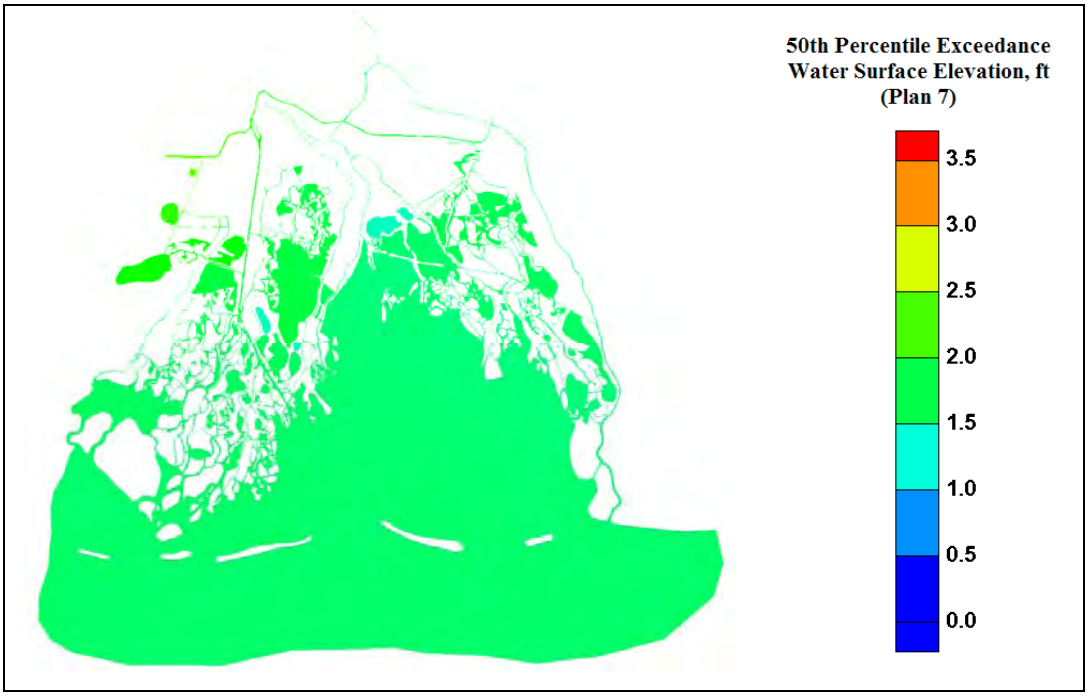

Figure 96. 50th Percentile exceedance water-surface elevation for the Plan 7 conditions.

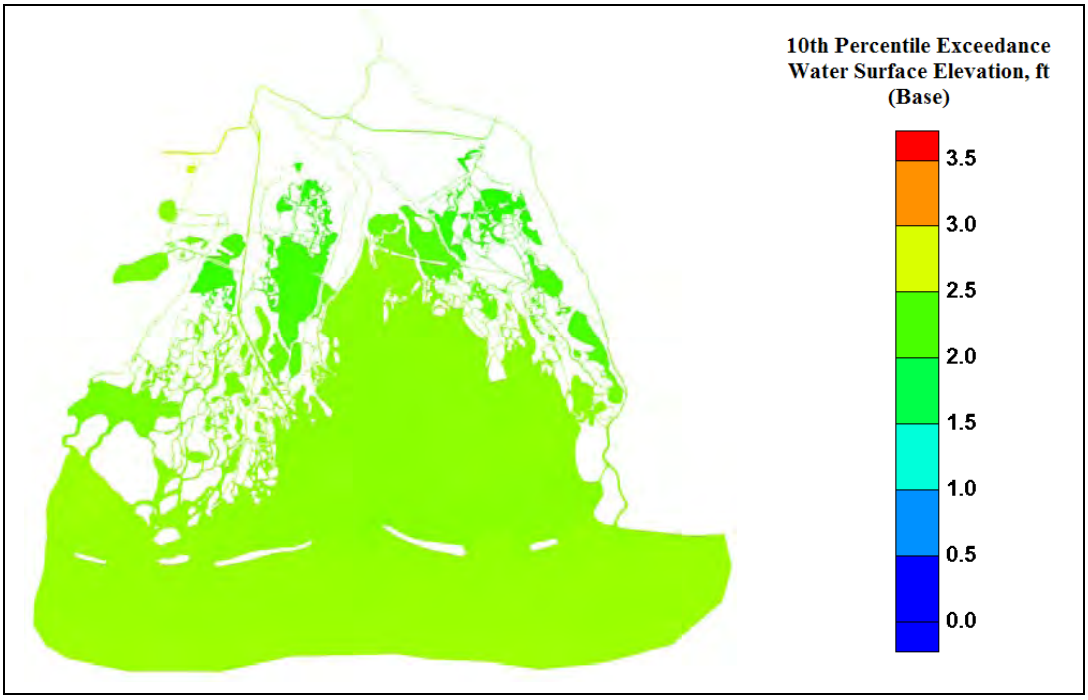

Figure 97. 10th Percentile exceedance water-surface elevation for the base conditions.

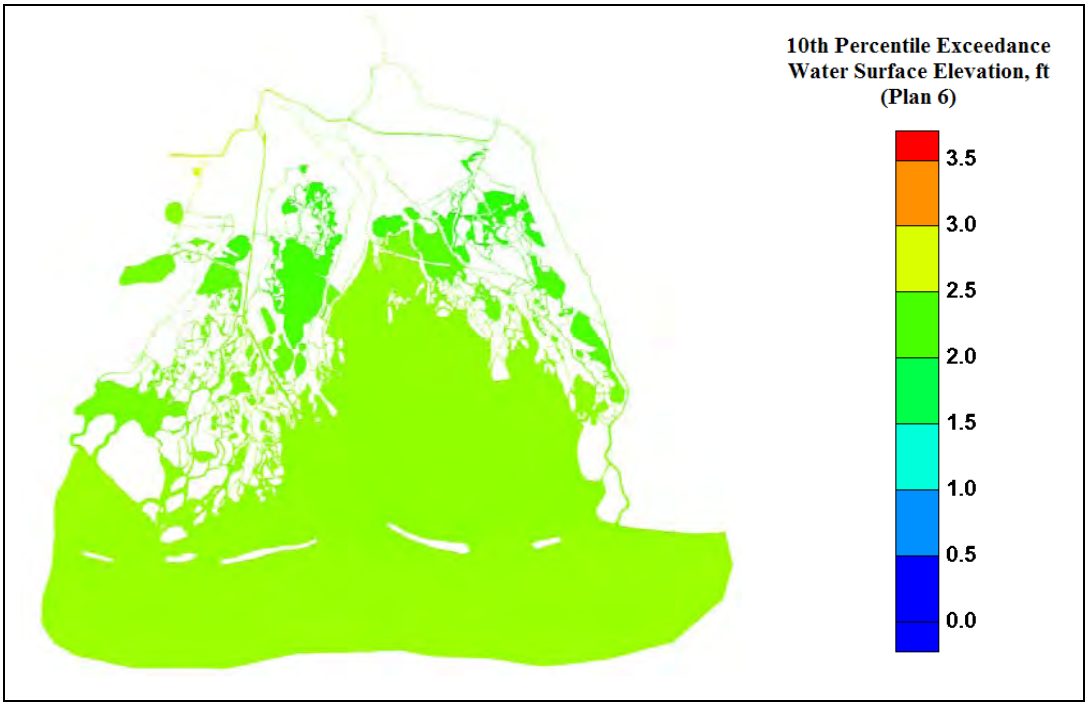

Figure 98. 10th percentile exceedance water-surface elevation for the Plan 6 conditions.

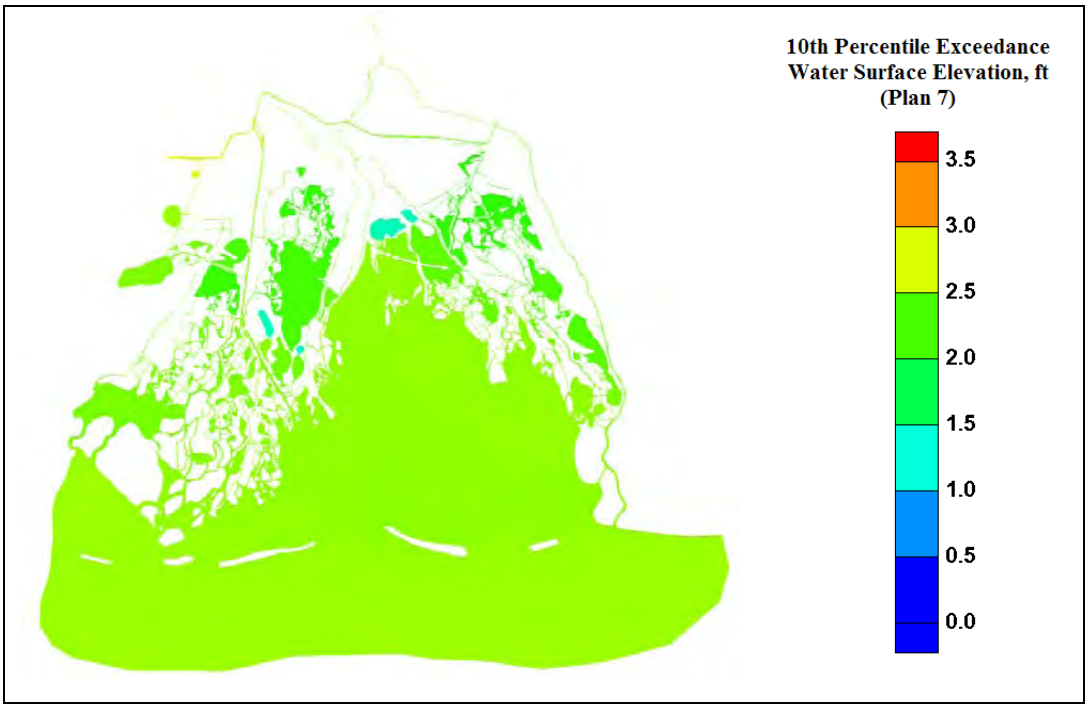

Figure 99. 10thpPercentile exceedance water-surface elevation for the Plan 7 conditions.

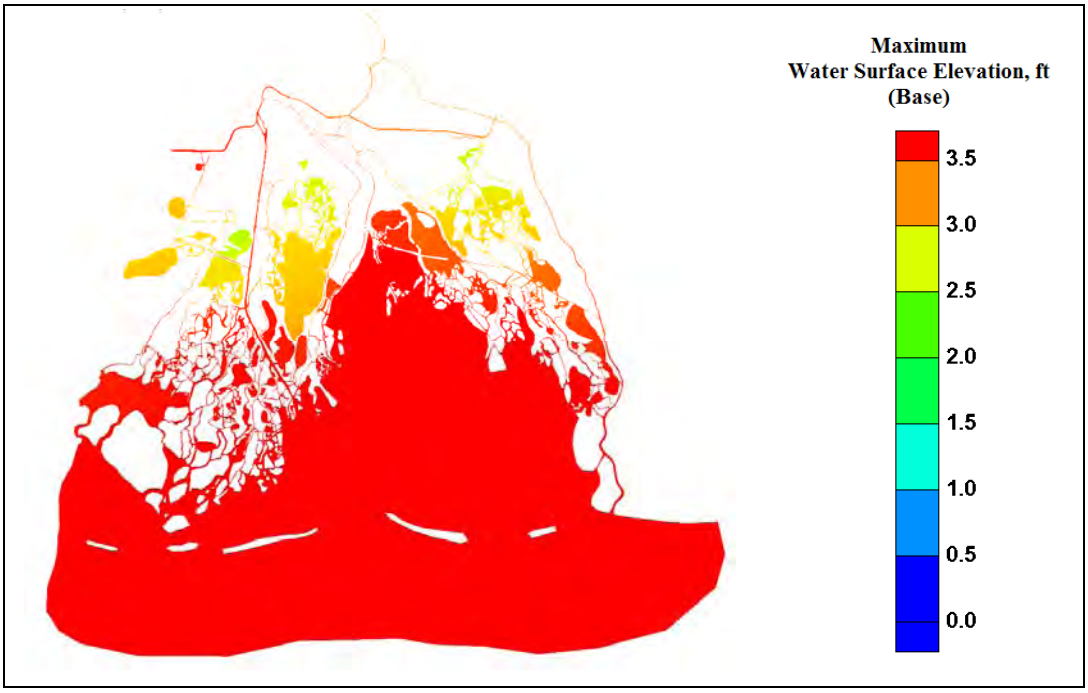

Figure 100. Maximum water-surface elevation for the base conditions.

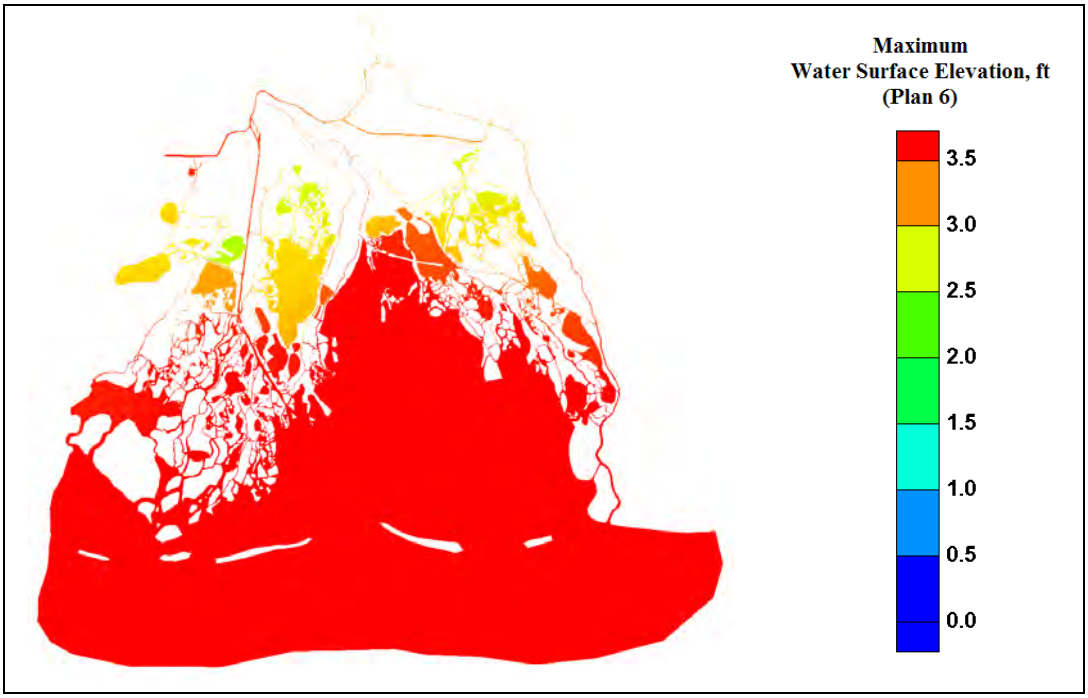

Figure 101. Maximum water-surface elevation for the Plan 6 conditions.

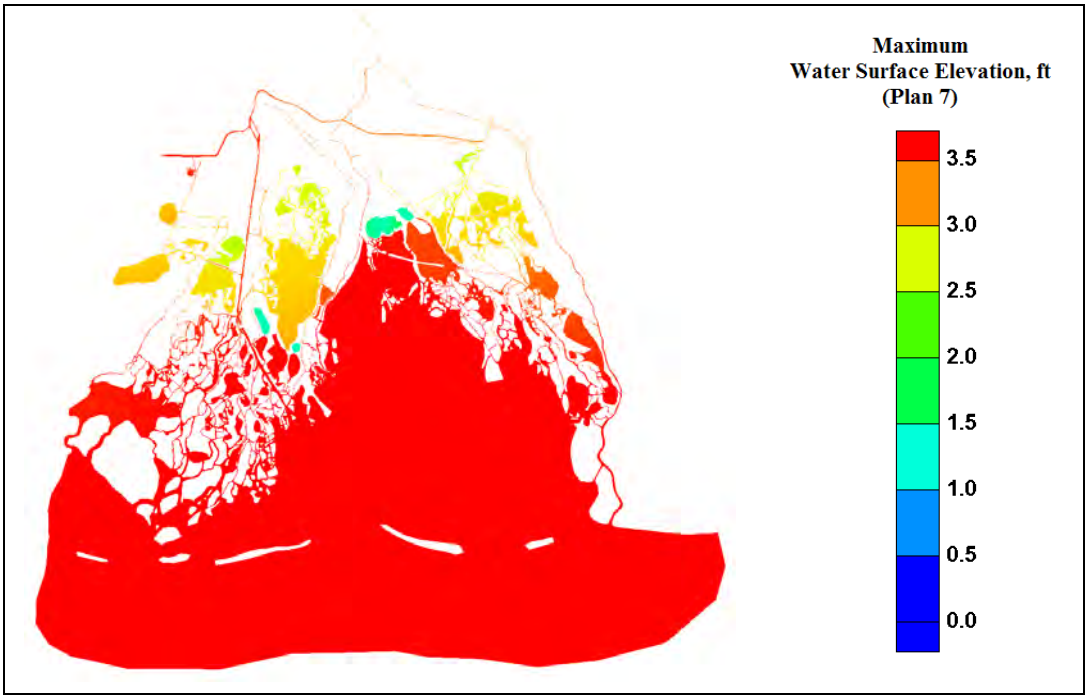

Figure 102. Maximum water-surface elevation for the Plan 7 conditions.

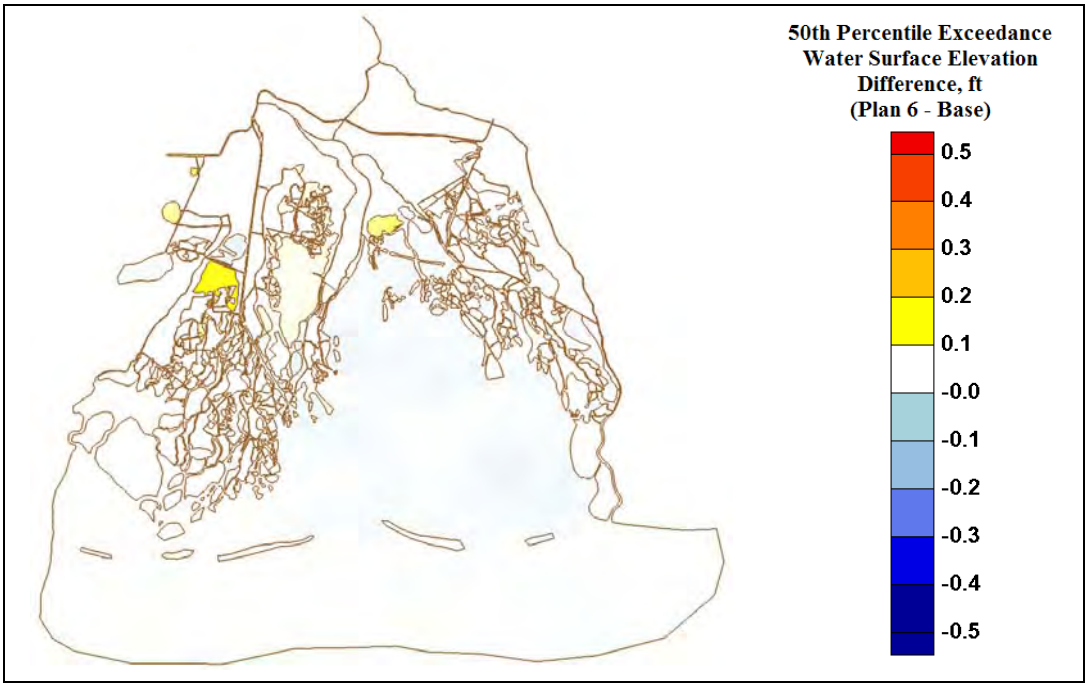

Figure 103. 50th percentile exceedance water level differences (Plan 6 – base).

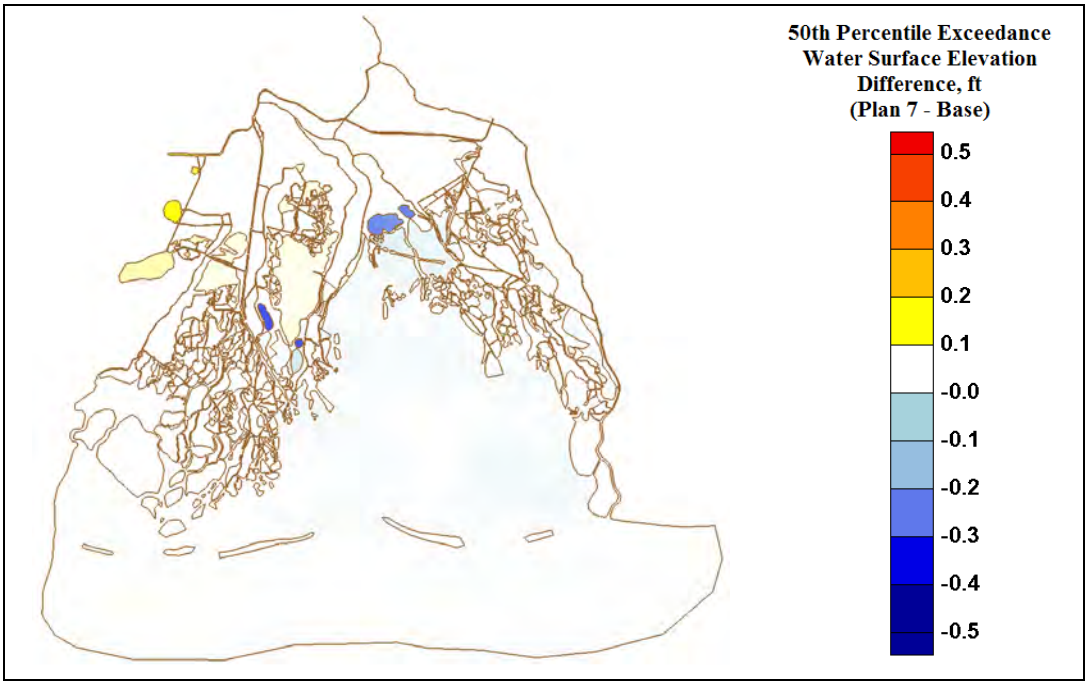

Figure 104. 50th percentile exceedance water level differences (Plan 7 – base).

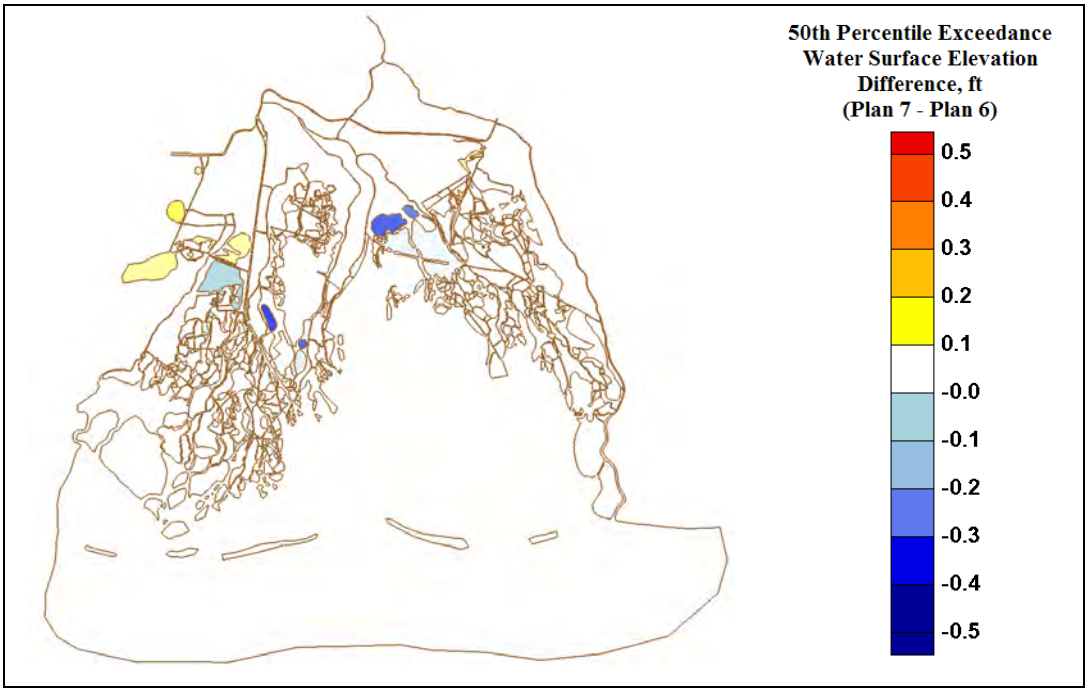

Figure 105. 50th Percentile exceedance water level differences (Plan 7 – Plan 6).

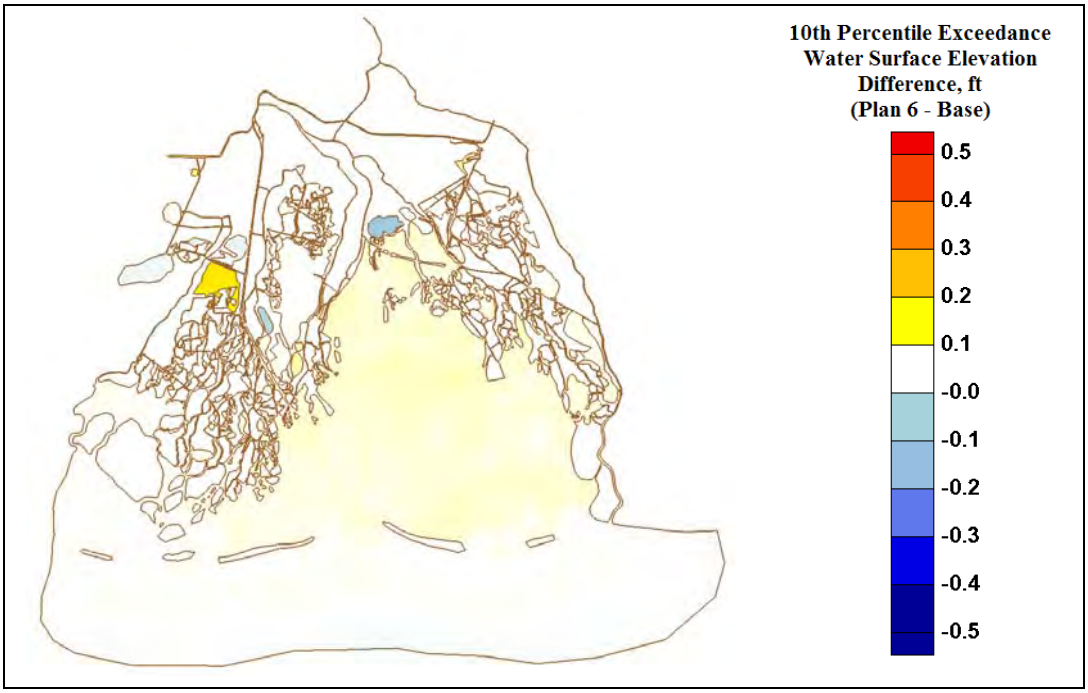

Figure 106. 10th Percentile exceedance water level differences (Plan 6 – base).

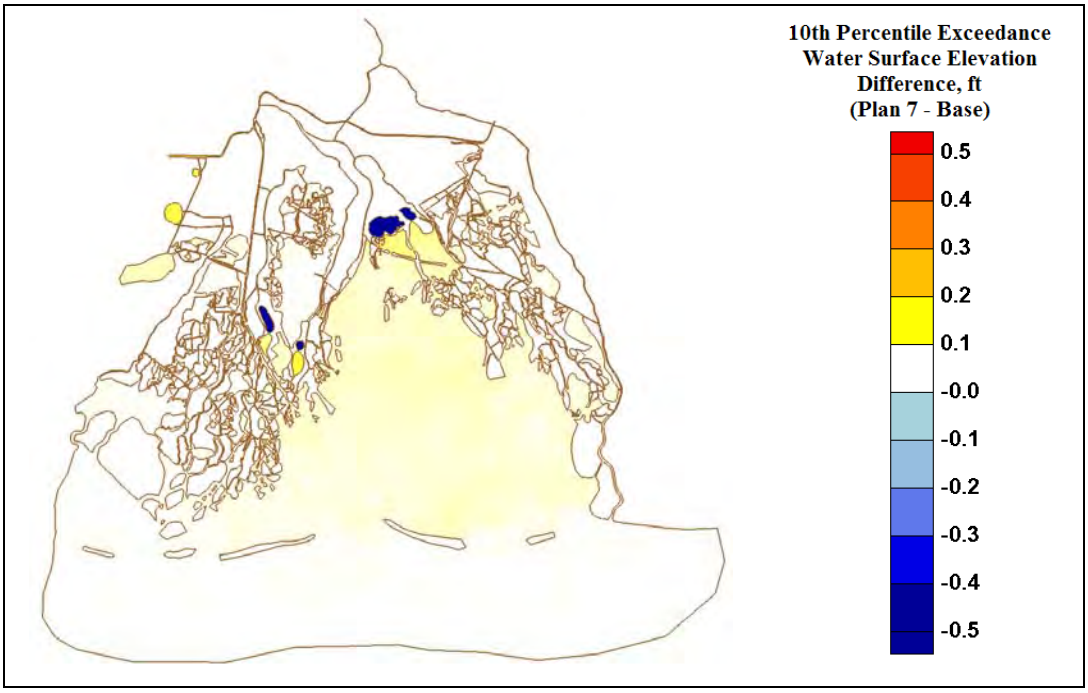

Figure 107. 10th Percentile exceedance water level differences (Plan 7 – base).

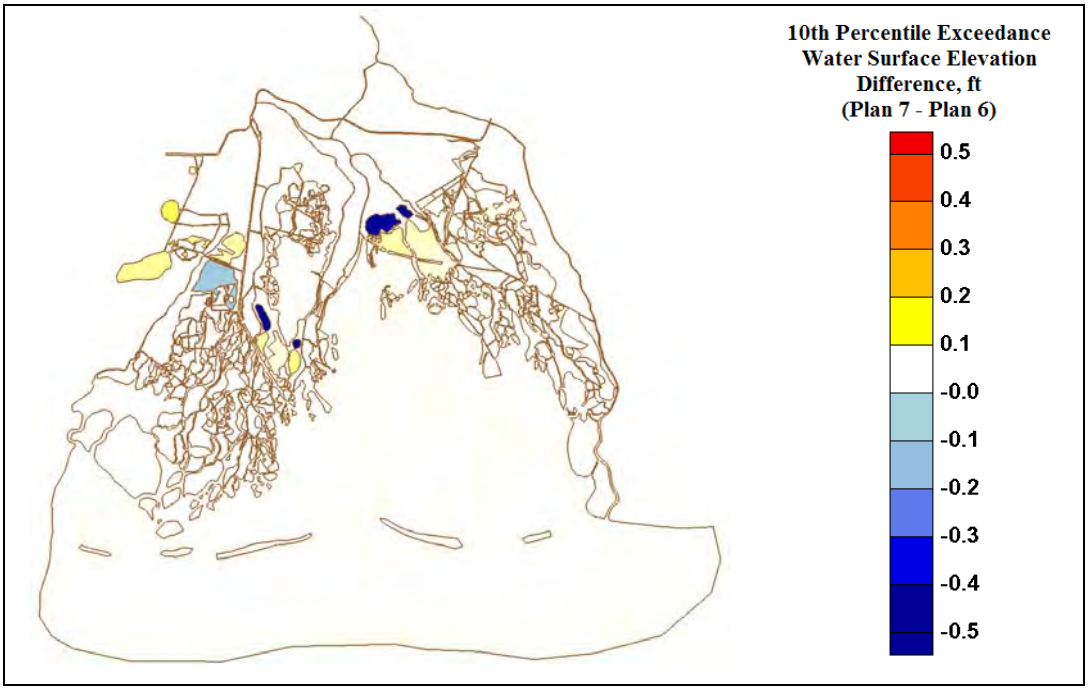

Figure 108. 10th Percentile exceedance water level differences (Plan 7 – Plan 6).

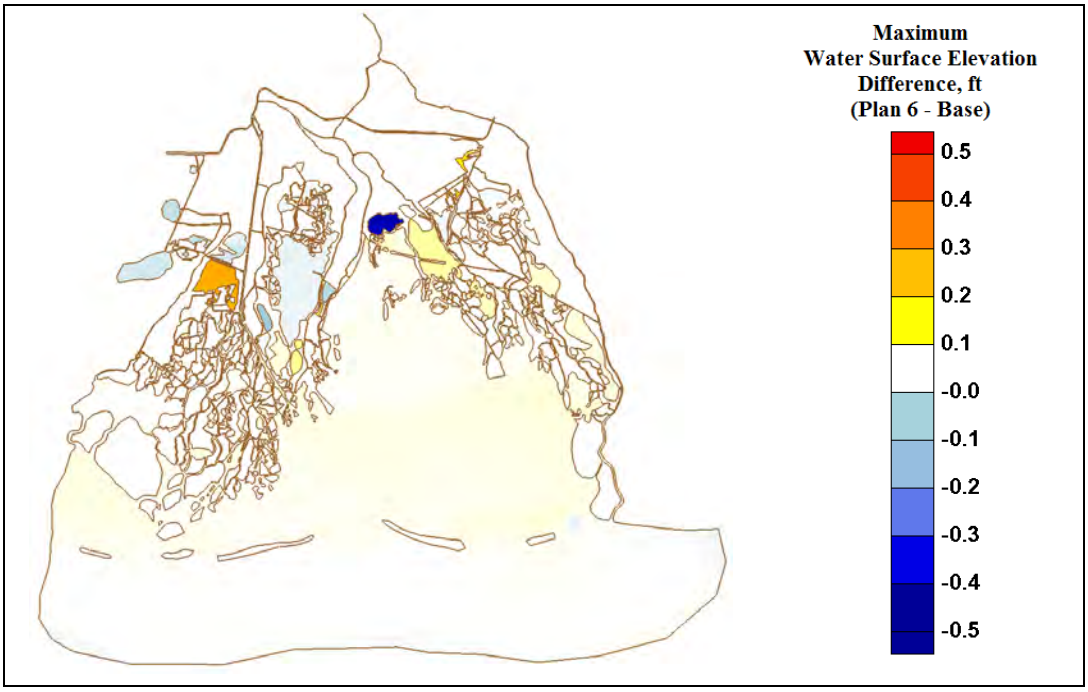

Figure 109. Maximum water level differences (Plan 6 – base).

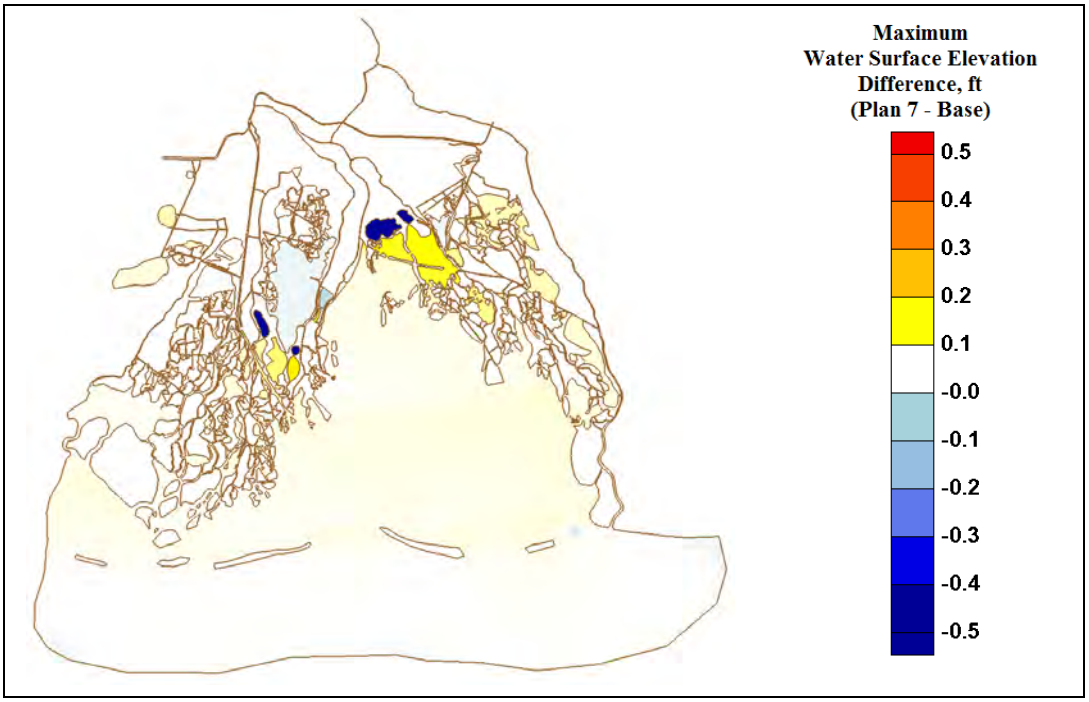

Figure 110. Maximum water level differences (Plan 7 – base).

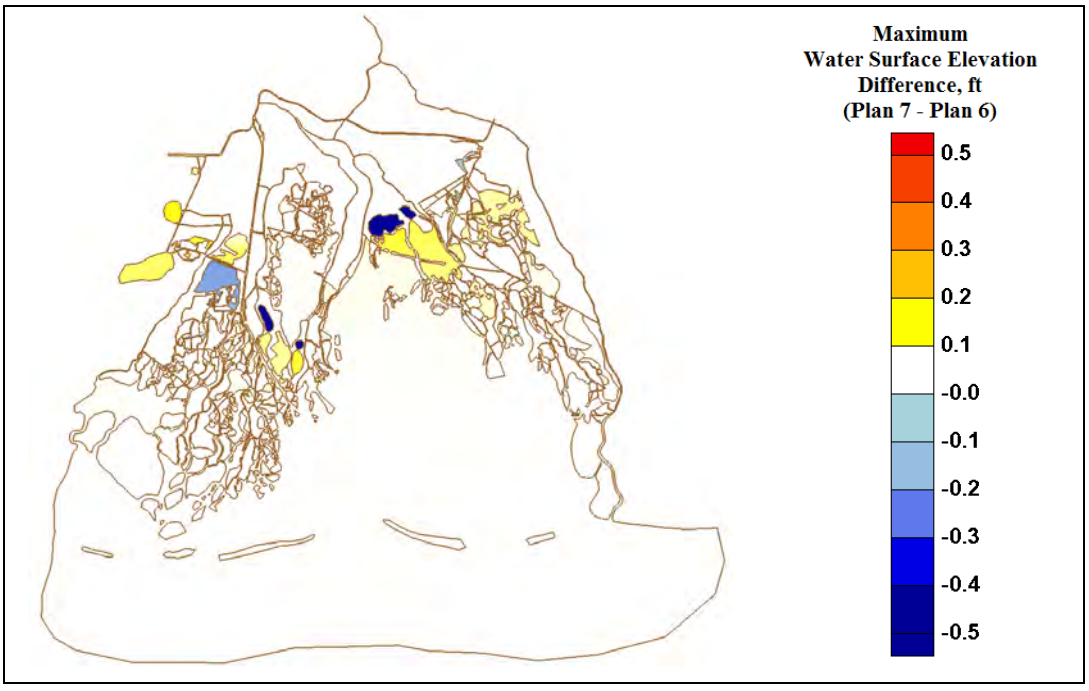

Figure 111. Maximum water level differences (Plan 7 – Plan 6).

While the base versus plan velocity comparisons were performed at all locations, there is expected to be a larger uncertainty in the velocities associated with the structure locations away from the current study area (GIWW West of Houma, Bayou Grand Caillou, Houma Navigational

Canal, Falgout Canal, Bayou Dularge, and Bayou Fourpoints) as these areas possessed less resolution and therefore could have larger errors associated with the velocity fields.

The results for the Pointe Aux Chenes and Grand Bayou structures are expected to have an even larger uncertainty than the previously mentioned structures as the area around these structures is less resolved with increased error associated with the geometry of the system. Less effort and time was expended accurately resolving this area due to its significant distance from the model study area. The less than ideal validation comparisons at Grand Bayou indicate a more cautious interpretation of the results for this area as well.

Bar plots showing the base, Plan 6, and Plan 7 velocity magnitudes are shown in Figures 91 to 93.

The water surface elevation differences show minimal differences between the base and plan configurations with some localized differences of as much as ~0.4 ft. The 50th percentile exceedance comparisons show the water levels for the system, on average, are only changed for the area south of Falgout Canal with a negligible increase in the water level (~0.01 ft) in Lake Boudreaux. For the 10th percent exceedance and maximum values, there is a slight increase in the water levels outside (south) of the new levee system with a slight decrease in the water levels inside (north) of the new levee system. This indicates that the new levee system, even with the structures open, can create a dampening of the surge due to frontal passages. The levee system allows slightly less water in during these more extreme frontal passages resulting in slightly lower water levels for the protected areas and slightly higher water levels for the unprotected areas.

8 Conclusions

Some of the maximum velocities did reach as high as 3.5 ft/s and above but those were maximum velocities over an approximately 3-month time frame consisting of multiple frontal passages. The previously provided exceedance curves, Figures 78 to 90, allow MVN the option of performing a cost to benefit analysis on select structures where the cost of increasing a particular structure size may not warrant the relatively minor decrease in the prevalent velocities. An example would be to increase a structure's size to reduce the maximum velocities below a given threshold when the velocities may only exceed that threshold during one event over a three month time frame. Depending on the amount of navigational traffic for a particular structure, the New Orleans District may be better served to occasionally restrict navigational traffic and construct a smaller structure at a much lower cost.

From the previously shown results, it can be observed that the changes associated with the Plan 6 and Plan 7 configurations produce minimal effects on the velocity fields (less than 1 ft/s change from the base) for the majority of the structures (Falgout Canal, Bayou Dularge, Houma Navigational Canal, Bayou Fourpoints, Bush Canal, Bayou Terrebonne, and Grand Bayou). The remaining structures (GIWW West of Houma, Bayou Grand Caillou, Bayou Petit Caillou, Placid Canal, and Pointe Aux Chenes) have higher velocity increases but the 10th percentile exceedance velocities are below 3 ft/s for all navigational structures. This indicates that velocities above 3 ft/s would not be regular occurrences.

The 50th percentile exceedance velocities are below 2 ft/s for all navigational structures except the GIWW West of Houma structure (2.5 ft/s). These 50th percentile exceedance velocities indicate that on average the velocities for all the structures (except GIWW West of Houma at 2.5 ft/s) are below 2 ft/s. These values should be taken as an indication of the expected velocities for each structure location.

Previous salinity modeling considered configurations with all navigational structures open and all environmental structures closed. To insure no significant changes occurred in the velocity fields due to the closure of these environmental structures, Plan 7 (Plan 6 with all environmental

structures closed) was modeled. As expected, the Plan 7 model results produced minimal changes in velocity (less than ~0.3 ft/s). This indicates that the closure of the environmental structures for ecological/biological reasons should not have a significant impact on the velocities in the navigational structures.

References

Aquaveo. 2009. *Surface-water Modeling System Version 10.1*. Aquaveo. http://www.aquaveo.com/pdf/SMS 10.1.pdf

Berger, R. C., and R. L. Stockstill. 1995. Finite element model for high-velocity channels. *Journal of Hydraulic Engineering* ASCE, 121(10), 710–716.

Berger, R. C., and S. E. Howington. 2002. Discrete fluxes and mass balance in finite elements. *Journal of Hydraulic Engineering*, ASCE, 128 (1), 87 – 92.

Berger, R. C., and L. M. Lee. 2004. *Multidimensional numerical modeling of surges over initially dry land*. ERDC/CHL TR-04-10. Vicksburg, MS: U.S. Army Engineer Research and Development Center.

Berger, R. C., J. N. Tate, G. L. Brown, and G. Savant. 2010. *Adaptive hydraulics: Users manual*. Vicksburg, MS: U.S. Army Engineer Research and Development Center. https://adh.usace.army.mil/.

Brown, C. T., L. A. Berg, J. Granberry, C. Herman,C. G. Miller, J. Pincoske, R. Saucier, S. B. Smith, D. D. Davis, P. P. Robblee, and R. C. Goodwin. 2000. *Morganza to the gulf feasibility study: Cultural resources literature and records review, Terrebonne and Lafourche Parishes, Louisiana (Volume I of II)*. New Orleans, LA: U.S. Army Engineers District, New Orleans.

Donnell, B. P., J. V. Letter, and A. M. Teeter. 1991. *The Atchafalaya River Delta, Report 11, Two-dimensional modeling*. Hydraulics Laboratory Technical Report, HL-82-15. Vicksburg, MS: U.S. Army Engineer Waterways Experiment Station.

Federal Emergency Management Agency (FEMA) 2010. *Flood insurance study: St. Landry Parish, Louisiana and incorporated areas*. Flood Insurance Study Number 2209CV000A.

Fraizer, D. E. 1967. Deltaic deposits of the Mississippi River: Their development and chronology. *Transactions of the Gulf Coast Association of Geological Societies*. 17: 287-315.

Fredrickson, H., J. Furey, C. Foote, and M. Richmond. 2007. *Environmental consequences of the failure of the New Orleans levee system during Hurricane Katrina*. ERDC/EL TR-08-26. Vicksburg, MS: U.S. Army Engineer Research and Development Center.

Gabutti, B. 1983. On two upwind finite difference schemes for hyperbolic equations in non-conservative form. *Computers and Fluids* 11(3), 207-230.

Higgins, J. 2006. *The radical statistician: A beginners guide to unleashing the power of applied Statistics in the Real World (5th Edition)*. Self-published.

Hughes, T. J. R., and A. N. Brooks. 1982. A theoretical framework for Petrov-Galerkin methods with discontinuous weighting functions: applications to the streamline-upwind procedures. *Finite elements in fluids*, R. H. Gallagher, et al., eds., J. Wiley & Sons, Inc., London, England, 4, 47–65.

Martin, S. K., G. Savant, and D. C. McVan. 2010. *Lake Borgne surge barrier study*. ERDC/ CHL TR-10-10. Vicksburg, MS: U.S. Army Engineer Research and Development Center.

Matlab. 2010. MATLAB 7 function reference: Volume 3 (P-Z). Natick, MA: The MathWorks, Inc. 01760-2098.

McCuen, R. H., Z. Knight, and A. G. Cutter. 2006. Evaluation of the Nash-Sutcliffe Efficiency Index. *Journal of Hydraulic Engineering* ASCE, 11(6): 597–602.

McAlpin, T. O., R. C. Berger, and A. M. Henville. 2009. *Bush Canal floodgate study*. ERDC/ CHL TR-09-9. Vicksburg, MS: U.S. Army Engineer Research and Development Center.

McLaughlin, J. W., A. Bilgili, and D. R. Lynch. 2003. Numerical modeling of tides in the Great Bay Estuarine System: Dynamical balance and spring-neap residual modulation. *Estuarine, Coastal, and Shelf Science* 57, (1-2)A: 283-296.

Moretti, G. 1979. The λ-scheme. *Computers and Fluids* 7(3), 191 – 205.

Savant, G., R. C. Berger, T. O. McAlpin, and J. N. Tate. 2010. An efficient implicit finite element hydrodynamic model for dam and levee breach. *Journal of Hydraulic Engineering* ASCE. Doi:10.1061/(ASCE)HY.1943-7900.0000372.

Sontek. Argonaut – *SL: Side Looking Doppler Current Meter*. Sontek, San Diego, California.

Steger, J. L., and R. F. Warming. 1981. Flux vector splitting of the inviscid gas dynamics equations with applications to finite difference methods. *Journal of Computational Physics* 40, 263 – 293.

Stockstill, R. L., and J. M. Vaughan. 2009. Numerical model study of the Tuscarawas River below Dover Dam, Ohio. ERDC/CHL TR-09-17.Vicksburg, MS: U.S. Army Engineer Research and Development Center.

Stockstill, R. L., J. M. Vaughan, and S. K. Martin. 2010. *Numerical model of the Hoosic River Flood-Control Channel, Adams, MA*. ERDC/CHL TR-10-01. Vicksburg, MS: U.S. Army Engineer Research and Development Center.

Suedel, B., J. Steevens, A. Kennedy, and S. Brasfield. 2008. Effects of Hurricane Katrina-related levee failures on wetland sediments. ERDC/EL TR-08-26. Vicksburg, MS: U.S. Army Engineer Research and Development Center.

Swarzenski, C. M. 2003. *Surface-water hydrology of the Gulf Intracoastal Waterway in south-central Louisiana, 1996-99*. Reston, VA: U. S. Geological Survey Professional Paper 1672.

Tate, J. N., T. C. Lackey, and T. O. McAlpin. 2010. *Seabrook fish larval transport study*. ERDC/CHL TR-10-12. Vicksburg, MS: U.S. Army Engineer Research and Development Center.

Teledyne RD Instruments. 2009. *Workhorse Rio Grande ADCP: Highly accurate river discharge measurement tool*. Poway, CA:Teledyne RD Instruments,

Teledyne RD Instruments. 2006. Channel Master H-ADCP. Poway, CA: Teledyne RD Instruments.

U.S. Army Corps of Engineers. 2008. MN-2008-518-CT. New Orleans, LA: U.S. Army Engineer District, New Orleans.

Wahl, K. L., W. O. Thomas Jr., and R. M. Hirsch. 1995. *Stream-gaging program of the U.S. Geological Survey*. Reston, VA: U.S. Geological Survey Circular 123.

Willmott, C. J. 1982. Some comments on the evaluation of model performance. *Bulletin American Meterological Society* 63(11), 1309 – 1313.

Willmott, C. J., S. G. Ackleson, R. E. Davis, J. J. Feddema, K. M. Klink, D. R. Legates, J. O'Donnel, and C. M. Rowe. 1985. Statistics for the evaluation and comparison of models. *Journal of Geophysical Research* 90(C5), 8995-9005.

Appendix A: Description of the Adaptive Hydraulics (AdH) Model

AdH is a state-of-the-art code developed by the U.S. Army Engineer Research and Development Center (ERDC) to simulate both saturated and unsaturated groundwater, overland flow, three-dimensional (3-D) Navier-Stokes flow, and 2- or 3-D shallow-water problems (Berger et al. 2010).

The 2-D shallow-water equations are a result of the vertical integration of the equations of mass and momentum conservation for incompressible flow under the hydrostatic pressure assumption (Berger and Lee 2004). Written in conservative form, the 2-D shallow-water equations are:

$$\frac{\partial \boldsymbol{U}}{\partial t}+\frac{\partial \boldsymbol{F}}{\partial x}+\frac{\partial \boldsymbol{G}}{\partial y}+\boldsymbol{H}=0$$

where

$$U=\begin{Bmatrix} h \\ uh \\ vh \end{Bmatrix}$$

$$F=\begin{Bmatrix} uh \\ u^2h+\frac{1}{2}gh^2-h\frac{\sigma_{xx}}{\rho} \\ uvh-h\frac{\sigma_{yx}}{\rho} \end{Bmatrix}$$

$$G=\begin{Bmatrix} vh \\ uvh-h\frac{\sigma_{xy}}{\rho} \\ v^2h+\frac{1}{2}gh^2-h\frac{\sigma_{yy}}{\rho} \end{Bmatrix}$$

and

$$H = \begin{Bmatrix} 0 \\ gh\dfrac{\partial z_b}{\partial x} + \tau_{bed_x} \\ gh\dfrac{\partial z_b}{\partial y} + \tau_{bed_y} \end{Bmatrix}$$

where ρ is the fluid density, g is the gravitational acceleration, z_b is the bed elevation, τ_{bed_i} is the bed shear stress drag where the subscript (i) indicates the direction (x and y), h is the flow depth, u is the x component of velocity, v is the y component of velocity, and the σ 's are the Reynolds stresses due to turbulence, where the first subscript indicates the direction, and the second indicates the face on which the stress acts.

The Reynolds stresses are determined using the Boussinesq approach to the gradient in the mean currents:

$$\sigma_{xx} = 2\rho\nu_t \frac{\partial u}{\partial x}$$

$$\sigma_{yy} = 2\rho\nu_t \frac{\partial v}{\partial y}$$

and

$$\sigma_{xy} = \sigma_{yx} = 2\rho\nu_t \left(\frac{\partial u}{\partial y} + \frac{\partial v}{\partial x} \right)$$

where ν_t = kinematic eddy viscosity (which varies spatially).

The AdH shallow-water equations are placed in conservative form to ensure mass balance and balance of momentum and pressure across an interface. This results in a locally mass conservative model (Berger and Howington 2002).

The equations are coded in a finite element approach with the velocities and depth being represented as linear polynomials on each element. AdH utilizes a streamline-upwind Petrov-Galerkin (SUPG) scheme similar to that reported in Berger and Stockstill (1995) and patterned after previous work by Hughes and Brooks (1982), Moretti (1979), Gabutti (1983), and Steger

and Warming (1981). Since the finite element scheme is not the primary focus of this report, a more in-depth description of this method is omitted.

AdH contains other essential features such as wetting and drying, completely coupled sediment and salt transport, and wind effects. A series of modularized libraries make it possible for AdH to include vessel movement, friction descriptions, as well as a host of other features. AdH can run in parallel or on a single processor and runs on both Windows systems and UNIX based systems.

Appendix B: Base versus Plan 6 Contour Plots of the Velocity

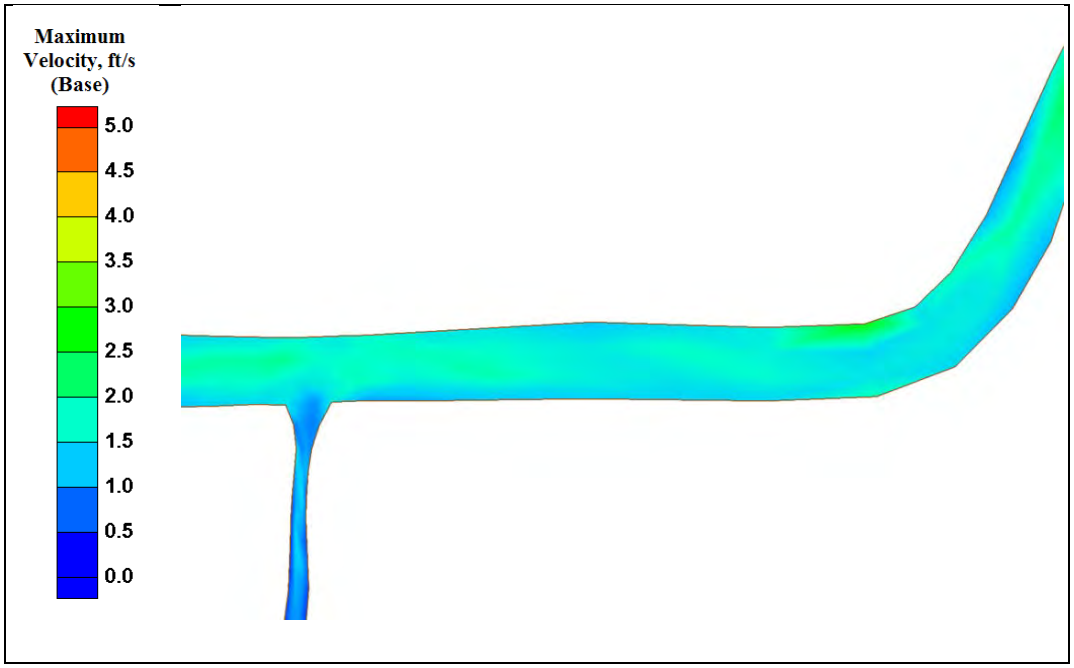

Figure B1. GIWW west of Houma structure maximum velocity (base).

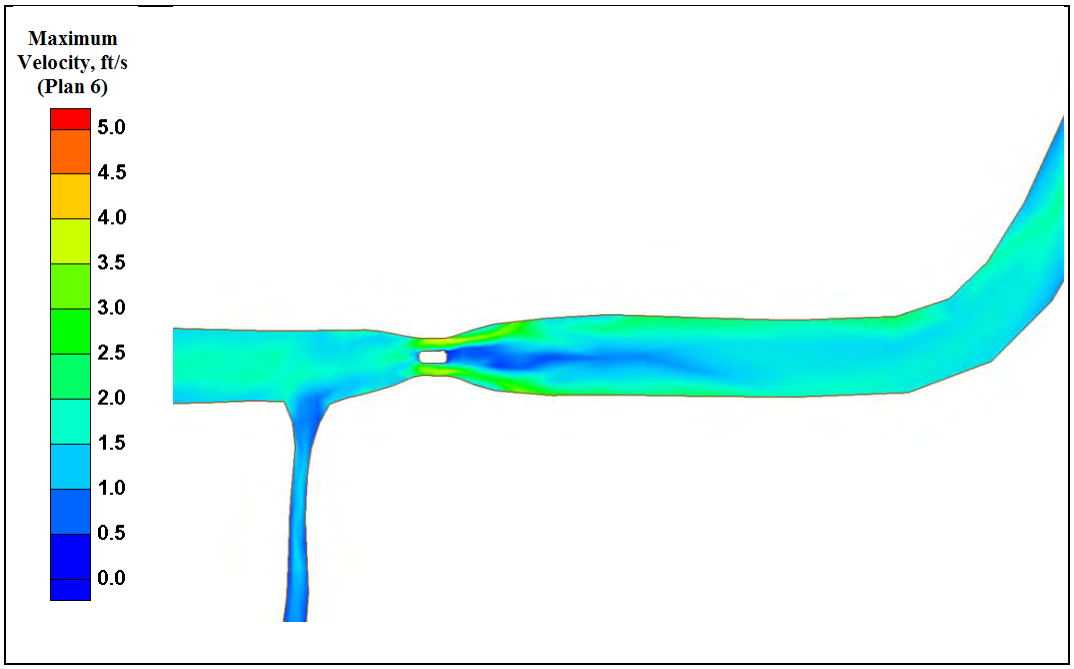

Figure B2. GIWW west of Houma structure maximum velocity (Plan 6).

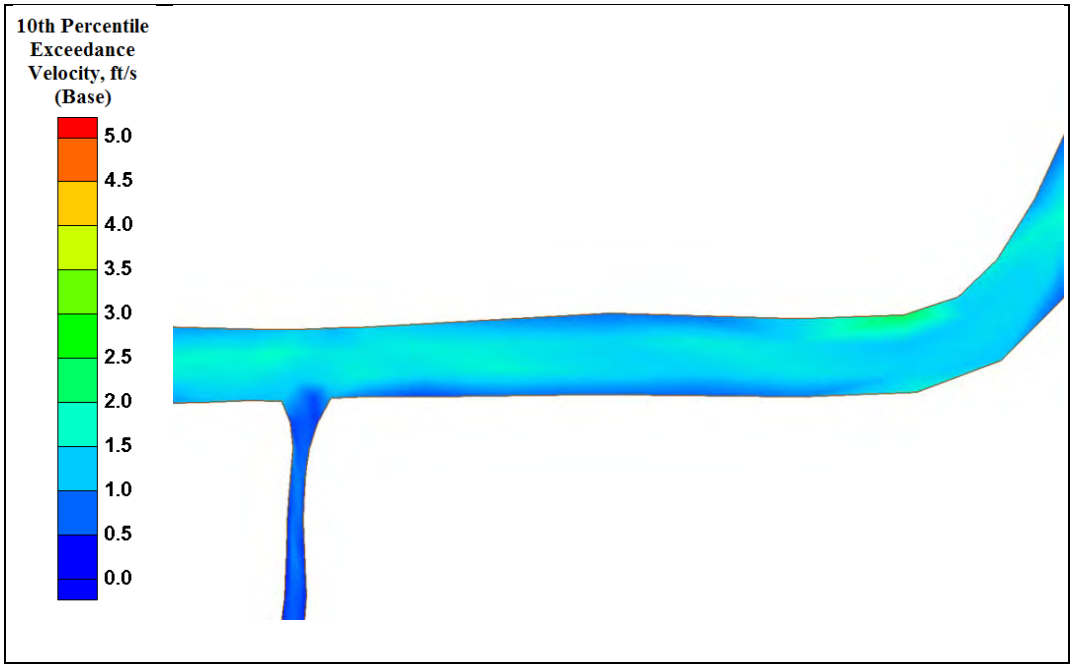

Figure B3. GIWW west of Houma structure 10th percentile exceedance velocity (base).

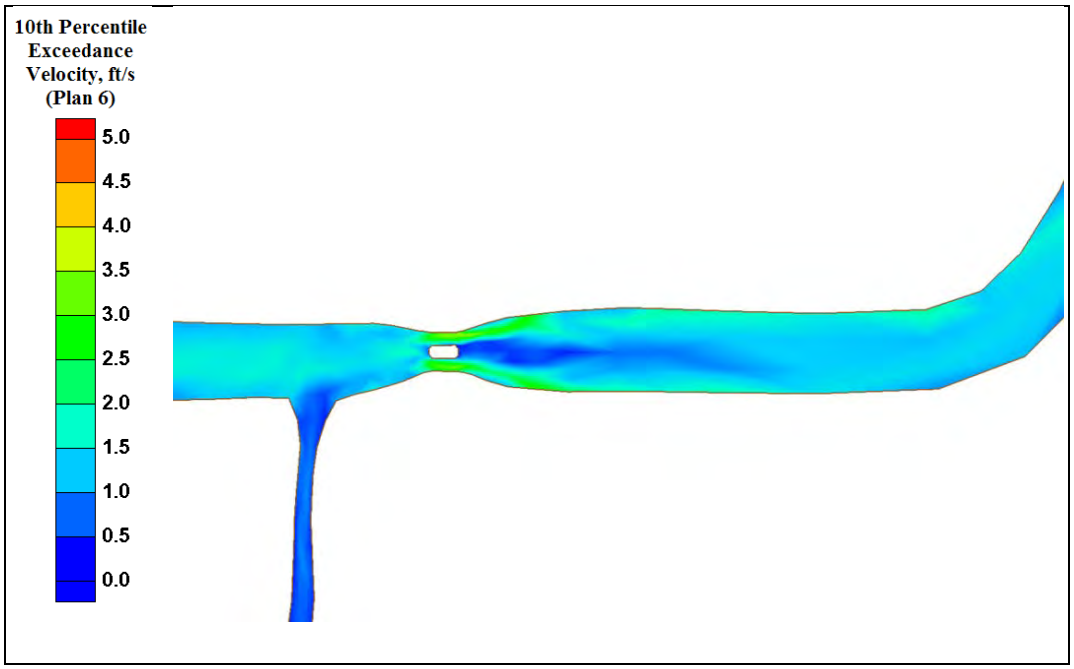

Figure B4. GIWW west of Houma structure 10th percentile exceedance velocity (Plan 6).

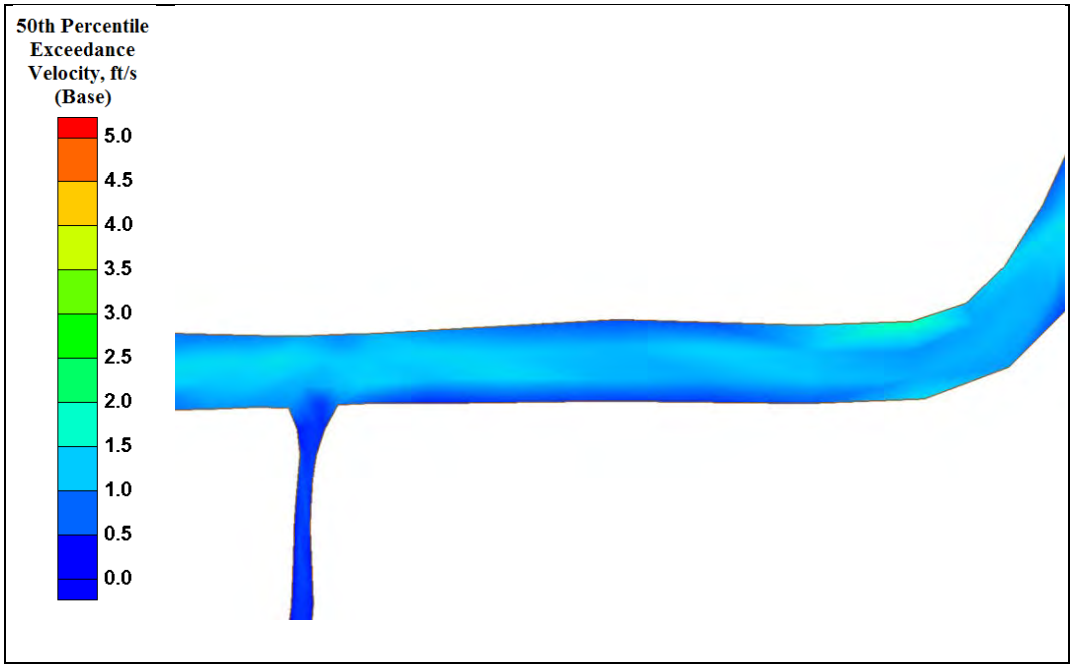

Figure B5. GIWW west of Houma structure 50th percentile exceedance velocity (base).

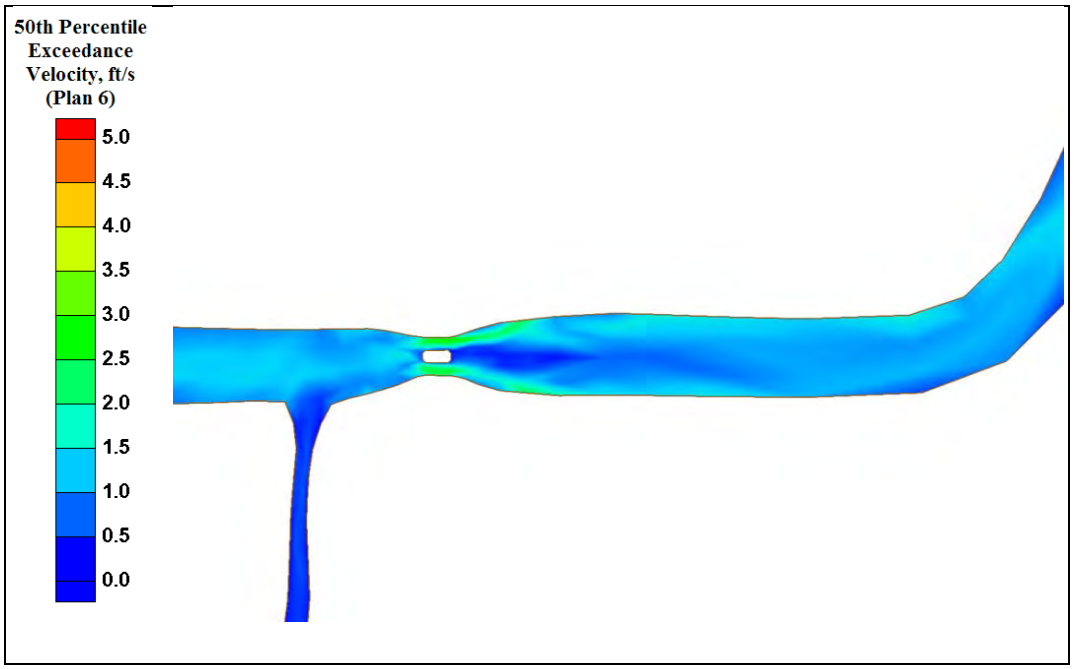

Figure B6. GIWW west of Houma structure 50th percentile exceedance velocity (Plan 6).

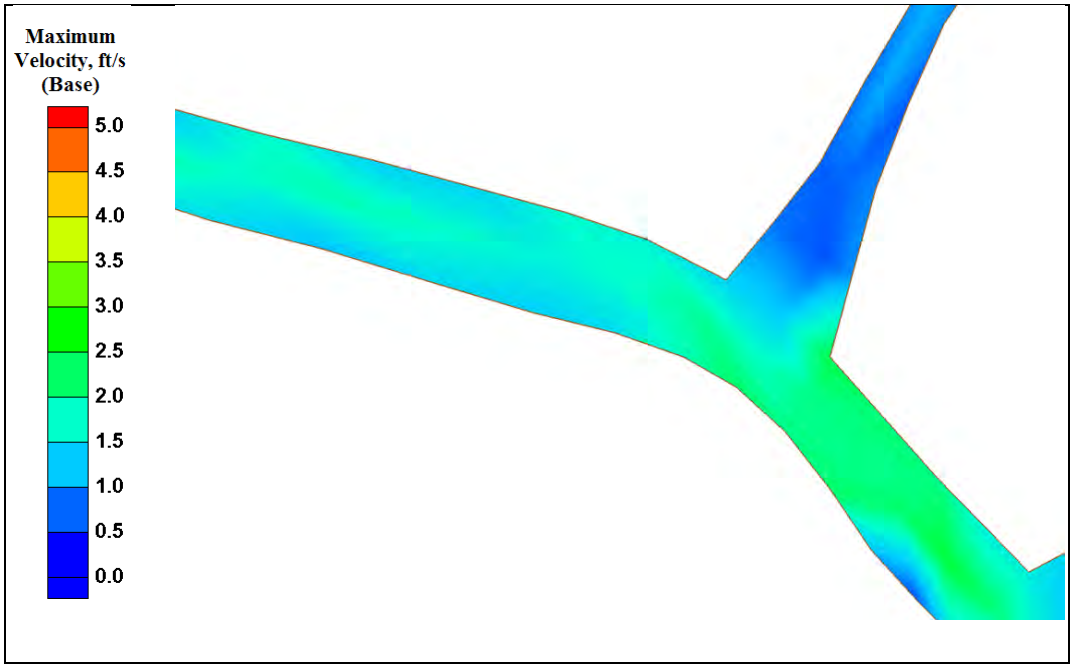

Figure B7. Falgout Canal maximum velocity (base).

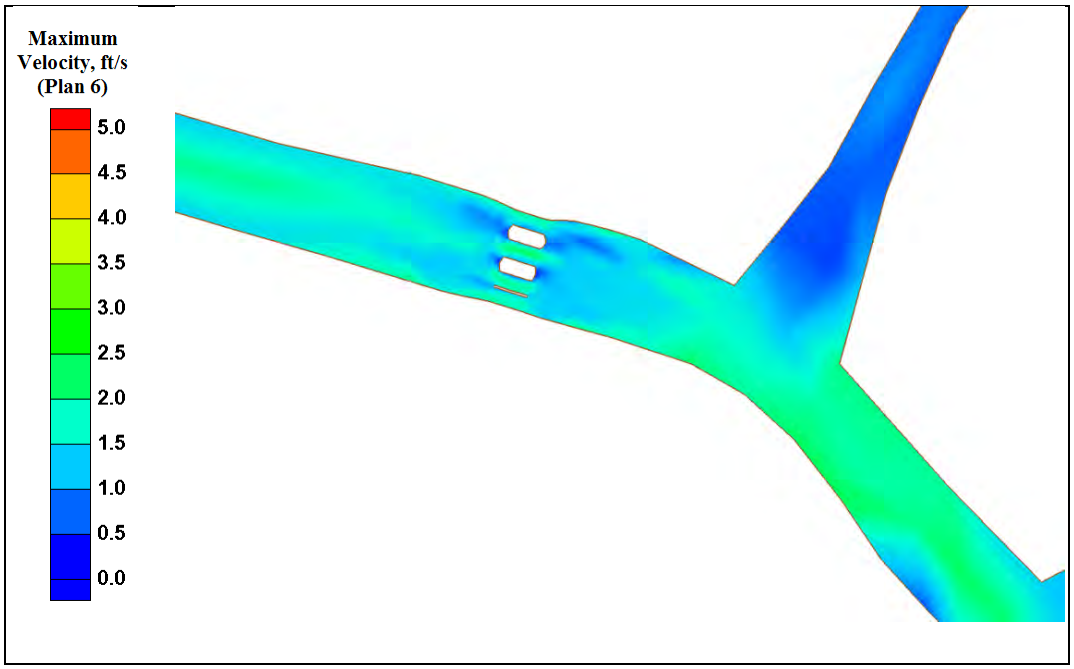

Figure B8. Falgout Canal maximum velocity (Plan 6).

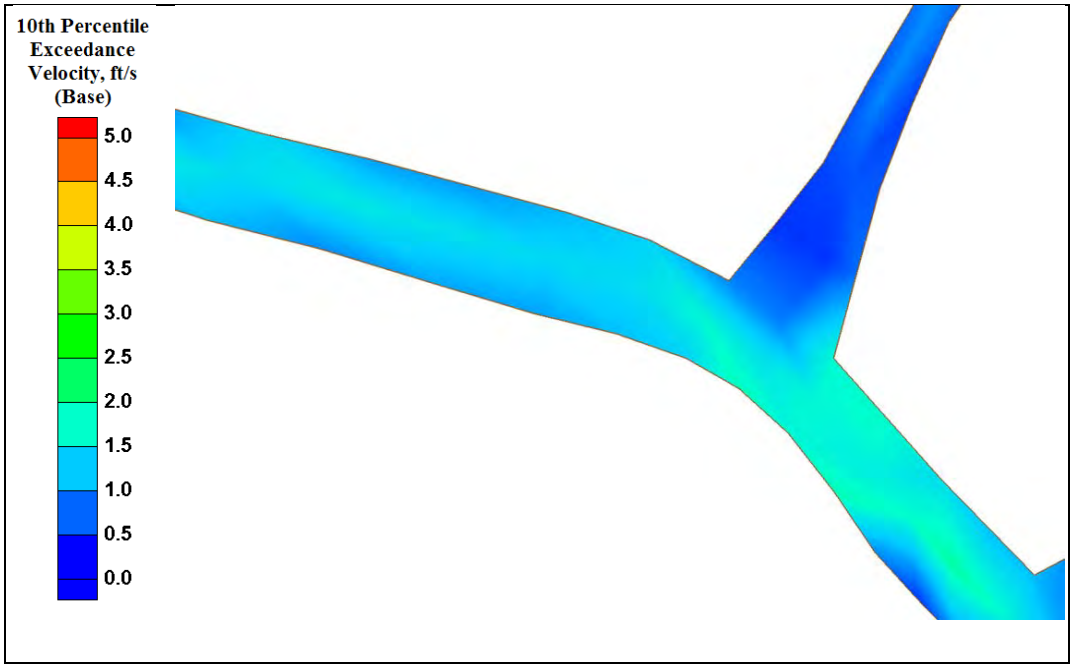

Figure B9. Falgout Canal 10th percentile exceedance velocity (base).

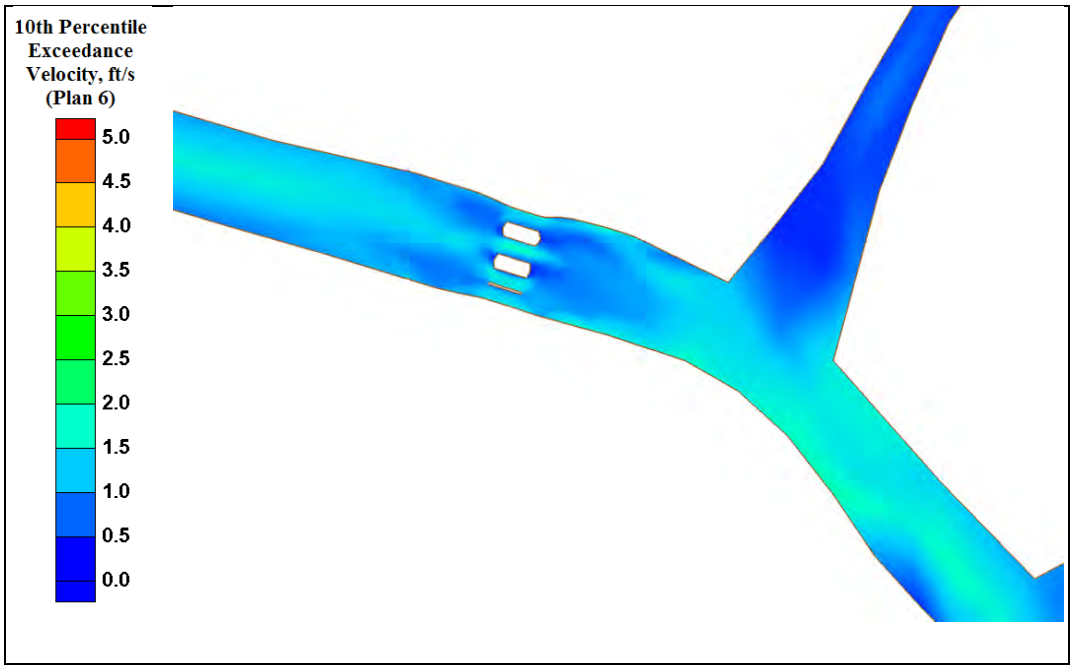

Figure B10. Falgout Canal 10th percentile exceedance velocity (Plan 6).

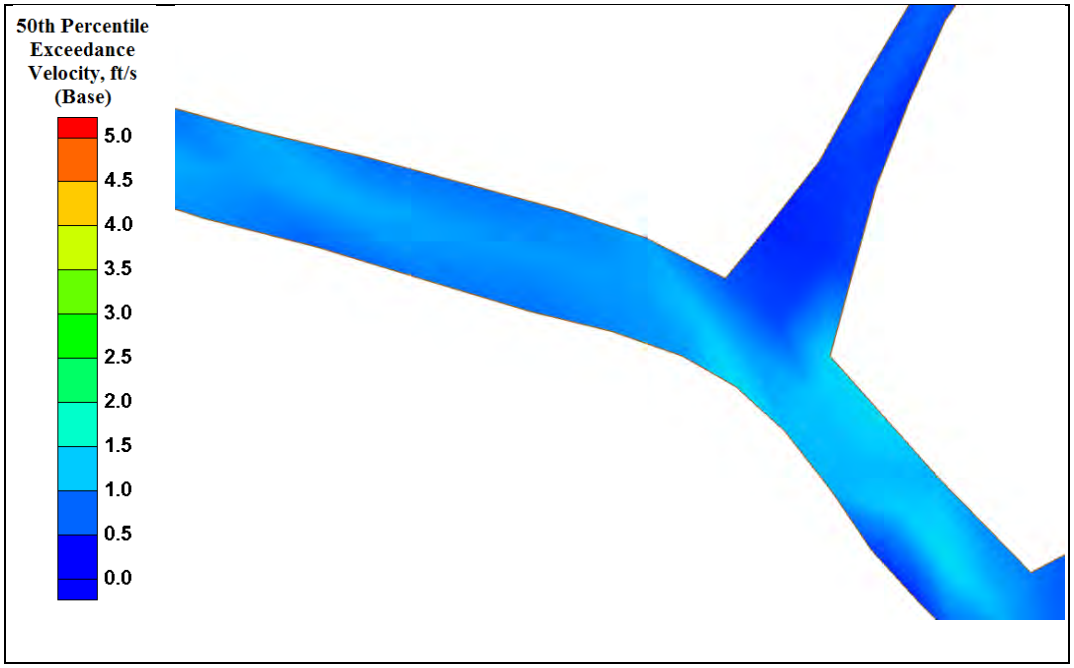

Figure B11. Falgout Canal 50th percentile exceedance velocity (base).

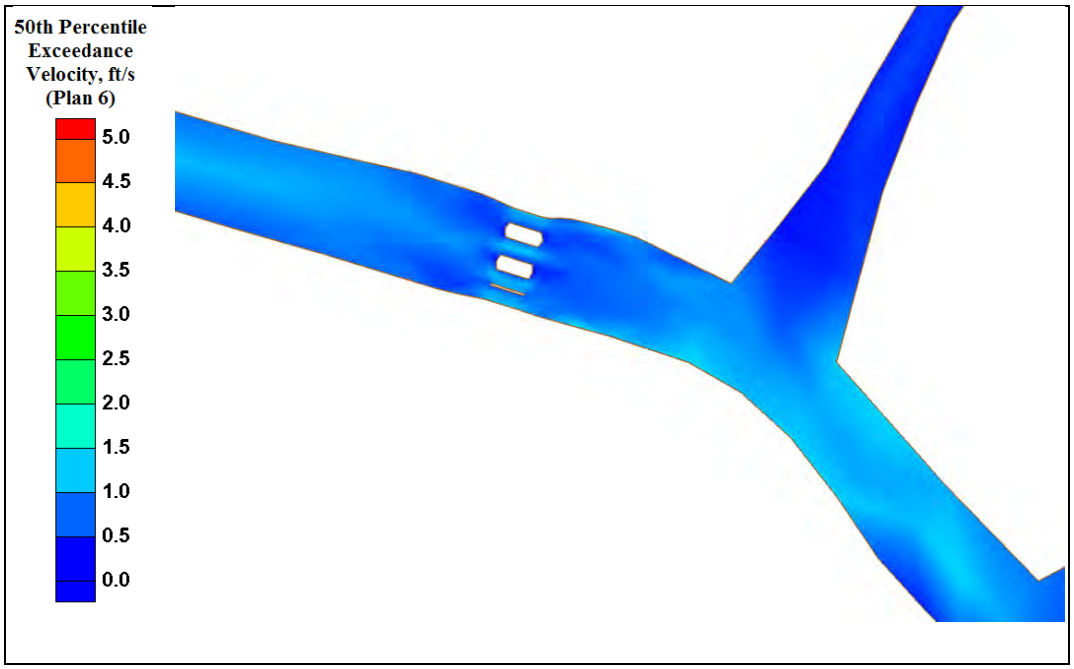

Figure B12. Falgout Canal 50th percentile exceedance velocity (Plan 6).

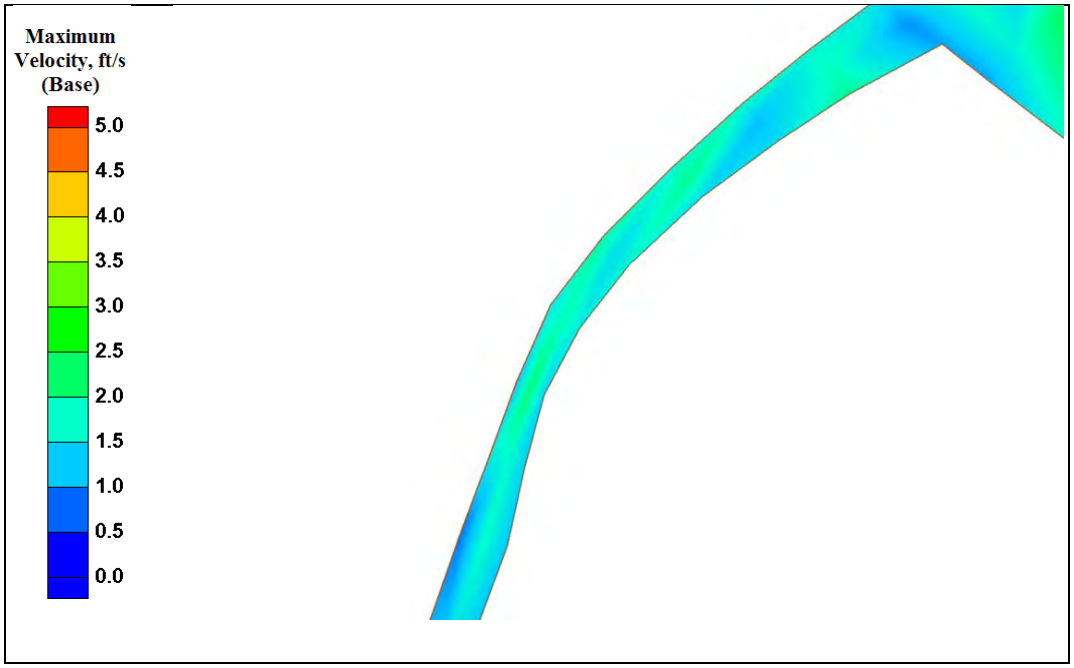

Figure B13. Bayou Dularge maximum velocity (base).

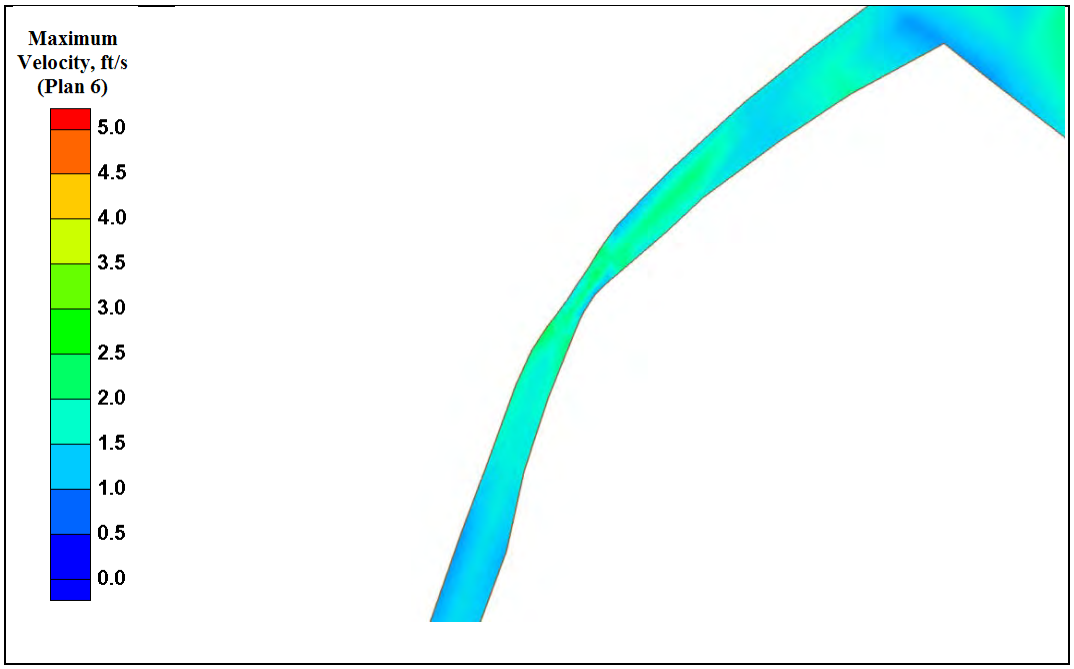

Figure B14. Bayou Dularge maximum velocity (Plan 6).

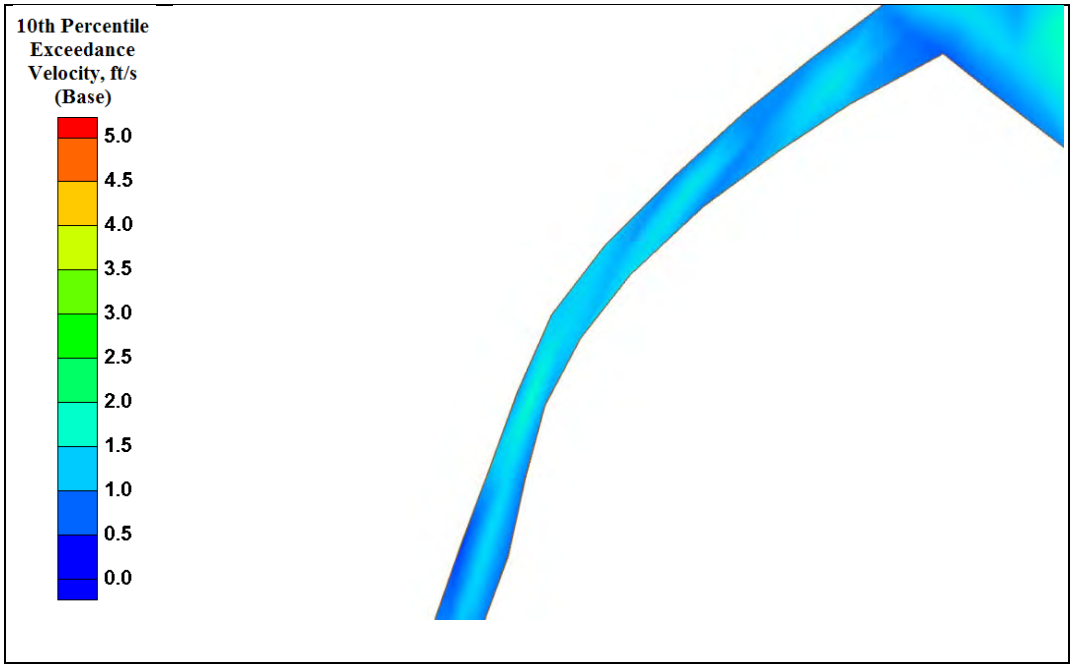

Figure B15. Bayou Dularge 10th percentile exceedance velocity (base).

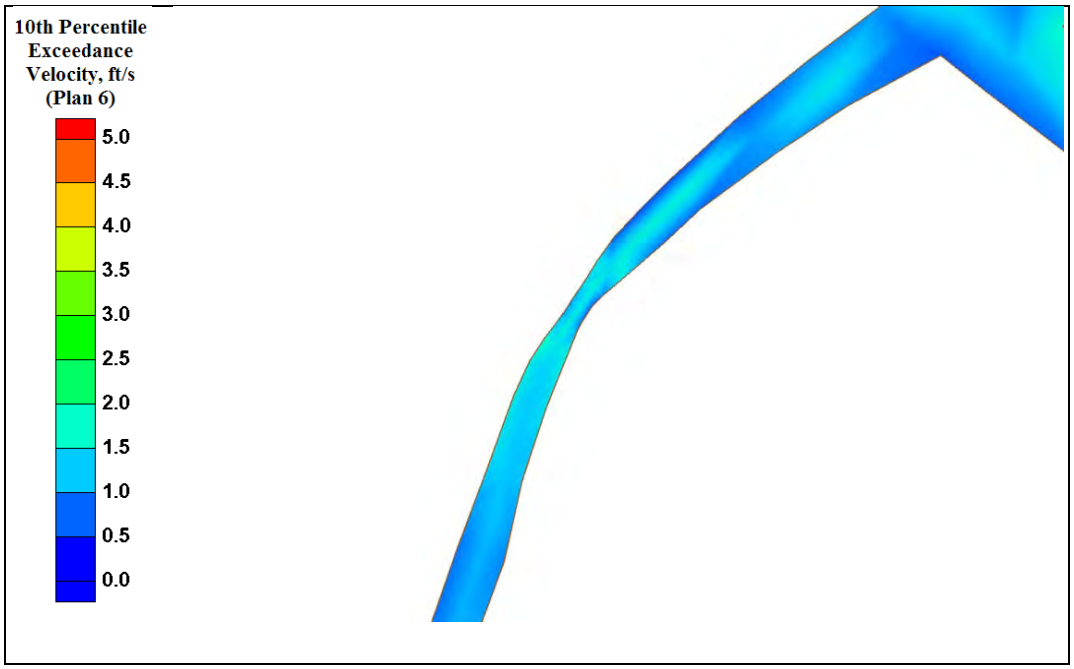

Figure B16. Bayou Dularge 10th percentile exceedance velocity (Plan 6).

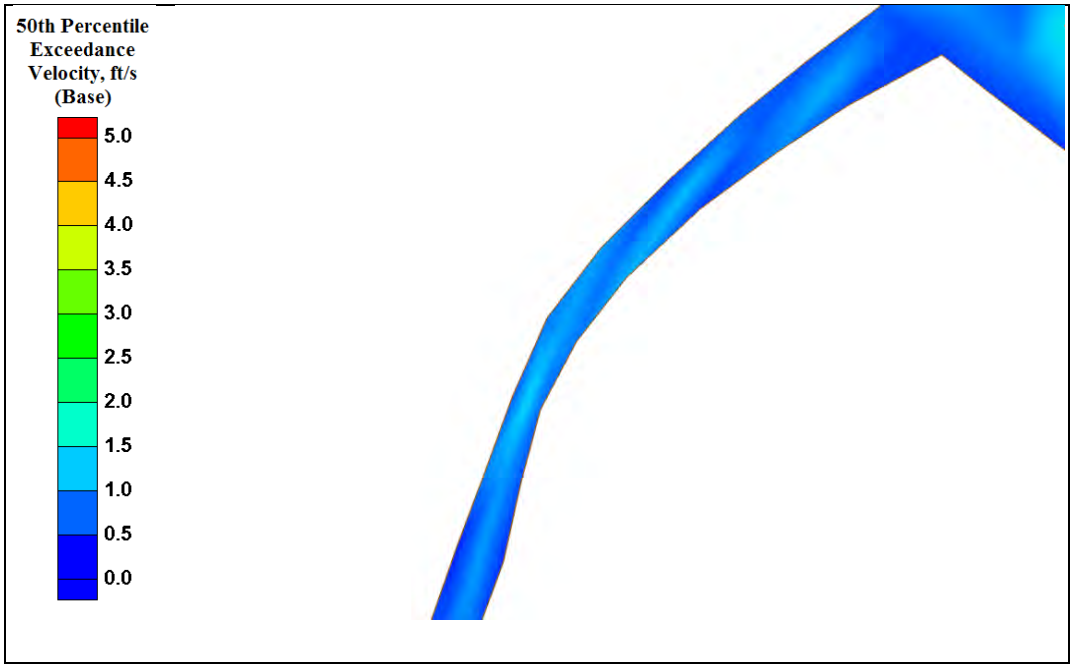

Figure B17. Bayou Dularge 50th percentile exceedance velocity (base).

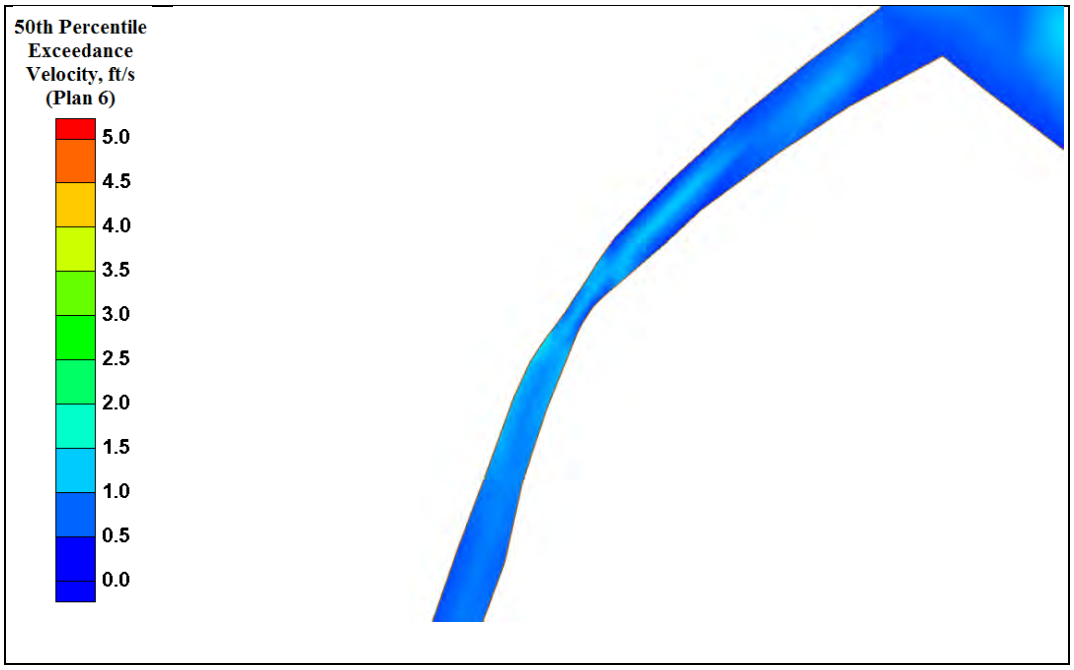

Figure B18. Bayou Dularge 50th percentile exceedance velocity (Plan 6).

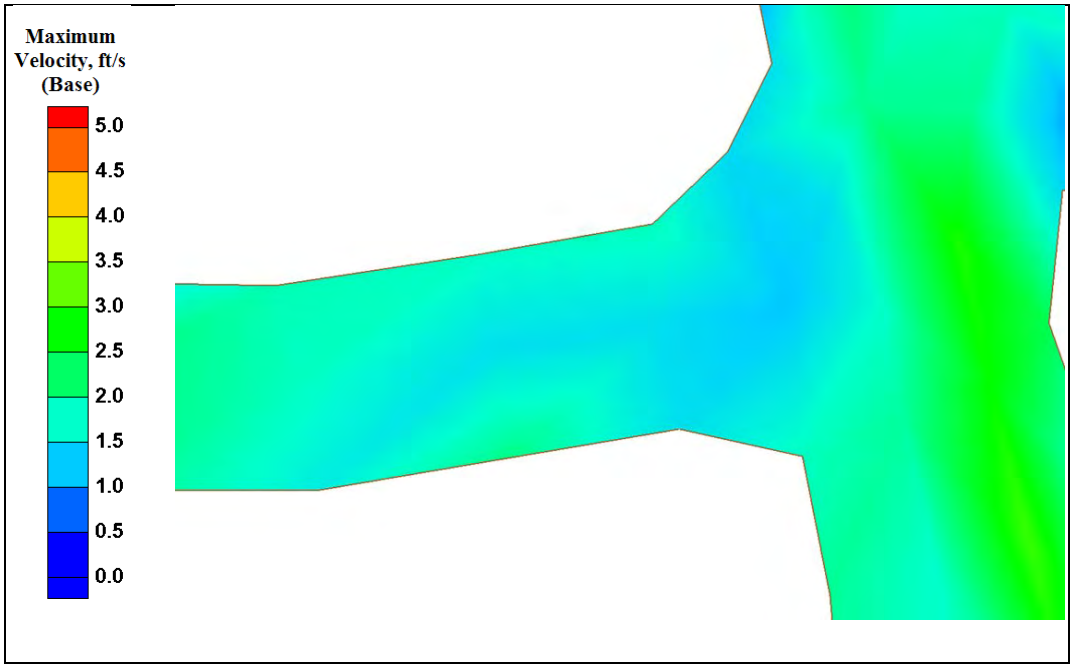

Figure B19. Bayou Grand Caillou maximum velocity (base).

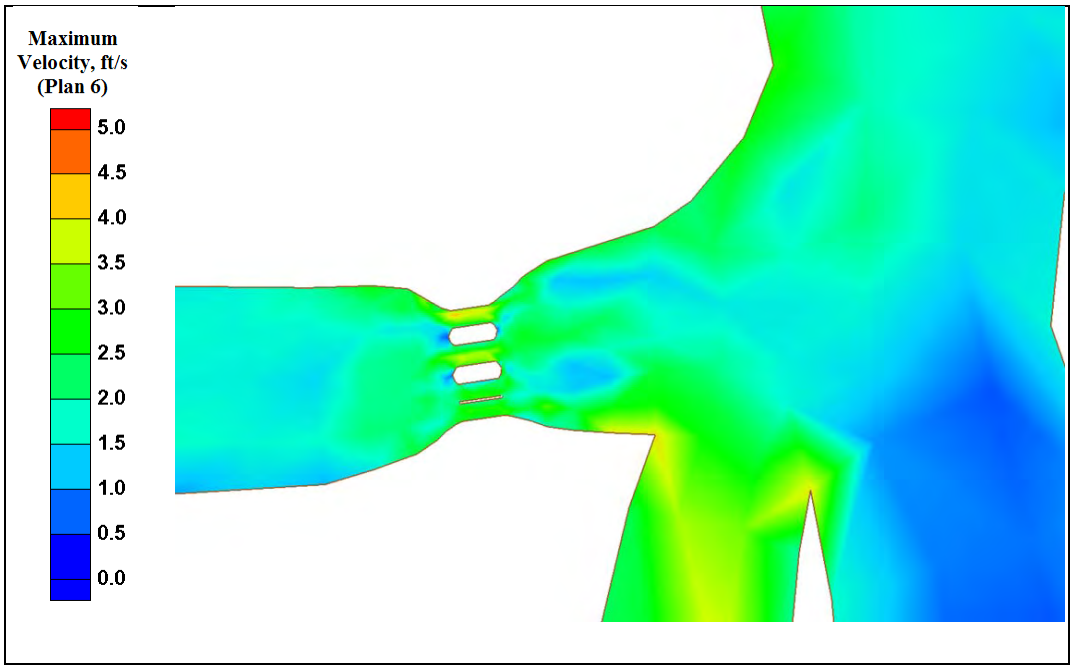

Figure B20. Bayou Grand Caillou maximum velocity (Plan 6).

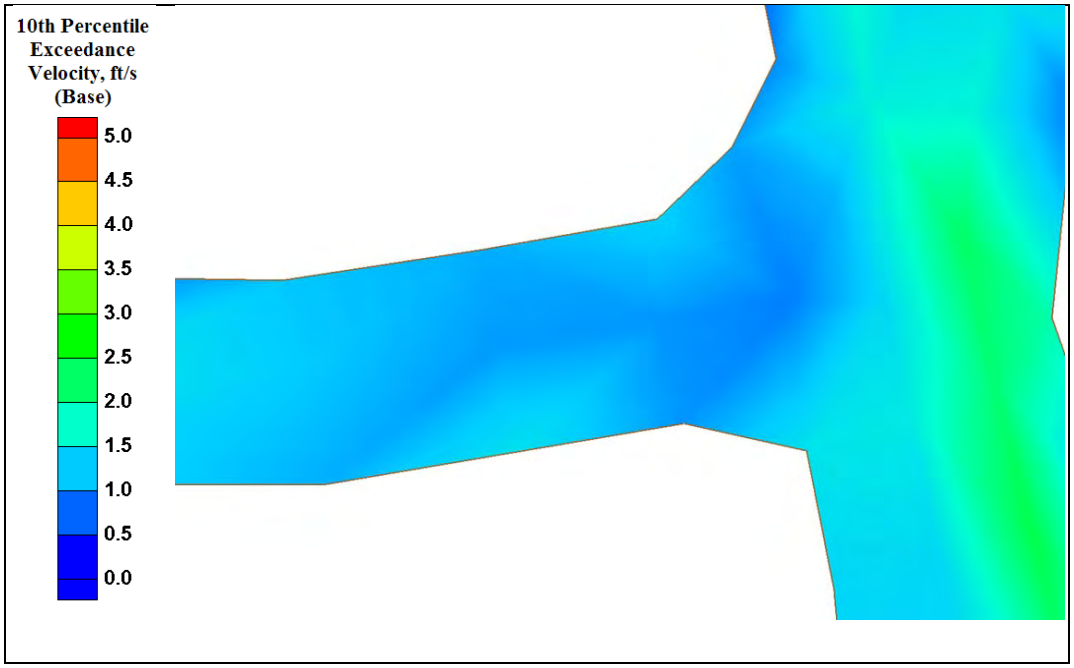

Figure B21. Bayou Grand Caillou 10th percentile exceedance velocity (base).

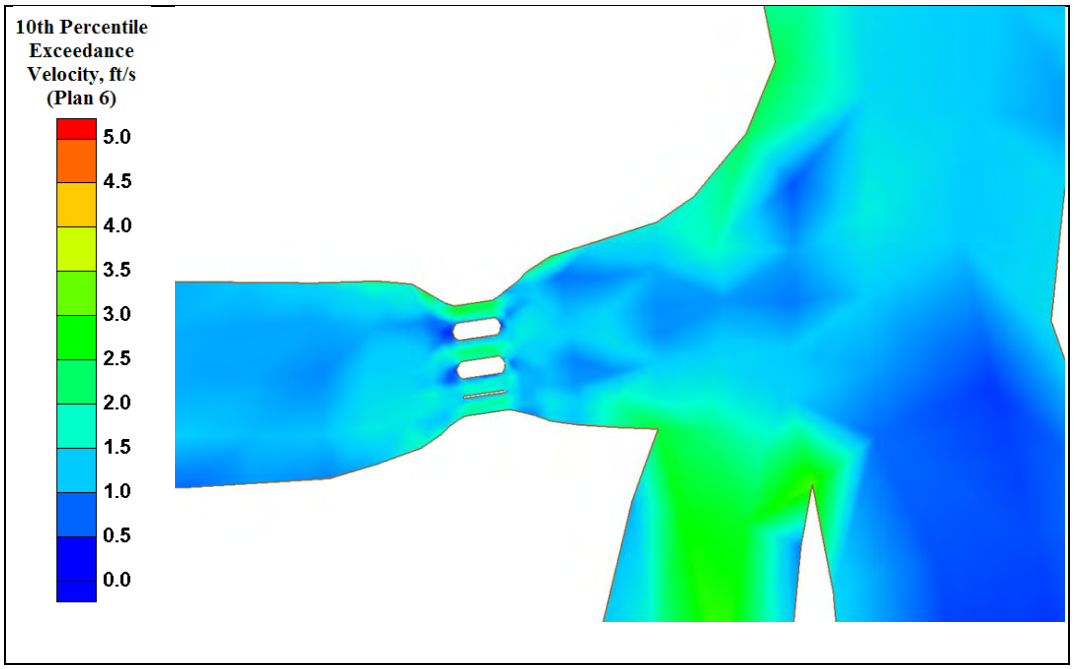

Figure B22. Bayou Grand Caillou 10th percentile exceedance velocity (Plan 6).

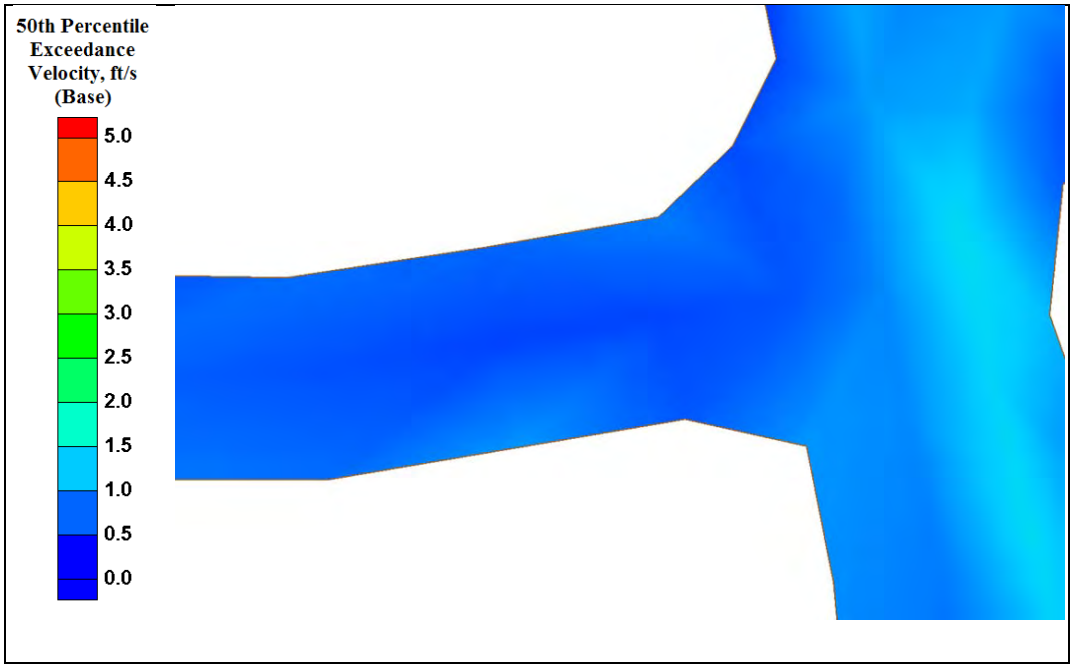

Figure B23. Bayou Grand Caillou 50th percentile exceedance velocity (base).

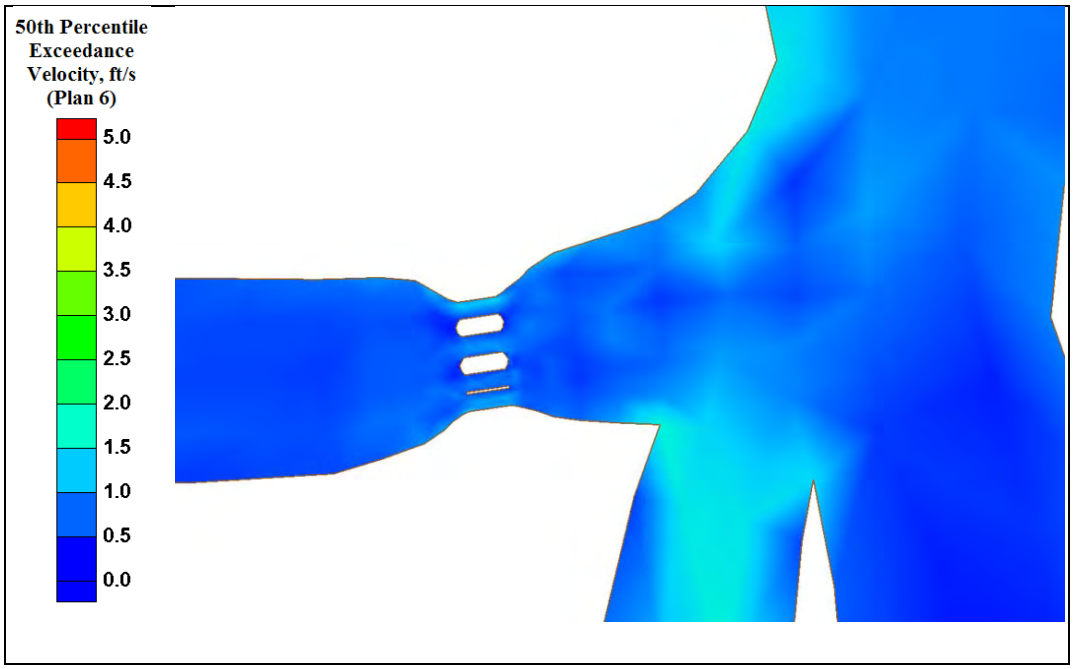

Figure B24. Bayou Grand Caillou 50th percentile exceedance velocity (Plan 6).

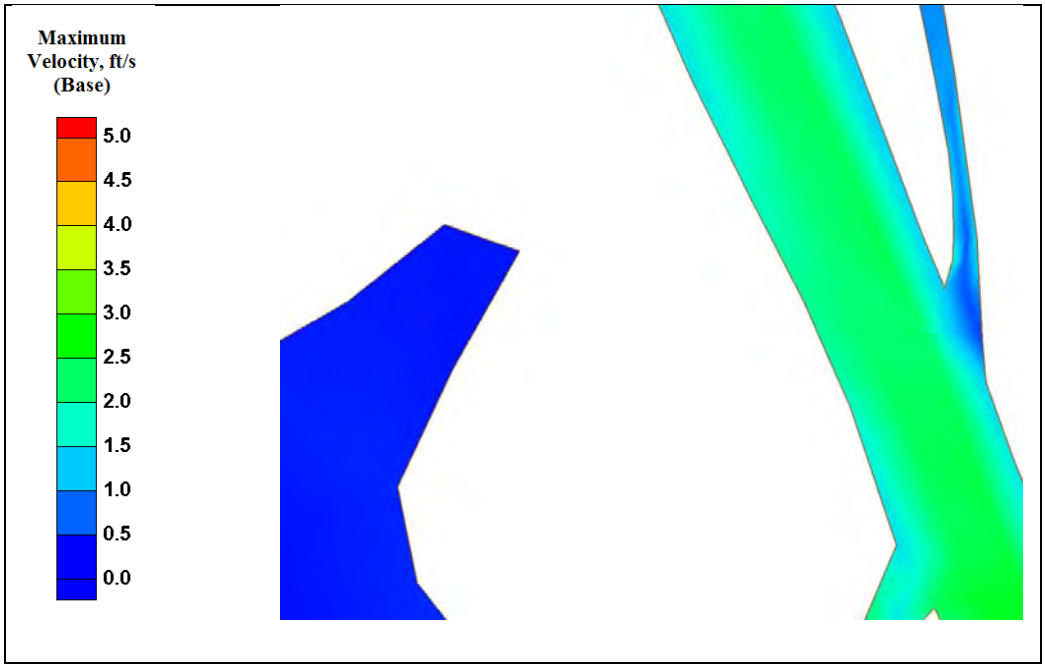

Figure B25. Houma Navigation Canal maximum velocity (base).

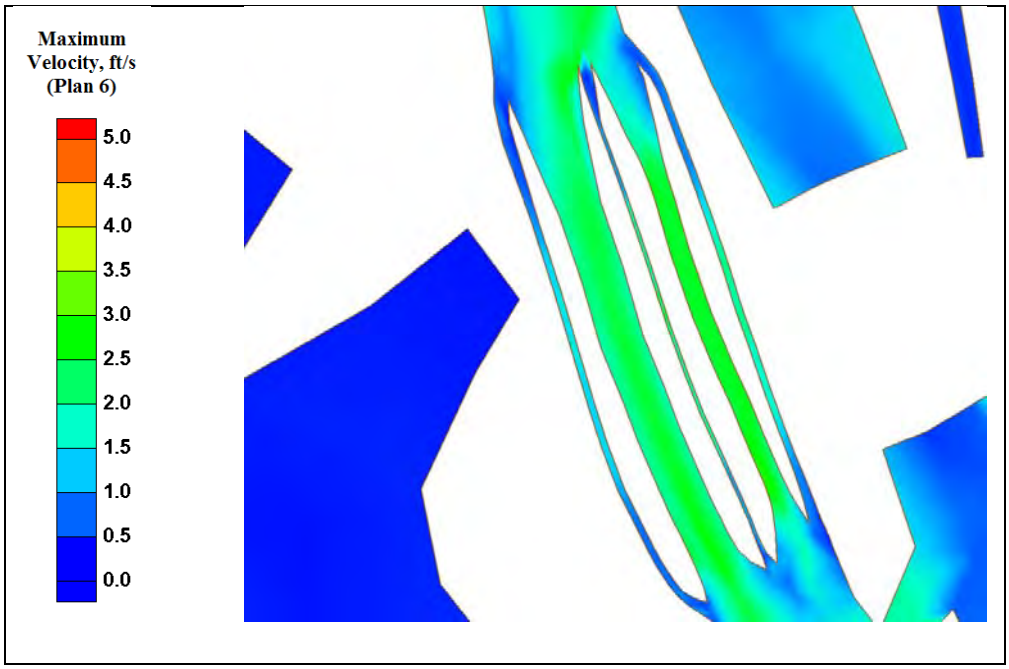

Figure B26. Houma Navigation Canal maximum velocity (Plan 6).

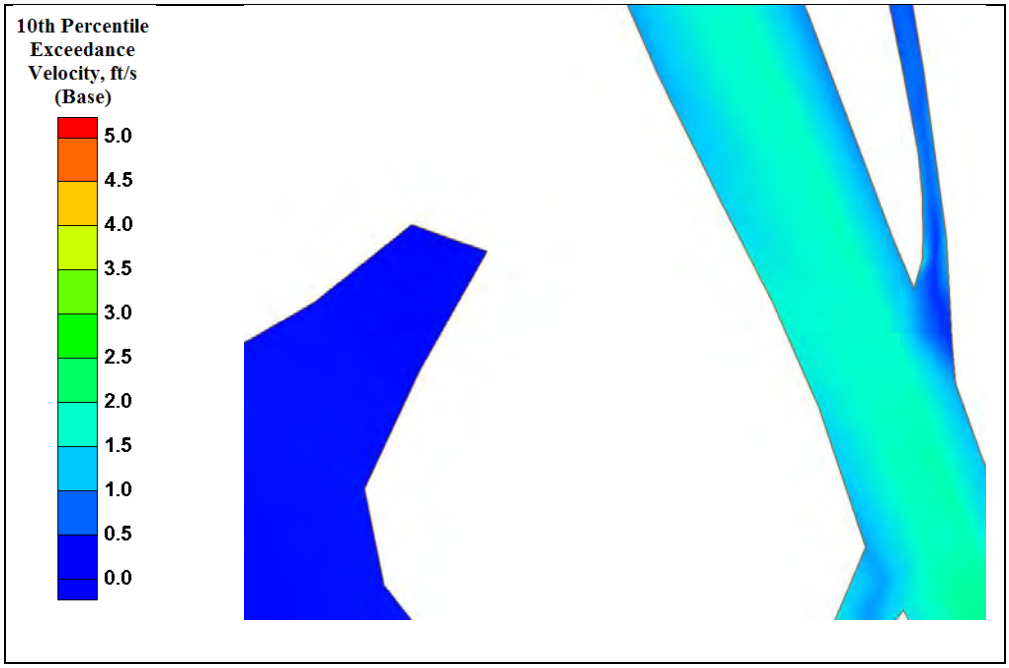

Figure B27. Houma Navigation Canal 10th percentile exceedance velocity (base).

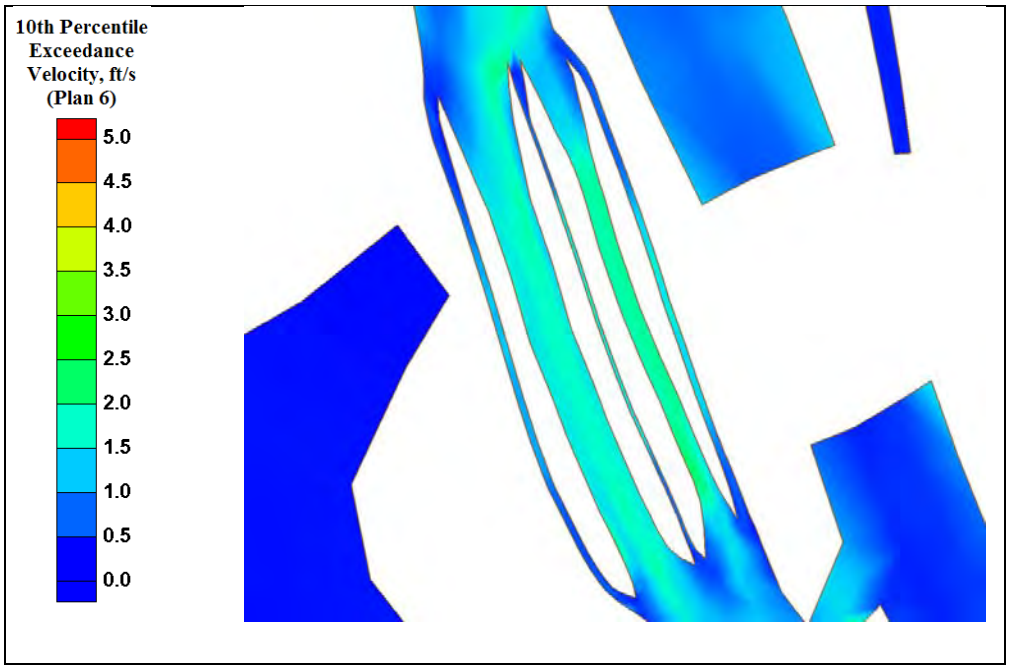

Figure B28. Houma Navigation Canal 10th percentile exceedance velocity (Plan 6).

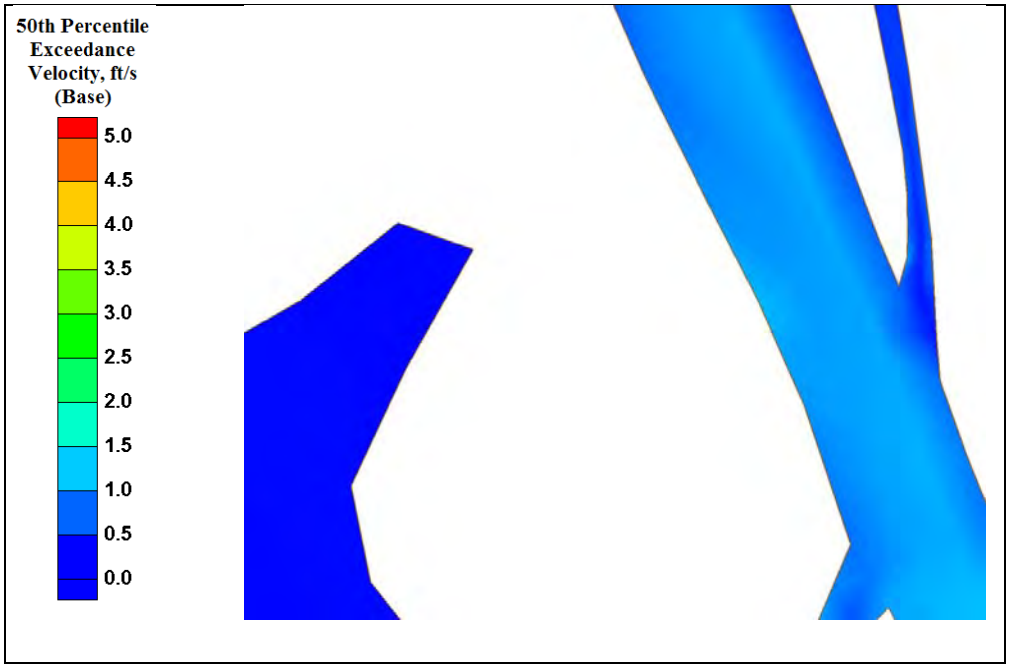

Figure B29. Houma Navigation Canal 50th percentile exceedance velocity (base).

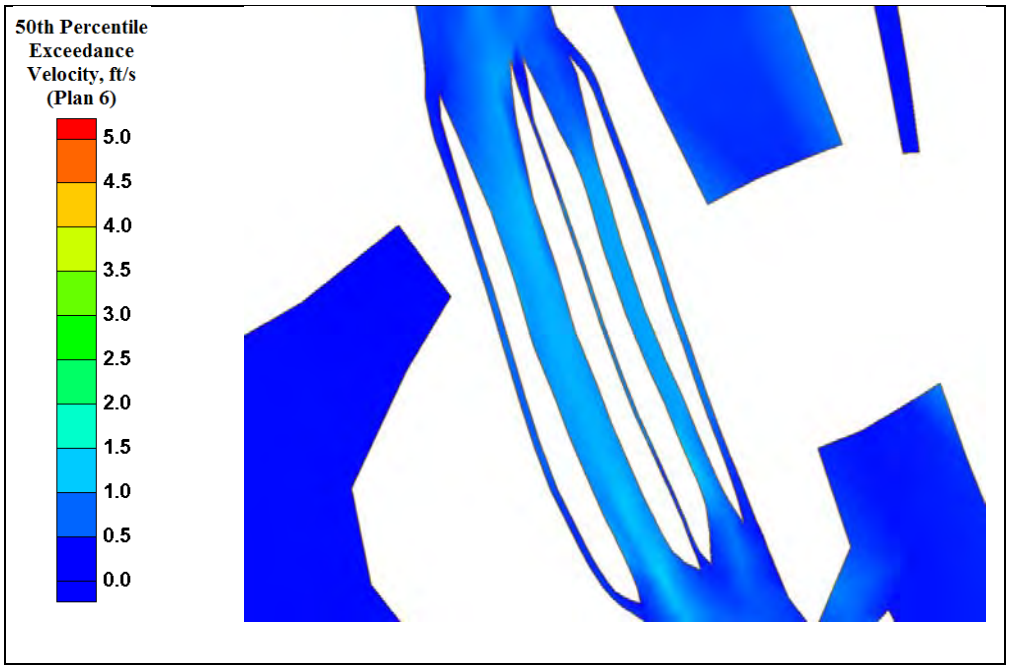

Figure B30. Houma Navigation Canal 50th percentile exceedance velocity (Plan 6).

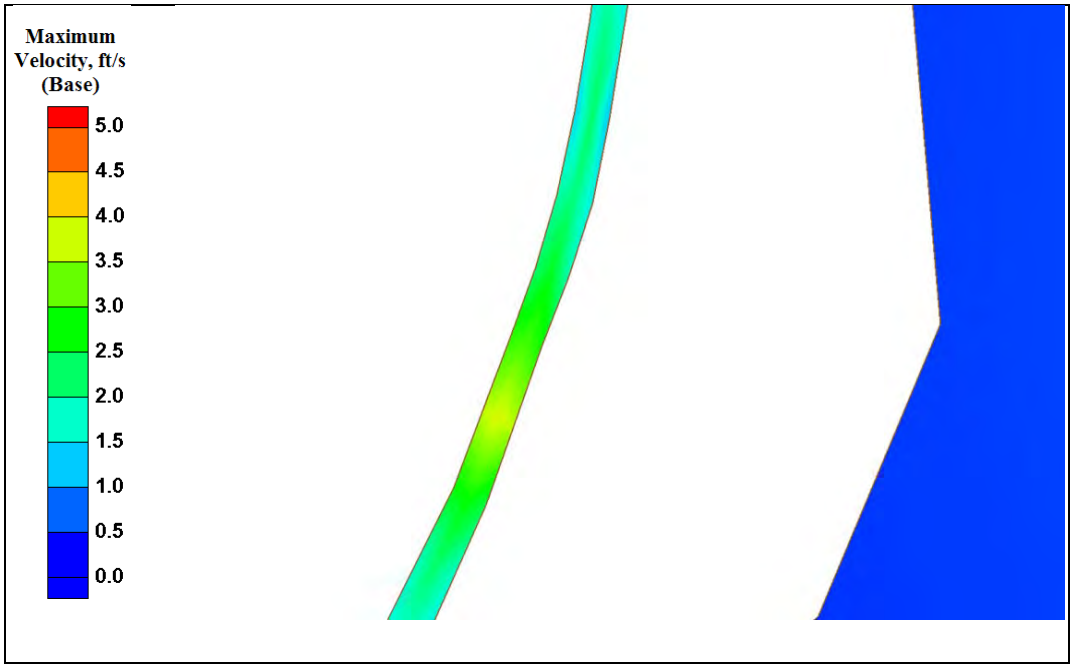

Figure B31. Bayou Fourpoints maximum velocity (base).

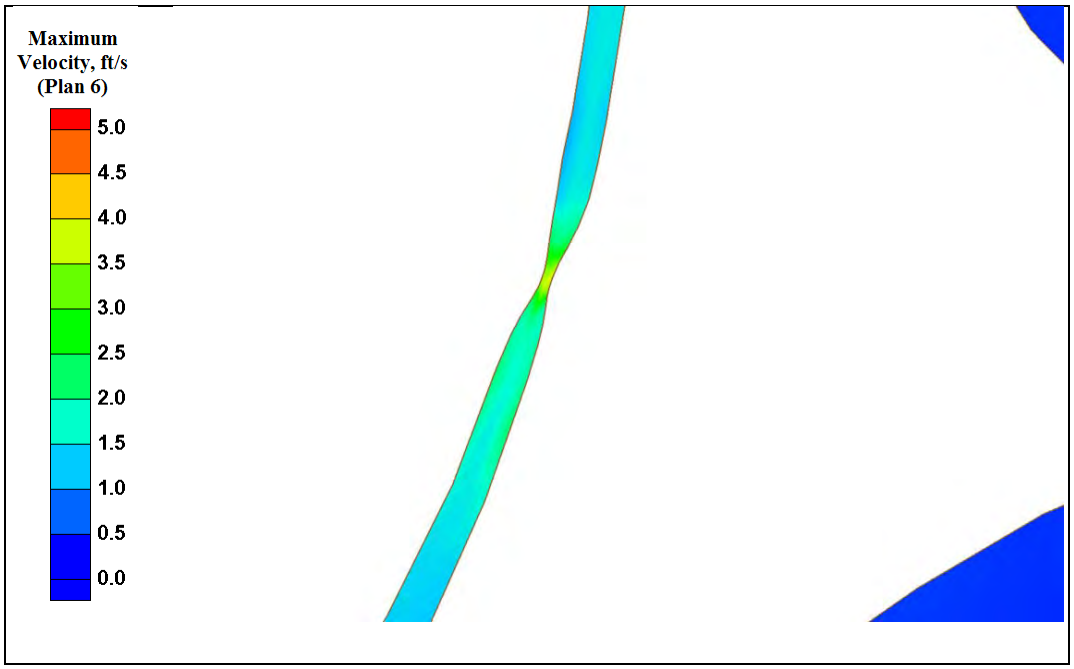

Figure B32. Bayou Fourpoints maximum velocity (Plan 6).

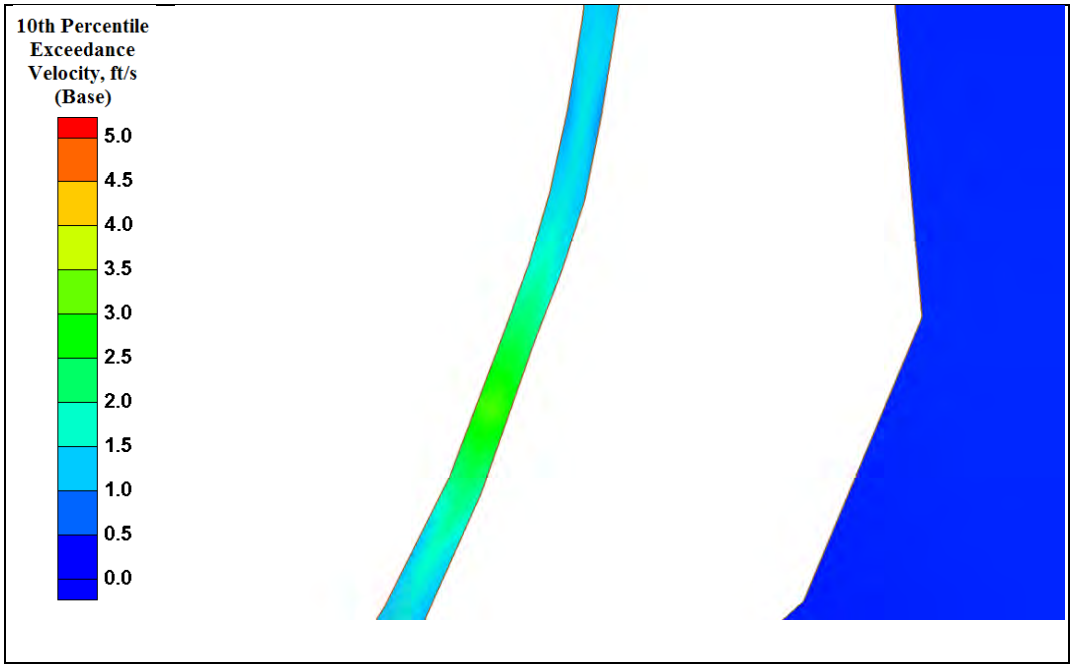

Figure B33. Bayou Fourpoints 10th percentile exceedance velocity (base).

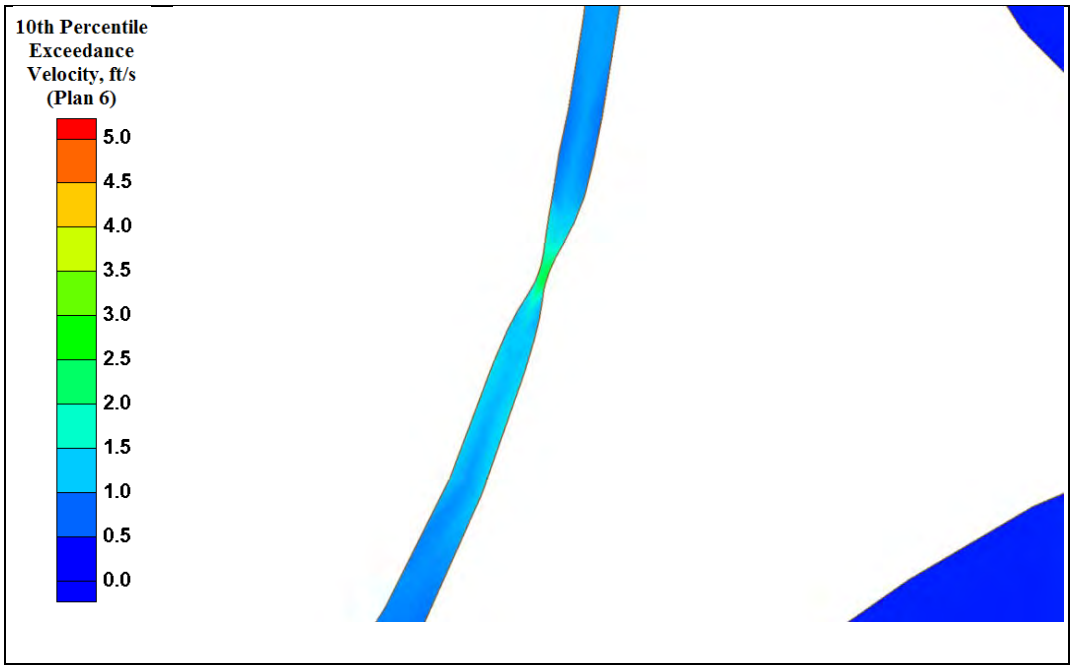

Figure B34. Bayou Fourpoints 10th percentile exceedance velocity (Plan 6).

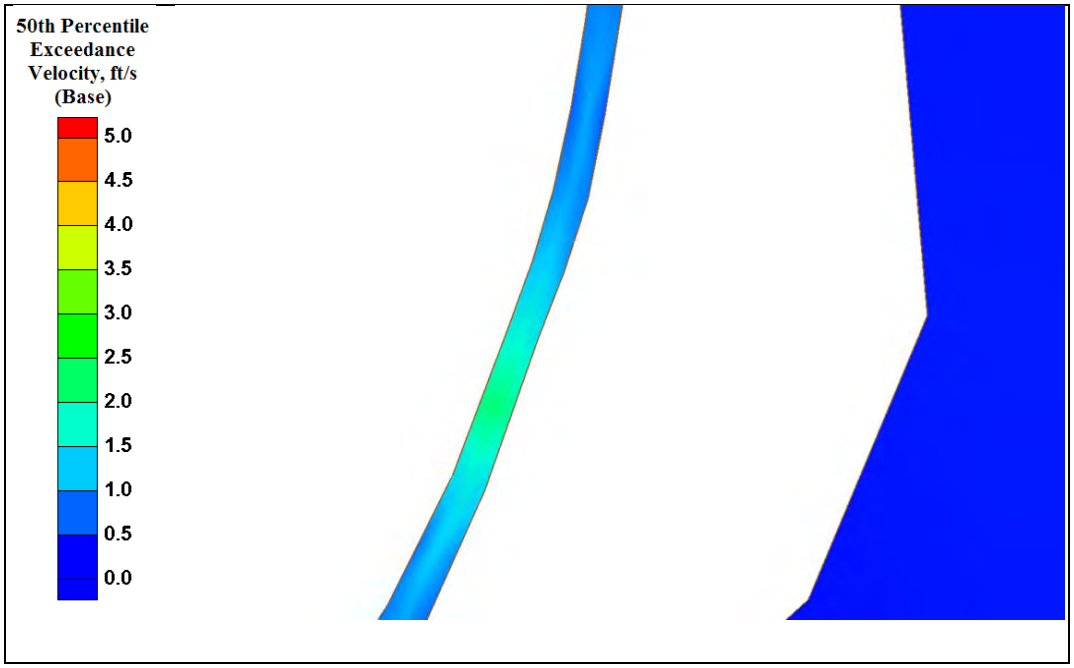

Figure B35. Bayou Fourpoints 50th percentile exceedance velocity (base).

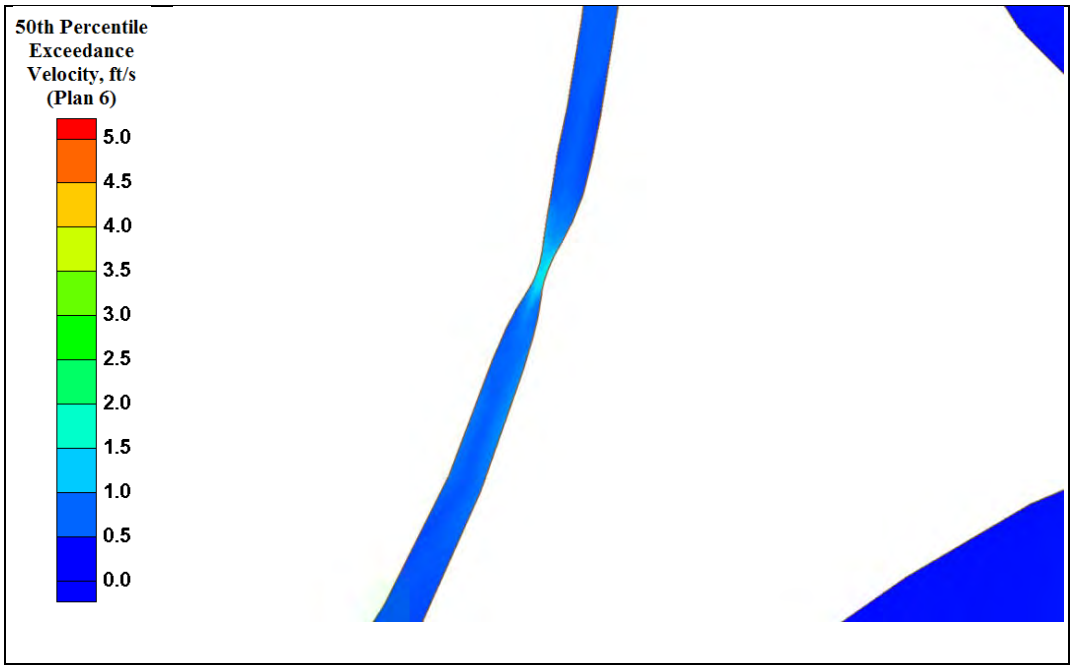

Figure B36. Bayou Fourpoints 50th percentile exceedance velocity (Plan 6).

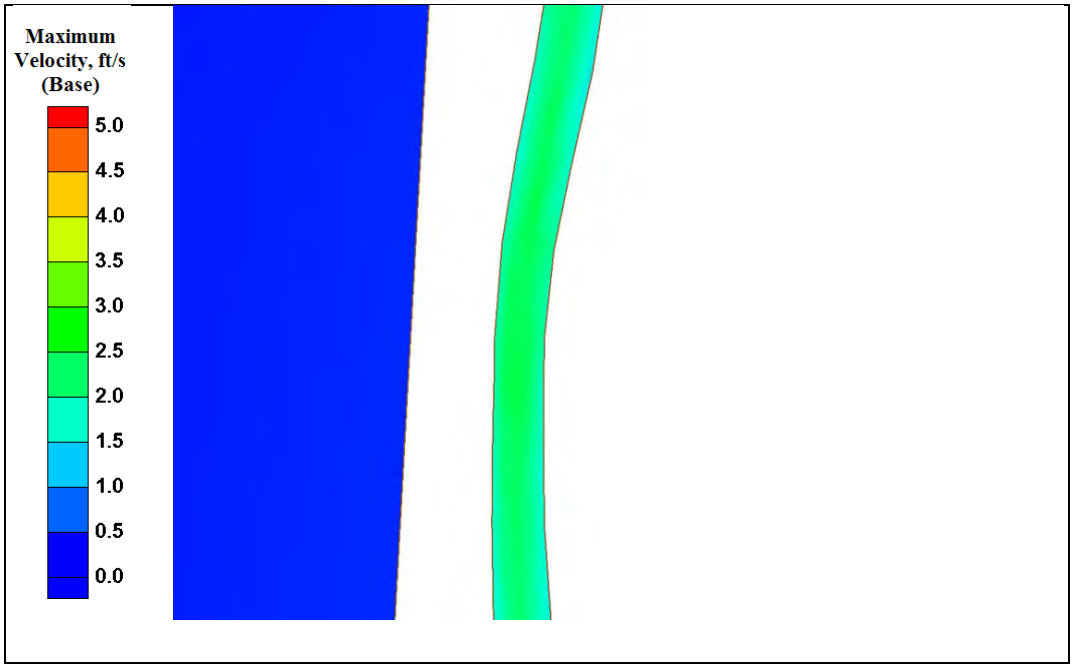

Figure B37. Bayou Petit Caillou maximum velocity (base).

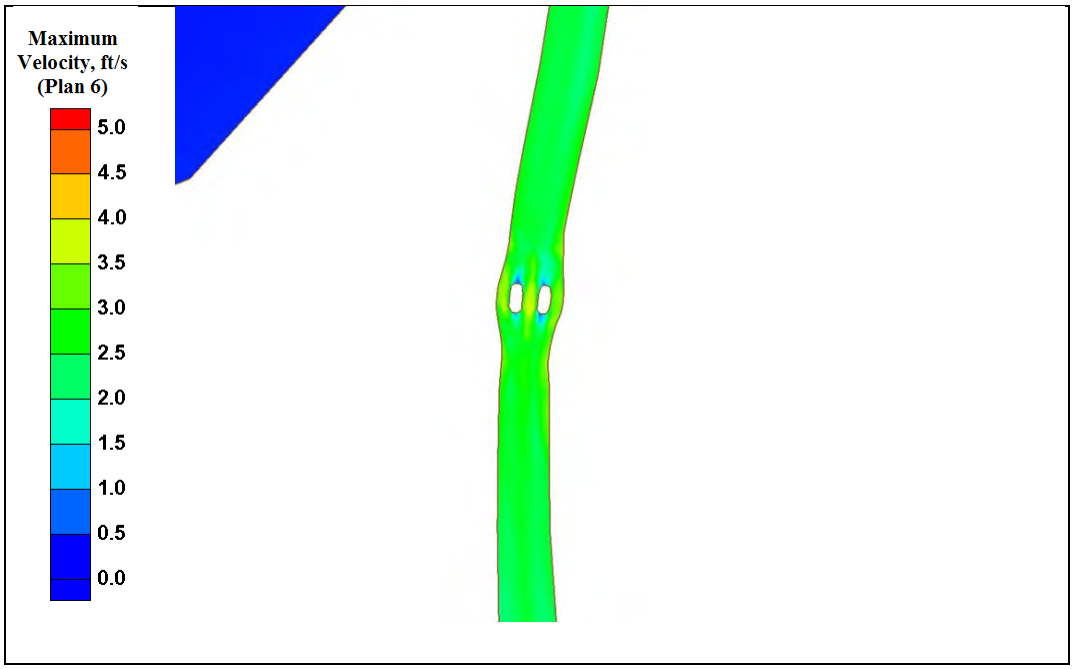

Figure B38. Bayou Petit Caillou maximum velocity (Plan 6).

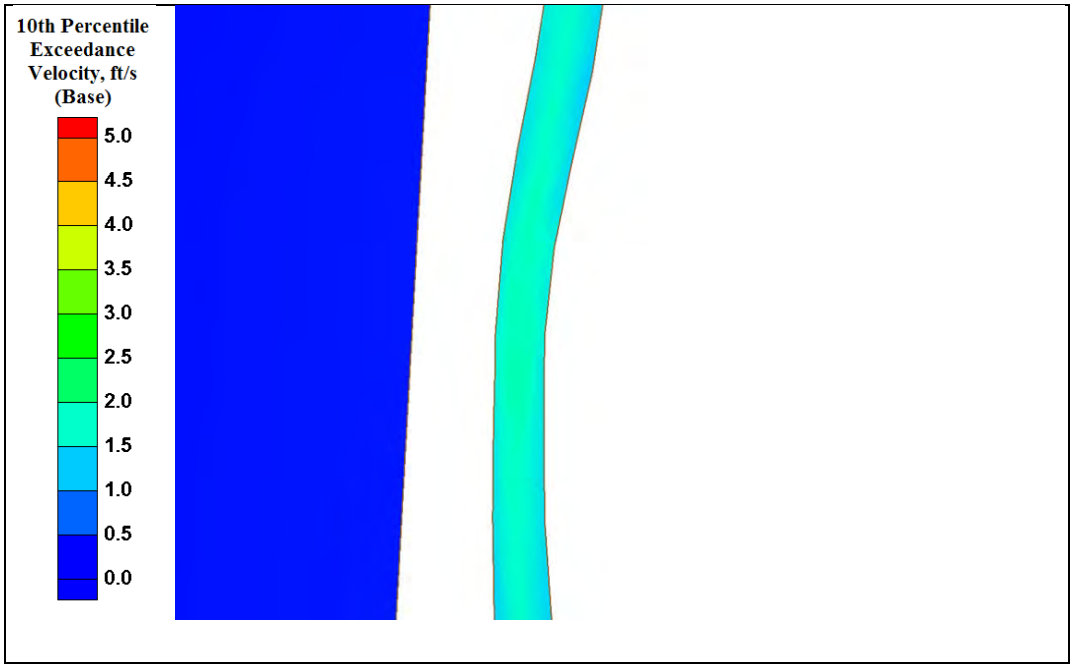

Figure B39. Bayou Petit Caillou 10th percentile exceedance velocity (base).

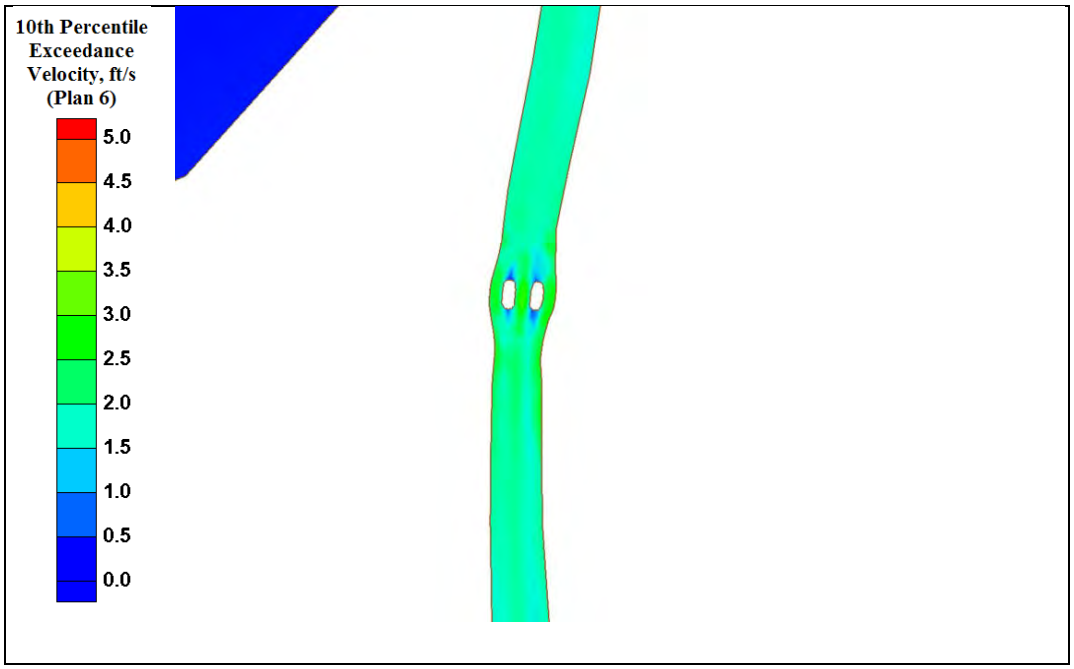

Figure B40. Bayou Petit Caillou 10th percentile exceedance velocity (Plan 6).

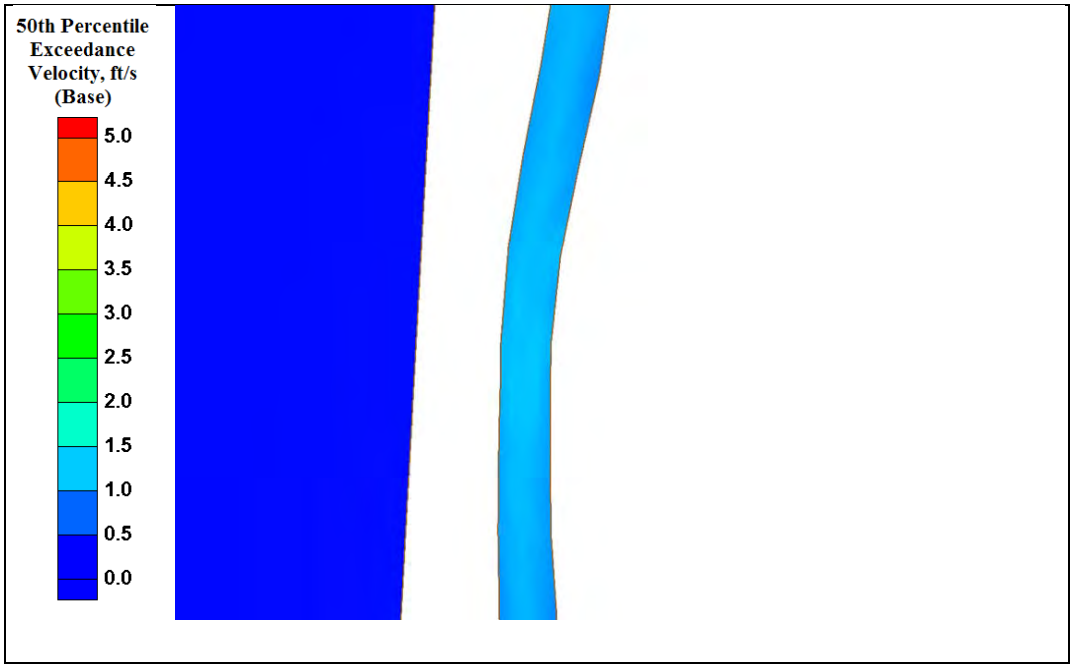

Figure B41. Bayou Petit Caillou 50th percentile exceedance velocity (base).

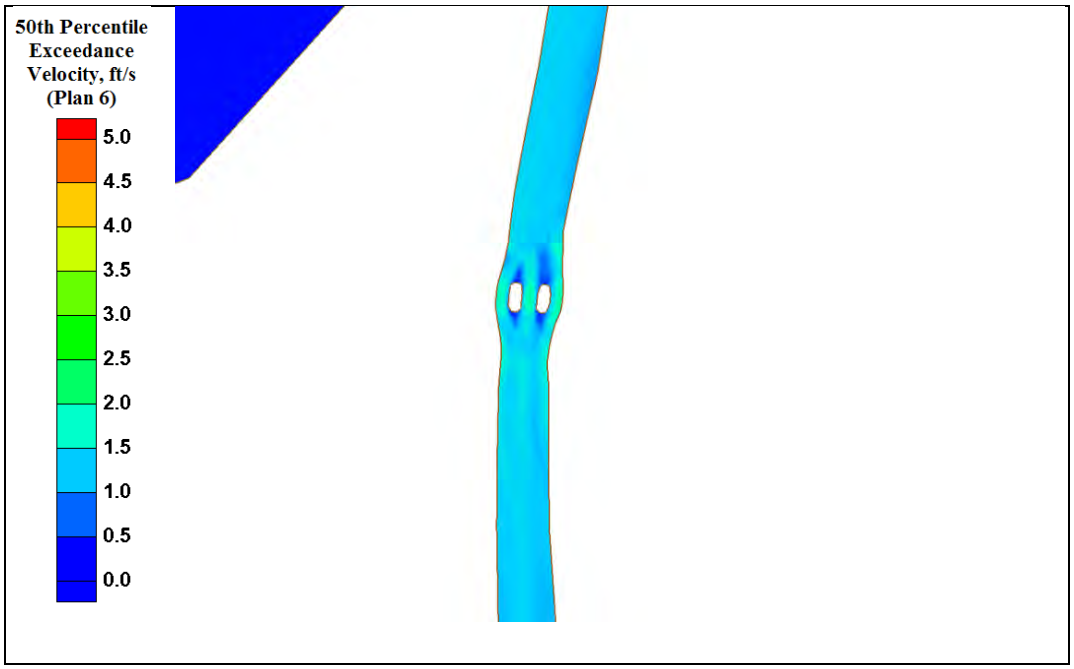

Figure B42. Bayou Petit Caillou 50th percentile exceedance velocity (Plan 6).

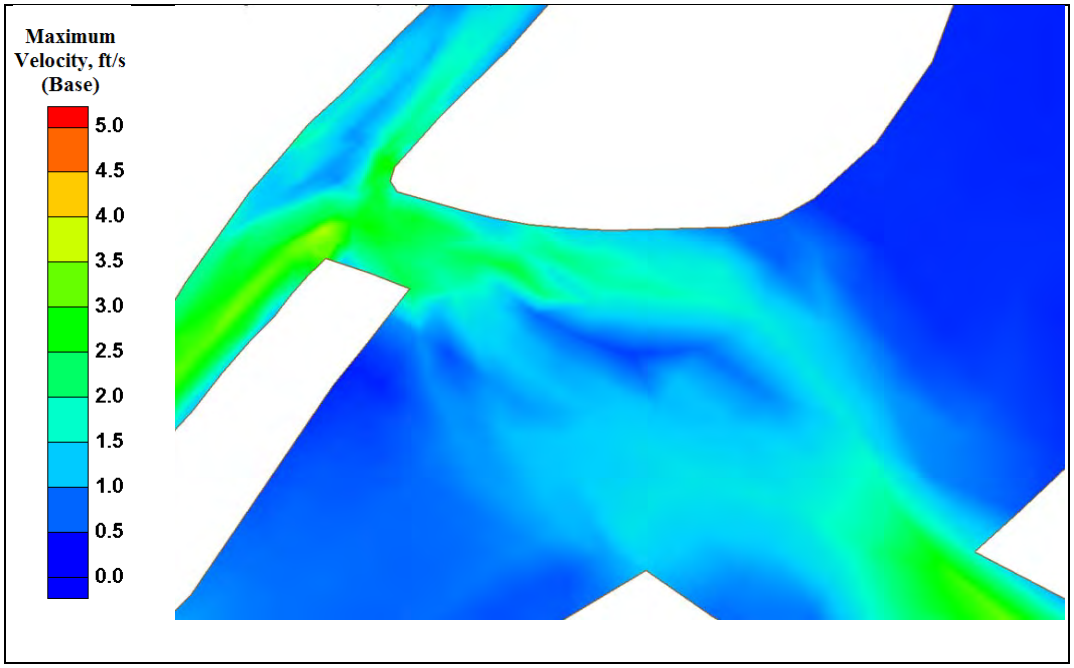

Figure B43. Placid Canal maximum velocity (base).

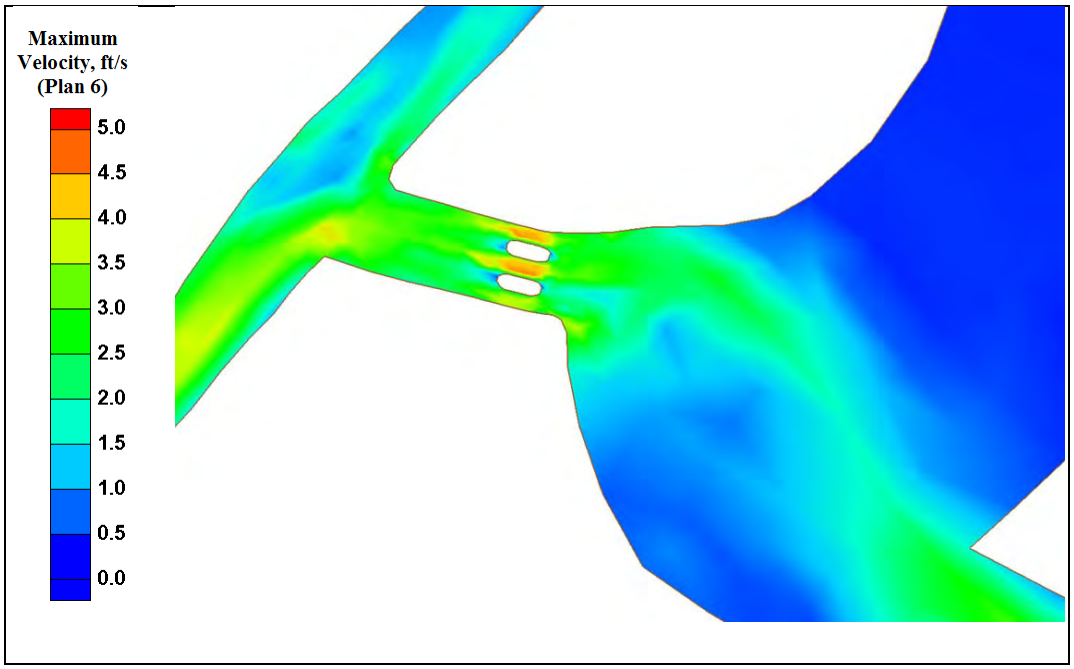

Figure B44. Placid Canal maximum velocity (Plan 6).

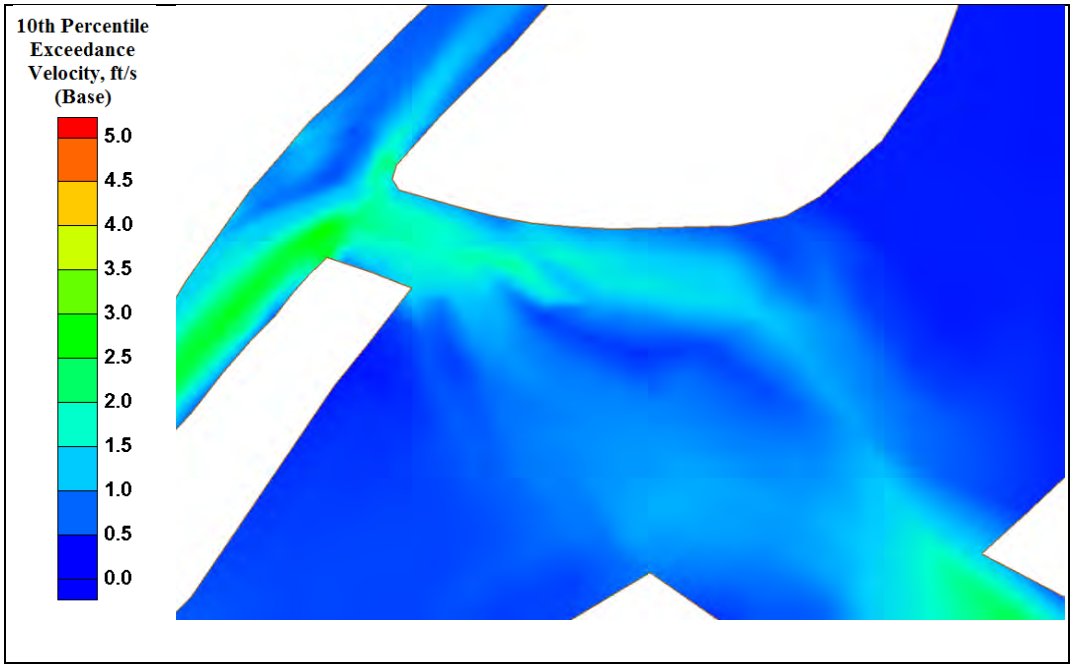

Figure B45. Placid Canal 10th percentile exceedance velocity (base).

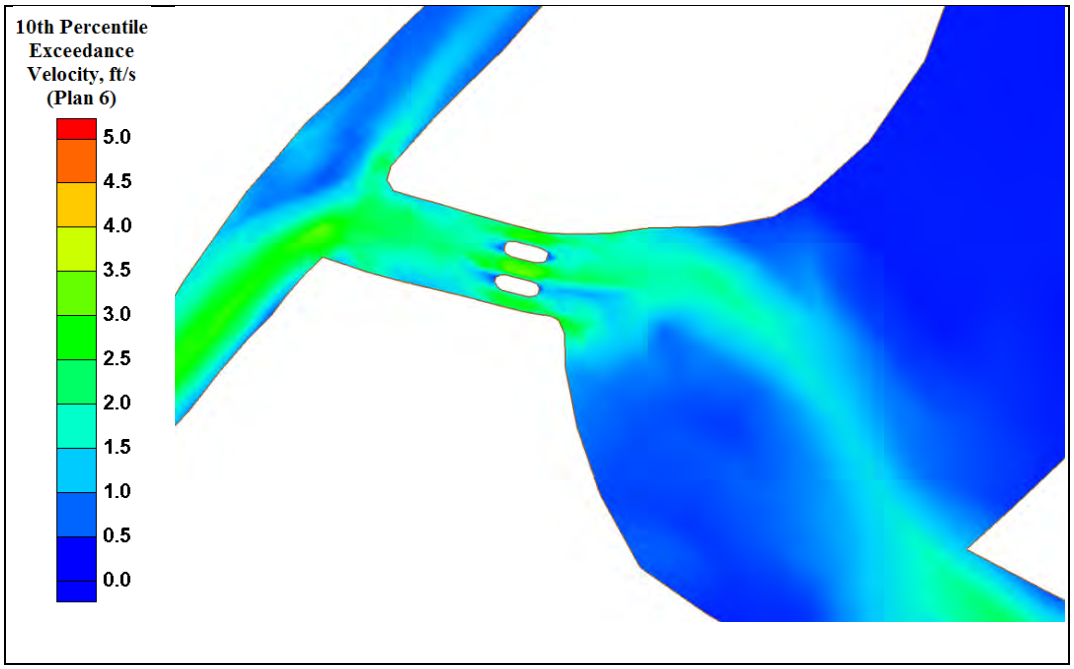

Figure B46. Placid Canal 10th percentile exceedance velocity (Plan 6).

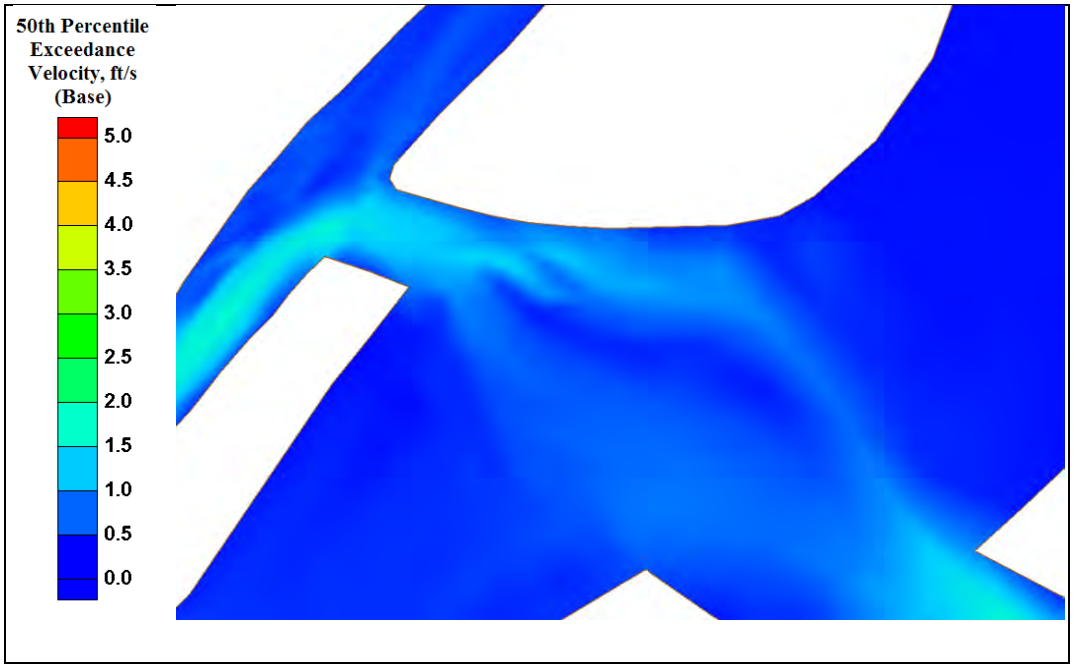

Figure B47. Placid Canal 50th percentile exceedance velocity (base).

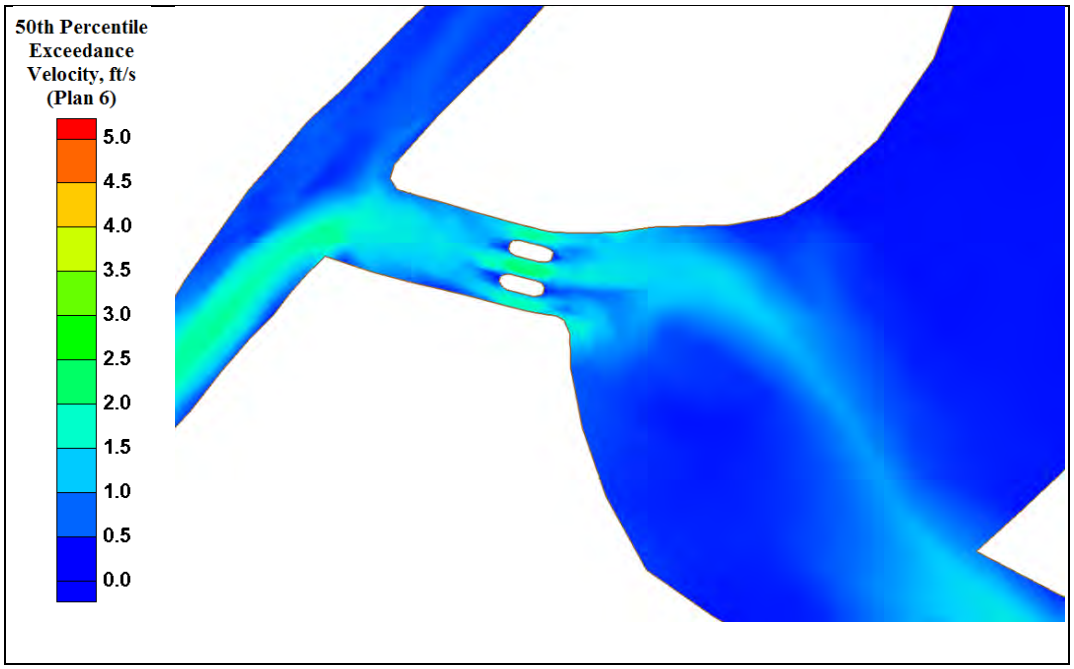

Figure B48. Placid Canal 50th percentile exceedance velocity (Plan 6).

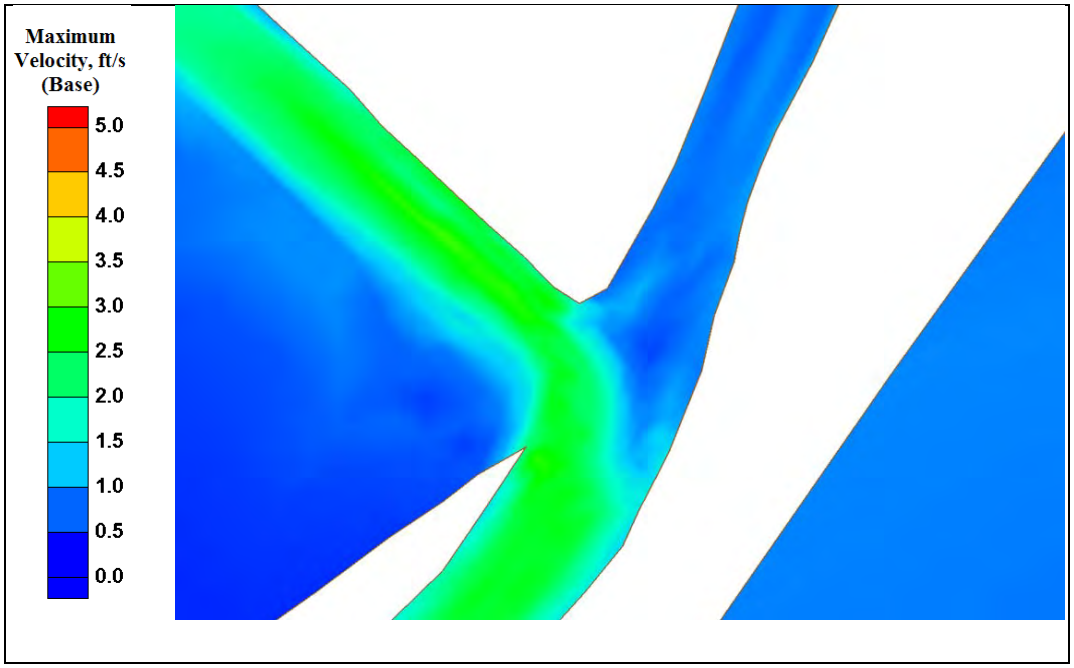

Figure B49. Bush Canal maximum velocity (base).

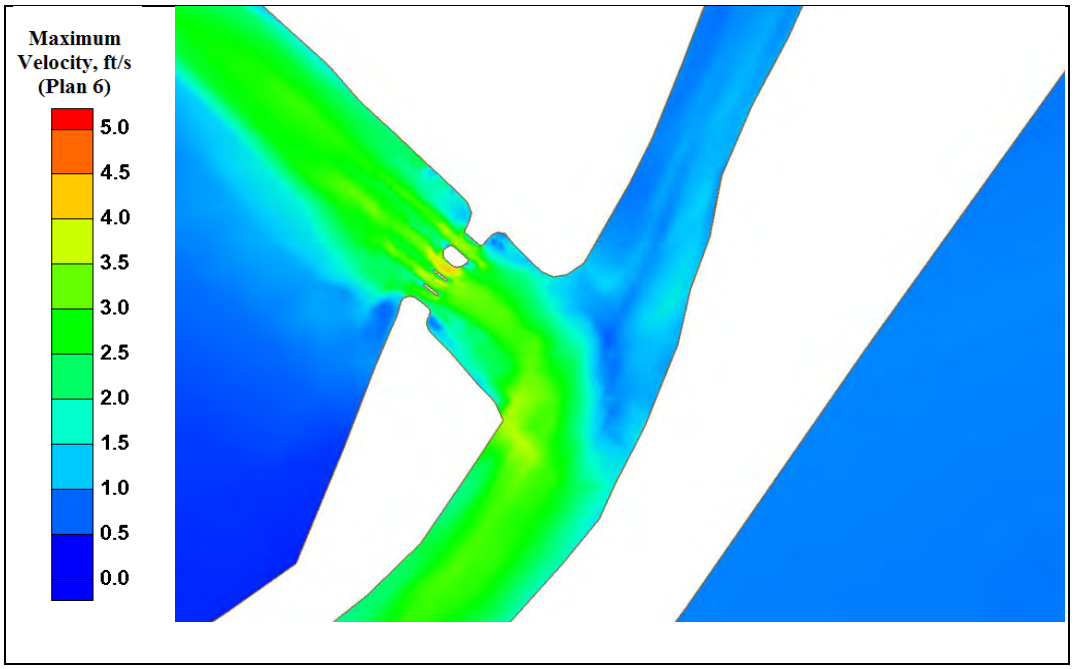

Figure B50. Bush Canal maximum velocity (Plan 6).

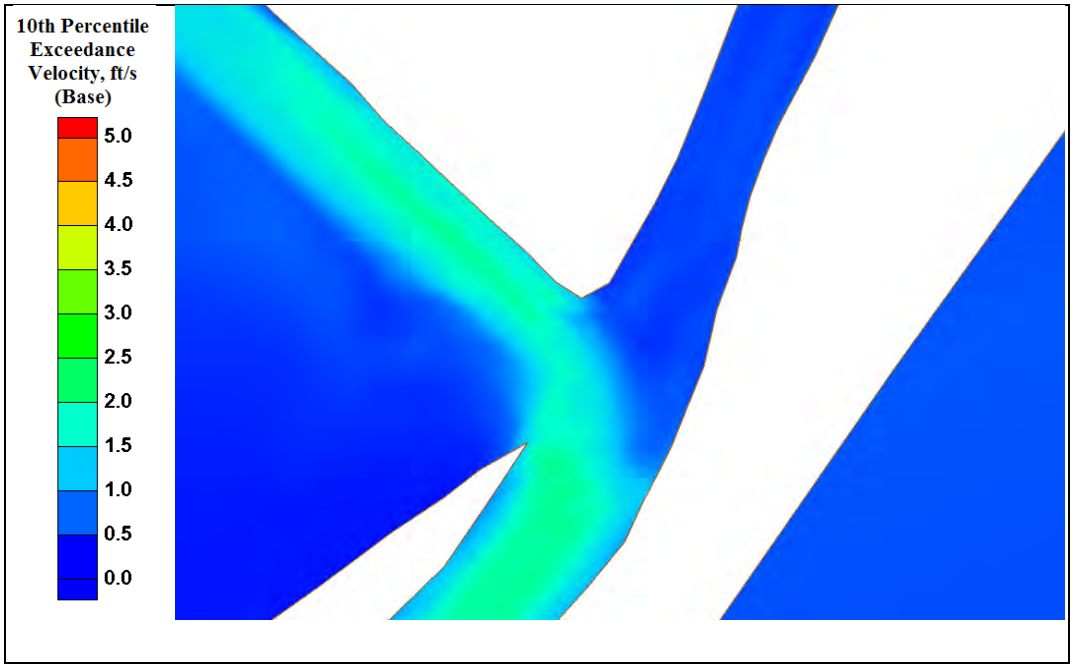

Figure B51. Bush Canal 10th percentile exceedance velocity (base).

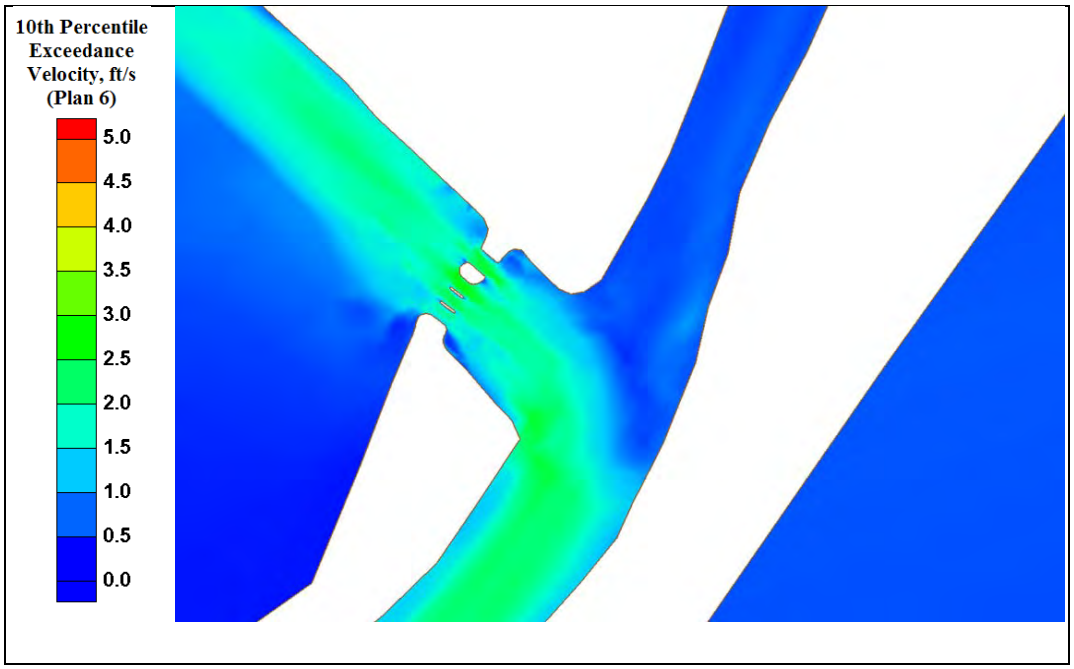

Figure B52. Bush Canal 10th percentile exceedance velocity (Plan 6).

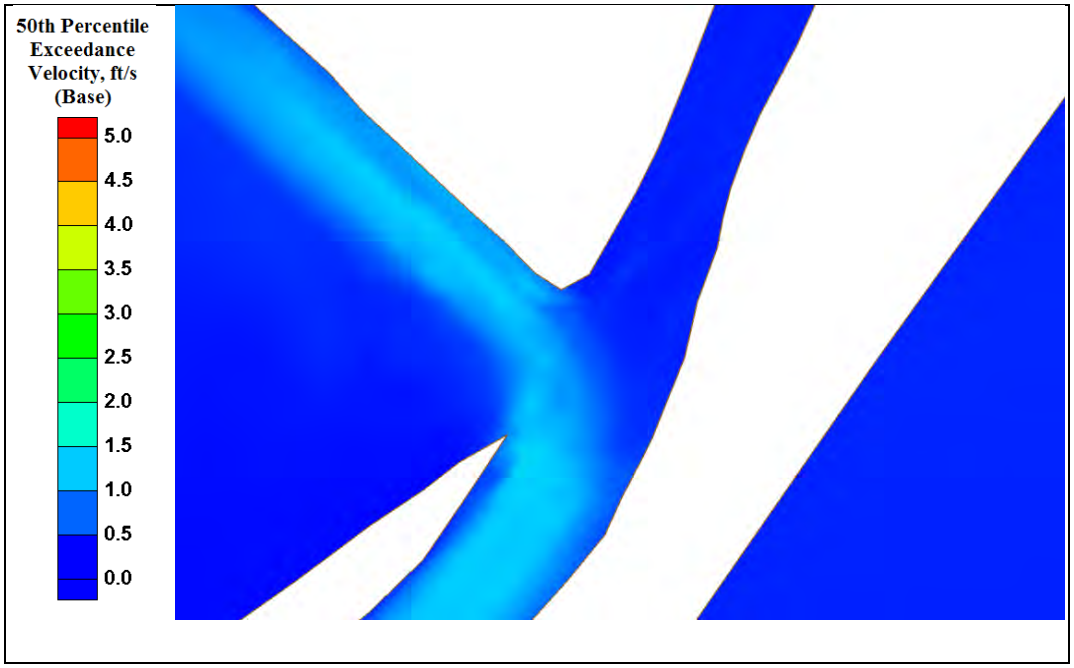

Figure B53. Bush Canal 50th percentile exceedance velocity (base).

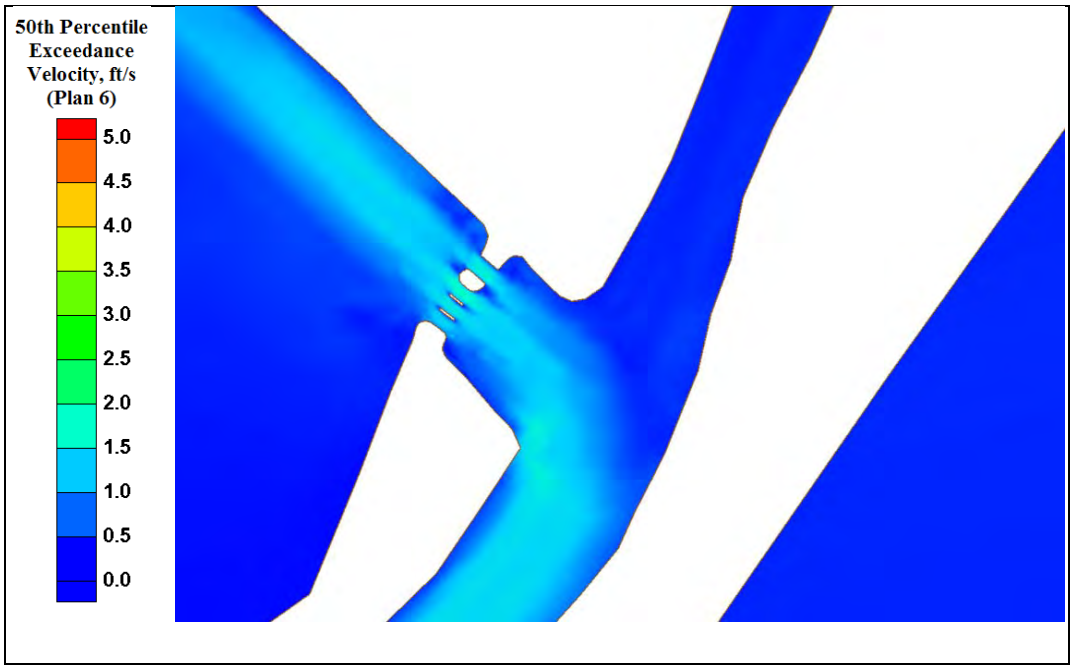

Figure B54. Bush Canal 50th percentile exceedance velocity (Plan 6).

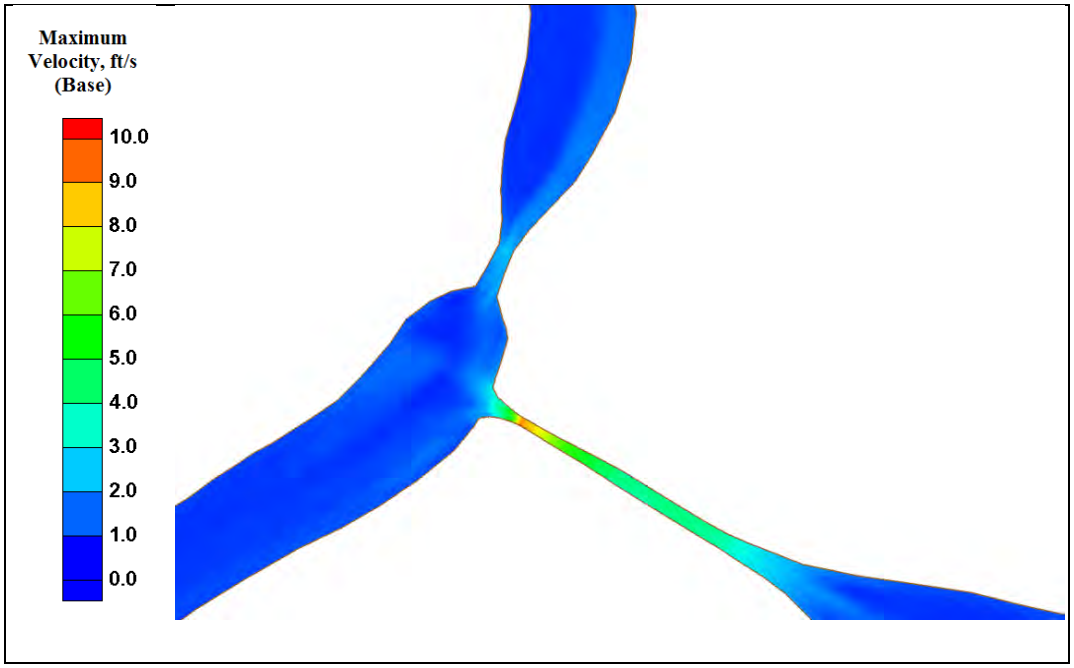

Figure B55. Bayou Terrebonne maximum velocity (base).

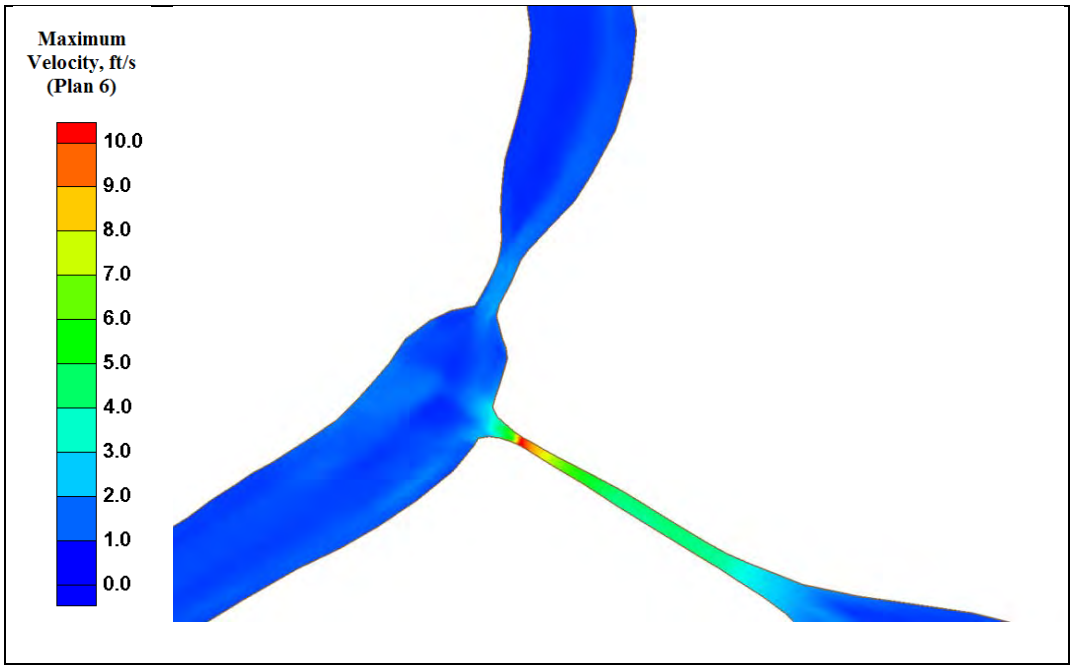

Figure B56. Bayou Terrebonne maximum velocity (Plan 6).

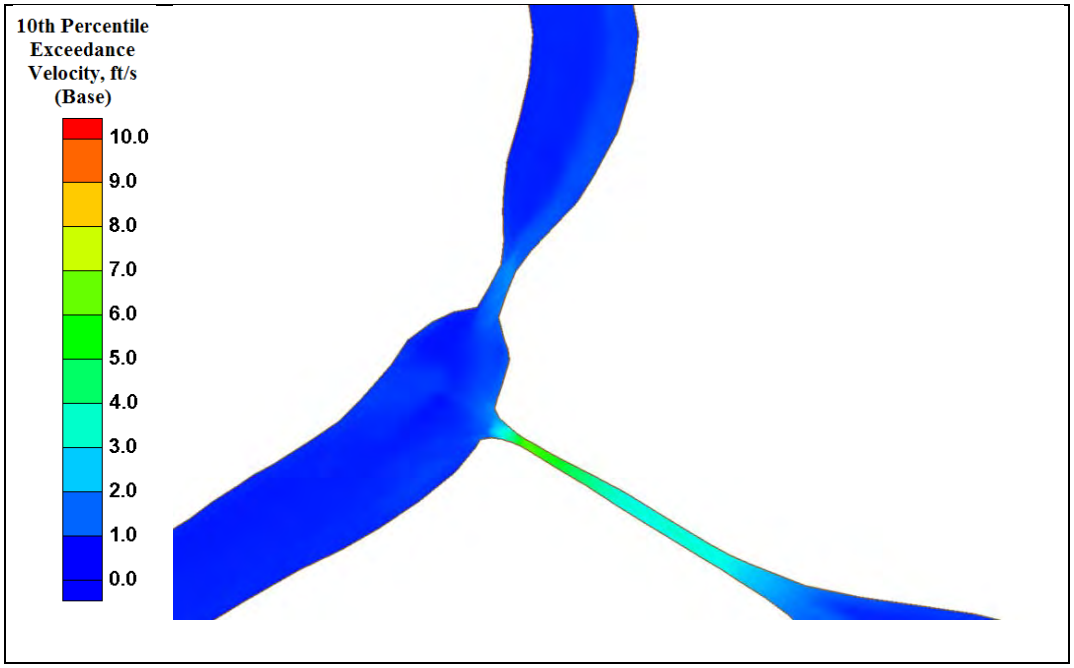

Figure B57. Bayou Terrebonne 10th percentile exceedance velocity (base).

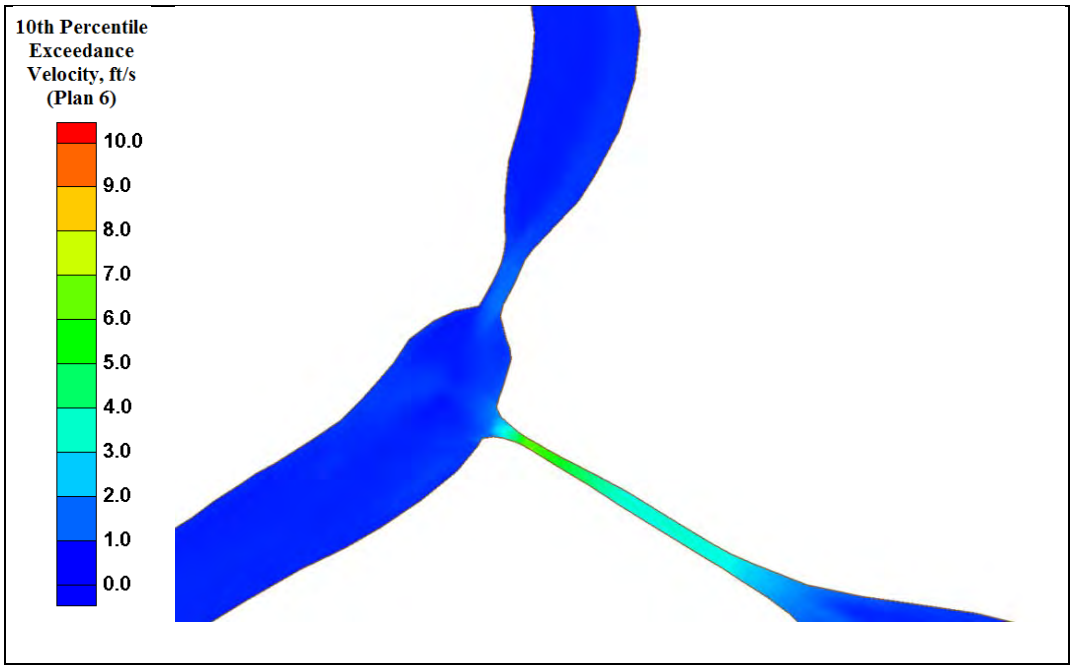

Figure B58. Bayou Terrebonne 10th percentile exceedance velocity (Plan 6).

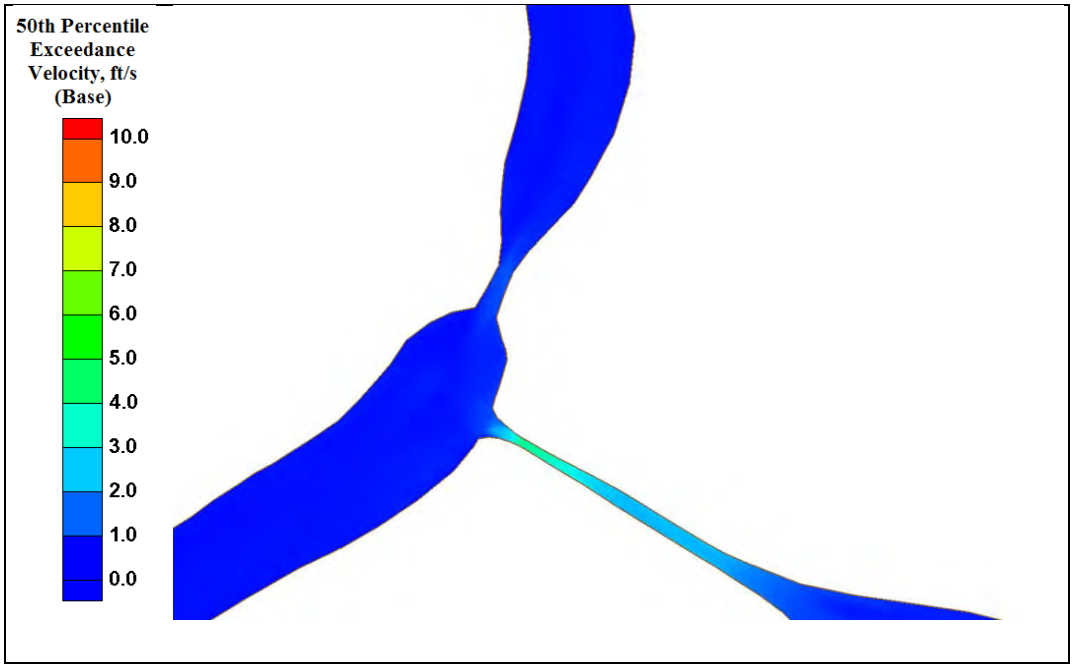

Figure B59. Bayou Terrebonne 50th percentile exceedance velocity (base).

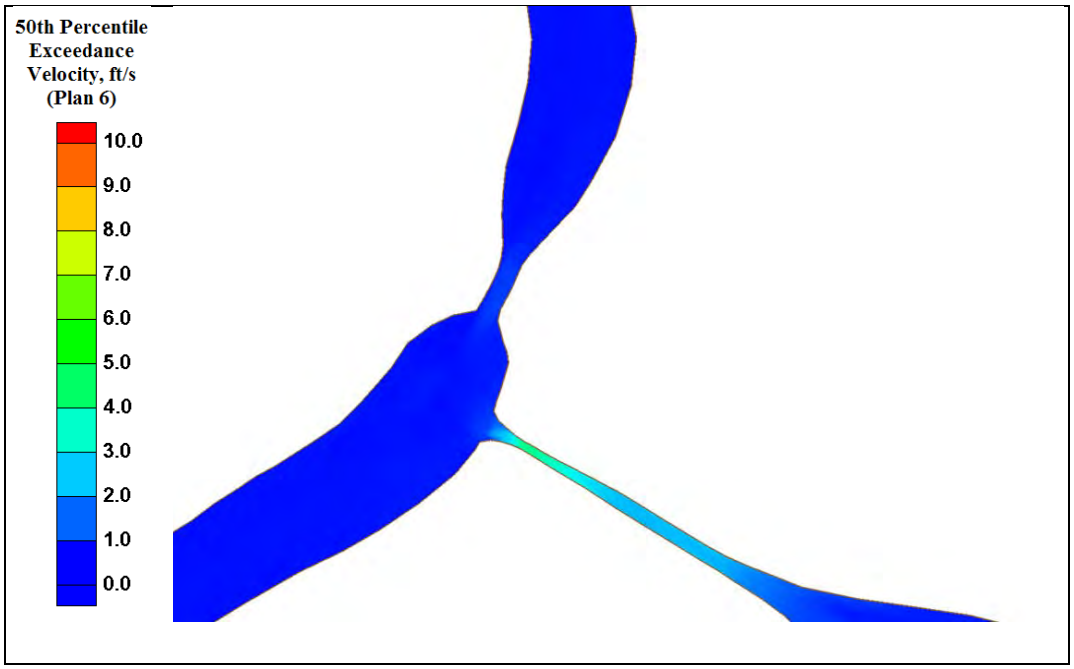

Figure B60. Bayou Terrebonne 50th percentile exceedance velocity (Plan 6).

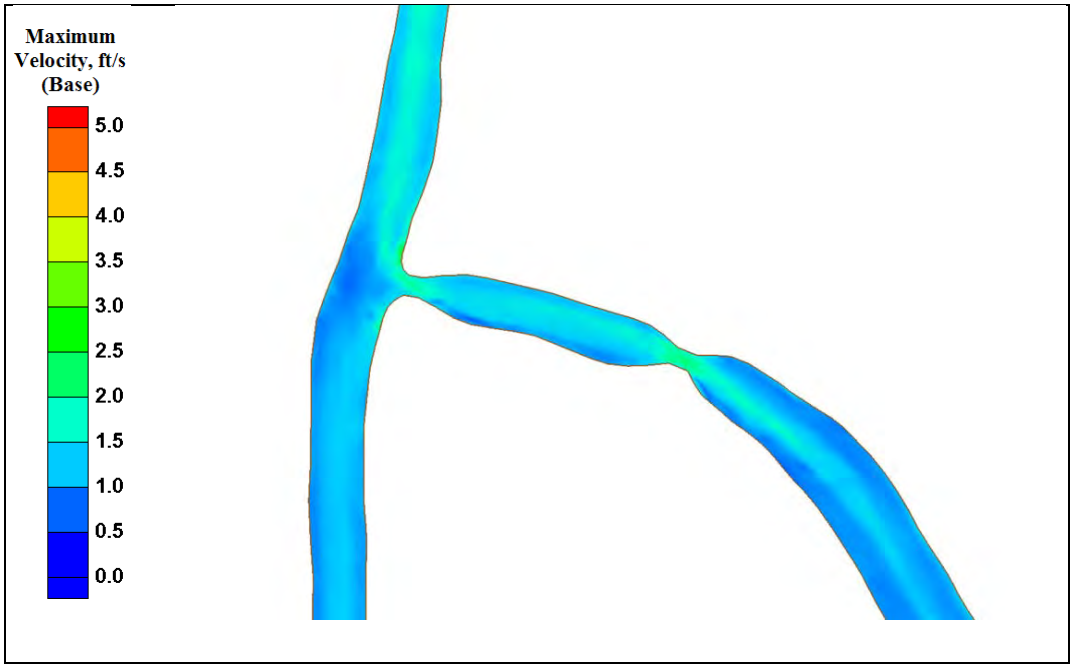

Figure B61. Humble Canal maximum velocity (base).

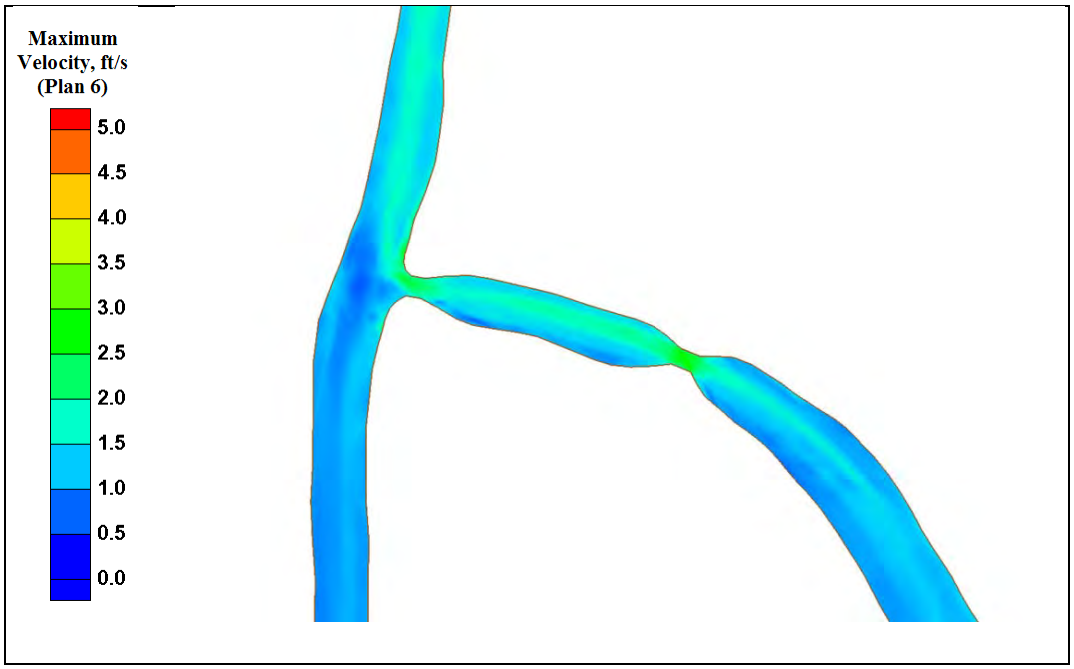

Figure B62. Humble Canal maximum velocity (Plan 6).

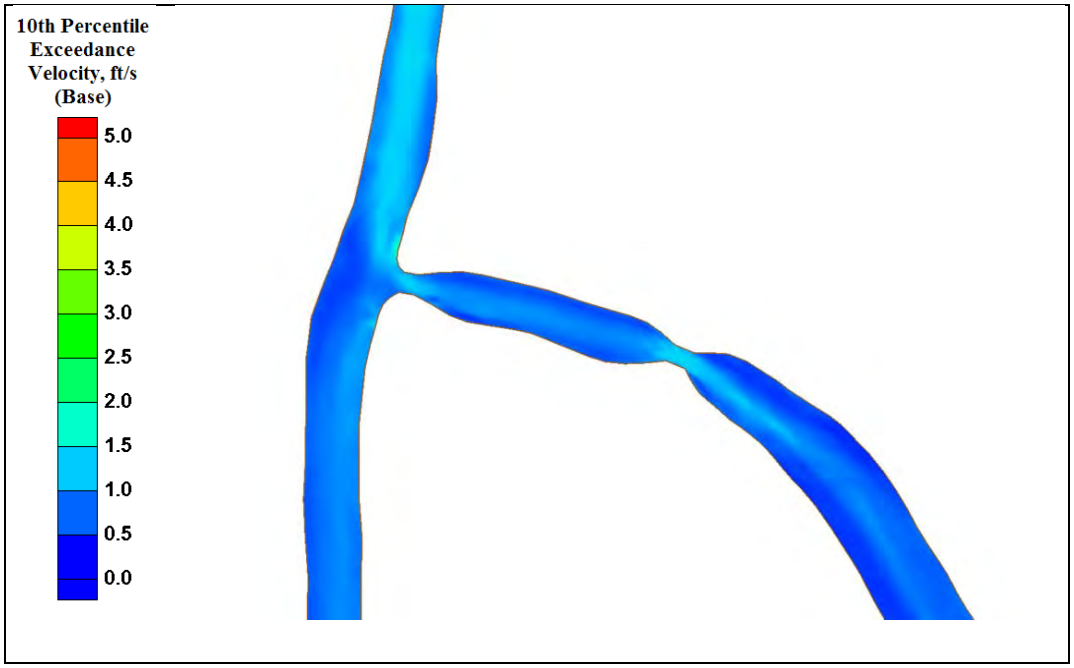

Figure B63. Humble Canal 10th percentile exceedance velocity (base).

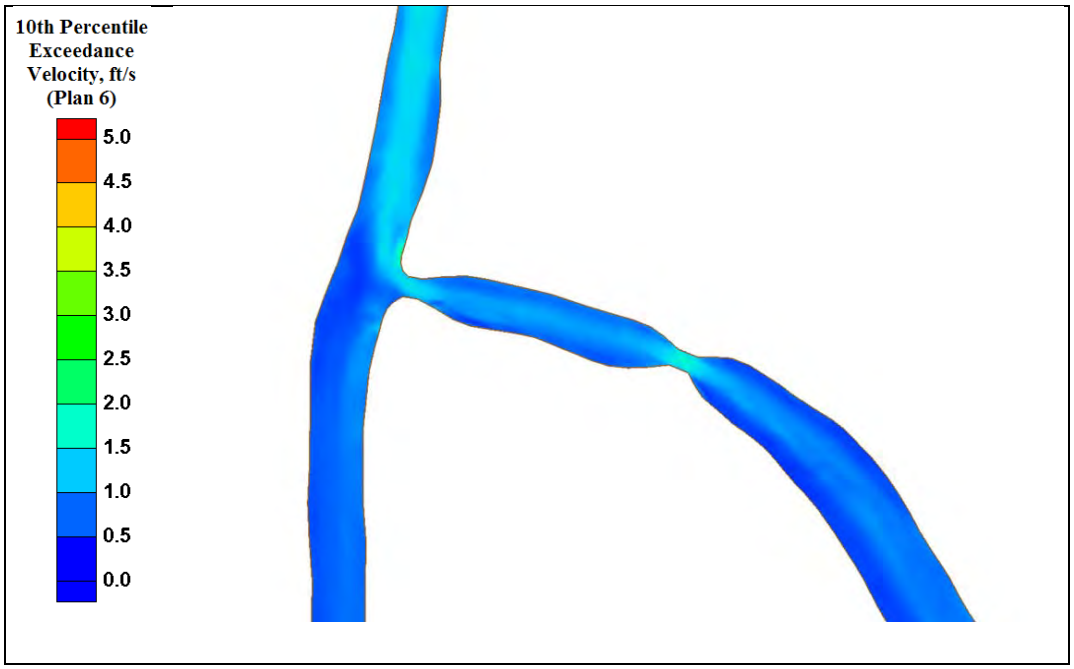

Figure B64. Humble Canal 10th percentile exceedance velocity (Plan 6).

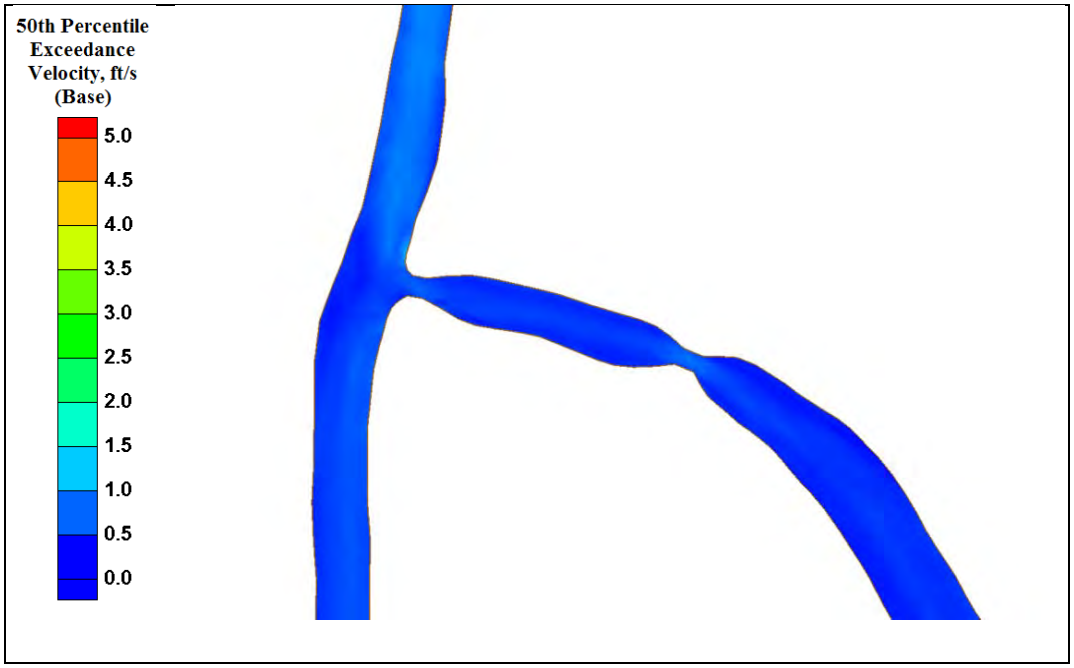

Figure B65. Humble Canal 50th percentile exceedance velocity (base).

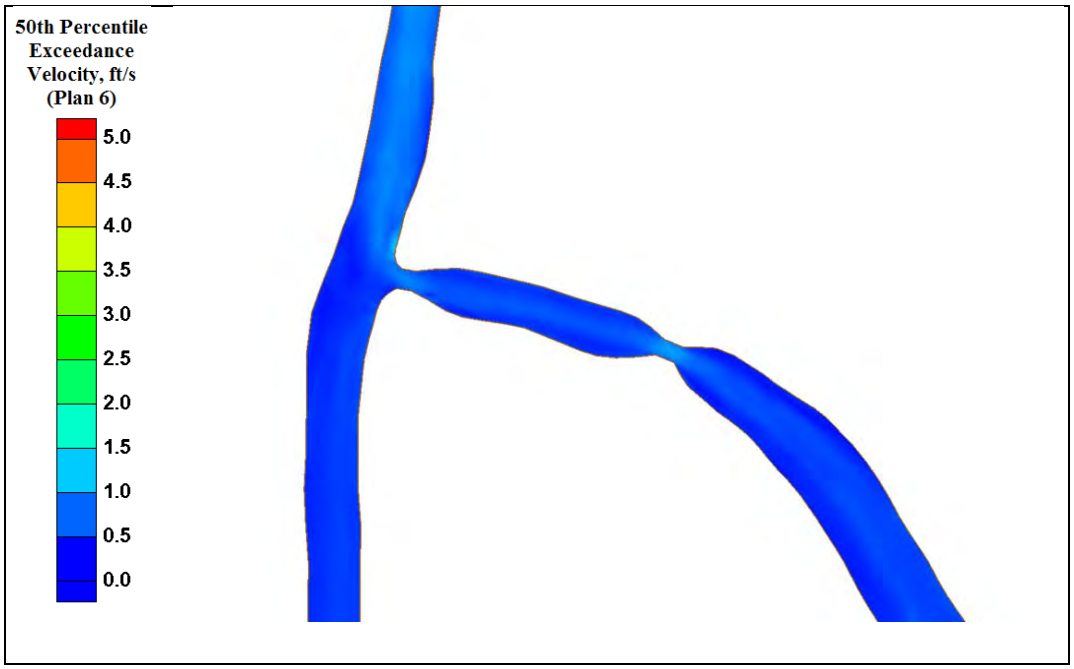

Figure B66. Humble Canal 50th percentile exceedance velocity (Plan 6).

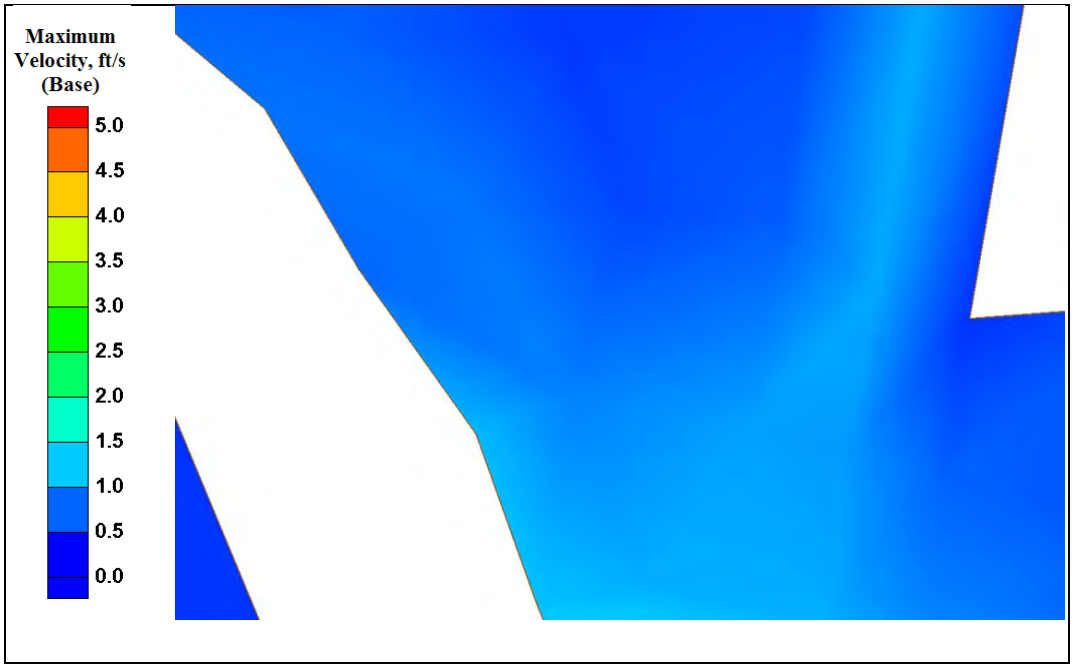

Figure B67. Pointe Aux Chenes maximum velocity (base).

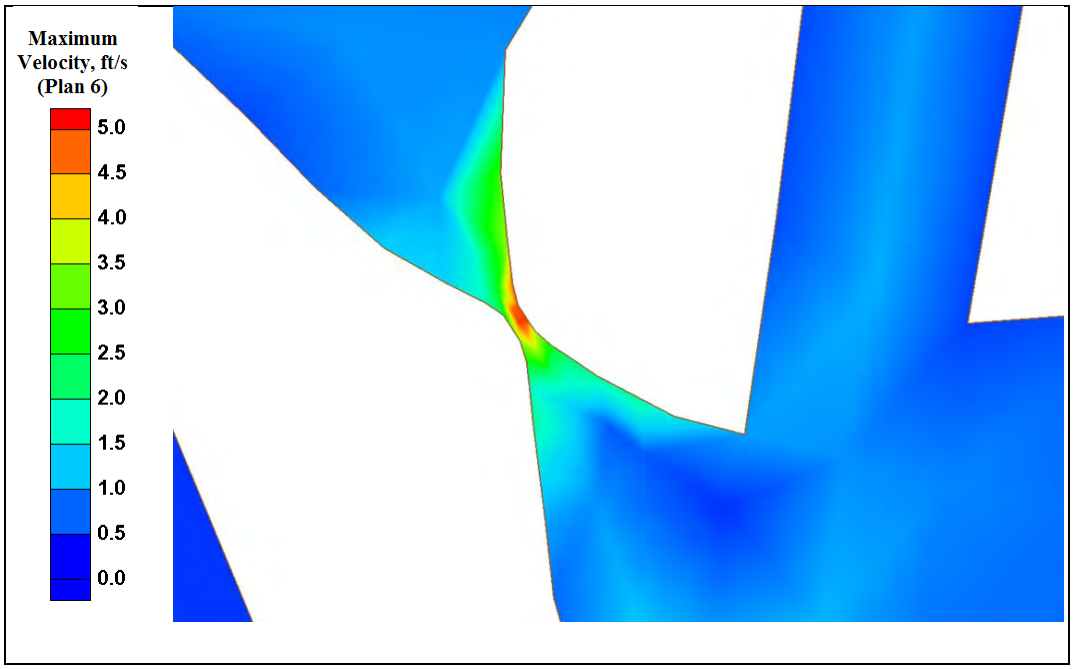

Figure B68. Pointe Aux Chenes maximum velocity (Plan 6).

Figure B69. Pointe Aux Chenes 10th percentile exceedance velocity (base).

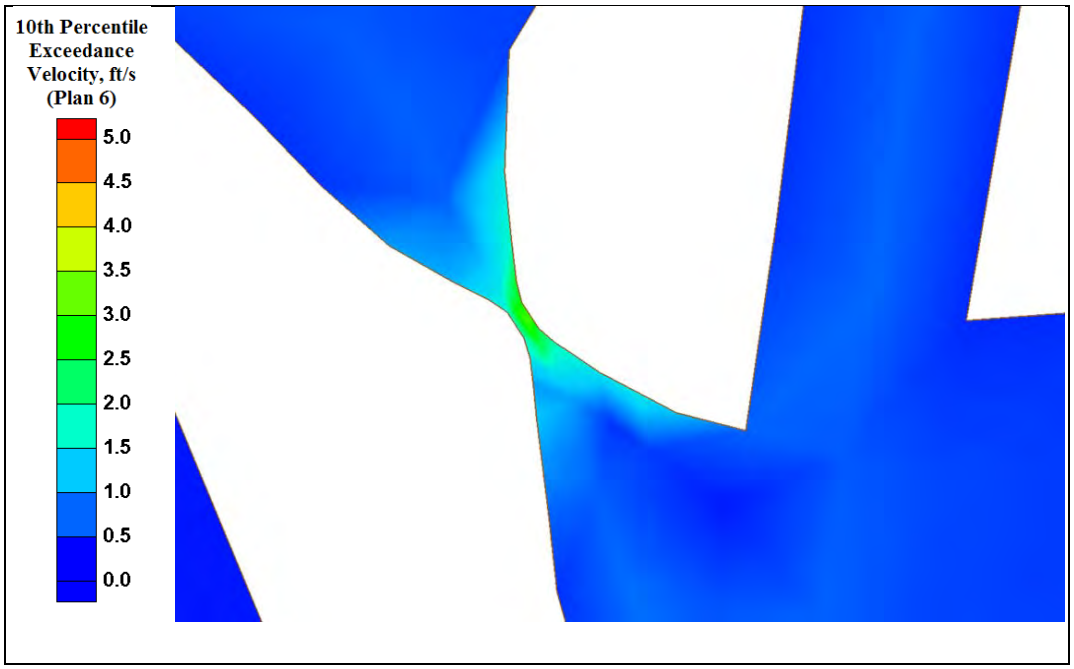

Figure B70. Pointe Aux Chenes 10th percentile exceedance velocity (Plan 6).

Figure B71. Pointe Aux Chenes 50th percentile exceedance velocity (base).

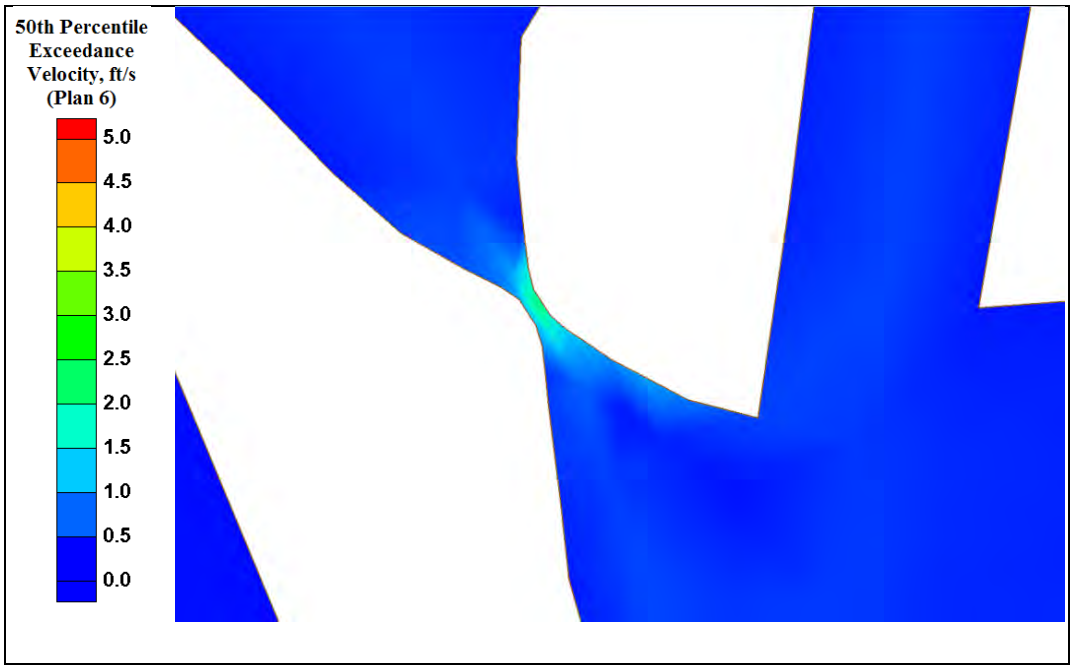

Figure B72. Pointe Aux Chenes 50th percentile exceedance velocity (Plan 6).

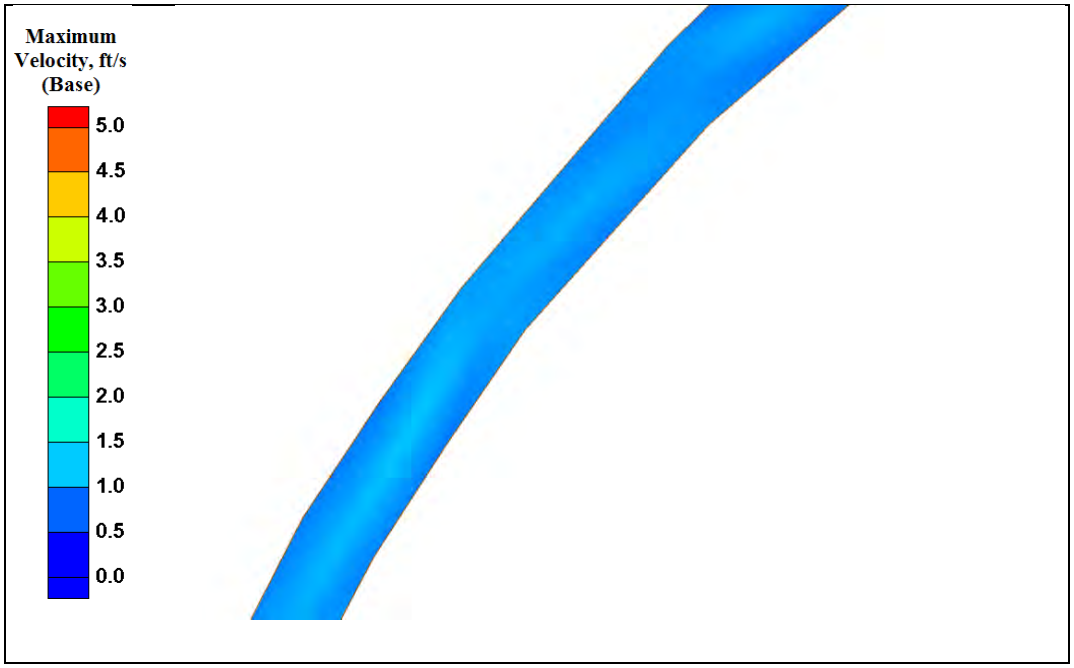

Figure B73. Grand Bayou maximum velocity (base).

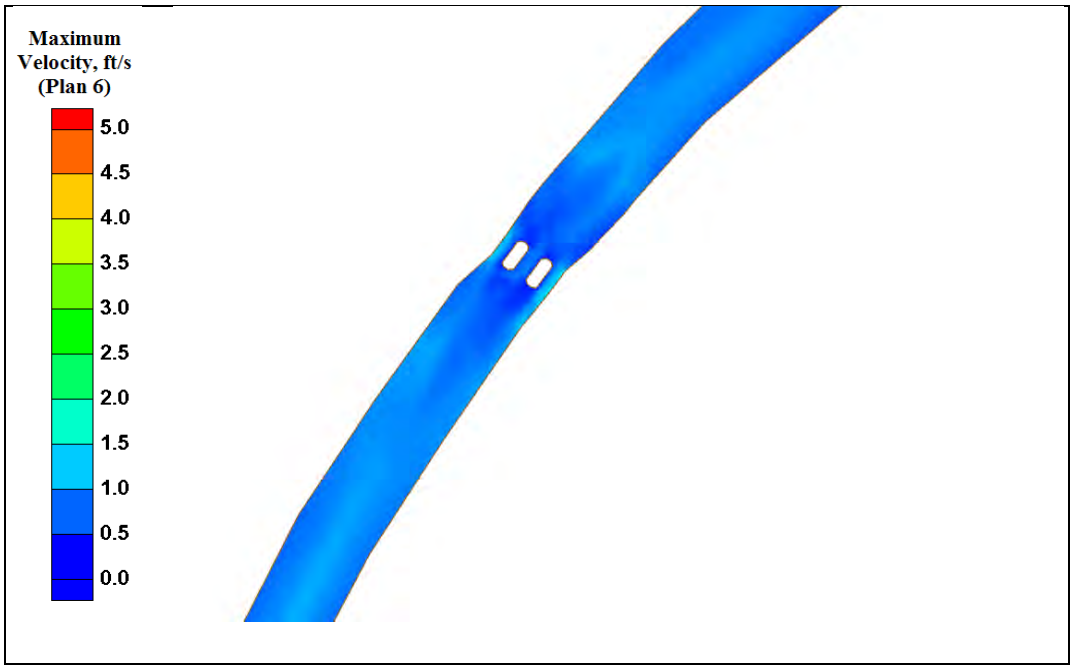

Figure B74. Grand Bayou maximum velocity (Plan 6).

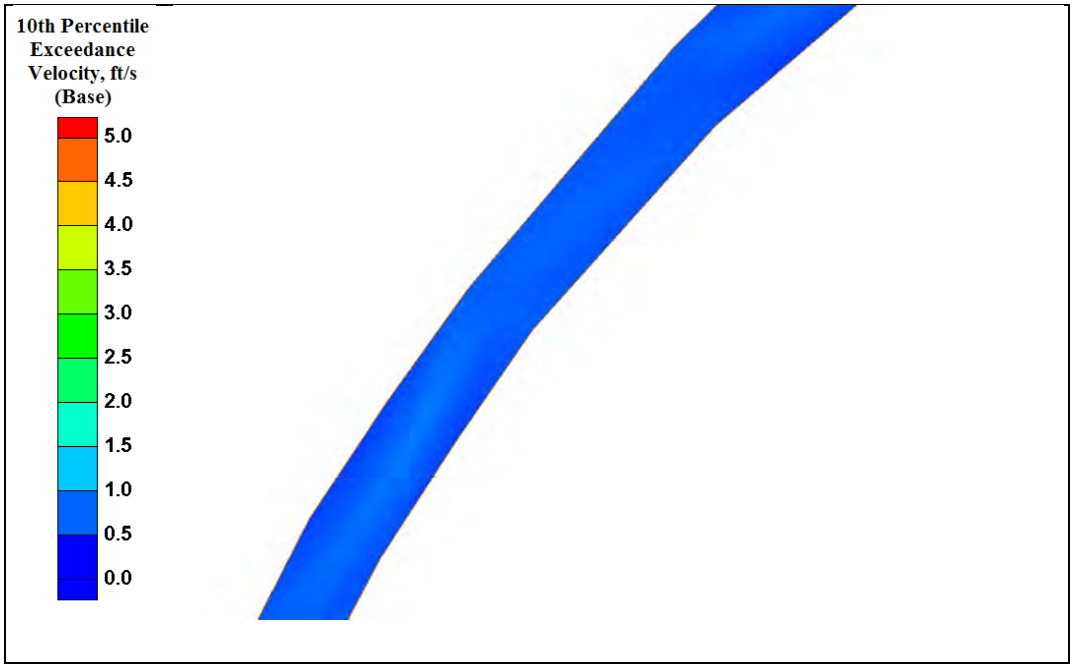

Figure B75. Grand Bayou 10th percentile exceedance velocity (base).

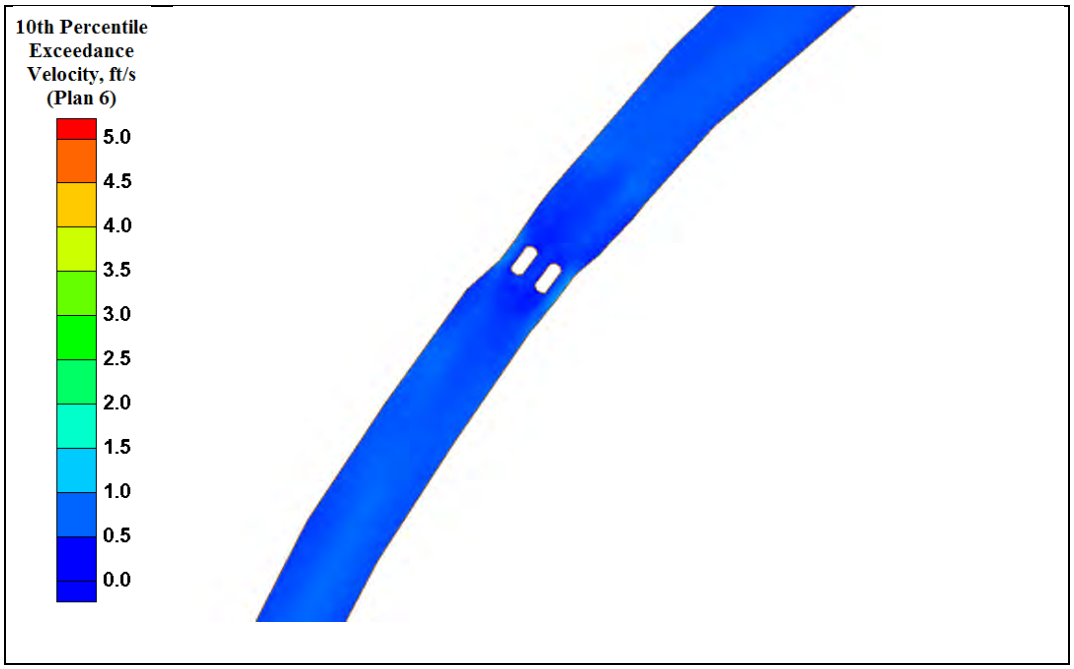

Figure B76. Grand Bayou 10th percentile exceedance velocity (Plan 6).

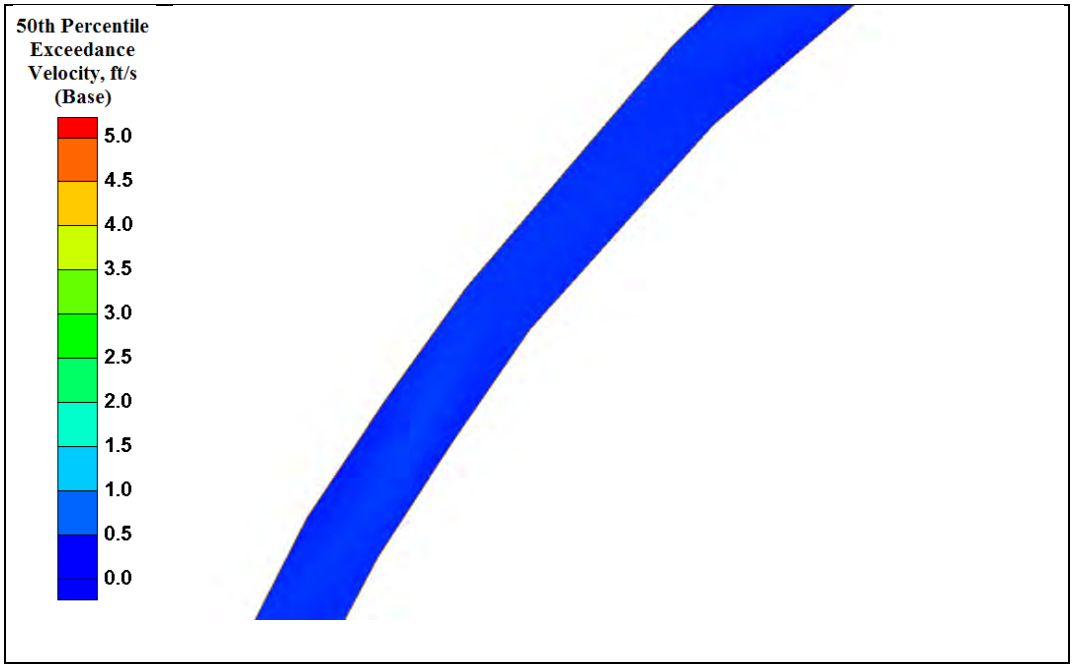

Figure B77. Grand Bayou 50th percentile exceedance velocity (base).

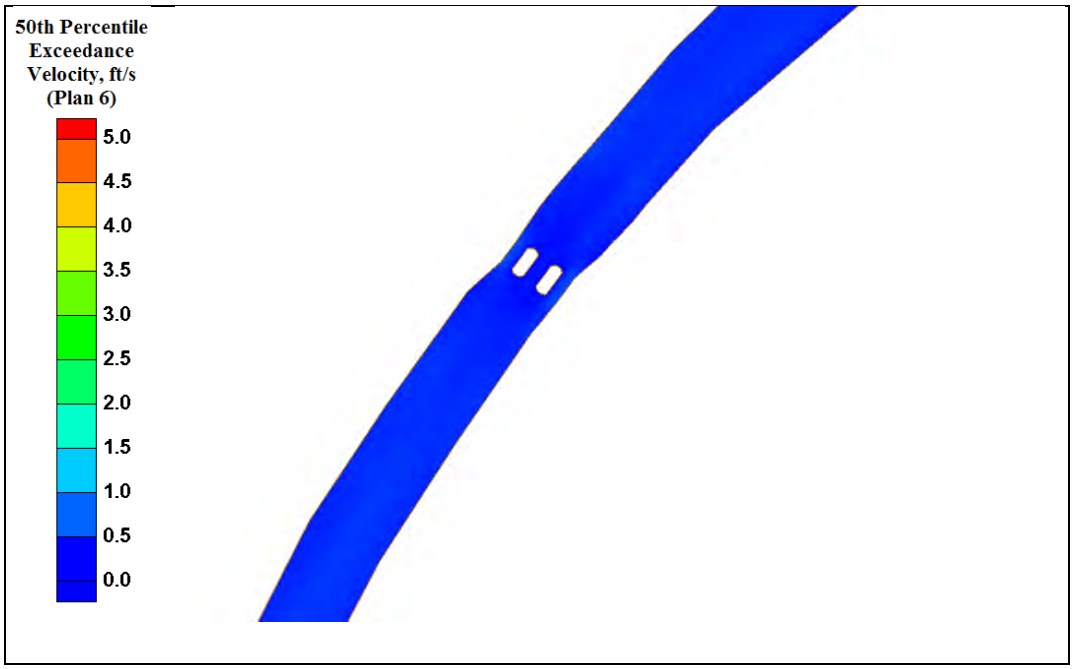

Figure B78. Grand Bayou 50th percentile exceedance velocity (Plan 6).

Appendix C: Base versus Plan 6 Contour Plots of the Maximum Flood and Ebb Velocities

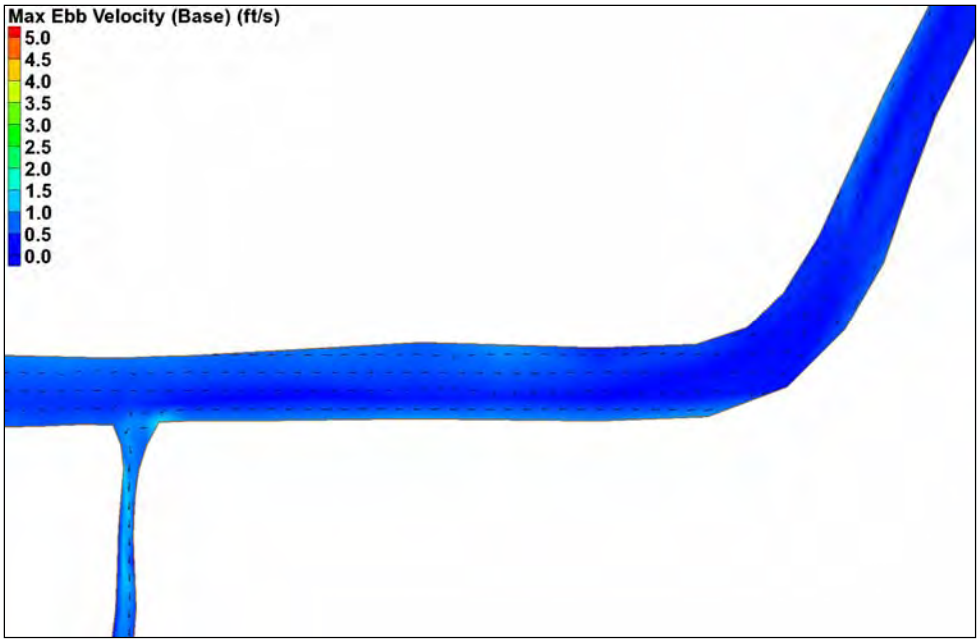

Figure C1. GIWW west of Houma max ebb velocity (base).

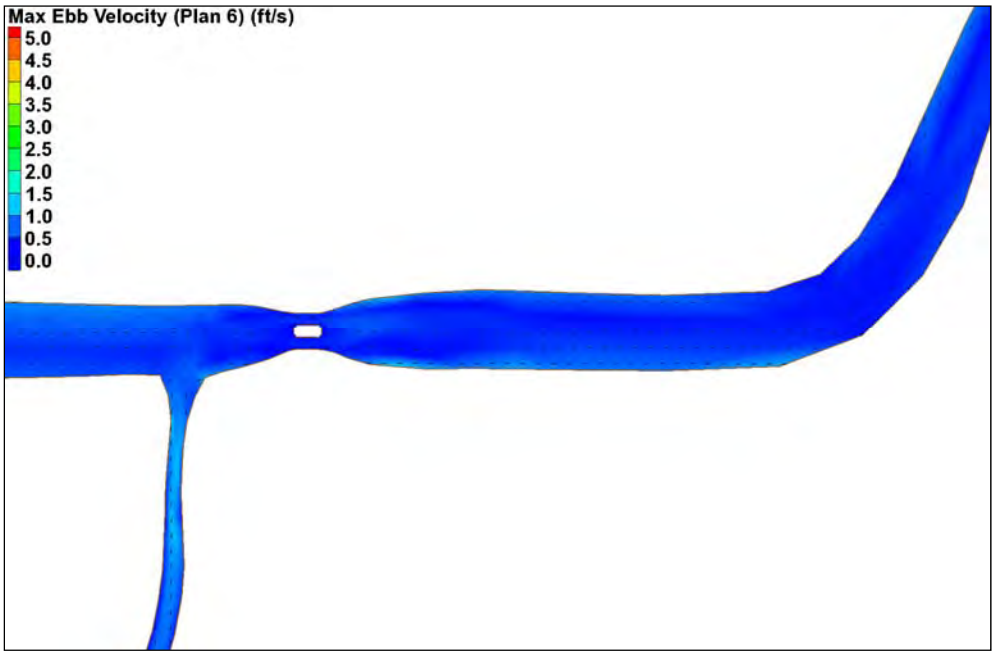

Figure C2. GIWW west of Houma max ebb velocity (Plan 6).

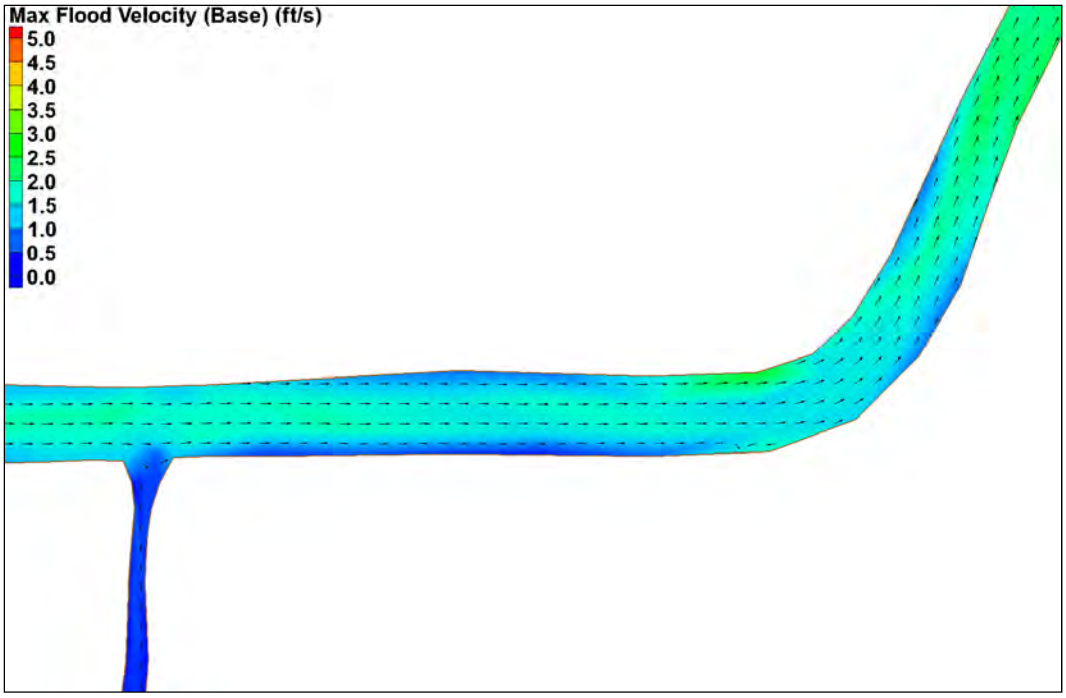

Figure C3. GIWW west of Houma max flood velocity (base).

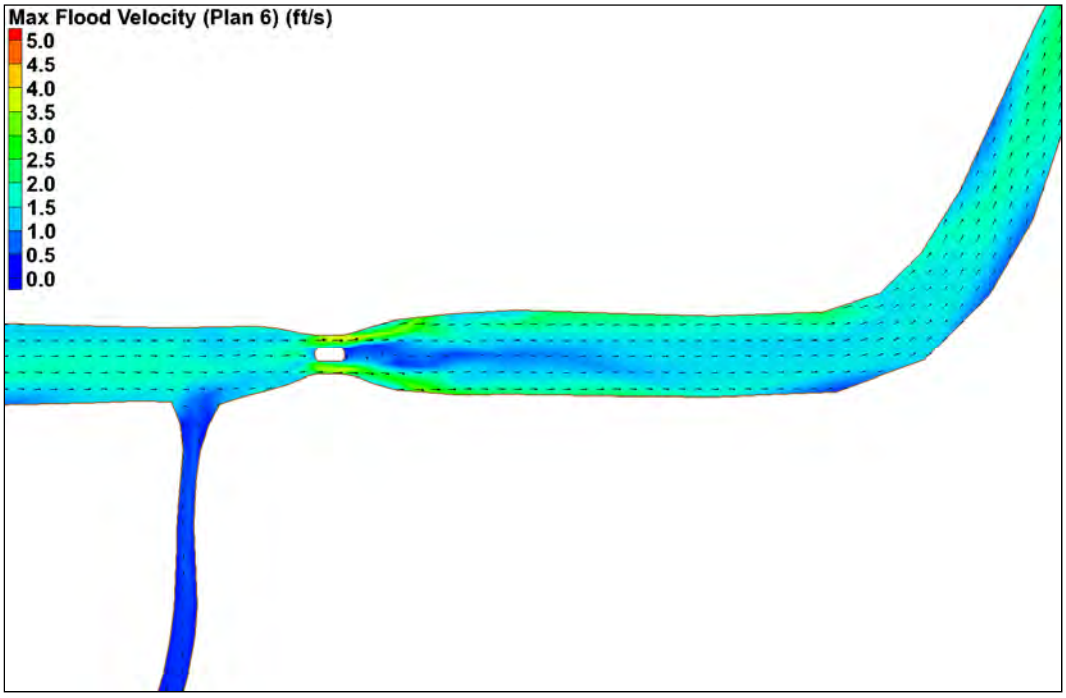

Figure C4. GIWW west of Houma max flood velocity (Plan 6).

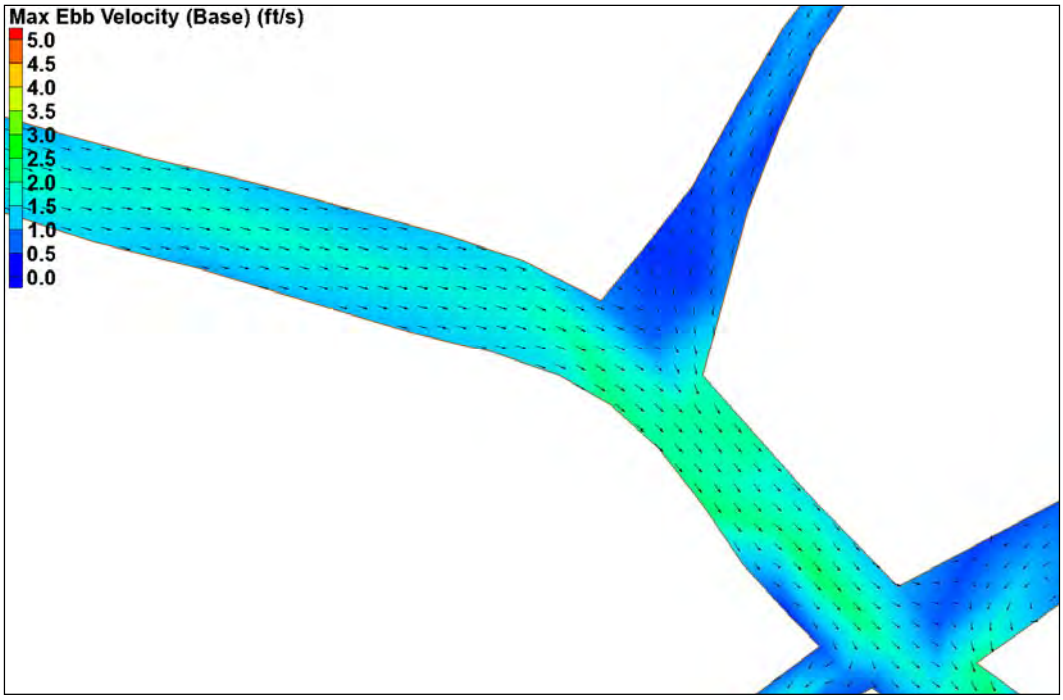

Figure C5. Falgout Canal max ebb velocity (base).

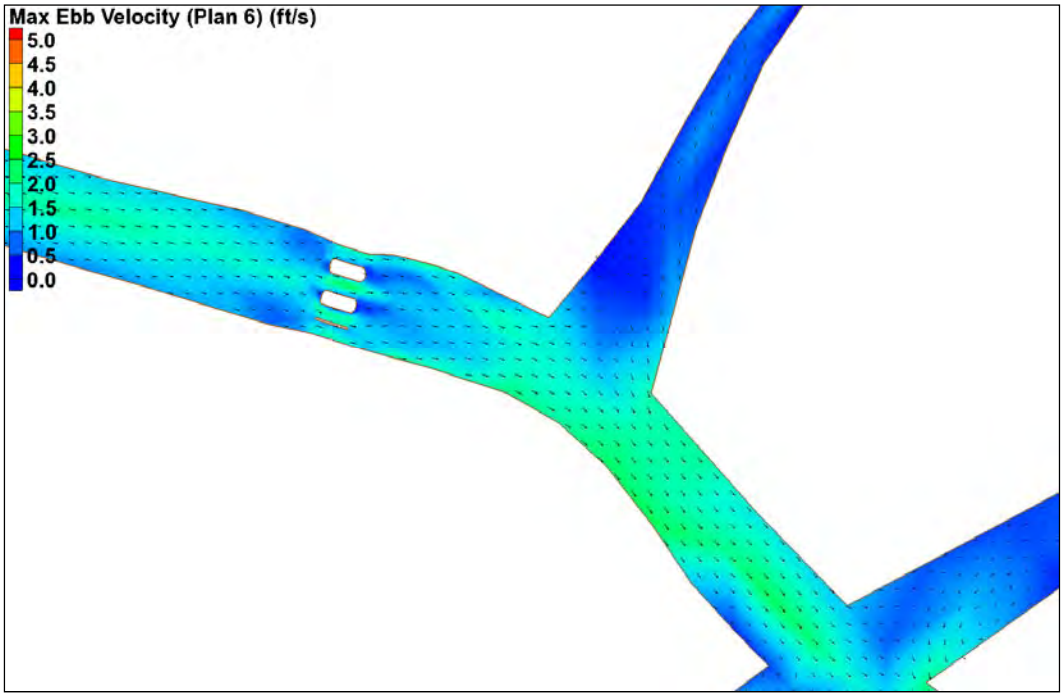

Figure C6. Falgout Canal max ebb velocity (Plan 6).

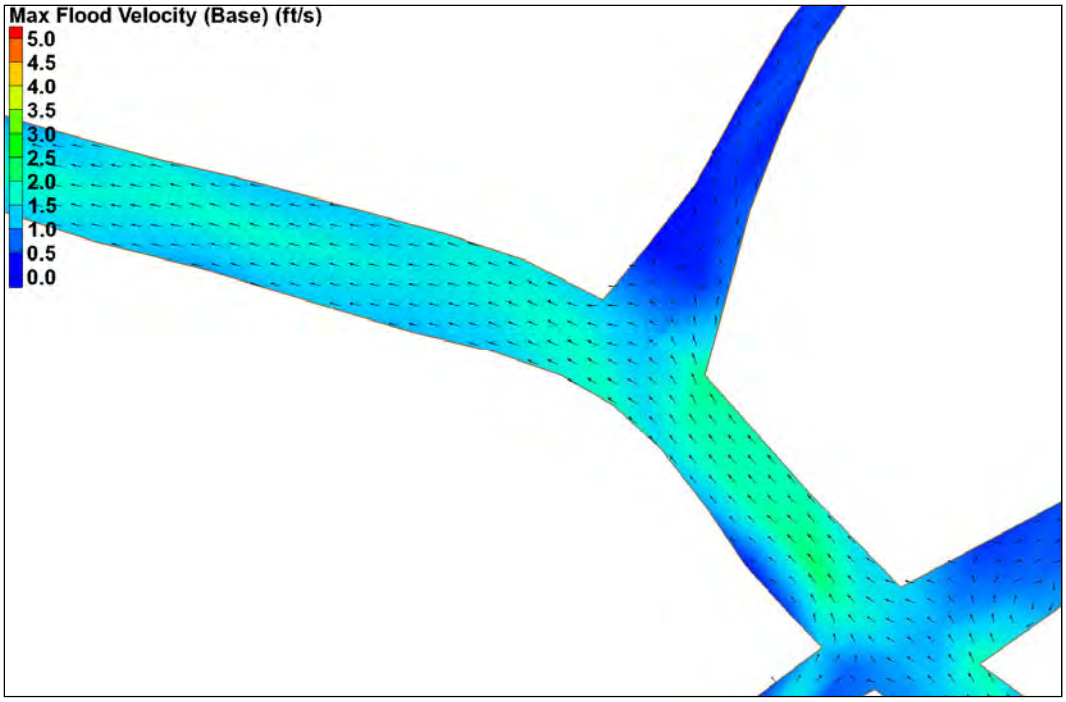

Figure C7. Falgout Canal max flood velocity (base).

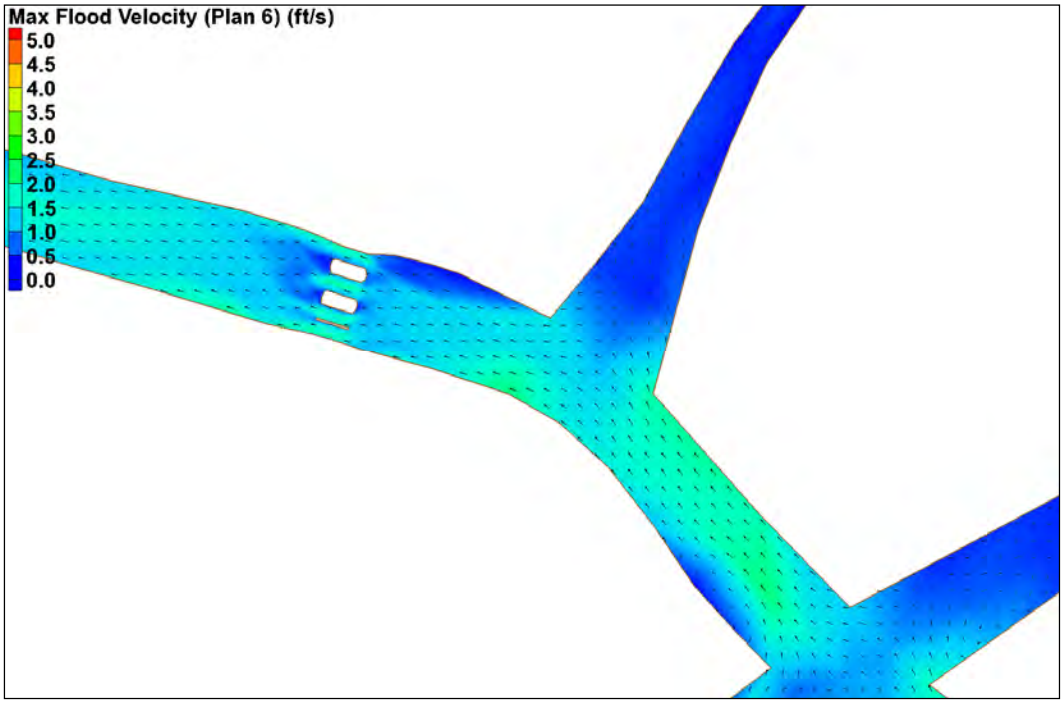

Figure C8. Falgout Canal max flood velocity (Plan 6).

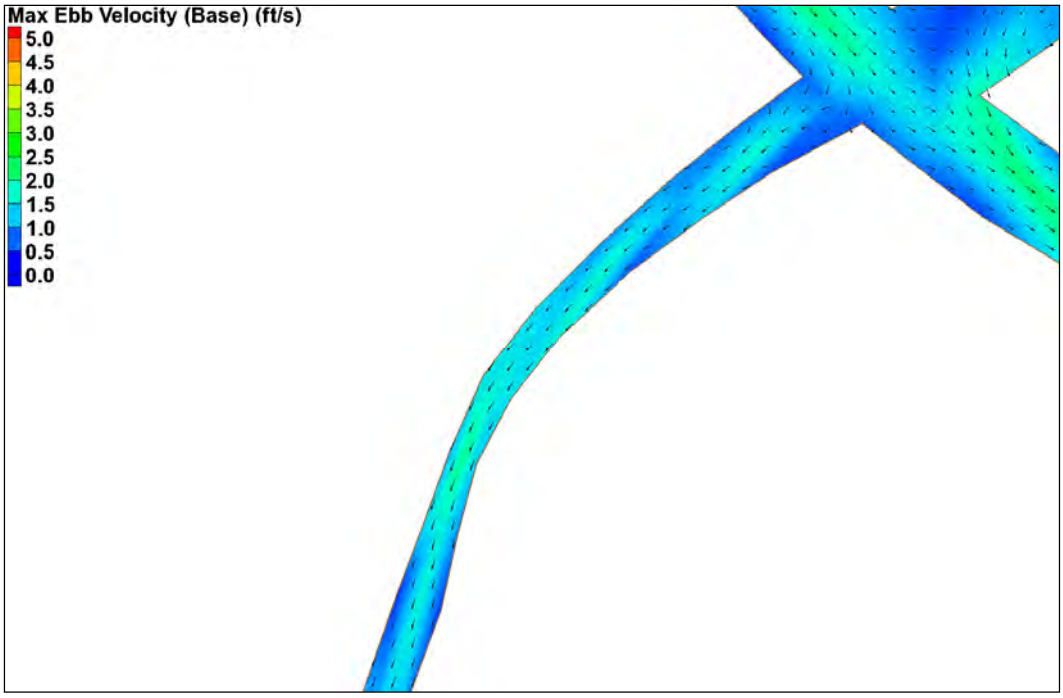

Figure C9. Bayou Dularge max ebb velocity (base).

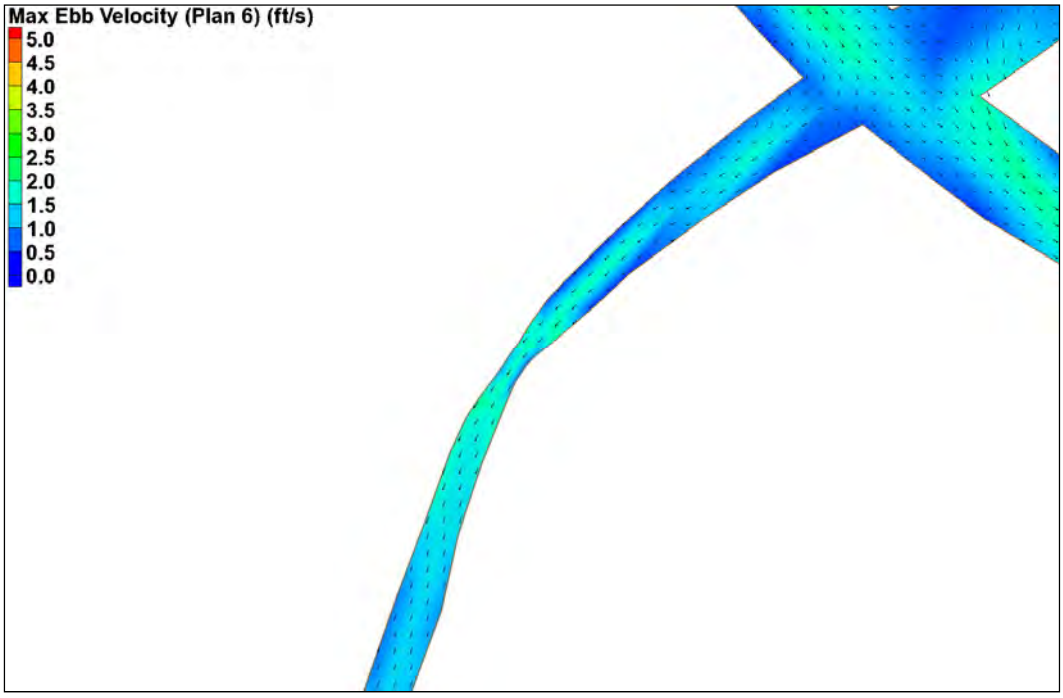

Figure C10. Bayou Dularge max ebb velocity (Plan 6).

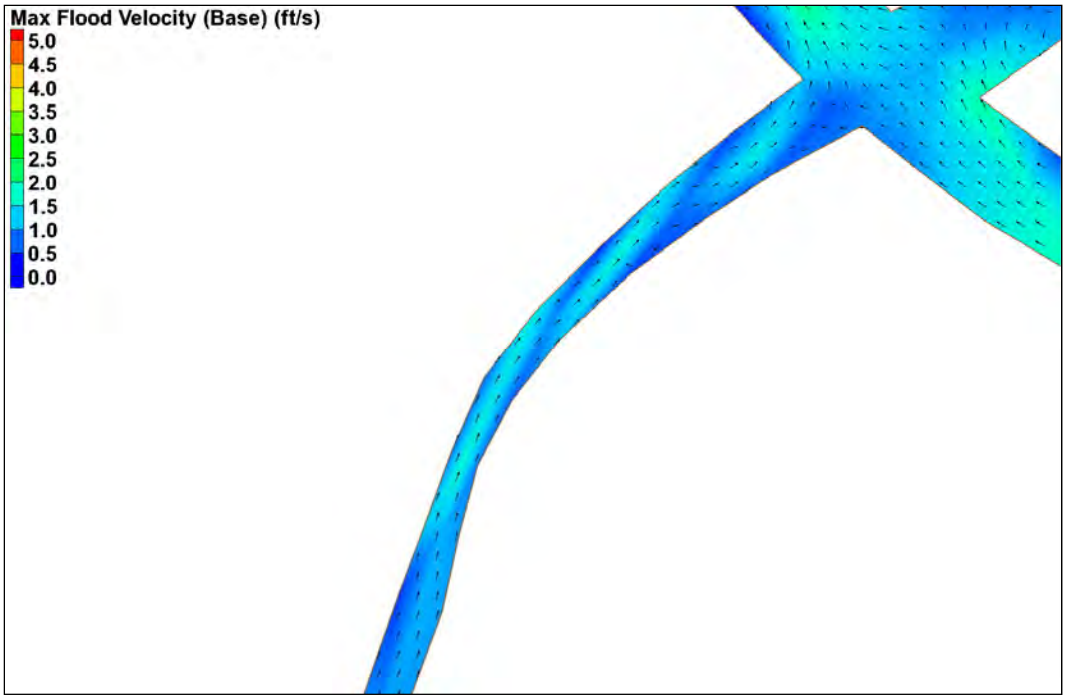

Figure C11. Bayou Dularge max flood velocity (base).

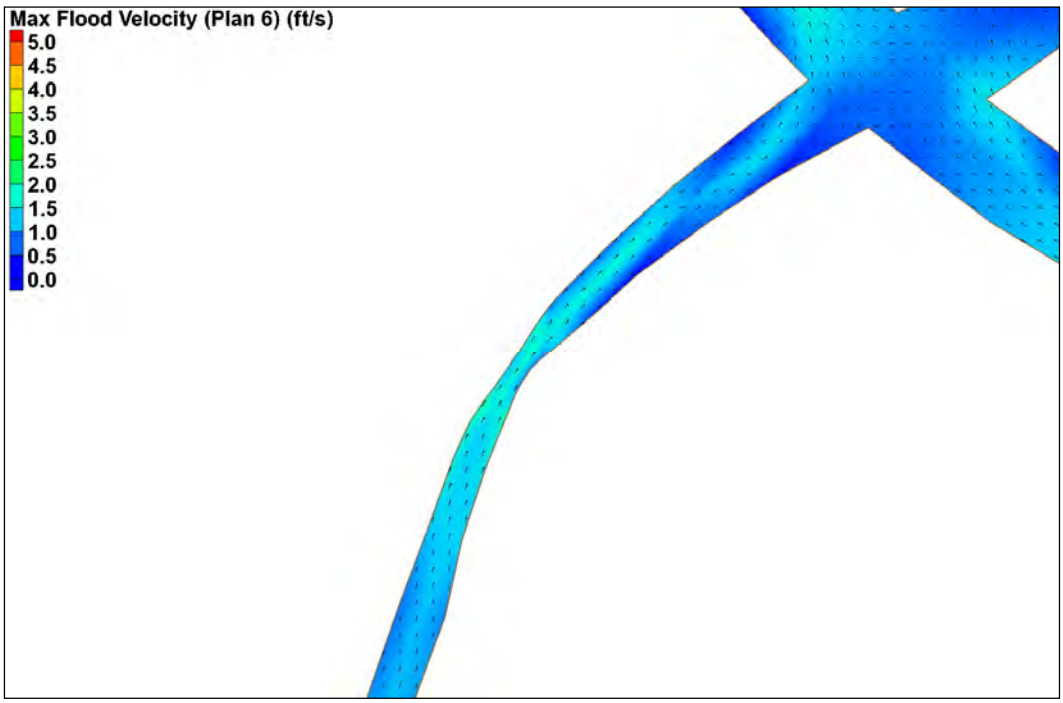

Figure C12. Bayou Dularge max flood velocity (Plan 6).

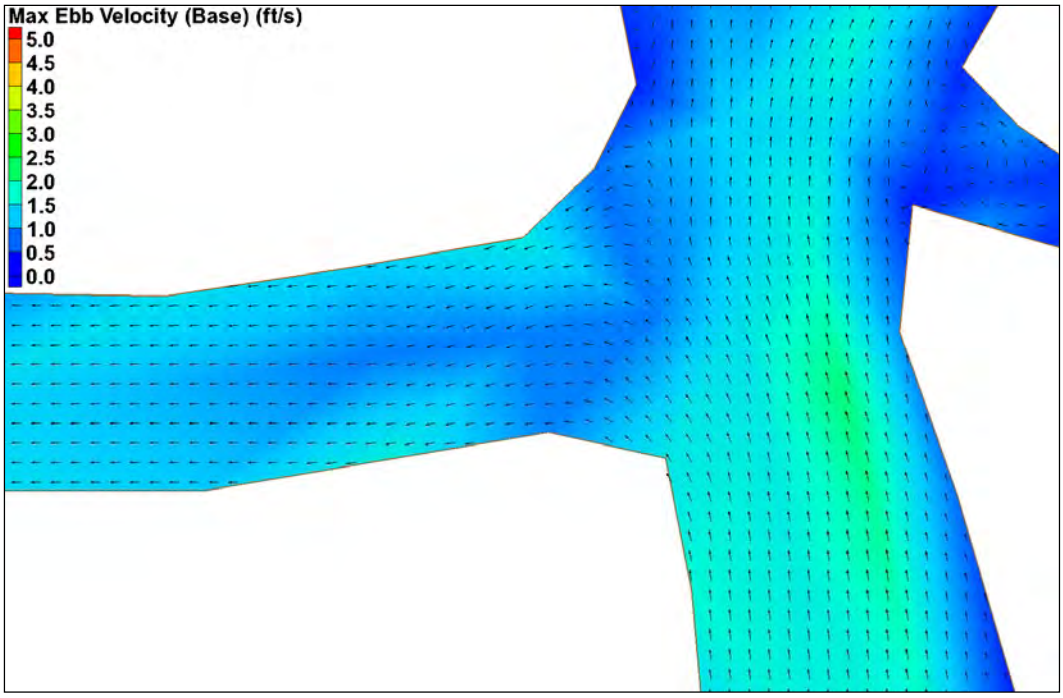

Figure C13. Bayou Grand Caillou max ebb velocity (base).

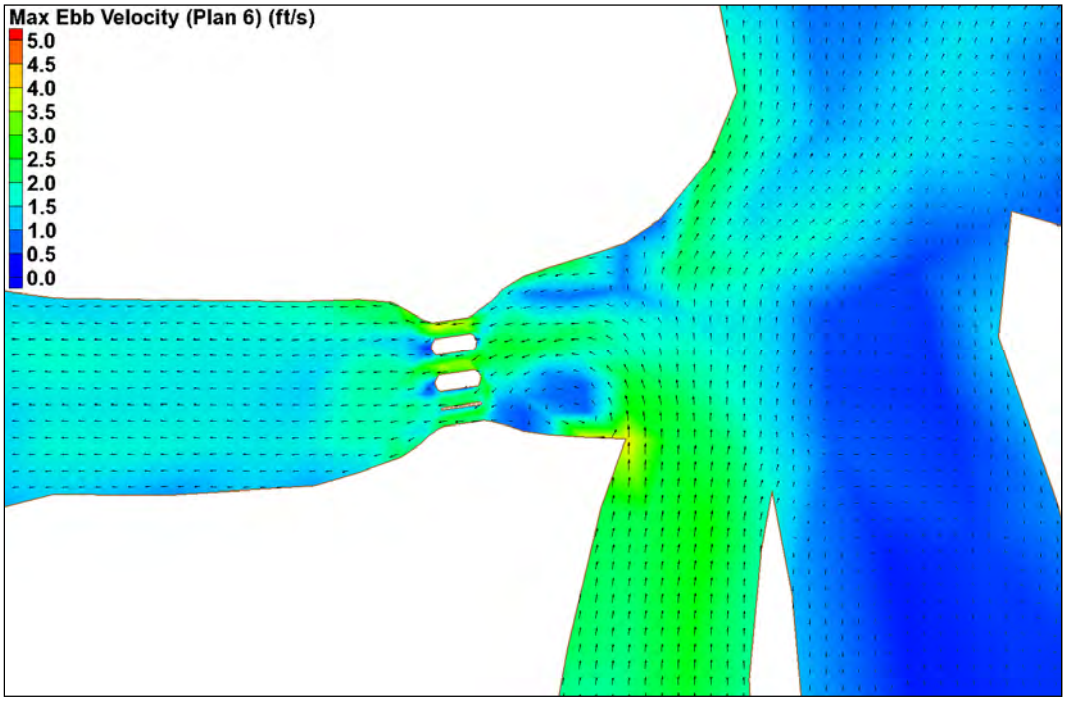

Figure C14. Bayou Grand Caillou max ebb velocity (Plan 6).

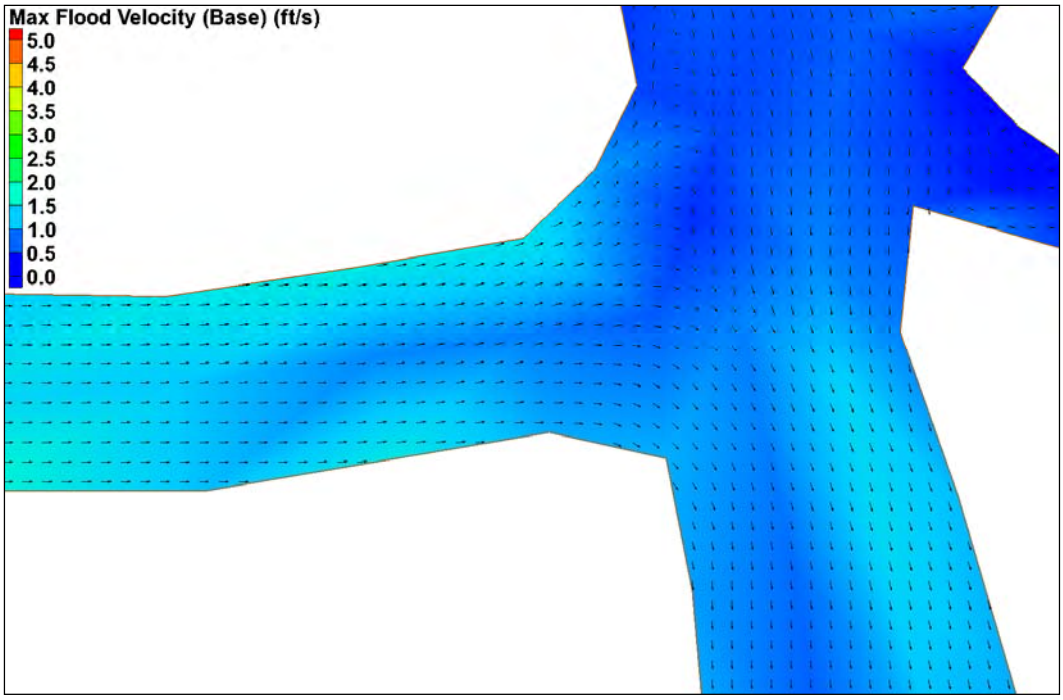

Figure C15. Bayou Grand Caillou max flood velocity (base).

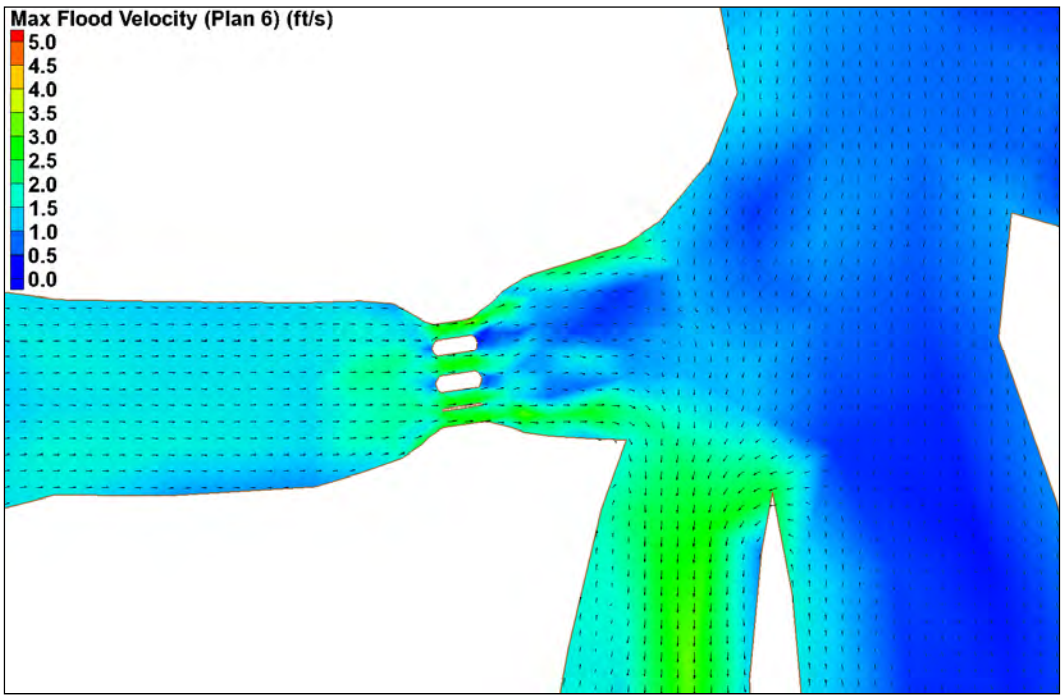

Figure C16. Bayou Grand Caillou max flood velocity (Plan 6).

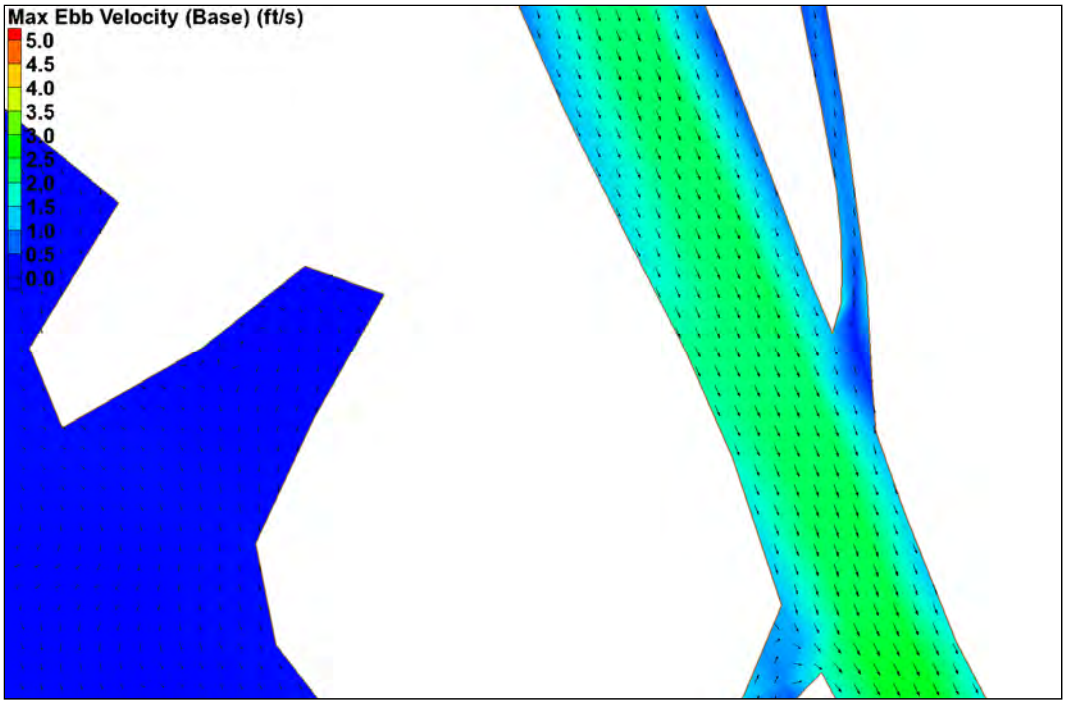

Figure C17. Houma Navigation Canal max ebb velocity (base).

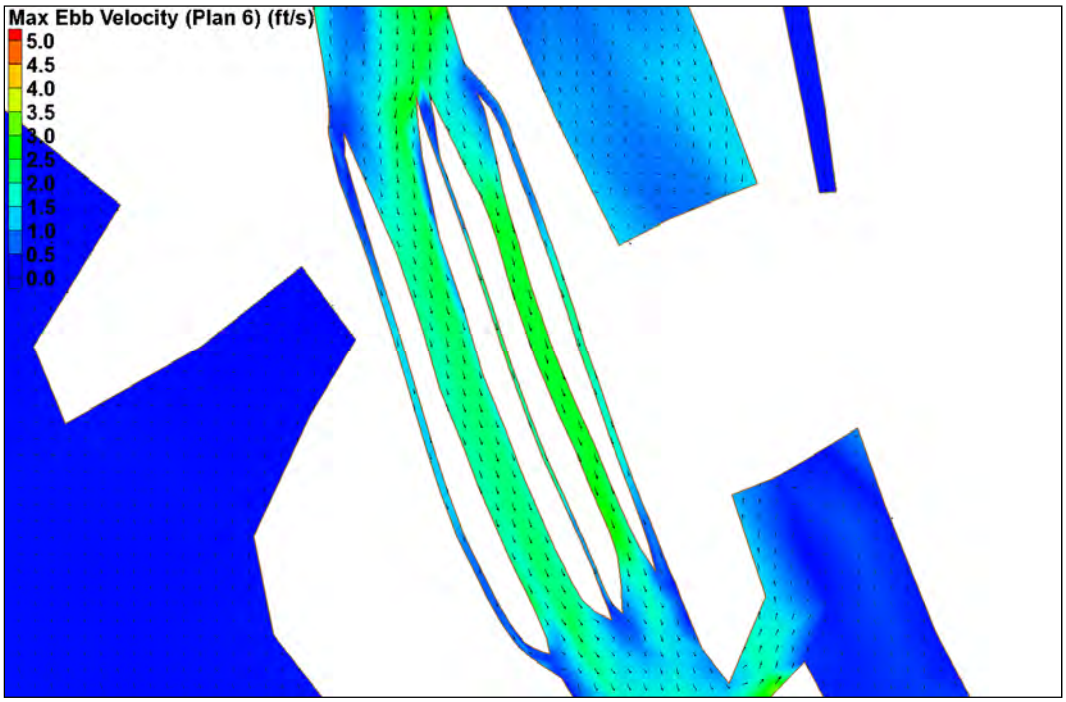

Figure C18. Houma Navigation Canal max ebb velocity (Plan 6).

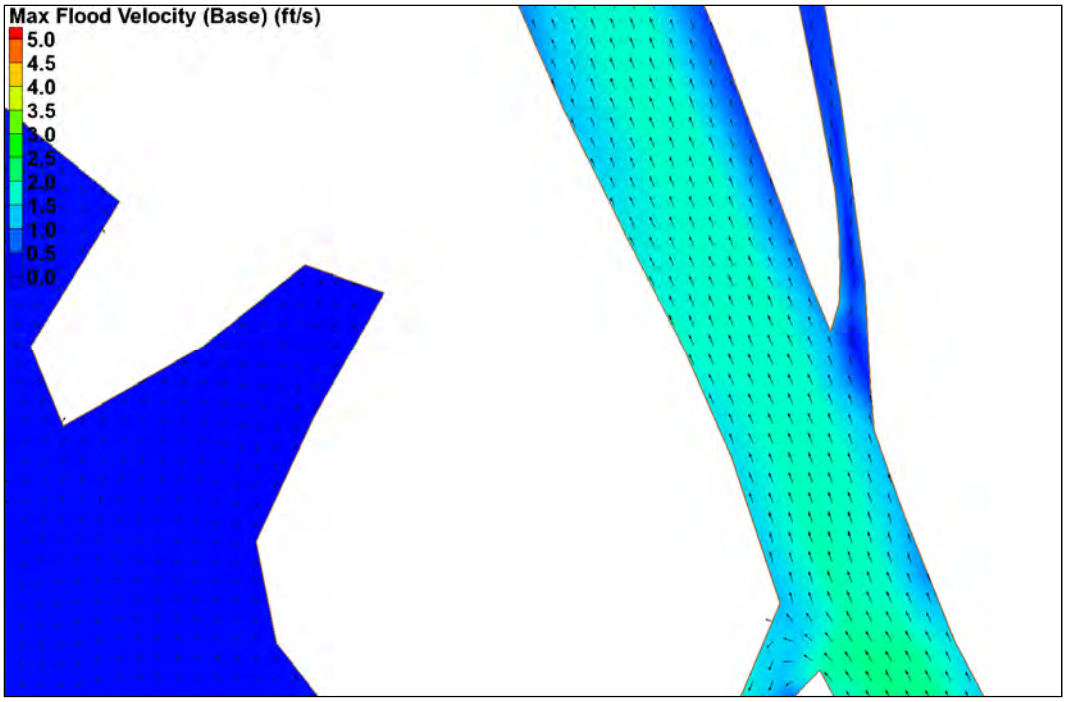

Figure C19. Houma Navigation Canal max flood velocity (base).

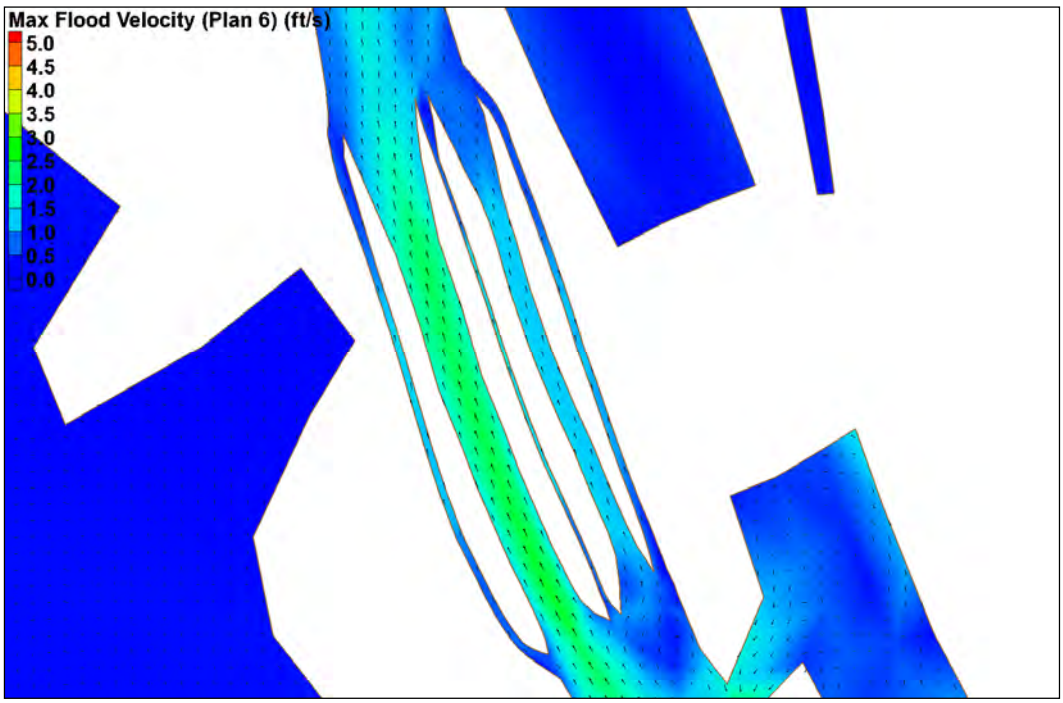

Figure C20. Houma Navigation Canal max flood velocity (Plan 6).

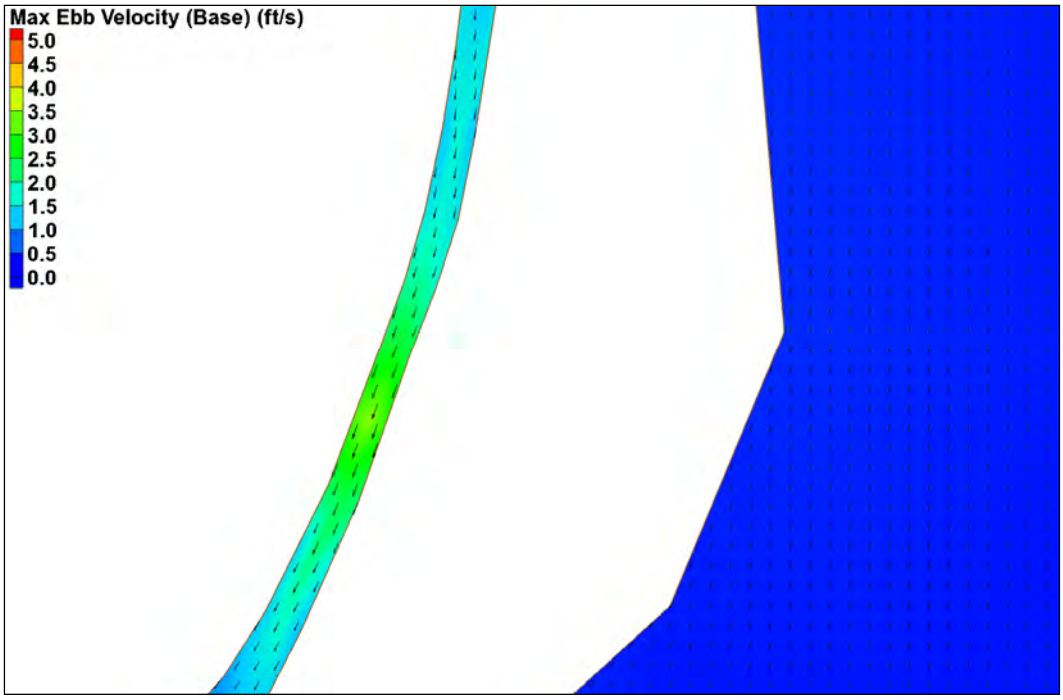

Figure C21. Bayou Fourpoints max ebb velocity (base).

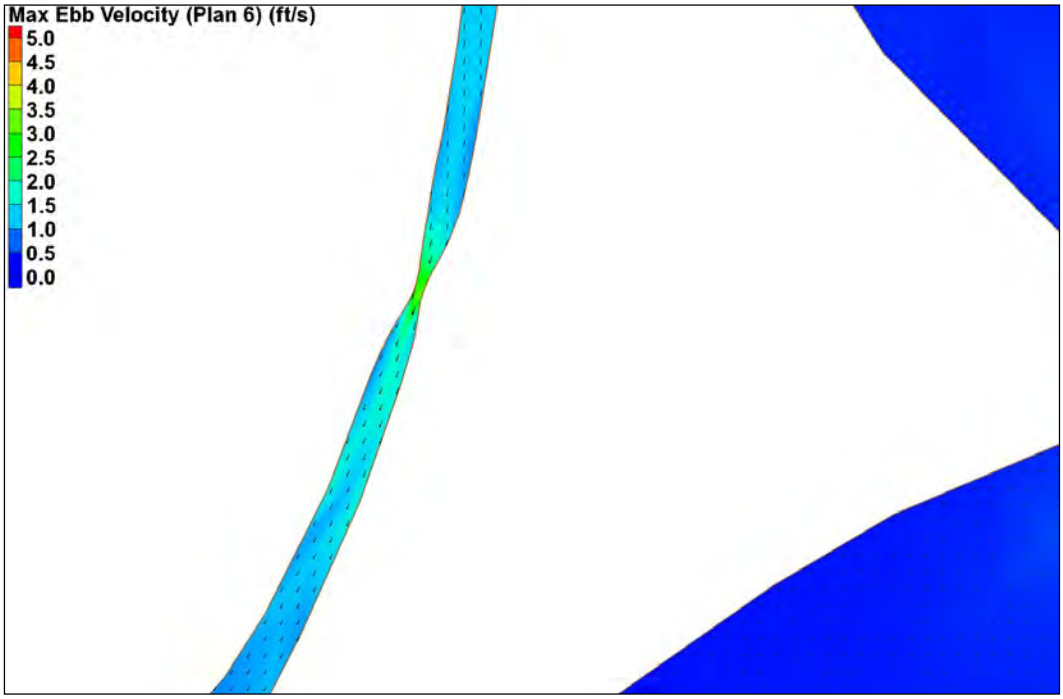

Figure C22. Bayou Fourpoints max ebb velocity (Plan 6).

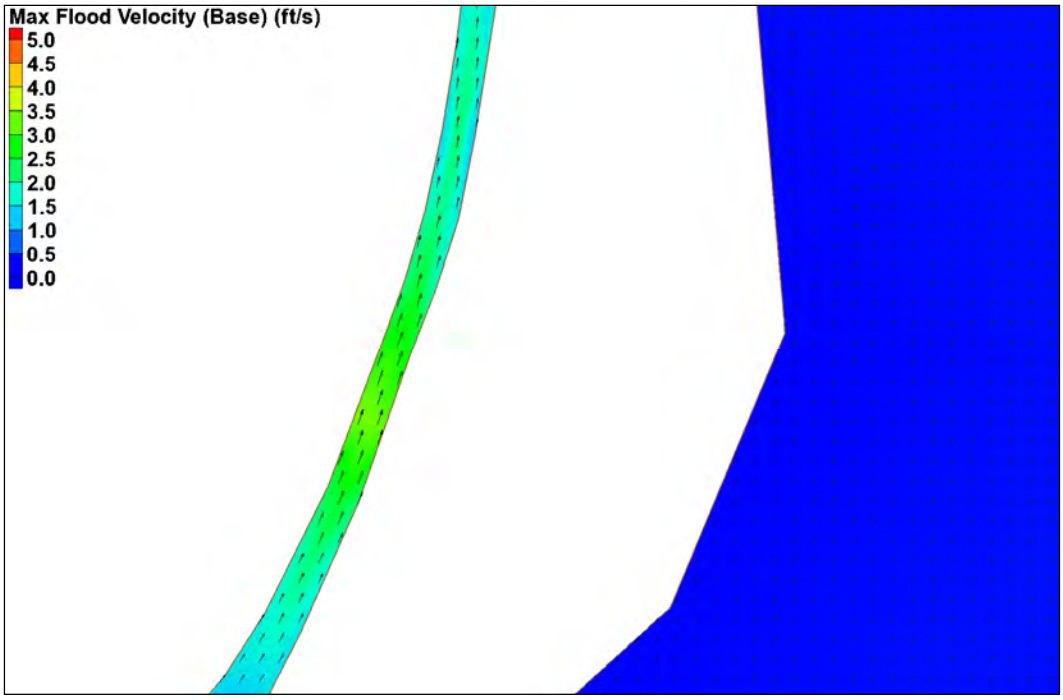

Figure C23. Bayou Fourpoints max flood velocity (base).

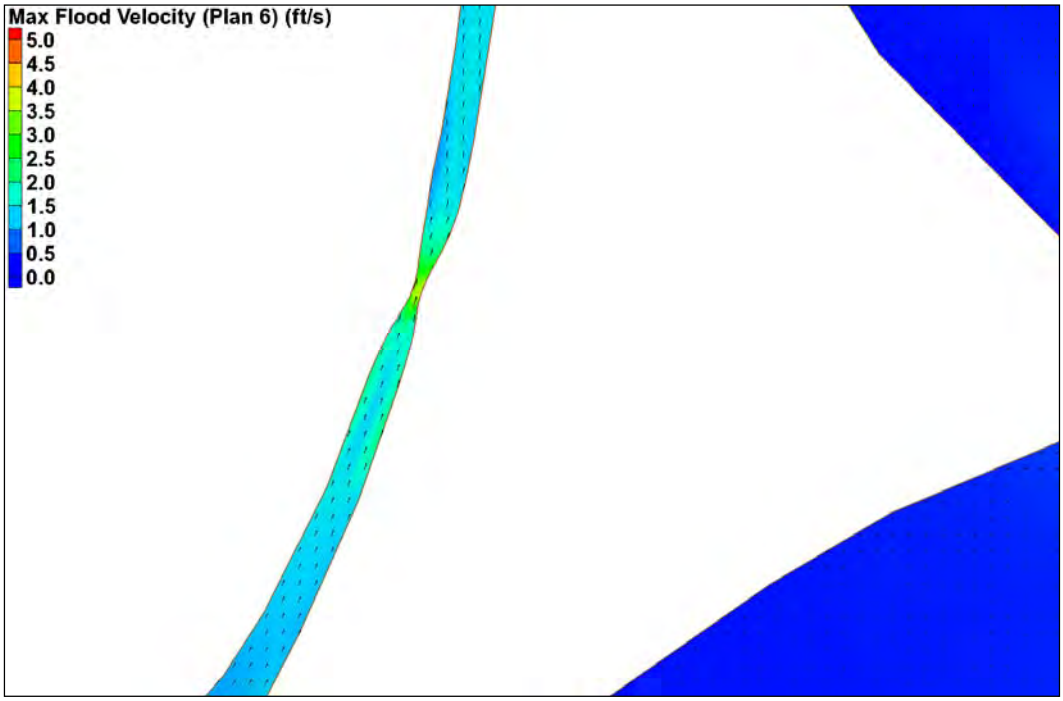

Figure C24. Bayou Fourpoints max flood velocity (Plan 6).

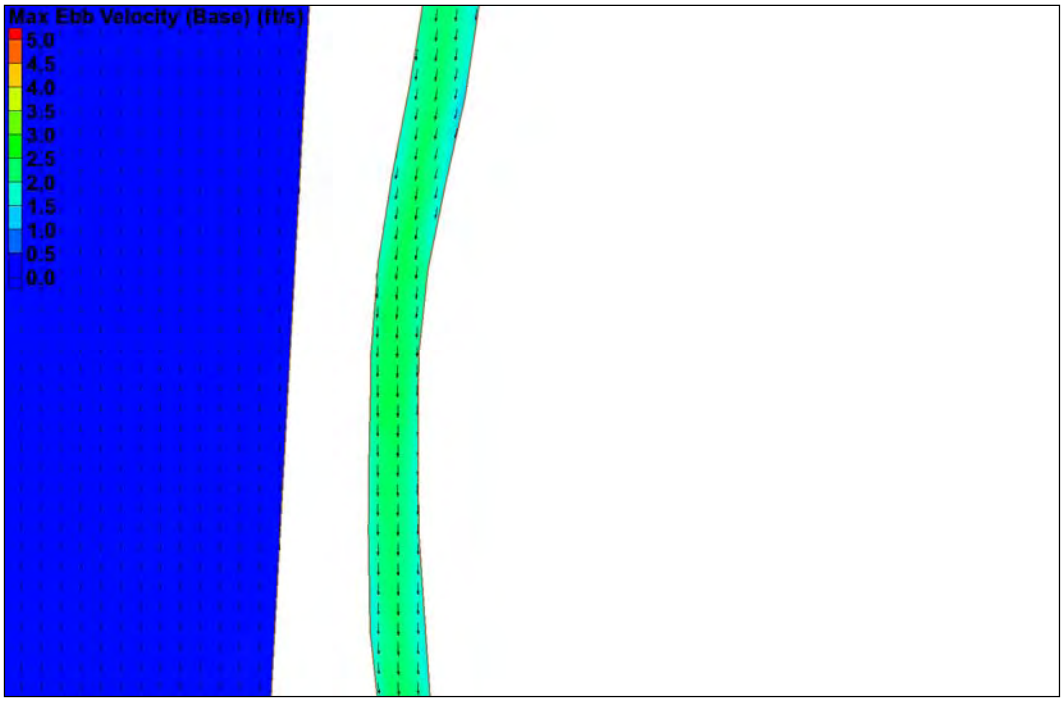

Figure C25. Bayou Petit Caillou max ebb velocity (base).

Figure C26. Bayou Petit Caillou max ebb velocity (Plan 6).

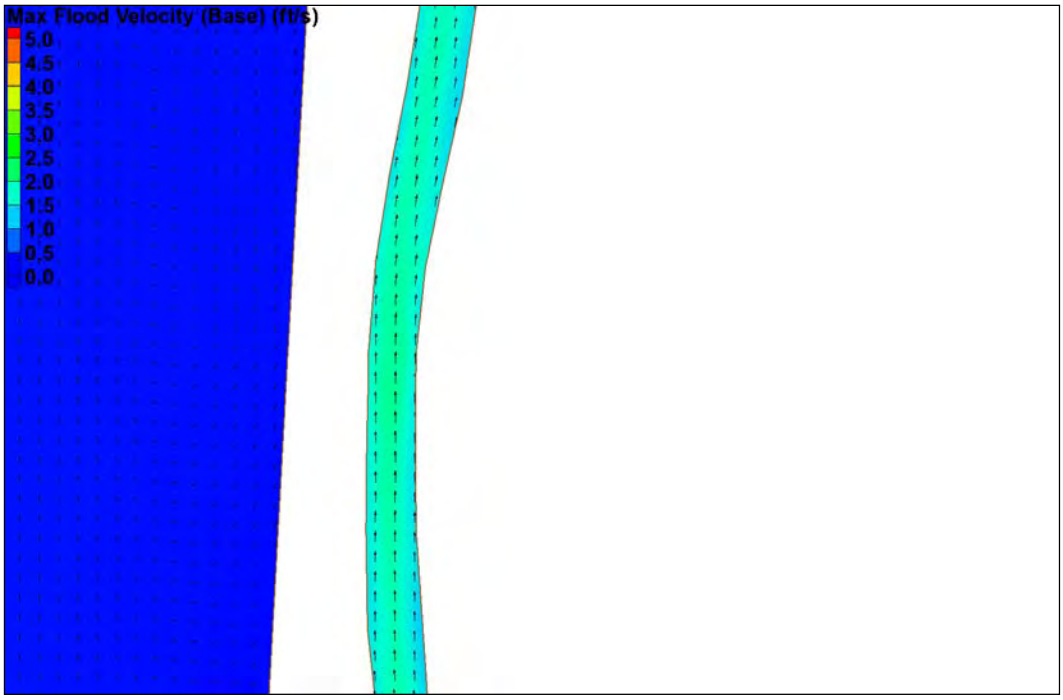

Figure C27. Bayou Petit Caillou max flood velocity (base).

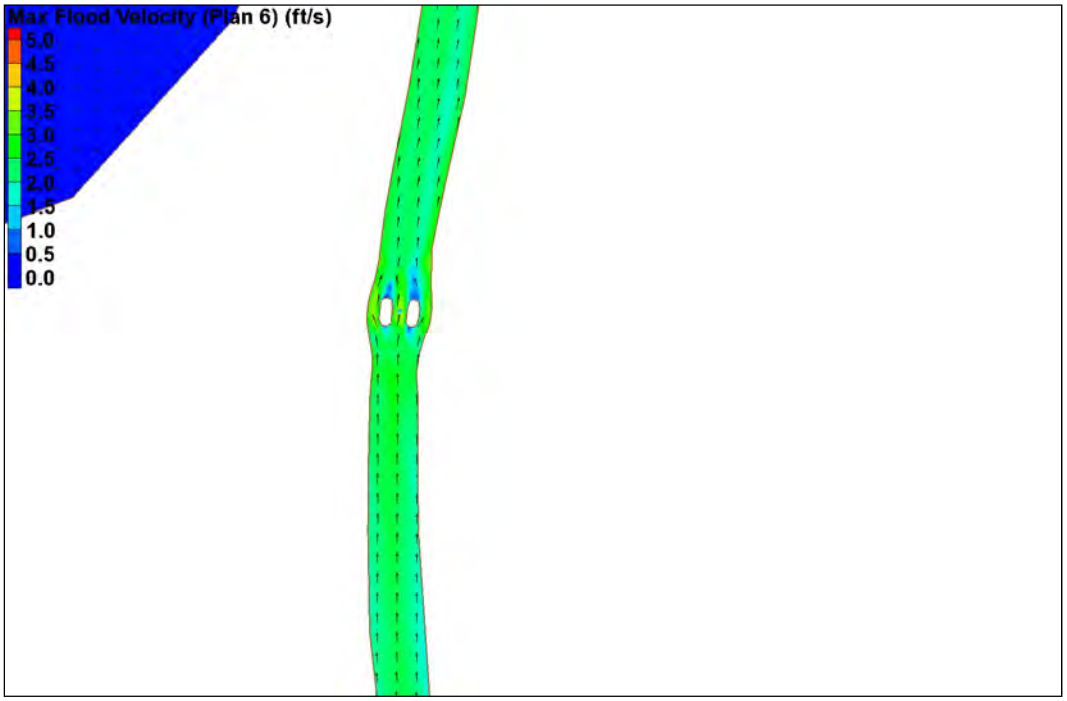

Figure C28. Bayou Petit Caillou max flood velocity (Plan 6).

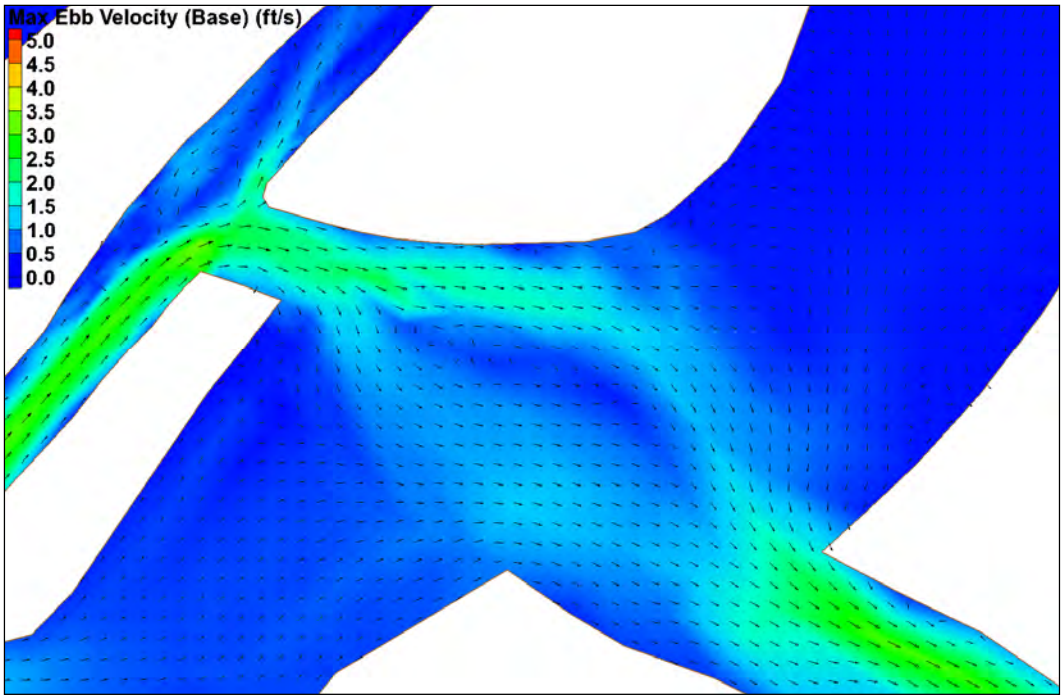

Figure C29. Placid Canal max ebb velocity (base).

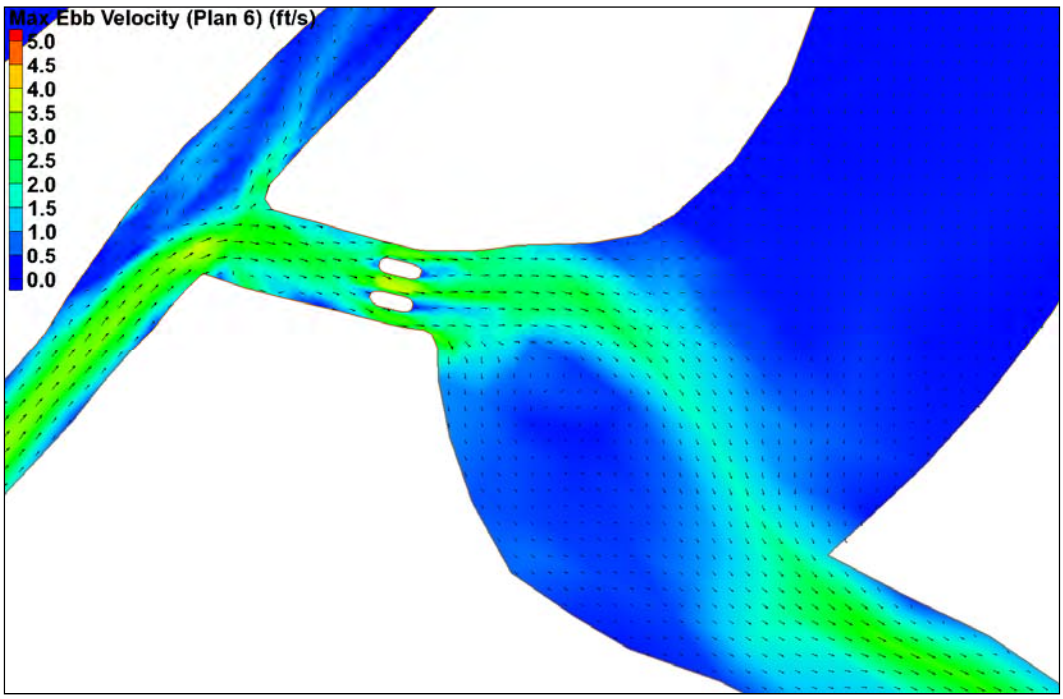

Figure C30. Placid Canal max ebb velocity (Plan 6).

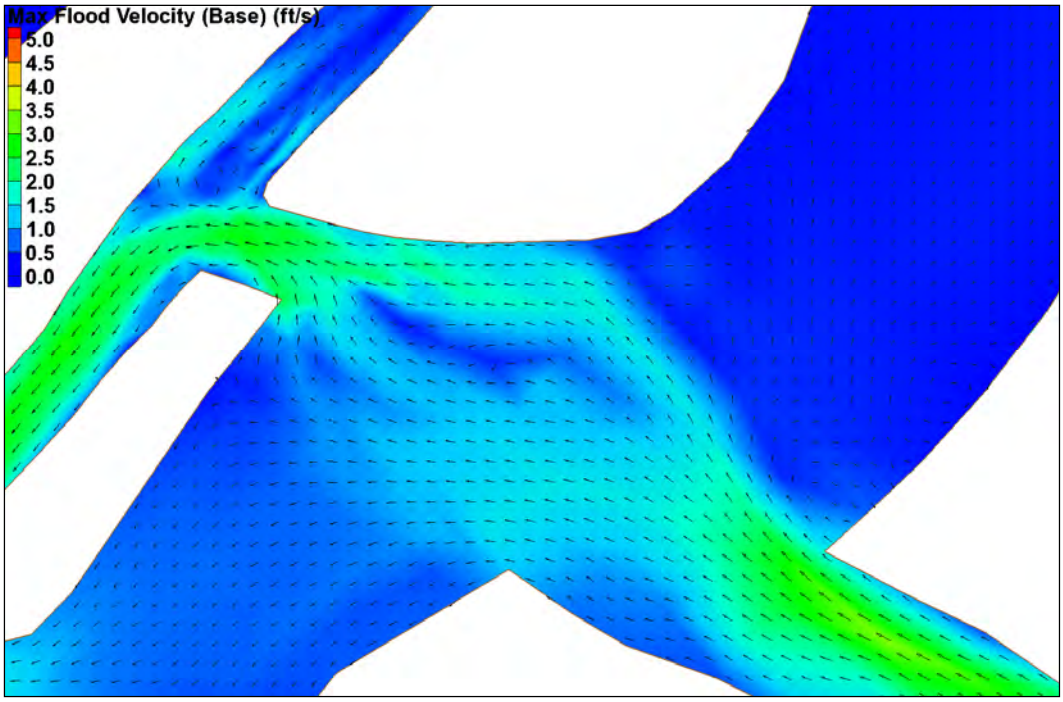

Figure C31. Placid Canal max flood velocity (base).

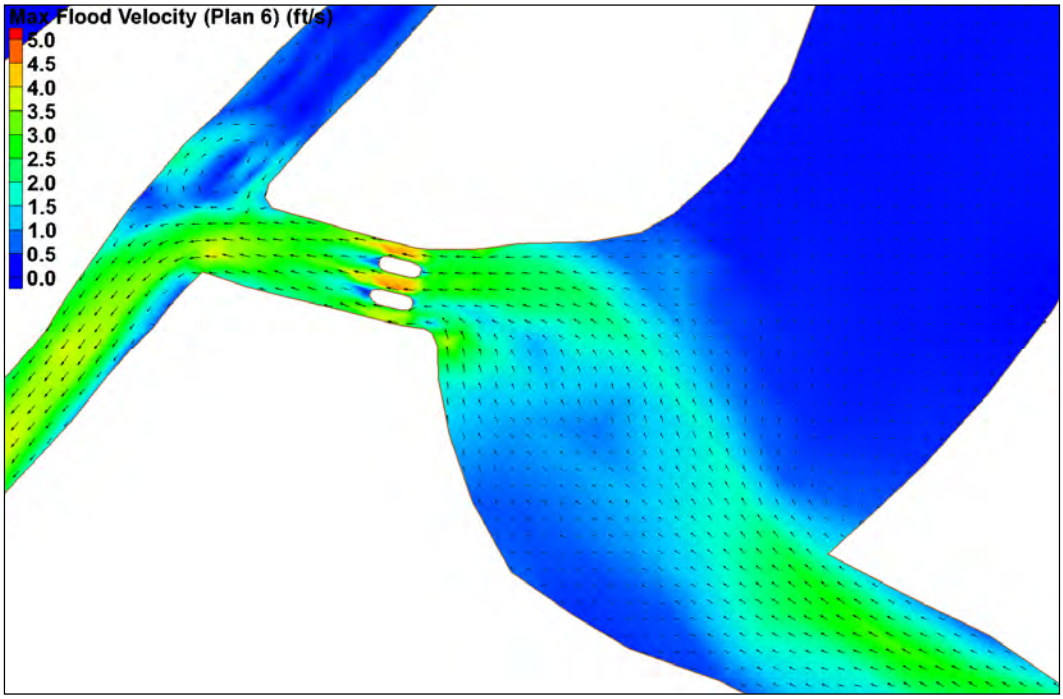

Figure C32. Placid Canal max flood velocity (Plan 6).

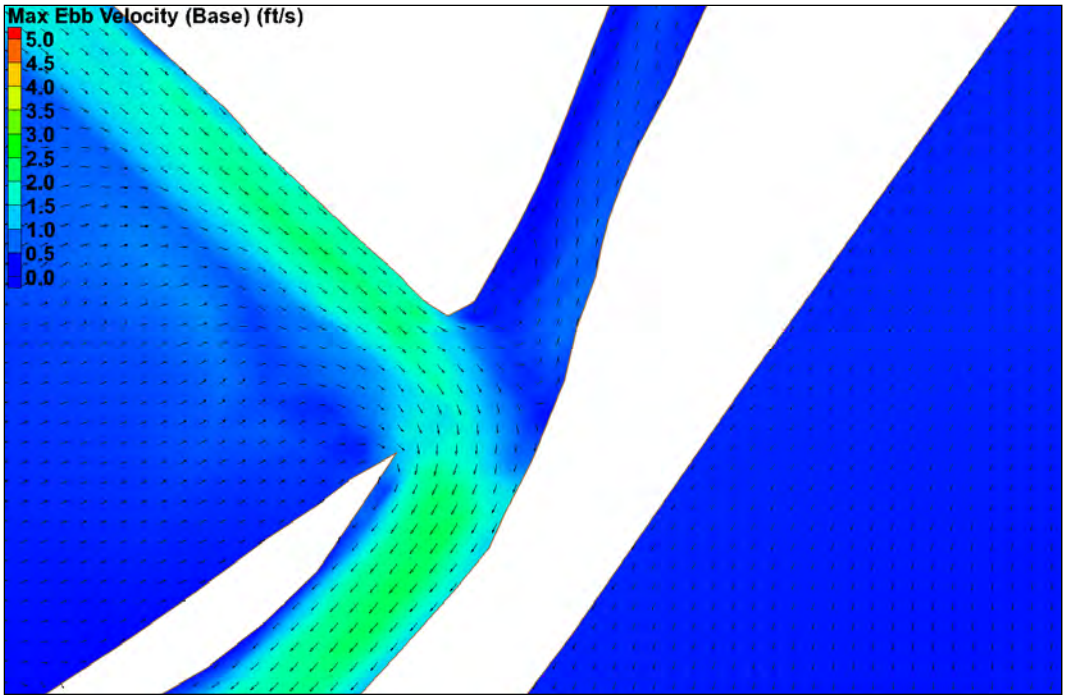

Figure C33. Bush Canal max ebb velocity (base).

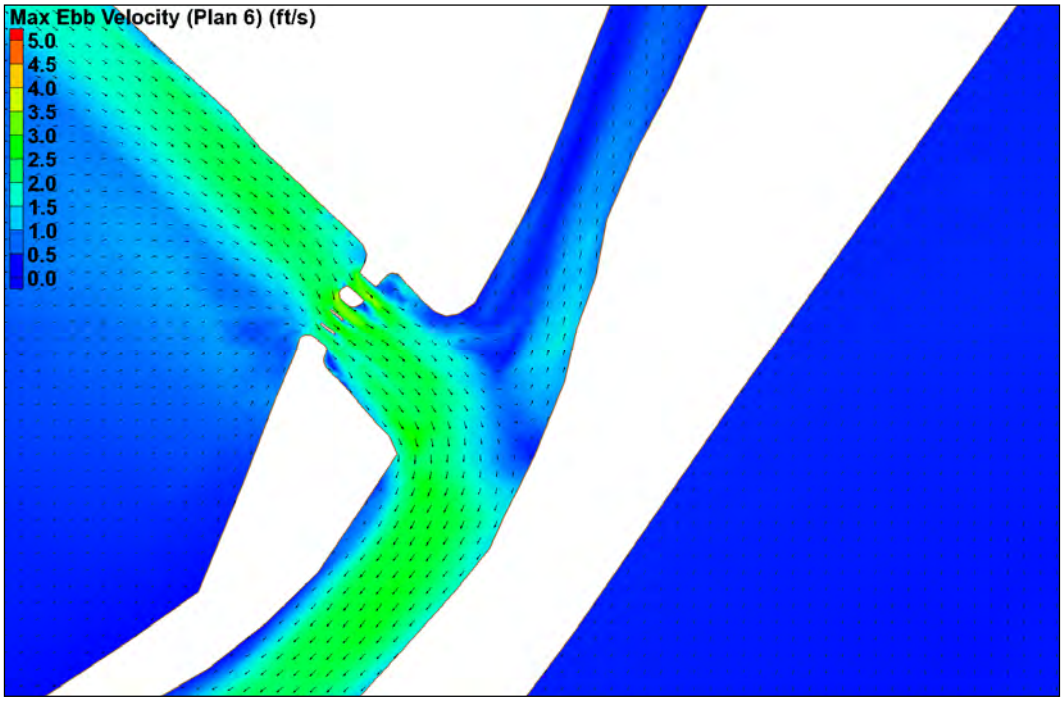

Figure C34. Bush Canal max ebb velocity (Plan 6).

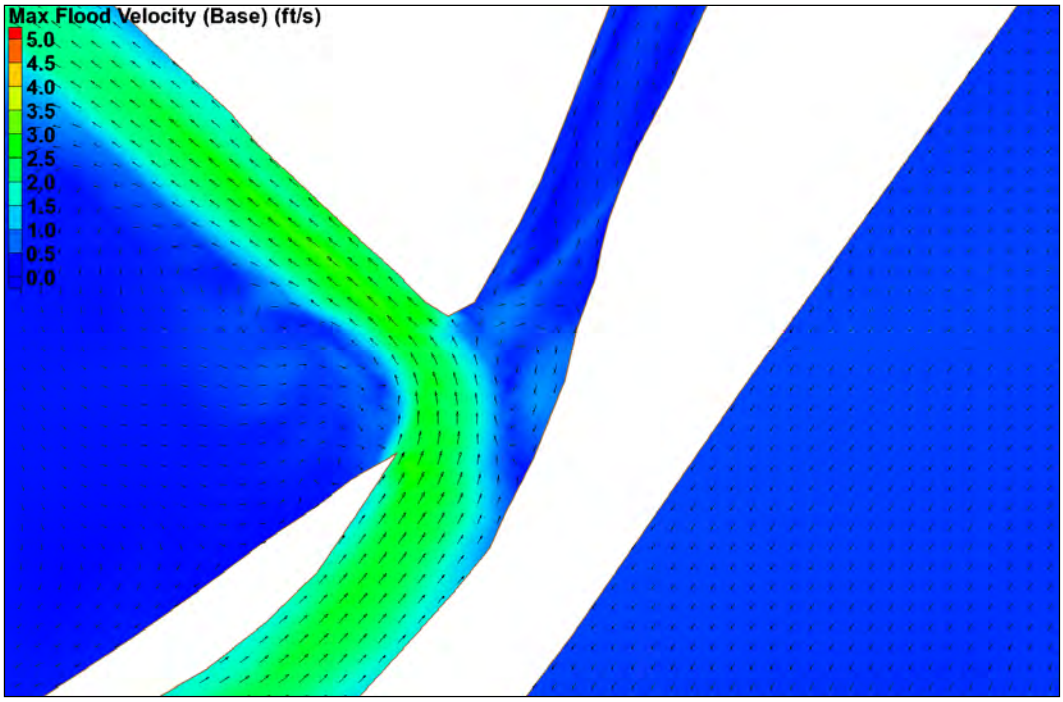

Figure C35. Bush Canal max flood velocity (base).

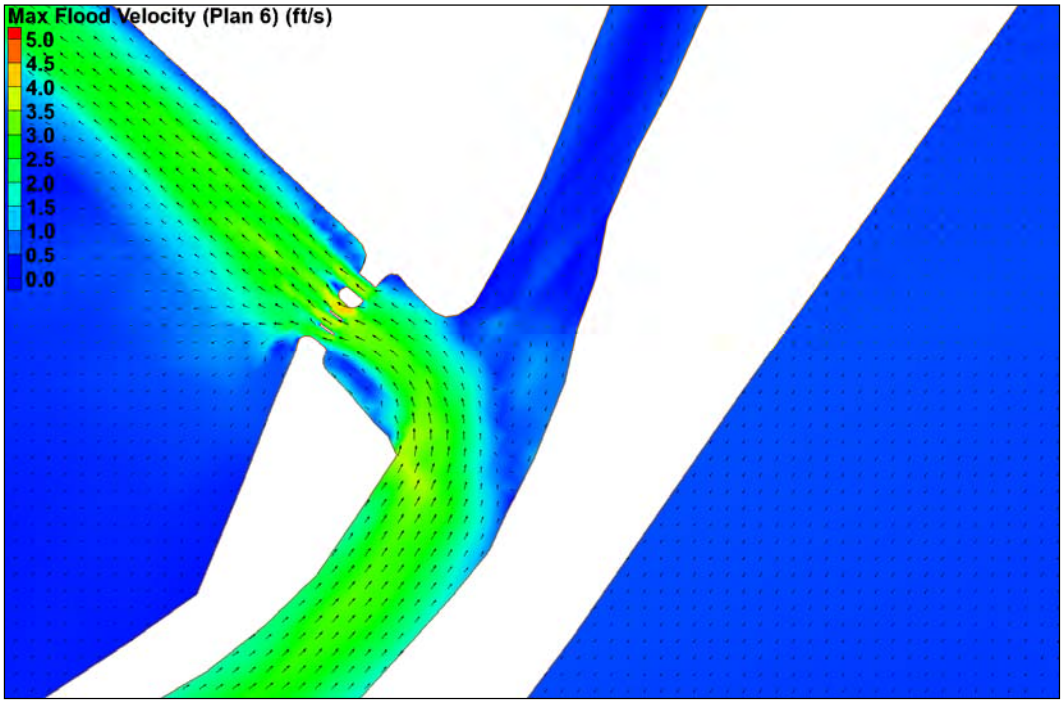

Figure C36. Bush Canal max flood velocity (Plan 6).

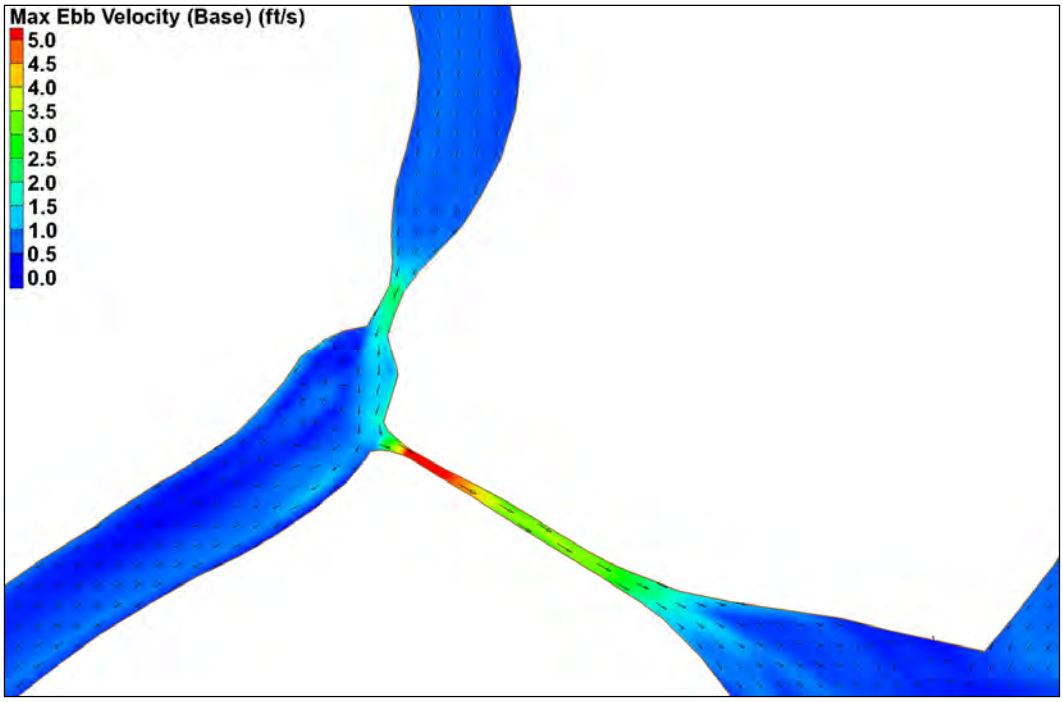

Figure C37. Bayou Terrebonne max ebb velocity (base).

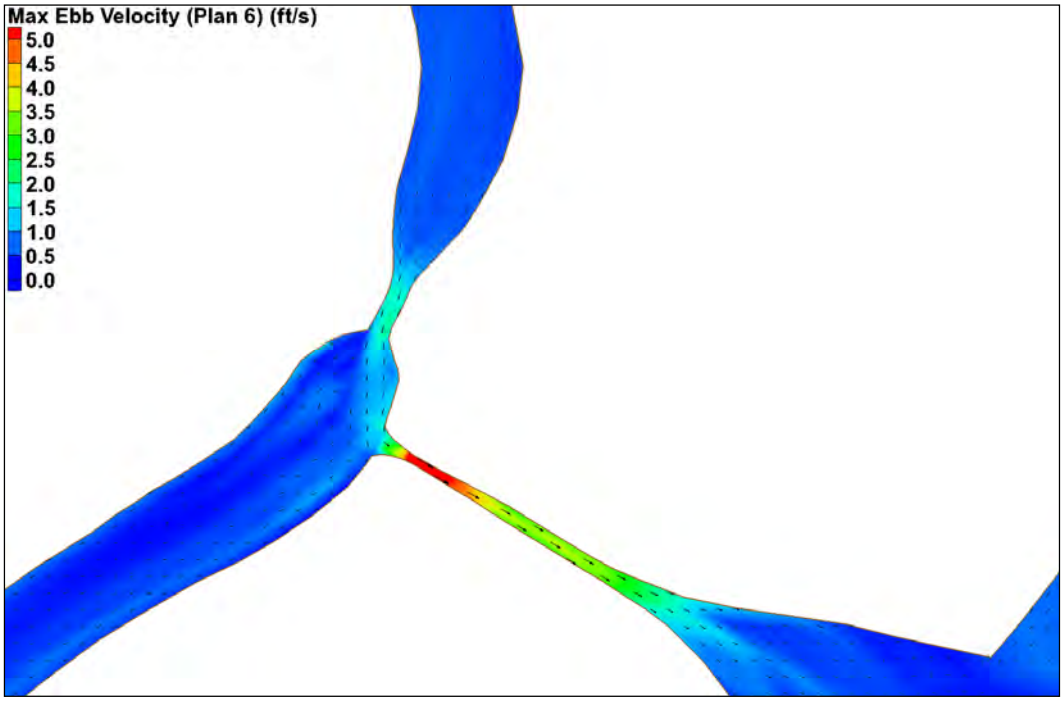

Figure C38. Bayou Terrebonne max ebb velocity (Plan 6).

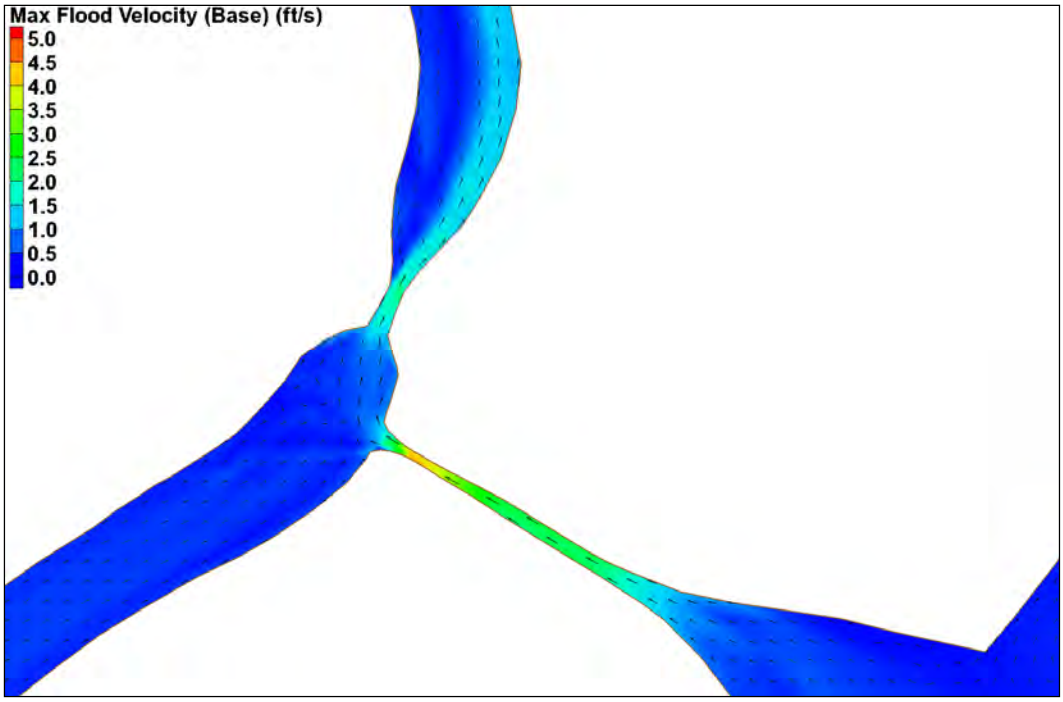

Figure C39. Bayou Terrebonne max flood velocity (base).

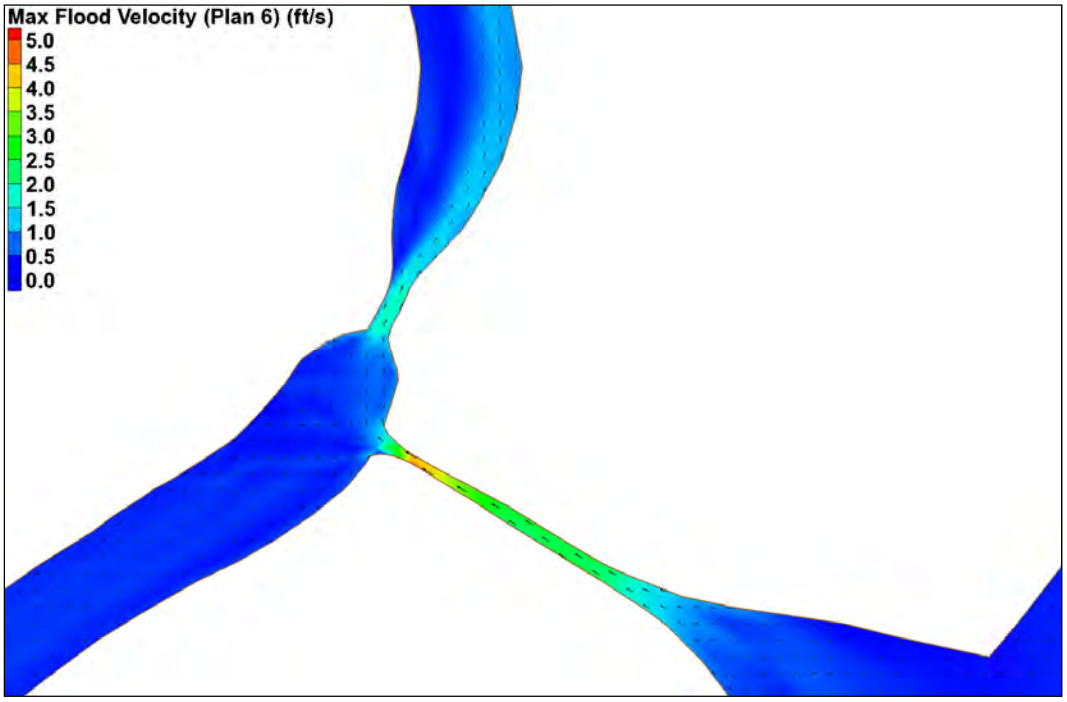

Figure C40. Bayou Terrebonne max flood velocity (Plan 6).

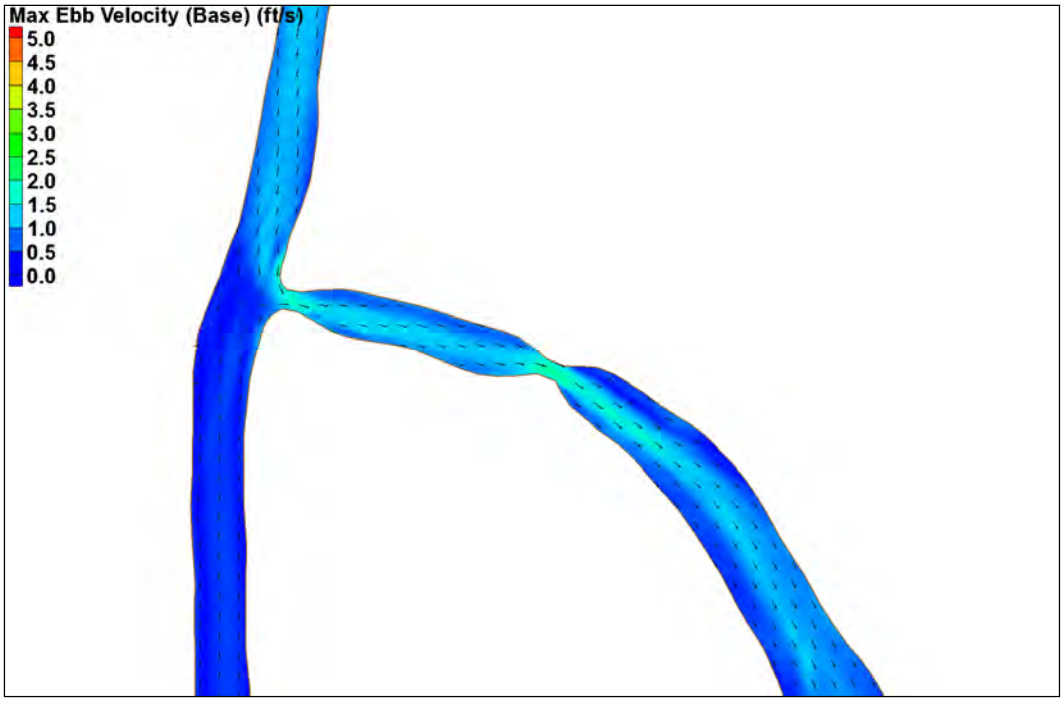

Figure C41. Humble Canal max ebb velocity (base).

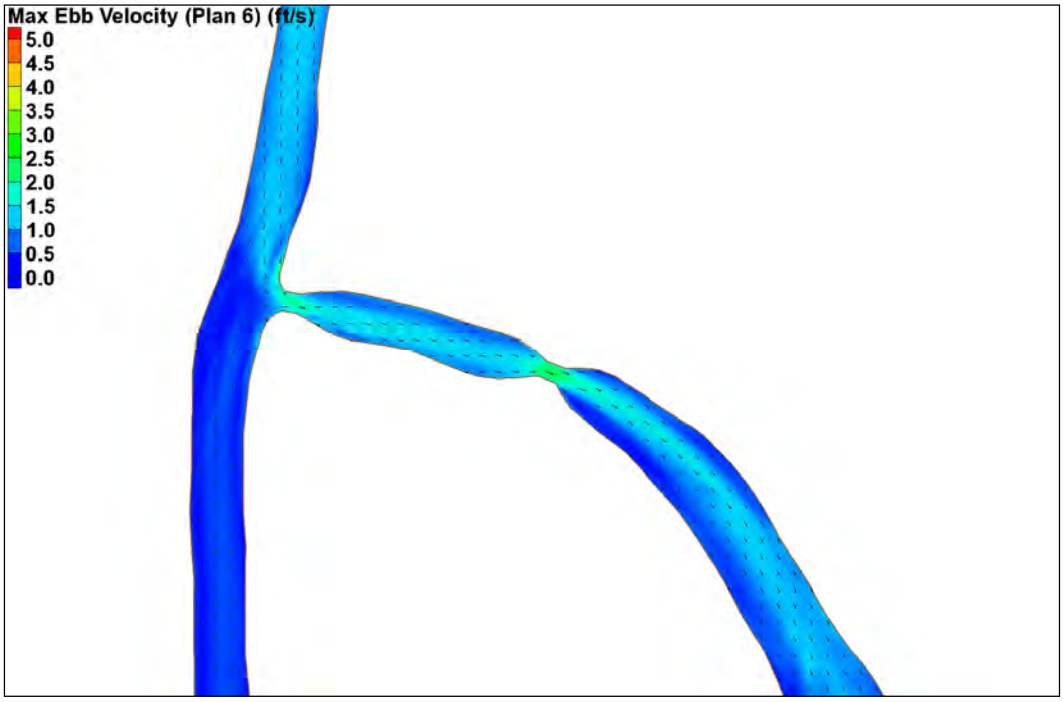

Figure C42. Humble Canal max ebb velocity (Plan 6).

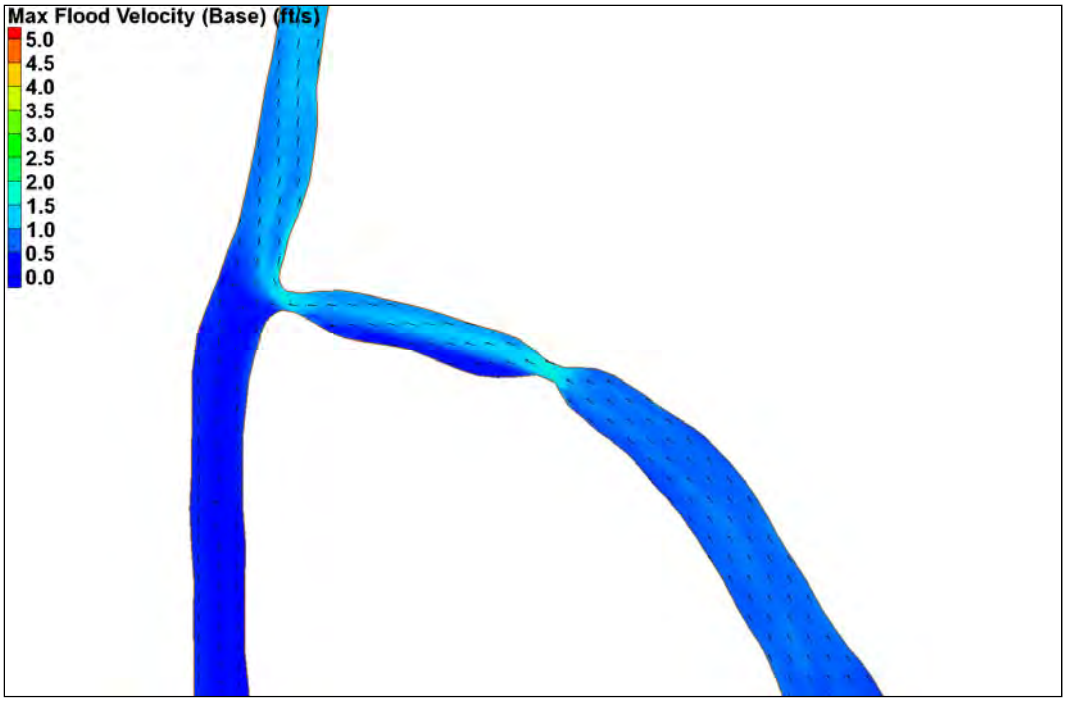

Figure C43. Humble Canal max flood velocity (base).

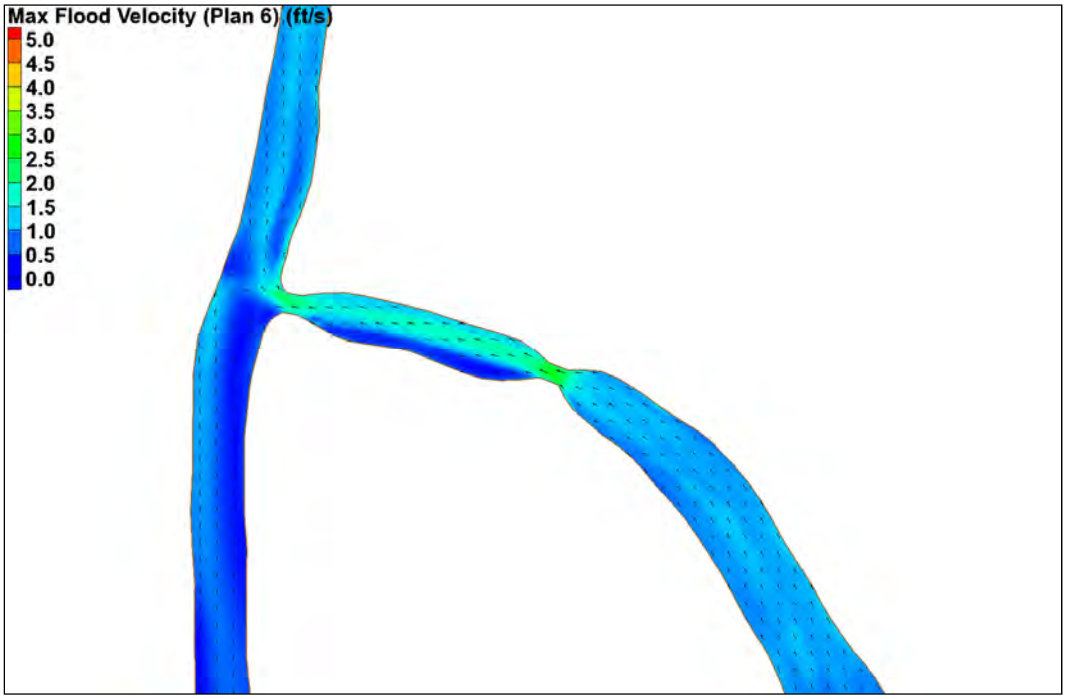

Figure C44. Humble Canal max flood velocity (Plan 6).

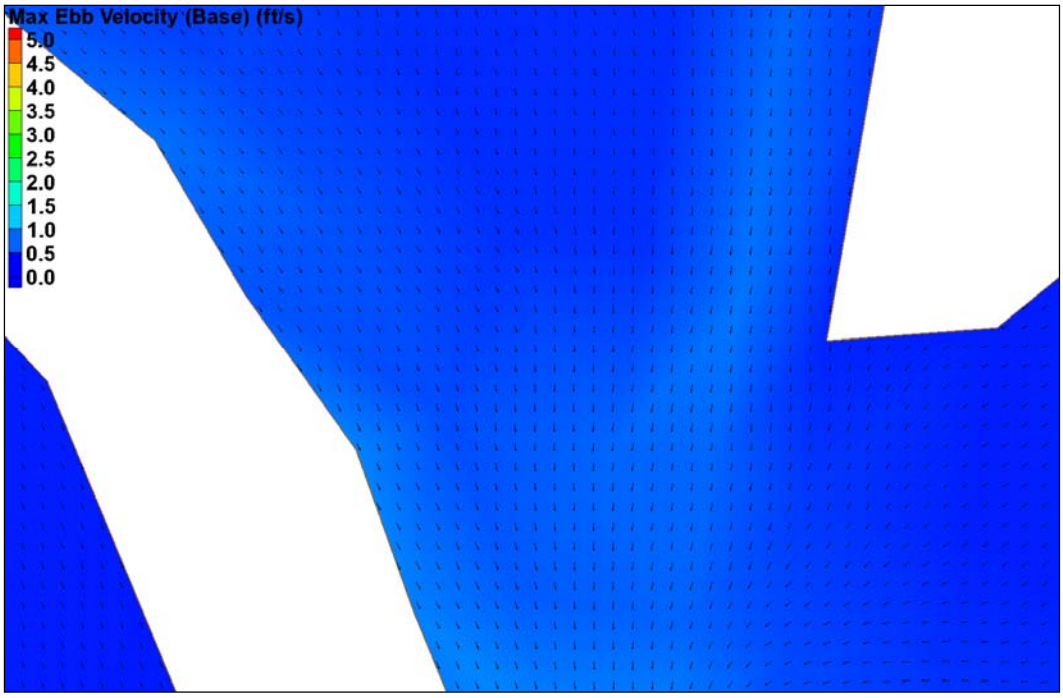

Figure C45. Pointe Aux Chenes max ebb velocity (base).

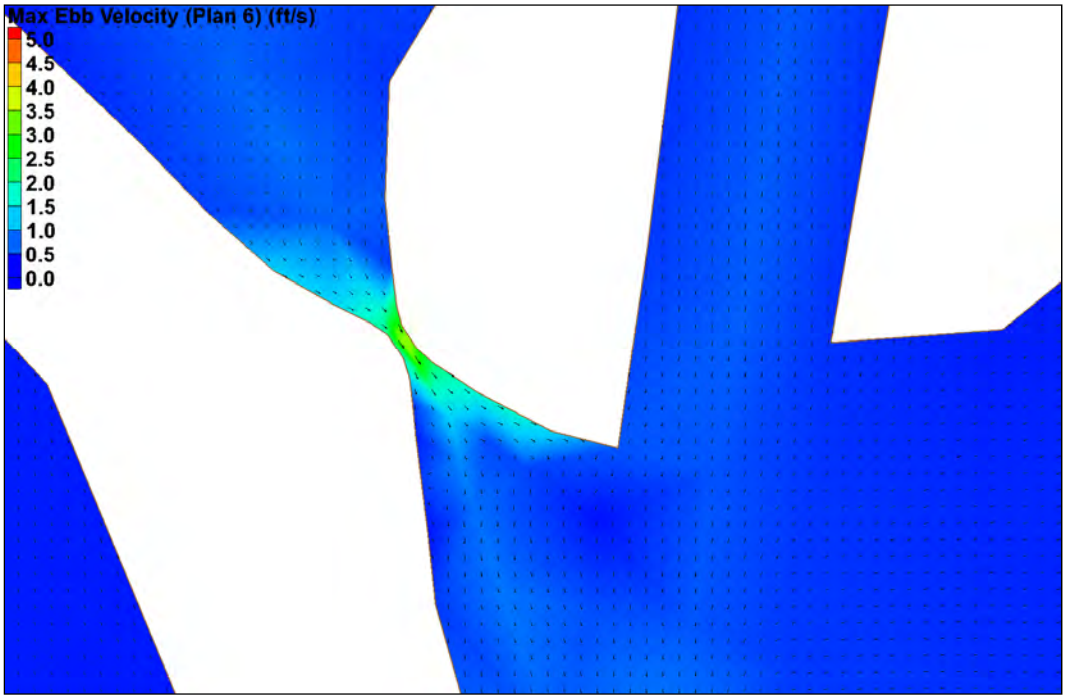

Figure C46. Pointe Aux Chenes max ebb velocity (Plan 6).

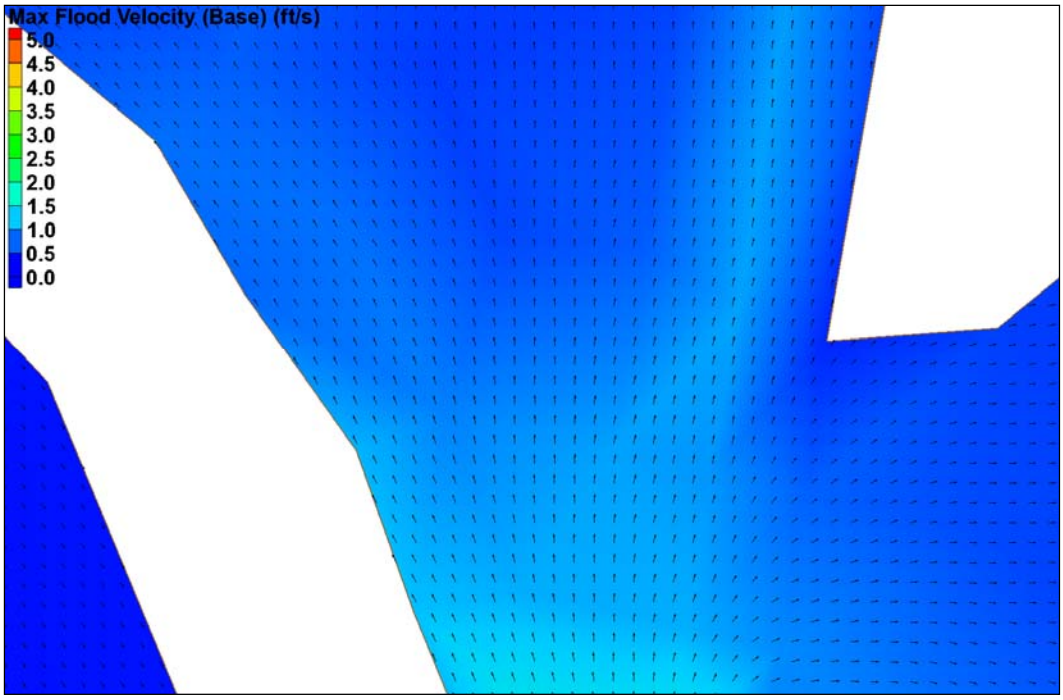

Figure C47. Pointe Aux Chenes max flood velocity (Plan 6).

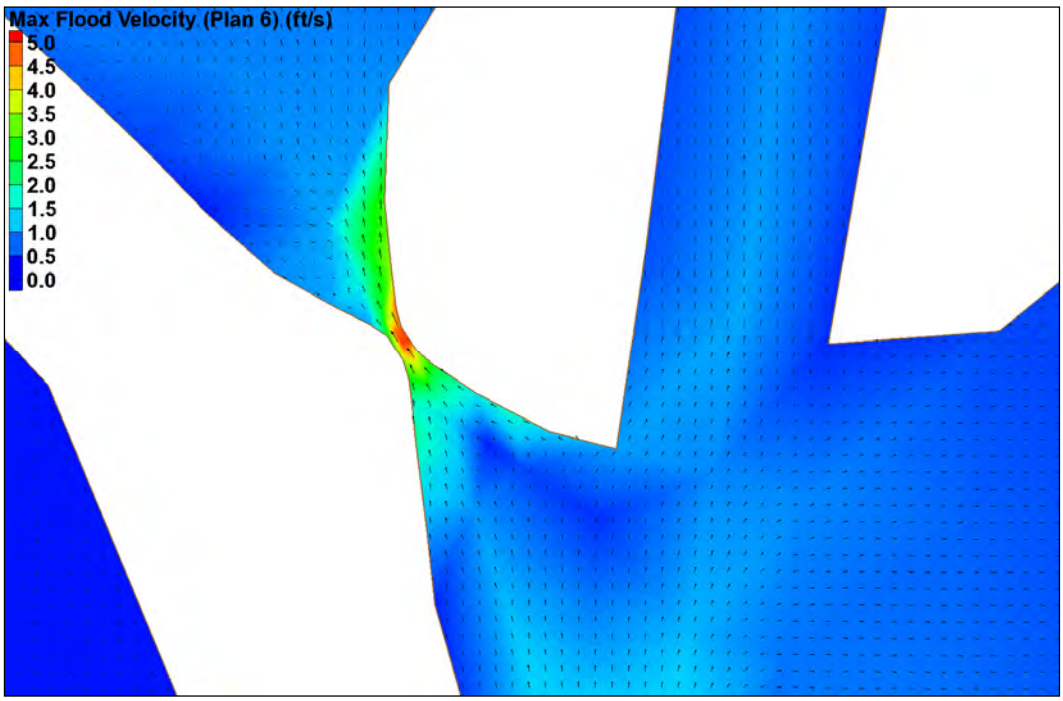

Figure C48. Pointe Aux Chenes max flood velocity (Plan 6).

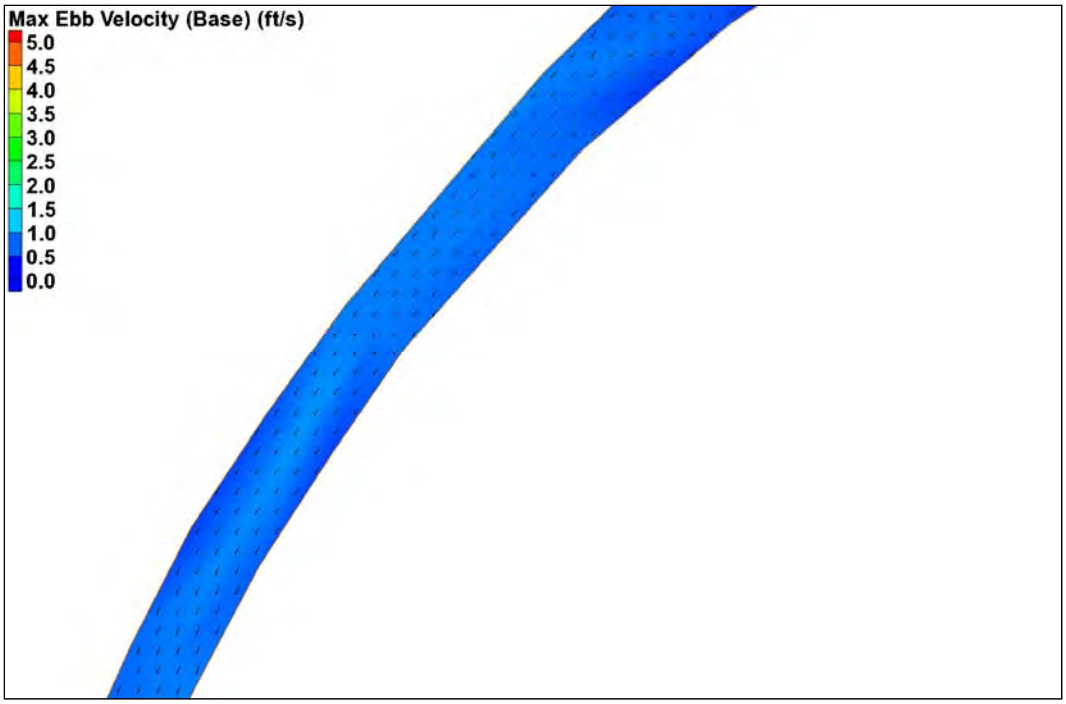

Figure C49. Grand Bayou max ebb velocity (base).

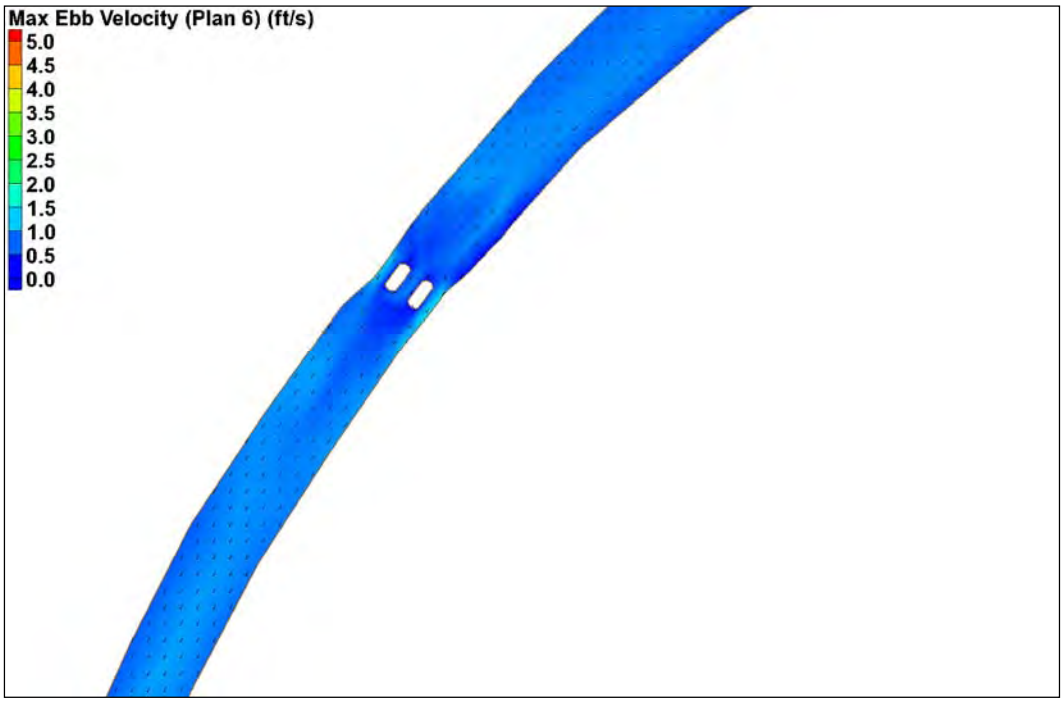

Figure C50. Grand Bayou max ebb velocity (Plan 6).

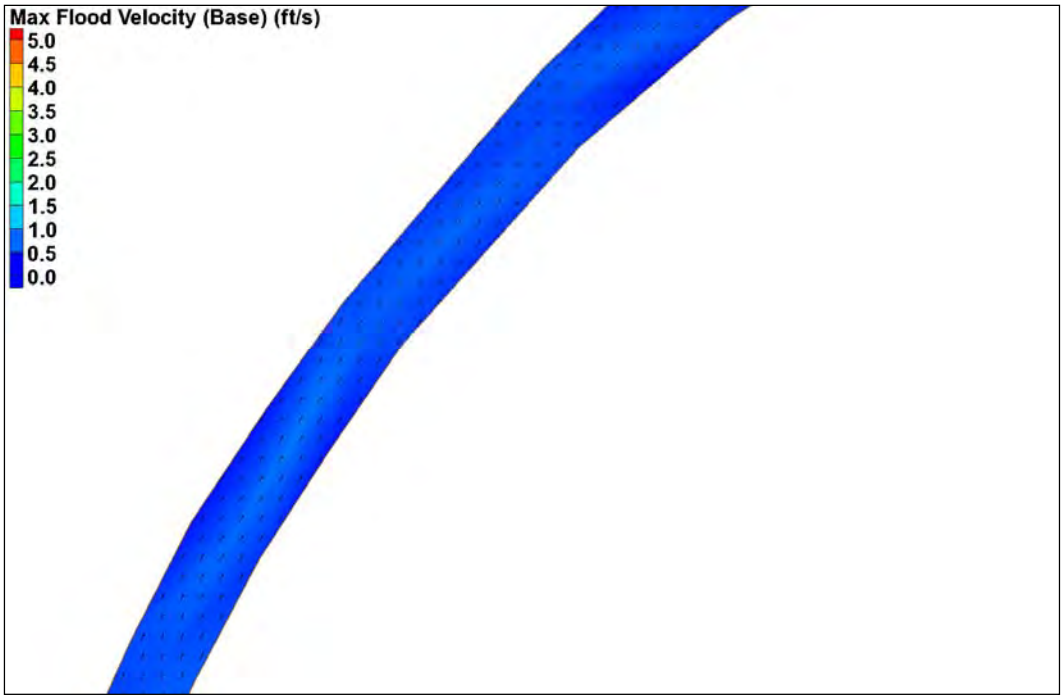

Figure C51. Grand Bayou max flood velocity (base).

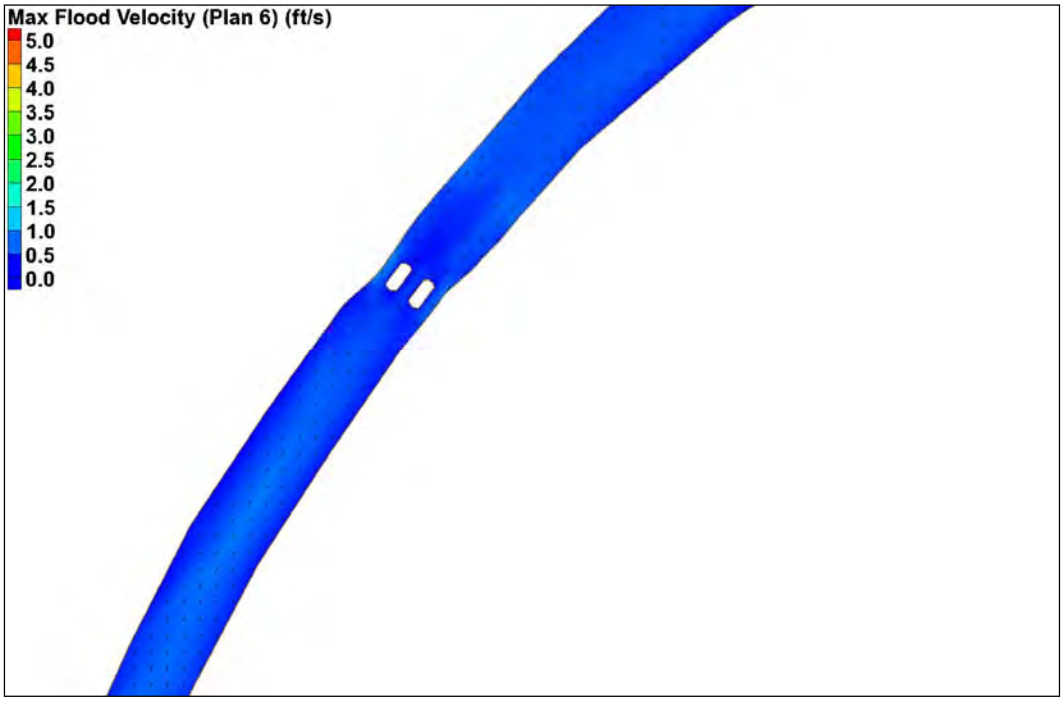

Figure C52. Grand Bayou max flood velocity (Plan 6).

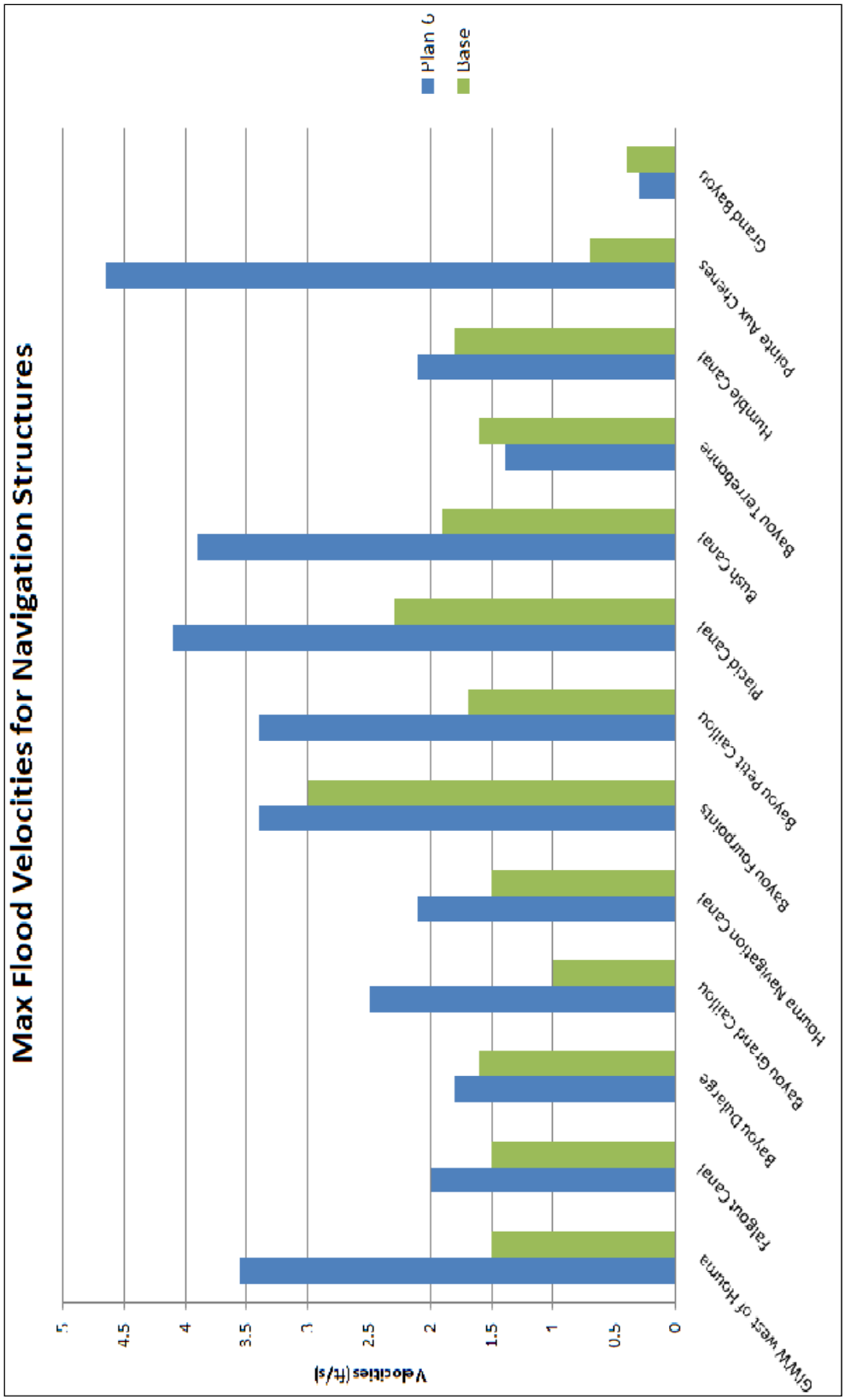

Figure C53. Maximum flood velocities for the navigation structures.

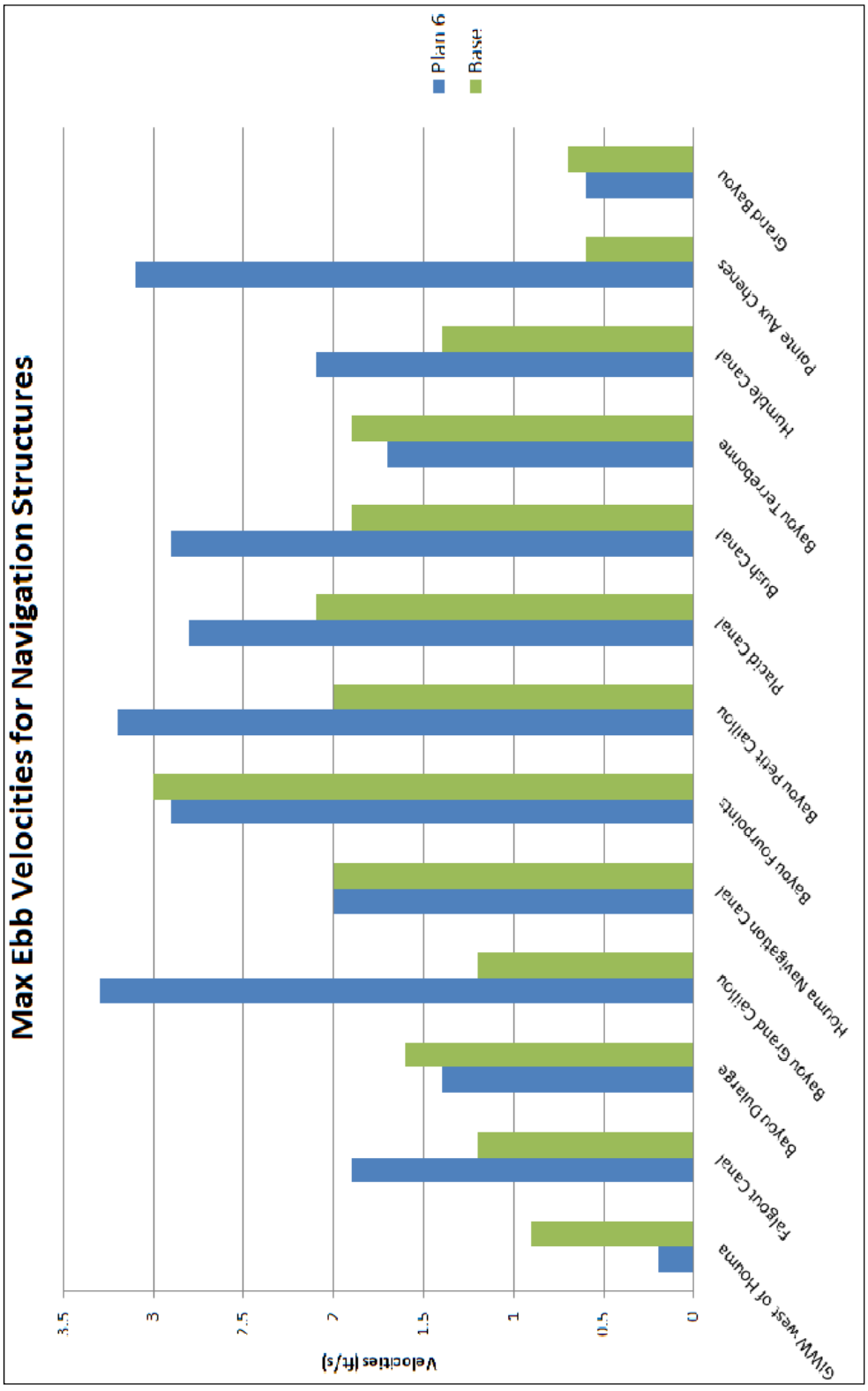

Figure C54. Maximum ebb velocities for navigation structures.

REPORT DOCUMENTATION PAGE

Form Approved
OMB No. 0704-0188

1. REPORT DATE *(DD-MM-YYYY)*	2. REPORT TYPE	3. DATES COVERED *(From - To)*
October 2011	Final report	

4. TITLE AND SUBTITLE
Morganza to the Gulf of Mexico Floodgate Study

5a. CONTRACT NUMBER

5b. GRANT NUMBER

5c. PROGRAM ELEMENT NUMBER

6. AUTHOR(S)
Tate O. McAlpin, Ian E. Floyd, Christopher J. Callegan, Thad C. Pratt, and Danielle M. Washington

5d. PROJECT NUMBER

5e. TASK NUMBER
MIPR W42HEM92266908

5f. WORK UNIT NUMBER

7. PERFORMING ORGANIZATION NAME(S) AND ADDRESS(ES)
U.S. Army Engineer Research and Development Center
Coastal and Hydraulics Laboratory
3909 Halls Ferry Road
Vicksburg, MS 39180

8. PERFORMING ORGANIZATION REPORT NUMBER
ERDC/CHL TR-11-6

9. SPONSORING / MONITORING AGENCY NAME(S) AND ADDRESS(ES)
U.S. Army Engineer District New Orleans
7400 Leake Ave.
New Orleans, LA 70118-3651

10. SPONSOR/MONITOR'S ACRONYM(S)
MVN

11. SPONSOR/MONITOR'S REPORT NUMBER(S)

12. DISTRIBUTION / AVAILABILITY STATEMENT
Approved for public release; distribution is unlimited.

13. SUPPLEMENTARY NOTES

14. ABSTRACT

The ADaptive Hydraulics model, AdH, was used to investigate the circulation tendencies in and around numerous proposed structure locations for the Morganza to the Gulf of Mexico project utilizing its two-dimensional shallow-water module. This study characterizes existing water levels and currents in the vicinity of six proposed structures and predicts any potential impacts that may result. Comparing model-generated currents and water-surface elevations between pre- and post-construction conditions provides insight into whether a particular alternative will adversely impact velocity conditions. AdH was used to develop time varying of current fields for the base and plan conditions.

15. SUBJECT TERMS		
ADaptive Hydaulics (ADH) model Bush Canal	Bayou Terrebonne Bayou Petit Caillou	Morganza to the Gulf of Mexico

16. SECURITY CLASSIFICATION OF:			17. LIMITATION OF ABSTRACT	18. NUMBER OF PAGES	19a. NAME OF RESPONSIBLE PERSON
a. REPORT	b. ABSTRACT	c. THIS PAGE			19b. TELEPHONE NUMBER *(include area code)*
Unclassified	Unclassified	Unclassified		183	

Standard Form 298 (Rev. 8-98)
Prescribed by ANSI Std. 239.18